2013

Characteristics of neotectonic faulting in the Mount Lofty and Flinders Ranges, South Australia

Chulantha Lakmal Jayawardena
University of Wollongong

UNIVERSITY OF WOLLONGONG

School of Earth & Environmental Sciences

Characteristics of neotectonic faulting in the Mount Lofty and Flinders Ranges, South Australia

Chulantha Lakmal Jayawardena

B.Sc. Eng. (Hons) University of Moratuwa

This thesis is presented as part of the requirements for the Award of the Degree of Doctor of Philosophy in the Faculty of Science of the University of Wollongong

December 2013

THESIS CERTIFICATION

I, Chulantha Lakmal Jayawardena, declare that this thesis, submitted in fulfilment of the requirements for the award of Doctor of Philosophy, in the School of Earth & Environmental Sciences, University of Wollongong, is wholly my own work unless otherwise referenced or acknowledged. The document has not been submitted for qualifications at any other academic institution.

.....

(Signature)

Chulantha Lakmal Jayawardena

12 December 2013

ABSTRACT

Ongoing seismicity is a characteristic feature of plate boundaries, which is not commonly observed in most continental interiors. Consistent low-level seismicity with anomalous higher magnitude events in the intraplate setting of the Mount Lofty and Flinders Ranges of South Australia, is an exception. The N-S elongated ranges are bounded by active faults, including the Eden-Burnside Fault, which produced a magnitude 5.5 Adelaide earthquake in 1954. Evidence of ongoing deformation from detailed mapping and trenching, highlights the potential seismic hazards in this intraplate setting, which requires a comprehensive characterization of faulting and a plausible driving mechanism.

The process of mountain building in the South Australian continental interior has been regarded as, E-W compressional uplift by reverse faulting on either sides of the Mount Lofty and Flinders Ranges. This is not in agreement with the local stress orientations, seismicity and fault characteristics revealed by the present study of individual fault contacts. Detailed geological mapping of stratigraphic offsets, discontinuity orientations, kinematic indicators and geomorphic features associated with the Willunga Fault at Sellicks Beach, have revealed reverse, normal and oblique fault movements. The unique orientations of these faults can be best explained through a sinistral strain-ellipse model, whereas subsidiary reverse fault splays with oblique movements radiating over a broad fault zone resembles positive flower structures. Oblique sinistral movements on the Eden-Burnside Fault and segments of the Wilkatana Fault, also display evidence of transpression, rather than purely E-W compression.

Extensive investigations on this intraplate neotectonic setting with rapid site exploration techniques, such as high resolution LiDAR digital elevation models, ground penetrating radar incorporated field trenches has revealed the presence of multiple faults in the shallow subsurface with limited surface expression. Results of the mapping and trenching indicate predominant reverse faulting towards the margins of the ranges, with comparatively steep fault contacts towards the centre. Identification of subtle, but important topographic and subsurface features, led to establish time constraints for relatively recent rupture events. Single grain OSL

results on a colluvial wedge developed over a disrupted soil profile in a trench at Tarlee has constrained the timing of ~1.6 m near surface offset on a low-angle thrust of the Williamstown-Meadows Fault to be ~15 ka. Single grain OSL dates on Alma and Burra faults also yielded late Pleistocene activity from a complicated depositional environment.

As the neotectonic faulting in the Mount Lofty and Flinders Ranges largely reflect reverse and oblique slip, a revised tectonic model is proposed with left-lateral movements. Accordingly, the faulting characteristics and much of the topographic features are accommodated by transpression instead of simplistic E-W compression. The model also better explains the distribution of regional seismicity. Frequent low-magnitude earthquakes along the middle of the ranges are largely due to the strike-slip movements, whereas intermittent higher magnitude earthquakes to the south and north are due to the terminal thrust faults that accumulate larger degrees of stress. Even though, the pre-historic structures are likely to continually evolve from a strike-slip behavioural perception, direct evidence of Delamerian structural influence on the neotectonic activities were not apparent on this localised and narrow zone of uplift.

The driving mechanism responsible for this intra-plate shallow-depth seismicity is difficult to reconcile, as the region has experienced multiple deformation episodes and the slow rates of ongoing deformation. However, it is possible to correlate major shifts in plate boundary conditions of the Indo-Australian tectonic plate, with deformations in the Australian continental interior. Renewed differential movements along the N-S striking crustal-scale southern oceanic transform faults due to the current NW-SE stress fields may have primarily impinged sinistral movements on the continental interior. The presence of these fracture zones south of the Mount Lofty and Flinders Ranges and the thermally weakened crust have been mutually facilitating the deformation, while the remainder of the plate boundary interactions are likely to enforce secondary controls. Furthermore, extensive fault branching, aseismic slip and structurally reworked, thermally weakened continental crust underneath the Mount Lofty and Flinders Ranges, may be collectively absorbing much of the seismic risk in this region. Nevertheless, neotectonic fault offsets suggest that the episodic large earthquakes are inevitable in this intraplate setting.

ACKNOWLEDGEMENTS

I would foremost like to thank Dr. Solomon Buckman, for his guidance towards successful completion of this fascinating research and the thesis. Input from Dr. Hendrik May with advice and support in crises is highly appreciated. Thank you very much Prof. Colin Murray-Wallace for keeping "*Chuzza*" on track. Thank you Prof. Robert Bourman for making me comfortable in writing, being supportive in the field, and sharing your research intellects. The four of you have been my inspiration as professional researchers both on and off the field, and the motivation to counteract the psychological dilemmas of isolated research.

Thank you very much Dr. Dan Clark and Dr. Andrew McPherson of Geosciences Australia, for allowing me to visit the trenches, being helpful in the field and accommodating lengthy GPR surveys. If not the trenching program of GA, I would never be able to compile an informative collection of data on unexposed fault contacts. The enthusiastic landowner Mr. Neil Weichert from Bethel is also acknowledged for his assistance in augering, to improve the GPR assessments. My sincere thank goes to A/Prof. Chris Fergusson and Dr. Amy Dougherty for their effective comments in getting this thesis to shine.

I owe a debt of gratitude to the University of Wollongong for sponsoring me to conduct the research, and to Ms. Lynne Wright and Prof. Buddima Indraratna for their support at various stages. I'm grateful to the entire staff and students of the School of Earth and Environmental Sciences for creating a comfortable environment to peacefully conduct my research activities. I'm also grateful to the academic staff of the Earth Resources Engineering, University of Moratuwa, for accommodating me during the hectic writing stages.

The stimulating speeches of Ven. Ajahn Brahm were the uninterrupted energy source throughout the years of hardship. Motivational discussions with Dr. Jocelyn Harper kept me on the track. Thank you, Dr. Senevi Kiridena, Ms. Mary Sparks for comforting me like family members and for all the friends who kept me well fed. I'm incredibly indebted to my parents and my brother for their love, understanding and looking after this lonely soul, remotely, but consistently.

TABLE OF CONTENTS

LIST OF FIGURES

LIST OF TABLES

PUBLICATIONS

Conference proceedings

Adelaide - seismicity and neotectonics. Buckman S & Jayawardena CL 2009.
(Poster presentation), Geodynamics of the Australian Plate research meeting, 8 & 9 June Monash University, Melbourne Australia.

What's up with the Willunga Fault? Strike-slip restraining bends in the Mount Lofty Ranges. Buckman S, Jayawardena CL, Bourman RP, Murray-Wallace, CV 2009.
(Poster presentation), 7th International conference on Geomorphology, 7-12 July – Melbourne Australia.

Strike-slip characteristics of the Willunga Fault at Sellicks Beach, Fleurieu Peninsula, South Australia. Jayawardena CL, Buckman S, Bourman RP, Murray-Wallace, CV 2010. *(Poster presentation).* What is driving intraplate deformation in South Australia? Buckman S, Jayawardena CL, Bourman RP, Murray-Wallace, CV 2010. *(Oral presentation.)*
Australian Earth Science Convention, 4-8 July Canberra Australia.

A field study on Willunga Fault at Sellicks Beach, South Australia – Implications on neotectonic mountain building. Jayawardena CL, Buckman S, Bourman RP, Murray-Wallace, CV 2011.
(Oral presentation), ANZGG conference 30 Jan to 4 Feb, Oamaru, New Zealand

Quaternary mountain building process in the Mount Lofty and Flinders, South Australia. Buckman S, Jayawardena CL, Murray-Wallace, CV, Bourman RP 2011. *(Oral presentation), Institute of Australian Geographers conference 3-6 July Wollongong, Australia.*

Nature of active faulting in Mount Lofty and Flinders Ranges: a study of intraplate mountain building. Jayawardena CL, Buckman S, Bourman RP, Murray-Wallace, CV 2012.
(Oral presentation), 15th Biennial ANZGG conference, 2-7 Dec, Bundanoon, Australia

Publications in preparation

The following publications are in preparation to be published in the Australian Journal of Earth Sciences, under the working title.

Field evidence of strike-slip transpressional movements along the Willunga Fault at Sellicks Beach, South Australia. Jayawardena C.L., Buckman S., Bourman R.P, Murray-Wallace C. V. (based on Chapter 3)

Neotectonics of Mount Lofty and Flinders Ranges from a strike-slip perspective. Buckman S., Jayawardena C.L., Bourman R.P. (based on Chapter 7)

Paleoseismological approach to quantify the nature and timing of active faults in the Mount Lofty and Flinders Ranges. Buckman S., May J. H., Meyer M., Jayawardena C.L., Bourman R.P., Murray-Wallace C. V., Clark D., McPherson A. (based on Chapters 4 and 5)

1 INTRODUCTION

1.1 Prologue

The world has witnessed destructive earthquakes during the recent past, many of which occurred on faults that had not recorded significant "historic" seismicity. In 2004, the *M* = 9.2 earthquake west of Sumatra, the second largest in recorded history, resulted in a tsunami that killed over 200 thousand people. In 2011, ~230 thousand people died following a *M* = 7.0 earthquake in Haiti. In the same year, *M* = 9.0 Tōhoku earthquake off the east coast of Japan spawned a tsunami which, resulted in ~19 thousand deaths and massive infrastructure damages. A *M* = 8.8 earthquake in Chile, in 2010, was fortunate to account for only 500 lives. However, in 2008, the *M* = 8.0 Chinese Sichuan earthquake (an intra-plate earthquake) killed ~69 thousand, leaving up to 11 million people homeless. These recent disasters highlight that earthquake hazards vary and depend not merely on the magnitude of the earthquake, but on the location of the epicentre, the population density and the strength of both the foundations and the infrastructure. Hence, it is important to document the history of seismicity in different tectonic settings and understand the processes responsible for crustal deformation. Such information is helpful for appropriate zoning and planning to reduce the impact of future earthquakes.

Countries situated within intra-plate settings, which experience infrequent earthquake activity are the least prepared in terms of building codes and emergency responses, as illustrated by the impacts of the *M* = 5.6 Newcastle earthquake in 1989, which killed 13 people and resulted in a damage bill in excess of $4 billion. A long temporal perspective is essential to help mitigate the impacts of earthquakes and to determine the fundamental driving mechanisms of intra-plate tectonism.

The interaction of the current stress field with major crustal discontinuities or weaknesses is probably creating the localised seismicity and mountain building activity in regions such as the Mount Lofty/Flinders Ranges. However, the exact nature and causes of faulting within intra-plate settings worldwide is still poorly understood (Sykes & Sbar 1973) compared with the more obvious mechanisms associated with plate collision or the tearing operating at plate boundaries.

1.2 Introduction

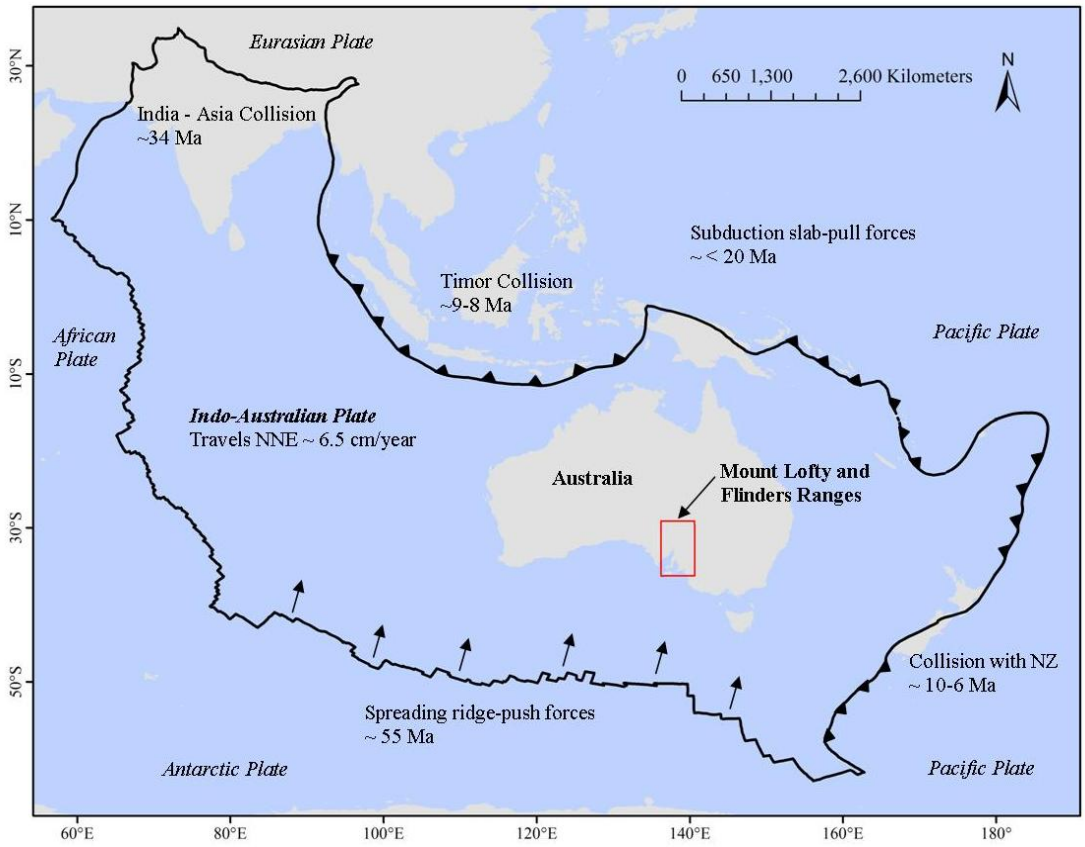

Figure 1.1 *Regional tectonic setting of Australia (source Hills et al. 2008), showing the timing of major plate boundary collisions and rifting events that resulted in the current Indo-Australian plate movement, and the location of the Mount Lofty and Flinders Ranges (Figure 1.2) in an intraplate setting*

The Mount Lofty and Flinders Ranges in South Australia represents one of the most seismically active regions in Australia (Greenhalgh *et al.* 1986, Belperio 1995, Hillis & Reynolds 2000, Hillis *et al.* 2008). The driving mechanism of this intra-plate deformation is a topic of much conjecture (Sandiford 2003a, Buckman *et al.* 2010, Bourman *et al.* 2010a) as the region is positioned in an intra-plate setting many thousands of kilometres from the nearest plate boundaries (Figure 1.1). To the north the Indo-Australian plate is being pulled by the subduction of dense oceanic crust beneath Indonesia. The collision of the Australian continent with the Indonesian volcanic archipelago occurred less than 20 million years ago and resulted in the formation of the highlands in Papua New Guinea (Findlay 2003), while further west the India-Asia collision, which started 34 million years ago (Aitchison *et al.* 2007) has had a profound effect on the stress field in Australia. To the east the Tasman Sea opened up 90-50 Ma and separated Australia from a convergent margin in New

Zealand, which developed ~10-6 Ma. To the south a mid-ocean ridge, which began spreading about 55 million years ago, separates Australia from Antarctica. The forces acting at these plate boundaries result in the overall northward migration of the Indo-Australian plate at a rate of 6.5 cm yr^{-1}, making Australia the fastest moving continent on Earth (Sandiford 2010a).

The Mount Lofty and Flinders Ranges extend some 700 km from the Fleurieu Peninsula in the south to Maree in the North Flinders (Figure 1.2) and attain elevations of up to 1171 m. Regionally these ranges form a distinctive *en echelon* or 'lazy S' shape with range-bounding reverse-faults occurring on the margins of the ranges (Twidale & Bourne 2004). The historic record of seismicity in this region shows a clear correlation between elevation and earthquake activity (Figure 2.2), revealing that the crustal deformation is young and ongoing (Crawford & Campbell 1973, Bourman & Lindsay 1989, Campbell 1996, Sandiford 2003a). The origin of range-bounding faults of the Mt Lofty and Flinders Ranges has long been discussed (Benson 1911, Fenner 1930, Sprigg 1942, 1946, Campana 1954, Talbot & Nesbitt 1968) and initially it was considered that the faults were normal types. Later the majority of the workers acknowledged the dominance of reverse faulting on the range margins and Wellman & Greenhalgh (1988) suggested that compressive forces have been important in the formation of the Mount Lofty Ranges. The orientation of the stress field is critical in terms of predicting the style of faulting as it interacts with pre-existing faults or zones of crustal weakness. Hillis and Reynolds (2000) attributed the overall N-S orientation of the Mount Lofty/Flinders Ranges to a predominantly E-W compressional stress field. However, reliable stress field indicators are few and far between in South Australia. The overall orientation of the maximum horizontal stress field as determined on the world stress map (Hillis *et al.* 2008) and subsequently modelled by Heidbach *et al.* (2010) shows a more NW-SE directed stress field through the Mount Lofty/Flinders Ranges. Hence, a re-evaluation of exposed fault contacts is required to resolve the nature of the faulting responsible for the uplift of the Mount Lofty Ranges in view of the recent structural mapping (Buckman *et al.* 2009b, Buckman *et al.* 2010), which indicates strike-slip faulting may have played a significant role in forming the mountains and generating earthquakes.

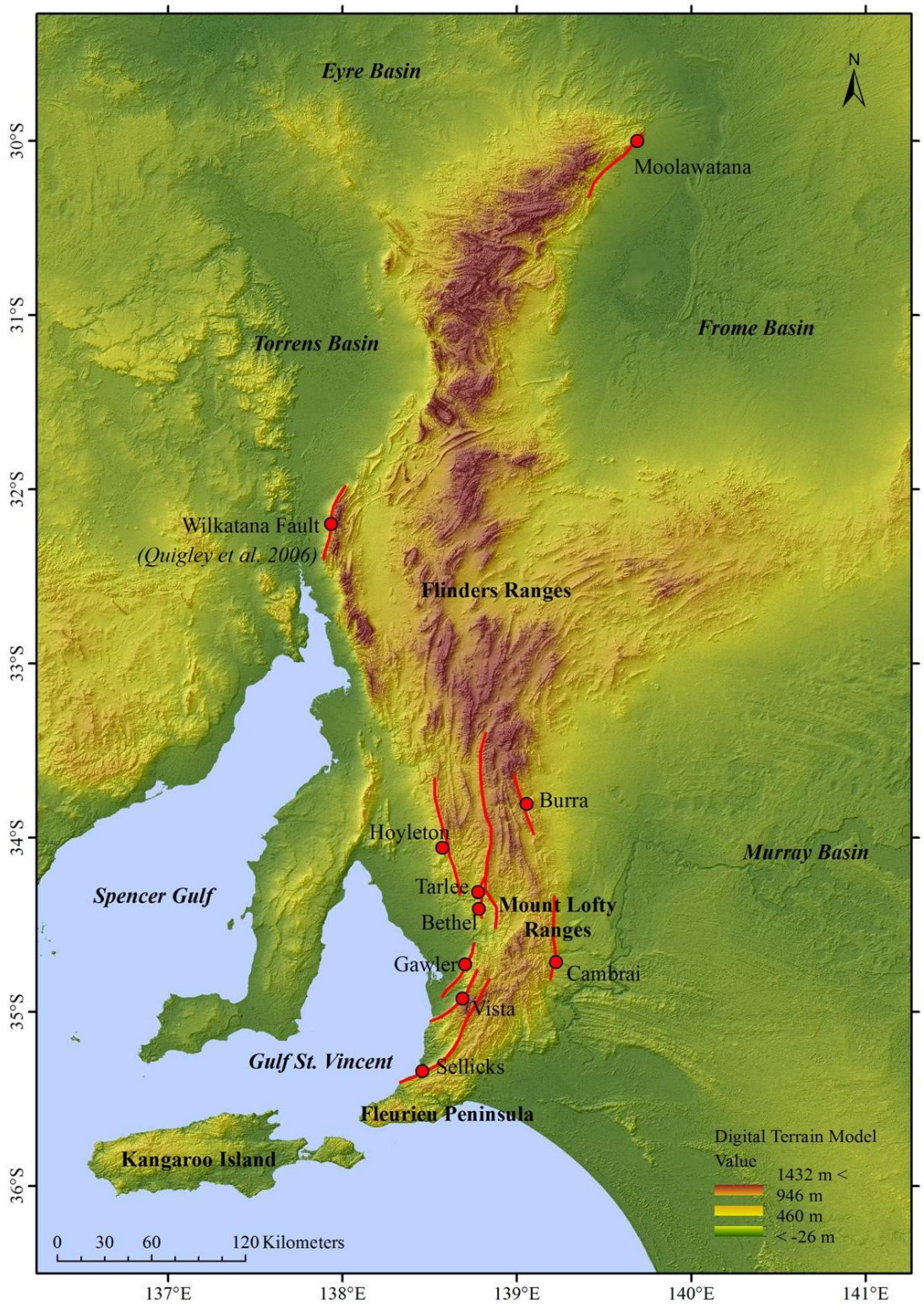

Figure 1.2 *Neotectonic study sites with corresponding faults in the Mount Lofty and Flinders Ranges*

Mountain building activity within the South Australian landscape throughout the Quaternary has been the subject of much discussion over the past century (Benson 1911, Fenner 1930, Sprigg 1942, 1946, Campana 1954, Cleary & Simpson 1971, Crawford & Campbell 1973, Twidale & Bourne 1975, Coward 1976, Daily *et al.* 1976, Ludbrook 1983, Bourman & Lindsay 1989, Marshak & Flöttmann 1996, Bourman & Pillans 1997, Sandiford 2003a, Tokarev 2005, Quigley *et al.* 2006, Bourman *et al.* 2010a). Despite these studies, the nature, origin and the timing of these neotectonic faults remain unclear and there have not been many attempts to explain the driving mechanism of this ongoing crustal deformation (McLaren & Sandiford 2001). On the rare occasions that neotectonic faults in the Mount Lofty/Flinders Ranges have been exposed and identified, they display a predominantly reverse sense of movement. Reverse faults have the potential to accumulate more strain than normal faults (Wesnousky & Jones 1994, Kelly *et al.* 1999) and thus generate strong ground motions and widespread damage when strain is released.

1.3 Aims and Objectives

The overarching aim of this project is to develop a tectonic model to re-evaluate the driving mechanisms responsible for localised zones of seismicity and mountain building activity in "stable" continental interior of Australia. The Flinders/Mount Lofty Ranges highlight the subtle complexities of tectonic processes operating within intra-plate settings that have not hitherto been explained by the more obvious and well established forces of subduction, rifting or transform faulting operating at plate boundaries. A key objective of this project was to characterise the nature and timing of large, pre-historic earthquakes on fault lines along the margins of the Mount Lofty and Flinders Ranges. Trenching in the Flinders and Mount Lofty Ranges in collaboration with Geosciences Australia demonstrated its usefulness in exposing recently active fault planes. A re-evaluation is necessary in the light of new Quaternary dating techniques, such as luminescence dating, which may extend the timing of depositional events to ~1 million years (Huntley *et al.* 1993, 1994), well beyond the ~50,000 year radiocarbon limit. This work is important because it provides the first attempt to systematically map, trench and date neotectonic fault

movements in the Flinders/Mount Lofty Ranges. The data from this project will help shed light on the broader question of possible mechanisms driving crustal deformation in so-called “passive” continental margins and intra-plate settings.

This project has been broken down into several specific, achievable objectives, which include:

1) To review literature relevant to the study
2) To conduct detailed geological and structural mapping of neotectonic faults exposed at selected sites, with structural mapping to be focused on identifying kinematic indicators and vertical/horizontal offsets in order to determine the overall nature of fault movement.
3) To produce detailed mapping and logging of trenches dug across neotectonic fault zones in conjunction with Geosciences Australia.
4) To date both offset and unaffected Quaternary units revealed by trenching to constrain the age of previous large events using optically stimulated luminescence (OSL) dating techniques where appropriate.
5) To develop a method and assess the viability of using ground penetrating radar (GPR) as a preliminary exploration technique to locate subsurface faults in the South Australian environment. The faults already identified by the aforementioned mapping or trenching programs were used for this purpose.
6) To propose a revised tectonic model that better explains the mode and cause of intraplate, continental deformation responsible for the ongoing mountain building activity within the Mount Lofty/Flinders Ranges, South Australia.

1.4 Methods

This study involves investigation of active faulting in the Mount Lofty and Flinders Ranges. In some places along the range front, active faults have been exposed in some places by recent erosion, removing the thin veneer of soil that usually masks the underlying geological features. Study sites are located in South Australia (Table 1.1) within the Mount Lofty and Flinders Ranges, covering significant locations along the mountain range. A total of 9 sites namely, Sellicks, Vista, Cambrai,

Moolawatana, Tarlee, Bethel, Gawler, Hoyeleton and Burra were selected and studied, covering 8 of the identified fault zones (Figure 1.2).

Study site	Fault name	Location coordinates	
		E	S
Sellicks	Willunga Fault	267709	6085146
Vista	Eden-Burnside Fault	297852	6198579
Gawler	Para Fault	291889	6161676
Cambrai	Milendella Fault	339147	6163147
Bethel	Williamstown-Meadows Fault	291951	6141469
Tarlee	Williamstown-Meadows Fault	296810	6202983
Hoyleton	Alma Fault	277655	6234150
Burra	Burra Fault	323473	6263068
Moolawatana	Paralana Fault	377267	6688740

Table 1.1 *Study sites with location coordinates*

1.4.1 Structural mapping and geomorphic analysis

Basic geological mapping of these fault zones provides a vital first step towards further understanding the nature and character of the stress field that currently makes the Mount Lofty/Flinders Ranges the most seismically active region in Australia. Fault exposures and surrounding structural geological features were recorded following basic structural geological mapping procedures (Marrett & Allmendinger 1990) and data plotted on stereonets for interpretation purposes. Recording *in situ* information on fault displacement of kinematic indicators such as slickensides, tension gashes and fault gouge textures were used to obtain localised movements along fault planes and to determine the palaeostress regimes (Dumont *et al.* 2005). Detailed geological maps of key fault exposures, presented in Chapters 3 and 4, were used in conjunction with ground penetrating radar (GPR) to better predict the strike extent of these faults in areas covered by thin veneers of soil or hillslope debris.

The study of drainage networks near the faults provided information relevant to the nature of fault movements and time constraints for regional deformation. Recognition and recording of knickpoints along valleys, restraining bends

(Cunningham 2007), flower structures (Harding 1985), splays of subsidiary thrust faults and offset of stratigraphic units were also considered in conjunction with digital elevation data and field mapping. Where the faults are exposed, as at Sellicks Beach, the orientation of the fault planes as well as kinematic indicators (slickensides) have been recorded and mapped to reveal the nature of past fault ruptures.

High resolution LIDAR elevation data from Airbourne Research Australia (ARA) have been used to create a detailed digital elevation model of the Sellicks region. SRTM and ASTER images were also used to extract Digital Elevation Models (DEM) using ArcGis and GeoMap App. Topographic profiles were created using Global Mapper and GoogleEarth software, sourcing SRTM data and were used to identify geomorphological features such as knickpoint retreats and topographical changes across fault zones in order to reconstruct the paleosurfaces. These data, along with high-resolution aerial photographs and elevation measurements through contouring, were used as a basemap to identify subtle geomorphic features, such as stream knickpoints (waterfalls) and terraces that may be related to neotectonic faulting.

1.4.2 Trenching

Trenching across active fault traces has been used effectively in other seismically active regions such as the San Andreas Fault in California, in order to more accurately constrain the timing of past fault ruptures (Williams 2007, McCalpin & Carver 2009). The method involves trenching across the fault line and identifying small colluvial wedges associated with erosion of the upthrown block and deposition of that material downslope. These colluvial wedges relate to individual earthquakes in the past and may be dated by radiocarbon or luminescence techniques depending on the age and nature of the sediments. Similarly, tension gashes can open up near the fault and be infilled with overlying soil. A trenching program undertaken by Geosciences Australia in 2010 and 2011 successfully excavated across several near-surface neotectonic faults and provided significant information for the investigations of this thesis. Examination of progressive offsets of Quaternary units affected by

ongoing faulting and associated colluvial wedges, and sampling of sheared fault gouge material for future textural and mineralogical analysis (Offler *et al.* 2009) formed considerable amount of fieldwork.

1.4.3 Optically Stimulated Luminescence Dating

Appropriately collected samples were analysed using luminescence dating techniques. Optically stimulated luminescence (OSL) dating was preferred due to its capability of dating quartz or feldspar grains obtained from a variety of depositional environments associated with faulting activities. Optical ages were calculated following the standard procedures and considering the environmental factors (Aitken 1998, Lian & Scott 2007b). Obtaining an age limit for the deposition of a colluvial wedge, alluvial or fluvial terrace can aid the interpretation of fault slip rates and recurrence intervals. The OSL dating was conducted in the Institute of Geology and Palaeontology, University of Innsbruck, Austria and at the School of Earth and Environmental Sciences, University of Wollongong, Australia.

1.4.4 Ground Penetrating Radar (GPR) survey

Ground penetration radar profiles on many fault zones have provided accurate information on the location and orientation of fault lines covered by thin veneers of alluvial/colluvial material (Benson 1995, Cagnoli & Russell 2000, Chow *et al.* 2001, Anderson *et al.* 2003, Rashed *et al.* 2003, Rossetti 2003, Taylor 2010). Unconformities, fault lines and offsets, deformations in sedimentary profiles, folding and colluvial/alluvial wedge structures may be recognised depending on the subsurface conditions and the antenna/GPR equipment capabilities. The applicability of GPR was tested within the southern South Australian region, in view of its *in situ* display capabilities of subsurface features and time/labour efficiencies. GPR was used to obtain subsurface details of selected sites with the aim of deploying it as a technique for preliminary site selection for trenching. Standard procedures were followed during field-work and data processing (Chow *et al.* 2001, Rashed *et al.* 2003, Jol 2009).

1.4.5 Development of a revised tectonic model

Structural data obtained through field-work and examination of existing literature, were incorporated into a suitable model to describes the fault activity. The nature of fault displacement was taken into account to present a revised behavioural tectonic model, the validity and applicability of which was generally tested through seismic trends and field observations, and to suggest possible driving mechanisms that are influencing the present seismicity. Age values obtained from dating were used to calculate the fault slip rates and to improve on the accuracy of recurrence rates.

1.5 Significance and Innovation

Continental interior earthquakes have the potential to cause extensive damage due to heavy ground motions as the attenuation of seismic energy is typically low in continental interiors (Atkinson 2007). The danger remains unaddressed as potentially hazardous faults could be aseismic at present and most of them are not identified due to a lack of geomorphic expression and long recurrence intervals of 10,000 to 100,000 years. The inadequate building codes developed in Australia at the time of the Newcastle earthquake in 1989 (Klose 2007) resulted in extensive damage and loss of life. There is a need to engage communities about the risk of earthquake activities even in apparently stable regions like Australia (Catchpole 2009).

The risk associated with seismicity increases as population grows, accompanied by general unawareness of the potential impacts of earthquakes. Even a low intensity earthquake may cause a significant impact on society and infrastructure if the risk of earthquakes is not adequately addressed (Rashed *et al.* 2003). The Mount Lofty and Flinders Ranges have a higher likelihood, among the earthquake prone regions of South Australia, of being affected by earthquakes. In the Mount Lofty Ranges, the largest recorded earthquake was a magnitude 5.5 at Adelaide in 1954 (Sinadinovski *et al.* 2006), generated on Eden-Burnside Fault (Belperio 1995). This earthquake resulted in ~$90 million worth of damage at the time (Dyster 1995) and it is estimated that if it were to occur today there would be in excess of ~$1 billion worth of damage. Recently, there were discussions as to whether the new Adelaide Hospital should have been located on one of these neotectonic faults (The Sydney Morning

Herald 2007). Detailed studies of recently active faults will help to determine the timing and recurrence interval of earthquake events, which will aid in future decision making in regards to appropriate building codes for major infrastructure in earthquake prone regions such as Adelaide and in the development of seismic hazard maps.

In terms of pure research this project will shed light on the poorly understood mechanisms that drive intraplate deformation in Australia. Unlike many seismically active regions of the world there has been no attempt to systematically trench and date neotectonic faults, using relatively new luminescence dating techniques near Adelaide to acquire an accurate palaeoseismic record. Hence this research represents a new and original contribution to the study of paleoseismology in Australia.

2 NEOTECTONICS OF THE MOUNT LOFTY AND FLINDERS RANGES – A REVIEW

2.1 Introduction

The term ‘neotectonic’ was introduced by Obruchev in 1948 when describing recent tectonic movements within the Neogene and Quaternary responsible for the present topography. The discipline of neotectonics focuses on understanding the most recent movements within the earth’s crust (Hancock 1988). Neotectonic deformations in the southern South Australian context are estimated to have evolved since ~10-5 Ma due to the present crustal stress regimes (Clark 2006, Mote *et al.* 2011). This chapter concentrates on a review of fault related processes responsible for Cenozoic mountain building that has given rise to the present relief of the Mount Lofty and Flinders Ranges in South Australia, with much of the focus given to the understanding of active faulting in response to the present stress regimes.

Australia is situated in an intra-plate setting (Hillis *et al.* 2008) and western and central Australia have long been regarded as tectonically inert since Permian times (Twidale & Bourne 1975). A stable continental region (Krishna *et al.* 2001) is defined as continental crust that has not experienced major orogenic, volcanic or extensional events, commonly associated with plate boundaries throughout the late Mesozoic to Cenozoic (Jonston *et al.* 1994, Crone *et al.* 1997, Clark *et al.* 2008). However, five of eleven worldwide historical surface rupturing earthquakes within ‘stable’ continents for the period 1819 to 1993, are recorded from Australia (Crone *et al.* 1997).

Trends in historical seismicity (Clark & Leonard 2003, Leonard 2006, Clark *et al.* 2008), geological studies, paleo-seismic evidence (Bourman *et al.* 2010a) and rates of landscape evolution (Crone *et al.* 2003, Sandiford 2003a, Quigley *et al.* 2006, Quigley *et al.* 2010) suggest that parts of the Australian continent are actively deforming and have deformed and eroded at geologically significant rates in the recent past (Sutton & White 1968, Bourman & Lindsay 1973, Crone *et al.* 1997, Sandiford 2003a). The recent seismicity signals the potential for significant crustal deformation by means of intraplate faulting. From the current seismic records and neotectonic features, four major zones of high seismic activity (Figure 2.2) can be

identified within the Australian continent (Hillis *et al.* 2008, Quigley *et al.* 2010). The Flinders Seismic Zone (FSZ) which consists of the Mount Lofty and Flinders Ranges of South Australia, experienced a magnitude 5.5 event on 1 March 1954 near Adelaide (Belperio 1995) and continues to demonstrate consistent low levels of seismicity with occasional higher magnitude events. The arid region of South Australia provides an ideal environment for neotectonic studies due to the lack of vegetation and the excellent exposures of bedrock and range bounding alluvial fans with a well-developed stratigraphy (Bourman *et al.* 2010b). Despite this, the nature and age of intraplate deformation in the area has received scant attention.

2.2 Tectonic setting

Australia is part of the Indian-Australian tectonic plate (Figure 1.1) which travels in a NNE direction at a rate of 6-7 cm/year (Muller *et al.* 1998, Schellart *et al.* 2007). In the north and east it is in contact along collision boundaries with the Pacific and Eurasian plates and in the west and south it is in contact along spreading ridges with the Antarctic and African plates. Despite the fact that the Australian continent has an intraplate setting and has been tectonically quiescent throughout the Mesozoic-Cenozoic, seismic records from the Mount Lofty and Flinders Ranges and historical earthquake information indicate active tectonism (Sutton & White 1968, Bourman & Lindsay 1973, Sandiford 2003a).

The Mount Lofty and Flinders Ranges are located in southern South Australia and extend more than 600 km inland from the Fleurieu Peninsula towards the Lake Eyre Basin (Figure 1.2). It displays the remnants of an ancient fold belt generated during the Delamerian Orogeny (~500 Ma) along the palaeo-Pacific margin of eastern Gondwana (Flottmann *et al.* 1993), which extends from Kangaroo Island to Lake Torrens and Lake Callabonna (Paul 1998). The present topography of the mountain belt is generally thought to be the result of the Cenozoic compressional reactivation of Delamerian structures (Benbow *et al.* 1995, Drexel & Preiss 1995, Love *et al.* 1995, Rowett 1997). However, Tokarev (2005) proposes that many of the neotectonic faults may have developed in line with stress fields generated during the Tertiary, independently of the older, sealed, Delamerian faults.

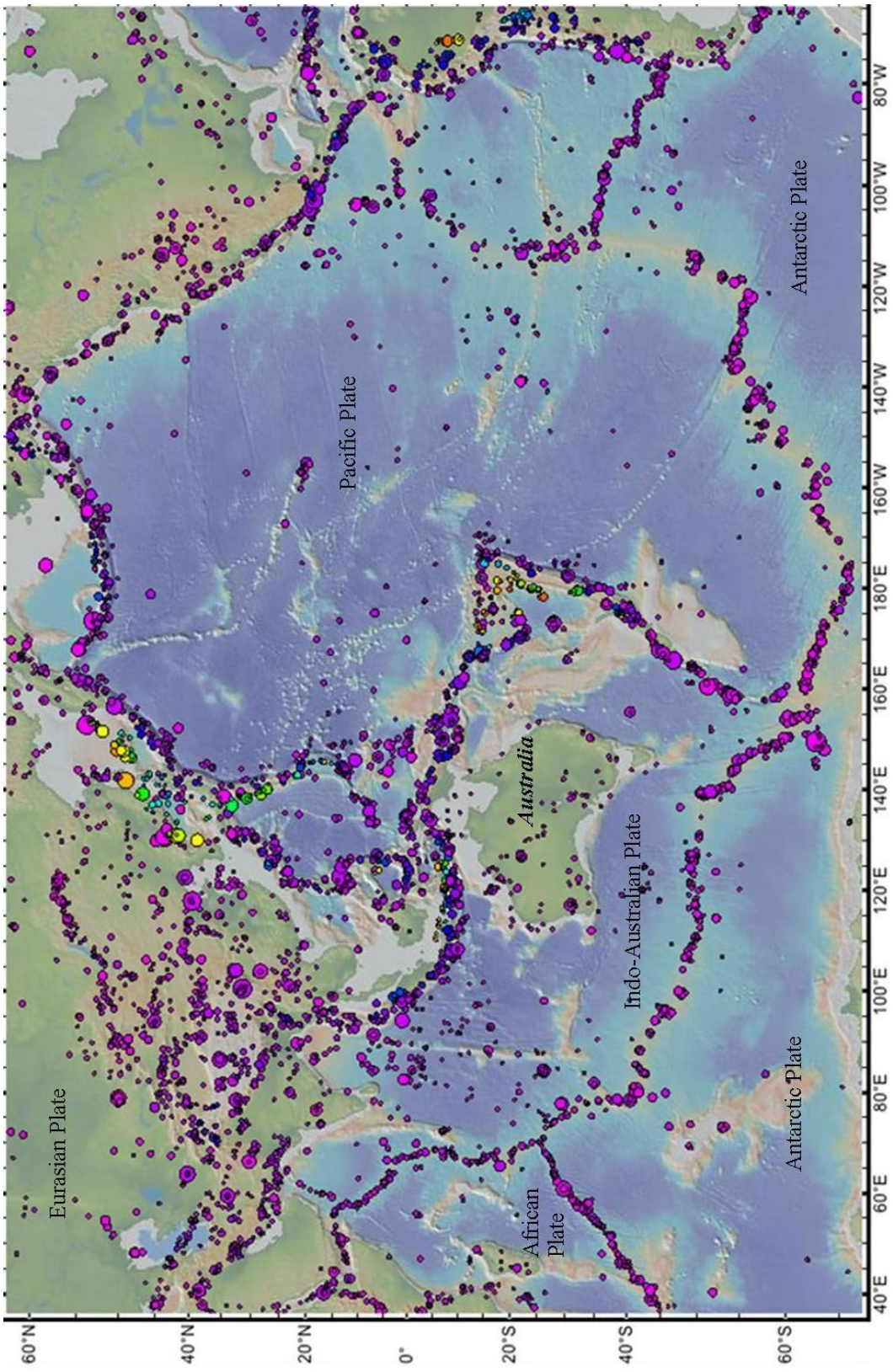

Figure 2.1 *Distribution and magnitude (proportional to the size of the circles) of global seismicity (from 1973 to 2009) dominates at plate boundaries. Regions such as Central Asia, USA and Australia show considerable intraplate seismicity (source USGS, presented through GeoMapApp).*

The north south trending *en echelon* or lazy 'S'-shaped mountain belt reaches elevations of more than 600 m and is variously referred to as the Eastern South Australian Ranges (Campana 1954), the Adelaide Rift Zone (Stewart 1976), the Adelaide Geosyncline (Sprigg 1946, Stewart & Sutton 1971, Shackleford & Sutton 1981, Preiss 1993), the Adelaide Fold Belt (May 1992, Paul 1998), the Adelaide Fold Thrust Belt (Marshak & Flöttmann 1996) and the Mount Lofty and Flinders Ranges (Doyle *et al.* 1968, Callen 1983, Tokarev 2005). In the present study mountainous regions from Fleurieu Peninsula up to Moolawatana are referred to as the Mount Lofty and Flinders Ranges respectively. They are specifically not referred to as the Adelaide Geosyncline or the Adelaide Fold Belt as these terms are genetically linked to Delamerian (Cambrian) convergent margin tectonics that resulted in the widespread folding, metamorphism and igneous activity, which affected the eastern margin of Gondwana during the Cambro-Ordovician period.

The Mount Lofty and Flinders Ranges have a high topographic relief, surrounded by Cenozoic basins (Figure 1.2), demonstrating consistent low magnitude seismicity mostly associated with elevated regions but also beneath some of the adjacent Cenozoic depocentres (Figure 2.1). Broadly, this region of active seismicity is referred to as the Flinders Seismic Zone (FSZ). High Quaternary slip-rates on identified faults indicate the significance of neotectonic activity (Sandiford 2003a). The range-bounding faults dominate, with thrusts on the western side of the Mount Lofty Ranges and the eastern side of the Flinders Ranges. The Mount Lofty and Flinders Ranges correspond with the seismically active Flinders Seismic Zone and the southern section of the Australian heat anomaly. However, the causative relationship between present stress fields, seismicity, heat anomalies and the nature of active faults do not show a clear association, leaving the actual cause of this intra-plate deformation speculative. Limited stress field data collected from focal mechanisms, borehole breakouts and the like, have restricted the compilation of a comprehensive stress field map for Australia (Hillis & Reynolds 2000). Only a handful of the active faults are exposed, making it difficult to validate the stress-field models with field evidence. However, several hundreds of metres of vertical displacement due to Cenozoic faulting have been suggested by many authors for some parts of the Mount Lofty and Flinders Ranges (Bourman & Lindsay 1989,

Tokarev *et al.* 1999, Sandiford 2003a, 2003b). Based on the range bounding Plio-Quaternary alluvial fan sequences, Sandiford (2003a) and Quigley *et al.* (2006) suggest as much as 30-50% (~800-1000 m) of the topographic relief has been produced since the end of the Miocene.

2.3 Seismicity

2.3.1 Seismicity of the Australian continent

Earthquakes are less frequent in intraplate settings relative to plate boundaries (Figure 2.1), but large and potentially damaging earthquakes are not uncommon in plate interiors (Hancock 1988). The driving mechanism and location of intra-plate deformation is a topic of much conjecture worldwide (Sykes & Sbar 1973). Even though Australia is categorised as a stable continental region there is evidence of an increase in seismicity during the recent past (Crone *et al.* 1997). The Australian continent is actively deforming at geologically significant rates, with mountainous regions correlating with areas of greater seismic activity. Active crustal deformation is indicated locally by the frequency of earthquakes (Sutton 1976, May 1992) and the Australian continent experiences magnitude $\geq$ 6.0 earthquakes about every five years, as indicated by the historical database (McCue 1990). Recurrence intervals for large surface rupturing faults within intraplate settings are likely to extend beyond the records kept since the European settlement of Australia (Crone *et al.* 1997, Crone *et al.* 2003). Therefore, high magnitude (>5.0) earthquakes are unlikely to have been recorded for many areas within the past 200 years (Sandiford *et al.* 2004) resulting in a potential underestimation of the seismic risk (Clark & McCue 2003) and an inadequate characterisation of long-term fault behaviour.

Four distinct zones of elevated seismicity within the Australian continent (Figure 2.2) have been identified (Leonard 2006, Hillis *et al.* 2008). Earthquake focal mechanism solutions, borehole breakouts, drilling induced tensile fractures in hydrocarbon wells, and hydraulic fracture sets were used to derive the maximum horizontal stress (σH^{max}) orientations of these zones (Denham *et al.* 1979, Hillis *et al.* 1995, Hillis *et al.* 1999, Hillis & Reynolds 2000, 2003). The NW Seismic Zone, located on the passive margin bordering the Indian Ocean and the Timor Sea, is

characterised by E-W to NE-SW oriented (σH^{max}) (Hillis *et al.* 1995). The SW Seismic Zone extends from SW Western Australia to the western edge of the Australian continent in a belt in line with the rifted western edge of the Yilgarn Craton and the Pinjarra Orogen, with E-W trending stress regimes. The SE Seismic Zone extends from central New South Wales through eastern Victoria into Tasmania, overlapping part of the Palaeozoic Tasman Orogen with NW-SE σH^{max}. The Flinders Seismic Zone, which includes the Flinders, Mount Lofty and Barrier Ranges and the eastern Gawler Craton, aligns with a major Neoproterozoic rift zone and subsequent Palaeozoic fold belt with a complex maximum horizontal stress regime.

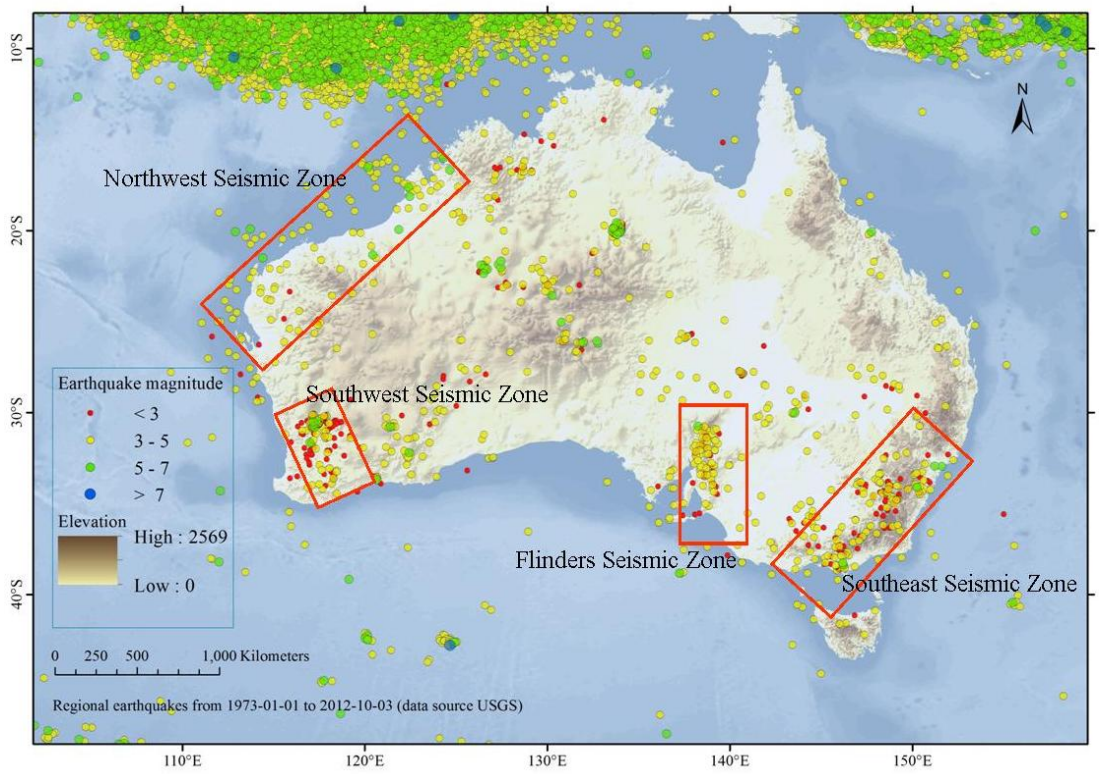

Figure 2.2 *Major seismic zones of Australia based on neotectonic features and earthquakes above magnitude-4 (source: Quigley et al. 2010, and seismic data from USGS)*

2.3.2 The Flinders Seismic Zone (FSZ)

The South Australian Flinders Seismic Zone (FSZ) displays a congested and consistent low level of seismicity (Figure 2.2 & Figure 2.3) compared to the rest of South Australia (Glanville 2010), with five magnitude > 5.0 earthquakes recorded in the past century (Greenhalgh *et al.* 1994). The Mount Lofty and Flinders Ranges within the Flinders Seismic Zone have a higher likelihood among the earthquake

prone regions of South Australia of being affected by earthquakes. A magnitude 5.5 event along the Eden-Burnside Fault in 1954, ~14 km south of Adelaide, at Darlington (Belperio 1995), registered as the largest recorded earthquake in the Adelaide suburbs.

More than 75% of South Australian earthquakes are recorded within the FSZ concentrated in the Mount Lofty and Flinders Ranges. Over 80% of recorded seismic events have taken place within the upper crust at depths less than 20 km, indicating the shallow nature of the seismicity (Wellman & Greenhalgh 1988, Belperio 1995, Tokarev 2005). The Quaternary fault record of the Mount Lofty and Flinders Ranges has mostly been interpreted as dip-slip reverse faulting (Clark & McCue 2003, Hillis *et al.* 2008). However, Greenhalgh *et al.* (1986) interpreted focal mechanism solutions for six earthquakes from 1978 to 1983 in the central Flinders Ranges, with dominantly steeply dipping strike-slip faults (Figure 2.4) subjected to northeast-southwest compression. Clark and Leonard (2003) and Hillis *et al.* (2008) obtained similar results but with large uncertainty.

Most of the above calculations are based on a limited number of observations, which dilutes the statistical validity and may not represent the actual stress fields. However, provided the recordings are comprehensive and accurate, the derived association between epicentres against mapped faults and the existence of large error ellipses (Figure 2.5) could be due to poor understanding of the Quaternary fault behaviour and inability to extensively describe the process through existing models. Accordingly, some of the range-bounding faults progressively flatten out at depth away from the actual fault exposures may account for the discrepancy between the seismic data and the actual known or suspected faults (Preiss 1993, 1999). Construction of a three dimensional frameworks under the ranges may be required to understand the nature of faults at depth, using more sensitive seismometers with a greater coverage. In an attempt to correlate the regional seismicity with the elevation of the Mount Lofty and Flinders Ranges, Love *et al.* (1995), have postulated that the present deformation is a result of the reactivation of ancient tectonic structures.

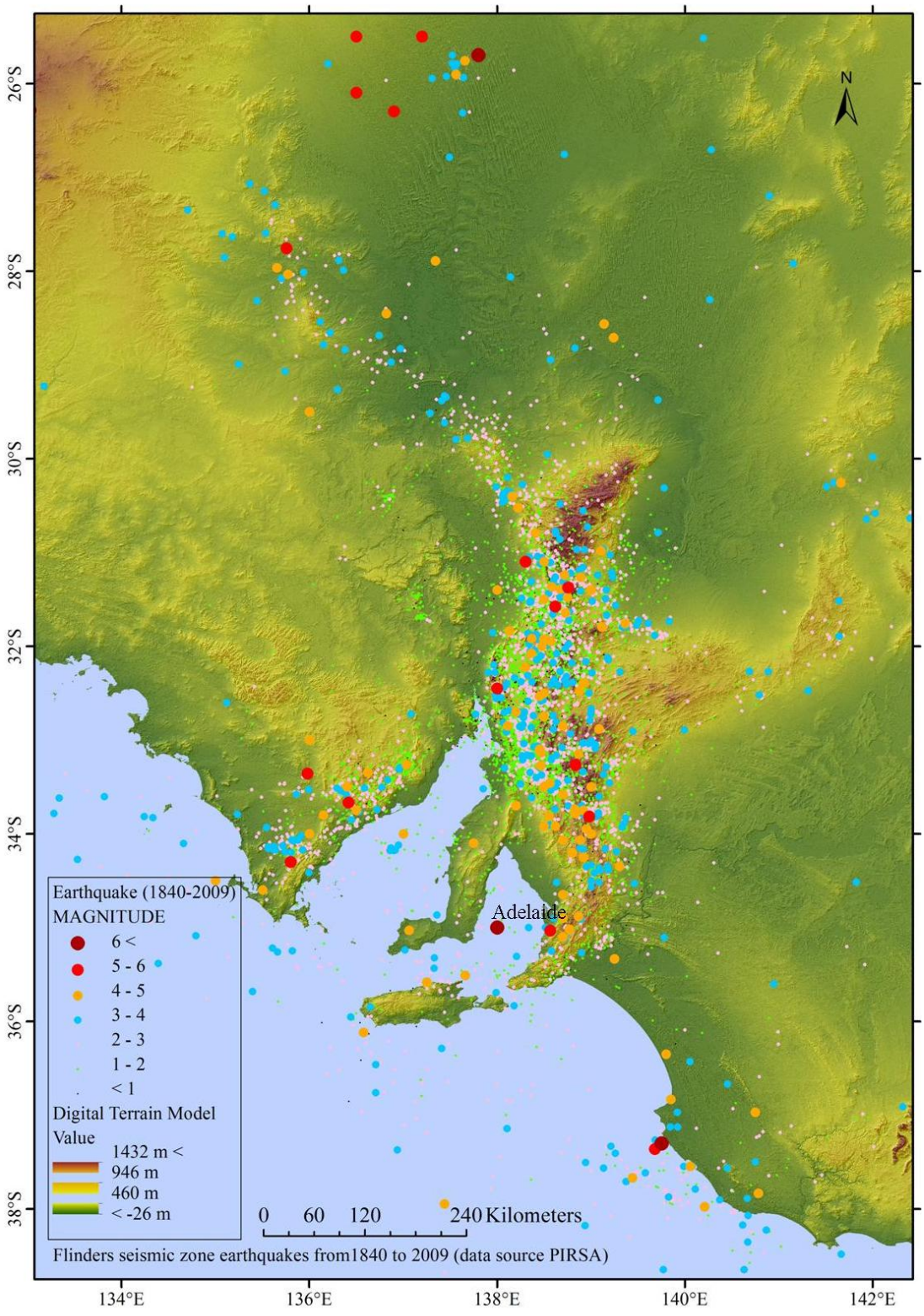

Figure 2.3 *Seismicity in South Australia displaying high concentrations in the Mount Lofty and Flinders Ranges (source PIRSA 2009)*

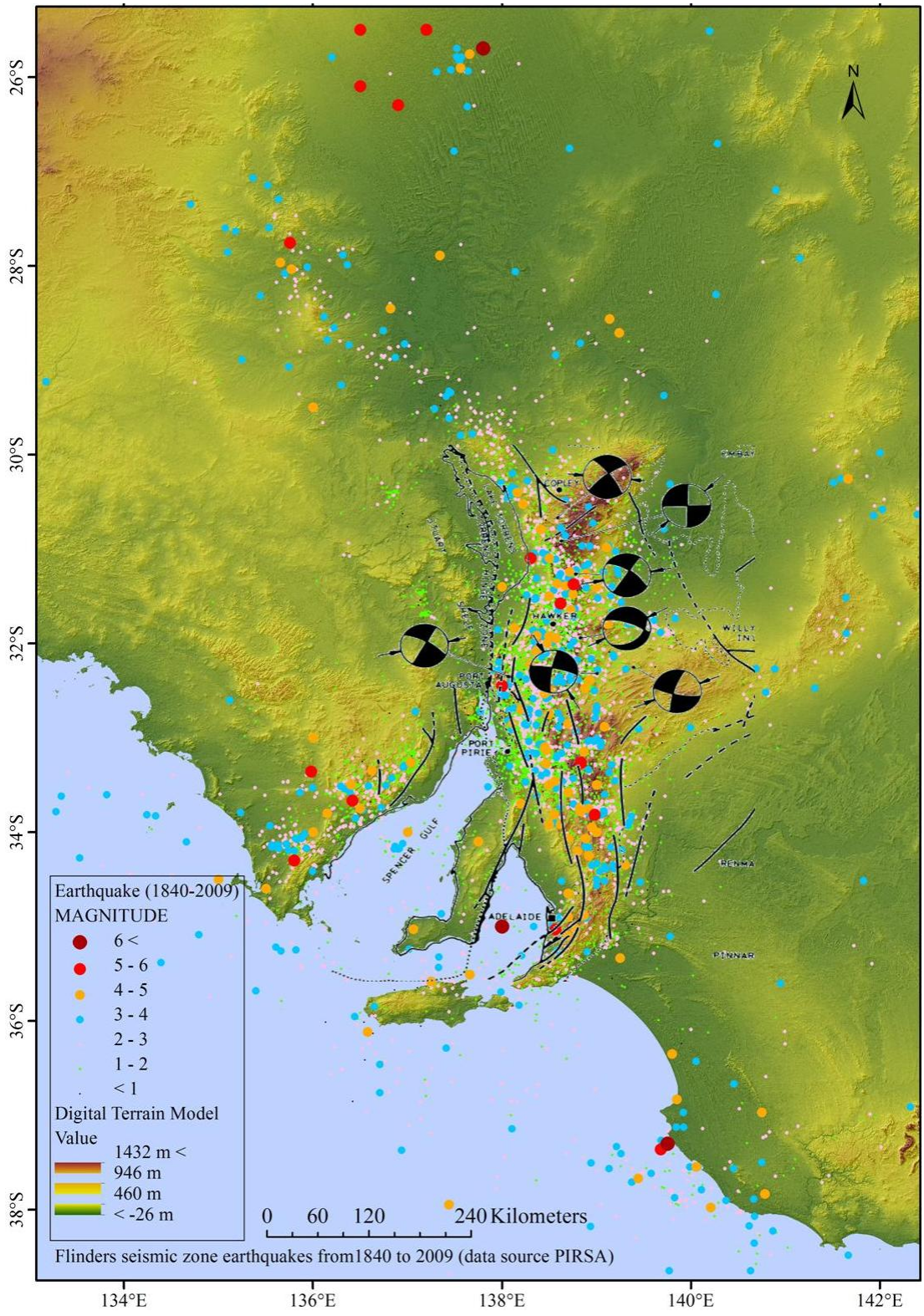

Figure 2.4 *Seven earthquake focal mechanism solutions for the Flinders Ranges, displaying strike-slip dominant behavioural patterns (source Greenhalgh et al. 1986)*

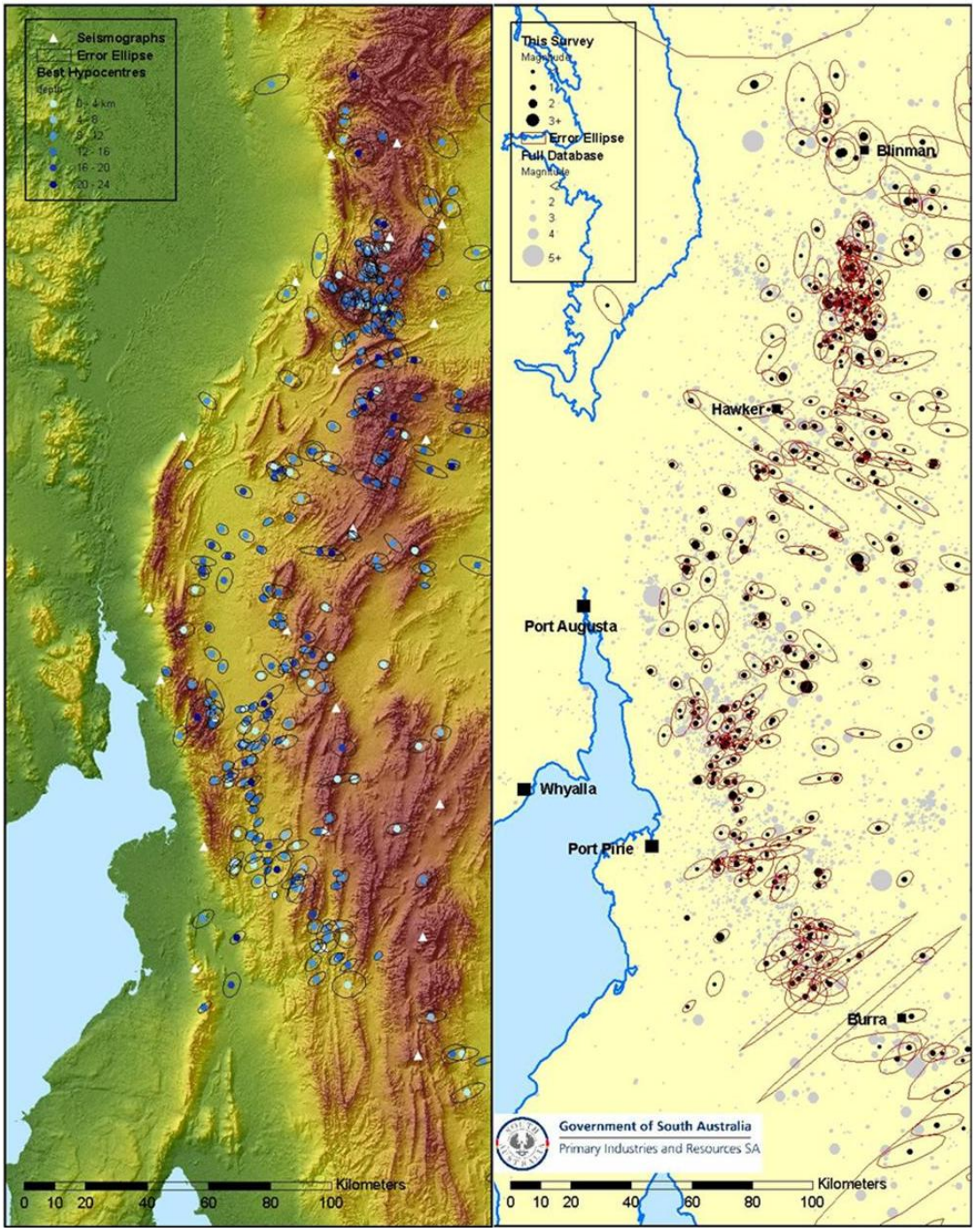

Figure 2.5 *Error ellipses recorded from seismic data on the western flanks of the Flinders Ranges near the Wilkatana Fault Zone (source: PIRSA) displaying the inconsistencies between topographic features and epicentres.*

Based on the available seismic records, the Flinders Ranges display consistently low levels of seismicity compared with the Mont Lofty Ranges, which have a relatively anomalous behaviour, producing some of the larger magnitude but less frequent earthquakes. This could result from differences in the nature of faulting due to changes in fault alignment against the complex stress fields. Furthermore, limitations of the seismic monitoring networks within the Mount Lofty and Flinders Ranges could also contribute to this situation. However, the larger error ellipses determined through seismic observations, and difficulty in locating the earthquake epicentres on identified faults, indicate inconsistency of the recordings with respect to the actual nature and extent of faulting.

2.4 Stress distribution and the plate boundary interactions

2.4.1 Continental scale stress distribution

The Indo-Australian tectonic plate has a complex stress profile aligned in many directions making stress orientations across the Australian continent highly variable (Figure 2.6). The maximum horizontal stress vectors (σH^{max}) do not show simple relationships with the north to northeast direction of its absolute plate motion (Zoback *et al.* 1989, Richardson 1992, Coblentz *et al.* 1995, Hillis & Reynolds 2000, Reynolds 2001, Reynolds *et al.* 2003). However, these studies indicate that the plate boundary forces have primary control over the Australian continental stress fields. The pattern of σH^{max} across Australia suggests that the *in situ* stress field reflects a combination of driving mechanisms such as ridge-push, slab-pull, absolute plate motion and collisional resistance (Richardson 1992, Coblentz *et al.* 1995, Coblentz *et al.* 1998). Increasing stress levels within the Indo-Australian Plate are reflected by Pliocene to recent deformations caused by the increased plate boundary forces from the Pacific and Asian plates (Coblentz *et al.* 1995, Sandiford 2003a, Sandiford *et al.* 2004). The brittle upper crust in most of South Australia is under the influence of compressive stress regimes, which have a higher probability to initiate reverse or strike-slip movements than normal faulting. Compared to normal faults, these reverse or strike-slip faults could generate strong ground motions and widespread damage (McGarr 1984, Bommer *et al.* 2003, Ma & Beroza 2008).

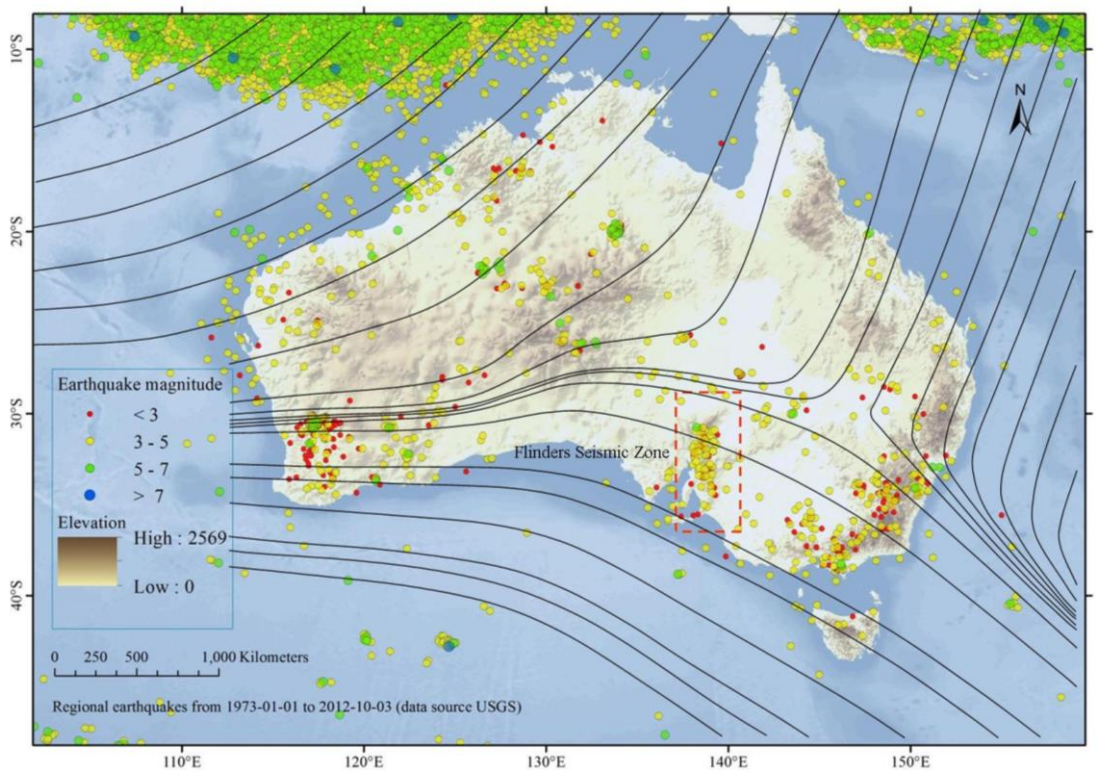

Figure 2.6 *Stress trajectories derived from the horizontal maximum stress data (source: Hansen & Mount 1990, Hillis & Reynolds 2000, Cull 2000)*

Results of finite element modelling of the Indo-Australian Plate and contemporary seismicity indicate that plate boundary forces play a major role in determining the first order stress fields in continental Australia (Cloetingh & Wortel 1985, Cloetingh & Wortel 1986, Coblentz *et al.* 1995, Coblentz *et al.* 1998). Geophysical data suggest that the torque generated on the Indo-Australian Tectonic Plate (IAP) by its Himalayan boundary is approximately balanced by the torque produced at the boundary south of New Zealand. Hence, the plate is deforming due to large forces acting on the New Zealand boundary as well as on the Himalayan boundary (Valenzuela & Wysession 1993, Spitzak & DeMets 1996, DeMets & Dixon 1999, Reynolds 2001). Discontinuities along the Antarctic ridge indicate that differences in spreading rates are governed by the inhomogeneous stress fields.

Using stress measurements recorded from focal mechanisms, borehole breakouts, drilling induced tensile fractures, hydro-fracturing, over coring and magnitude and quality wise poor geological indicators, Reynolds (2001) suggests that Australia is dominated by reverse faulting stress regimes with areas facilitating strike-slip faulting. The analysis used available stress information, which demonstrated that of

all the earthquakes with sufficiently high magnitudes to allow solving of accurate focal mechanisms, 30% are reverse, 13% strike-slip, 3% normal, 3% oblique faulting, with the remaining 51% being difficult to determine.

2.4.2 South Australian stress distribution

Focal mechanisms are considered to be a consistent indicator of local stress (Bergman 1986). The stress field of the Flinders Seismic Zone (Figure 2.6) is primarily constrained using earthquake focal mechanisms, even though there are not nearly enough earthquake focal planes to build an accurate picture of the stress field in the region. A few of the focal mechanisms that do exist suggest roughly E-W compression and strike-slip deformation (Greenhalgh *et al.* 1994, Hillis & Reynolds 2000, Clark & Leonard 2003). Analysis of seven earthquake focal mechanisms has revealed three dip slip thrusts and four strike-slip fault plane solutions, with N to NE striking focal planes (Greenhalgh *et al.* 1986, Greenhalgh *et al.* 1994). Clark and Leonard (2003) documented a similar combination of strike-slip and pure thrust mechanisms in the Flinders Ranges and derived a horizontal compressive stress azimuth of 82° on strike-slip dominant faults.

The faults bounding the Flinders Ranges indicated an ~E-W oriented σH^{max} (Hillis *et al.* 2008), which is consistent with σH^{max} orientations derived from historical seismicity (Quigley *et al.* 2006). Towards the Mount Lofty Ranges, borehole data suggest a more NW-SE trend for the compressional stress regimes (Hillis *et al.* 1999), which would promote oblique movements on the active faults of N-S trending range. Palaeostress orientations derived from Pliocene and Quaternary range-bounding reverse faults (Quigley *et al.* 2006) indicate the presence of a modern compressional tectonic regime for at least the past 5 Ma (Sandiford 2003a, Quigley *et al.* 2006).

Even though the complex maximum horizontal stress regime in this region is considered to be approximately E-W dominant, the models suggest a more NW-SE orientation (Müller *et al.* 2012). Local NW-SE maximum compressive stress orientations in South Australia are orthogonal to the collision boundary forces

generated at the Australian-Pacific plate margin. The magnitude of the stress is controlled by interactions along the Pacific-Australian plate boundary associated with the Southern Alps since the latest Miocene (Coblentz *et al.* 1995, Reynolds 2001, Sandiford 2003a, Sandiford *et al.* 2004). However, the paucity of data hinders the statistical validity of these observations in a situation where it is important to have a good understanding of current stress fields for a region like Adelaide.

2.5 Heat and gravity anomalies

The heat flow of continents reflect both mantle derived heat loss and heat production from U, Th and K within the lithosphere (Paul 1998). The contribution of each of these sources to heat flow depends on the age, tectonothermal evolution, lithological makeup, heat source distribution in the crust, thickness of lithosphere, and geodynamic settings (Cull 1982, Paul 1998, Sandiford *et al.* 1998b). The general surface heat flow of continents is known to be around 65 mW/m^2 (McLennan & Taylor 1996) and the majority of the heat is derived from transient heat associated with comparatively young tectonic activity.

The elevated heat provinces in Australia (Figure 2.7) have a north-south alignment, spanning sections of South Australia, Victoria, New South Wales, Queensland and the Northern Territory. Most of the heat is thought to derive from crustal sources within the basement, supported by the mantle heat flow (Sandiford 1989). The Mount Lofty and Flinders Ranges overlap with a heat flow of 90 mW/m^2 on average, whereas, a maximum of 125 mW/m^2 is observed in the northern Flinders Ranges (Neumann *et al.* 2000), which is situated in the centre of the central Australian heat flow province (Cull 1982, Paul 1998, McLaren *et al.* 2003).

High concentrations of U, Th & K in Meso-Proterozoic rocks within the mountain belt imply thermal weakening of the lithosphere (Sandiford *et al.* 1998b, Neumann *et al.* 2000, Celerier *et al.* 2005, Hillis *et al.* 2008). The southern parts of the mountain range display higher grades of metamorphism with the presence of migmatites (Offler & Fleming 1968, Sandiford *et al.* 1995, Paul *et al.* 1999), whereas in most of the northern Flinders Ranges metamorphic grade is a sub-greenschist facies. Biotite

grade metamorphism during the Delamerian Orogeny (Preiss 2008) generally affected most parts of the present mountain belt. The Delamerian deformations are reflected from the differential burial of the basement (Paul 1998), which is rich in heat producing elements, having heat production rates over 10 μW/m^3 (Neumann *et al.* 2000).

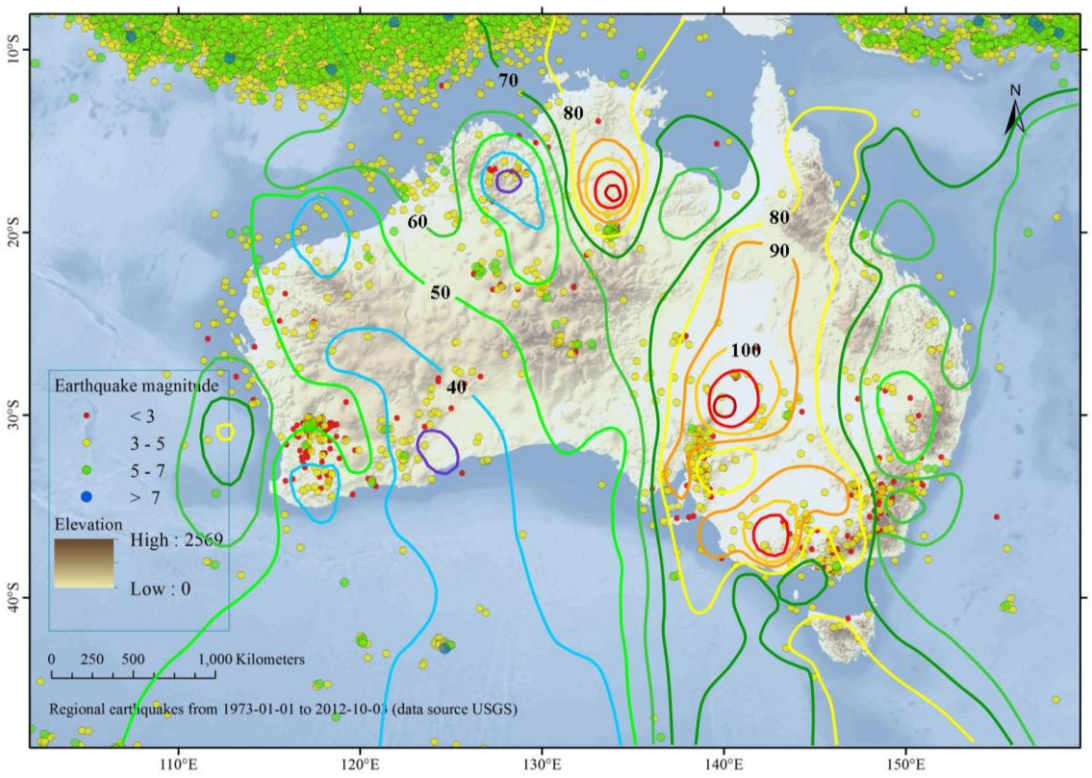

Figure 2.7 *Australian heat flow distribution (mW/m^2) overlapped with the seismic observations (source: Cull 1982; McLaren 2003)*

A consistent gravity field may represent a mechanically stable lithosphere irrespective of the thermal variations (Houseman & Molnar 2001). Inconsistent gravity fields reflect lateral contrasts in the density of subsurface rocks. Deformational episodes in continents are generally associated with lithospheric gravity field variations. The Bouger gravity field for southern South Australia shows generally a positive anomaly with a series of ~N-S oriented sub-parallel structures overlapping the Mount Lofty and Flinders Ranges (Wellman & Greenhalgh 1988). The elongated positive gravity field along the highlands may have resulted from a combination of high-density basement material and the absence of isostatically compensating crustal root (Wellman & Greenhalgh 1988, Sandiford *et al.* 1998b). A weak lithosphere may not substantially contribute to regional isostatic compensation

(Wellman & Greenhalgh 1988). Therefore, isostatic rebound of the region in response to erosion and unloading of a long-lived mountain range may not have significantly contributed to the uplift of the Mount Lofty and Flinders Ranges

A gravity survey conducted by Geosurveys of Australia Limited during June-July 1963, on the south-eastern flank of the Mount Lofty Ranges recorded relative gravitational minima on Permian sediment-filled valley systems. Two such gravity anomalies were clearly identified, separated by the south-eastern boundary of the Mount Lofty Ranges (Stackler 1963). The geophysical report by Stackler (1963) identified buried Permian glacial troughs offset across the fault zone along the eastern side of the southern Mount Lofty Ranges, suggesting significant sinistral transcurrent offsetting.

2.6 Evidence of deformation

Deformation of surface deposits, prominent scarp formation and range fronts with active alluvial fan deposits reflect regions with active fault systems. Neotectonic activity in the South Australian landscape is reflected in youthful mountain building and subsidence (Belperio 1995, Sandiford 2003a, Tokarev 2005, Hillis *et al.* 2008). Consistent low level seismicity is a significant feature in the Mount Lofty and Flinders Ranges and the undulating surface expression, deeply incised escarpments, well developed alluvial fans and range-bounding thrust faults are evidence of neotectonism (Twidale & Bourne 1975, Sandiford 2003b). Rugged catchment geomorphology, recent river channel offsets and headword propagation of knick-points provide further evidence for ongoing deformation (Quigley *et al.* 2006). Cenozoic sediments in direct contact with the Neoproterozoic rocks denote recent uplift but structural complexities and poor exposure of fault contacts have restricted the exploration of this anomalous intraplate behaviour (Crawford & Campbell 1973). However, vertical offsets in late Tertiary and Quaternary stratigraphy across the fault zones act as important marker units that help to identify the time of deformation (Bourman *et al.* 1999, Murray-Wallace & Bourman 2002, Bourman *et al.* 2010b).

River channels represent regional landscape development, being sensitive to tectonic or climatic changes. Tectonic movements are considered to be the major factor

affecting channel gradients, and ~4 to 30 m/km increase in gradient occurs in the River Torrens associated with uplift along the Eden-Burnside Fault (Tokarev 2005). Development of drainage systems in the Mount Lofty and Flinders Ranges are largely neotectonically influenced, being independent of the pre-Tertiary basement structures (Tokarev 2005); as most of the river systems flow obliquely across older tectonic fabrics (Tokarev *et al.* 1999). The Onkaparinga and Torrens Rivers in the southern Mount Lofty Ranges provide examples of neotectonic alterations to drainage systems and catchments (Benson 1911, Sprigg 1946). The southward flowing Cox Creek, a tributary of the Onkaparinga River, has been reversed due to surface deformation and is now linked with the River Torrens. Directional changes in Milendella Creek at Palmer and the northward displacement of the Onkaparinga River mouth may suggest river channel migration due to neotectonic activity (Howchin 1911). As well, streams on the Willunga scarp display youthful and undeveloped characteristics. Furthermore, the absence of terraces with a tectonic origin on upstream of waterfalls and on the western flanks of the Mount Lofty Ranges together with deep incision of the stream beds can be attributed to recent uplift (Sprigg 1946, Bourman 2006).

Evidence of substantial post Middle Eocene faulting is noted in Bourman *et al.* (2010a) near the Highbury Quarry, south of the Gun Emplacement (Figure 4.23), where the middle Eocene North Maslin Sand has been gently folded by compressive forces and steeply tilted at the Eden Burnside Fault, which dips at 60^{o}-80^{o} to the west. Slickensided fault surfaces, highly sheared fault gouge material and the nature of a recent fault scarplet were attributed to oblique sinistral reverse movements. A study by Quigley *et al.* (2006) and Quigley (2006) further confirms the contribution of active faulting at Wilkatana, Burra and Mundi-Mundi within the Flinders Ranges.

2.7 Neotectonic faults

The Mount Lofty and Flinders Ranges are controlled by north-northeast striking range-bounding faults subjected to east-west compression (Sandiford 2003a, Celerier *et al.* 2005, Hillis *et al.* 2008). Most youthful faults are on the western and eastern flanks of the Mount Lofty and Flinders Ranges respectively (Belperio 1995). Reverse

faulting is a characteristic feature of most of the documented neotectonic faults, whereas evidence of normal or reverse oblique movements is sparse. There is no direct field evidence for pure strike-slip faulting, but there are signs of its occurrence from the fault kinematics derived from the handful of fault plane solutions and slickenside data within Flinders Seismic Zone. A high angle west dipping thrust with a sinistral movement has been recorded by Bourman *et al*. (2010a) on the Eden-Burnside Fault on the western Mount Lofty Ranges. Similar sinistral movement on the Wilkatana Fault Zone and dominant reverse oblique faulting has been suggested by Quigley *et al.* (2006) for the western flanks of the central Flinders Ranges.

A range of 20-150 m/Ma vertical slip rates has been derived from the fault related Cenozoic stratigraphic offsets throughout the Mount Lofty and Flinders Ranges (Sandiford 2003a, Quigley *et al.* 2006) but there is lack of evidence to support the approximate contribution of the individual faults with respect to their spatial distribution (Crone *et al.* 1997, Crone *et al.* 2003). However, some of the recent studies reveal, about 15 m of uplift during the last 67,000 years at the Wilkatana Fault Zone in the Central Flinders Ranges (Quigley *et al.* 2006) and about 30-100 m of uplift during the 1 Ma at the Willunga and Milendella fault zones in Southern Mount Lofty Ranges (Sandiford 2003a).

Traditional understanding of compressional reactivation of the basement structures of the Delamerian Thrust Fold Belt in the core of the ranges (Drexel & Preiss 1995) has been challenged by Tokarev (2005) showing that most of the pre-Tertiary basement structures are obliquely superimposed by neotectonic faults. Development of the main river systems completely ignore the basement structures within the Mount Lofty and Flinders Ranges, often being perpendicularly superimposed onto the basement fabric (Yassaghi *et al.* 2004). The obliquity of neotectonic and Delamerian structures as a result of neotectonic faults being spatially inconsistent with the geometry of Palaeozoic faults, emphasise deformational independence with limited inheritance (Tokarev 2005).

2.8 Geology and Cenozoic stratigraphy

Geology and stratigraphy help to identify the historic fault offsets and deformational structures linking a pathway to an understanding of landscape evolution. South Australian geology is dominated by Neoproterozoic and Cambrian bedrock (Dalgarno *et al.* 1968, Riordan 2009) without major sedimentation taking place until Permian times (May 1992). The bedrock geology within the Mount Lofty and Flinders Ranges consists of Proterozoic to Cambrian metasedimentary rocks, granites, Neoproterozoic and Cambrian quartzites, sandstones, limestones, shales and argillites (Coats 1973, Stevens & Corbett 1993, Preiss 1995). Overturned anticlines having early Proterozoic basement gneisses and late Proterozoic and Cambrian metasediments resemble the bedrock structures underlying the Mount Lofty and Flinders Ranges (Daily *et al.* 1976, May 1992). The degree of metamorphism and grade of granite intrusions varies across the mountain belt (Offler & Fleming 1968, May 1992). The basement is exposed within various sections of the mountain range due to deformations that are mainly fault bounded (Preiss 1993, Paul 1998). Low to moderate regional strains are observed throughout the mountain belt (Paul 1998). A high strain imbricate thrust fan, in conjunction with a regional high strain deformation, is observed towards the south where structural reactivation took place during the Neoproterozoic (Flöttmann *et al.* 1994, Marshak & Flöttmann 1996, Paul 1998). Regional maps reveal the influence of Mesoproterozoic high-grade metamorphism and the Delamerian Orogeny for most of the outcropping basement (Howchin 1926, Preiss 1993, Paul 1998).

Particle size and analysis of the clay content on coastal stretches of the western side of the southern Mount Lofty Ranges have shown that the sediment sources and depositional conditions have not changed dramatically during the Quaternary. Study of the sedimentary and diagenetic history of the Quaternary sequences indicates that sediments were deposited on alluvial fans originating from the Mt Lofty Ranges. The Cenozoic stratigraphy at Sellicks consists of Tertiary to early Pleistocene marine sedimentary sequences overlain by the non-marine younger material commonly known as the Robinson Point Formation (May 1992). The non-marine sequences consist of inter-bedded clays, sands, and gravel beds. Coarser and thick sequences of

gravel beds are present closer to the Willunga Fault, suggesting a fault generated debris source.

Late Tertiary and Quaternary stratigraphic units have been offset across the fault zones and constrain the time of deformation and amount of vertical movement (Bourman *et al.* 1999, Murray-Wallace 2002). For example, the Early Miocene Port Willunga Beds, which are 200 m below sea level in the Adelaide area, reach sea level just north of the Willunga Fault at Sellicks Beach and elevations up to 240 m in the Myponga Basin (May & Bourman 1984). Similarly, the Pleistocene Burnham Limestone (Pillans & Bourman 2001) varies in elevation between 82 m below sea level at Port Adelaide, 17 m above sea level at Marino, 30 m at Hallett Cove, 20 m at Maslins Beach, 15 m at Port Willunga, 8 m at Sellicks Beach (May & Bourman 1984) and the time equivalent Port Ellen formation above 50 m at Cape Jervis (Belperio 1995). Bourman *et al*. (1999), Murray-Wallace (2002) and Murray-Wallace and Bourman (2002), have attributed the dislocation of Miocene and earliest Pleistocene coastal sediments on Fleurieu Peninsula to ongoing tectonism. To quantify tectonic uplift over the past 125 ka, last interglacial sediments (the Glanville Formation) are used as marker units. From the vertical distribution of the last interglacial shoreline sediments, an uplift of 3 m at Sellicks Beach and 10 m at Normanville has been calculated to have occurred since the Last Interglacial. Furthermore, a subsidence of 1 m over the last 125 ka has occurred in the Murray Basin with respect to the elevation of the Glanville Formation (Murray-Wallace & Belperio 1991, Passchier *et al.* 2005). Fault slip rates derived from the Pliocene-Quaternary offsets across the active faults within the Mount Lofty and Flinders Ranges have shown between ~ 20-150 m of uplift during the last 1 Ma (Sandiford 2003a, Quigley *et al.* 2006).

2.9 Mountain building and landscape evolution

Mountain building in southern South Australia occurred during the Delamerian Orogeny (514-485 Ma) in mid to late Cambrian times. Most of inland Australia was planated during the Paleozoic and Mesozoic, particularly during the Gondwanian glaciations (Tokarev 2005). However, the distribution of Permian glacial deposits

and erosion surfaces indicate that significant topography did exist during the Permian (Alley & Bourman 1984). Post-Permian tectonic quiescence up to the Middle Eocene is displayed by preserved Permian landforms and relict glacial valley slopes in parts of the Fleurieu Peninsula of South Australia.

The neotectonic activity experienced in eastern and southern Australia during the late Tertiary to Quaternary has been referred to as the 'Kosciuskan Orogeny' (Fenner 1930, Andrews 1933, Sprigg 1946, Glaessner 1953, Campana 1954, Glaessner & Wade 1958, Crawford & Campbell 1973, Bourman & Lindsay 1989) or locally for South Australia as 'Sprigg's Orogeny' (Sandiford 2003a). The Cenozoic Kosciuskan Orogeny marked the beginning of rejuvenated mountain building to produce the current topography of the Mount Lofty and Flinders Ranges (Sandiford 2003a).

Ambiguities in Pleistocene sea levels led Ward (1966) to conclude that most of the topography in South Australia could have been shaped as a result of higher sea levels rather than base level tectonic uplifting. However, accurate dating of Pleistocene coastal sediments marking past interglacial sea-level incursions and comparisons of the elevation with undisturbed equivalent deposits along the Great Australian Bight (Bourman & May 1984, Bourman & Pillans 1997, Murray-Wallace 2002) indicate that tectonic uplift was responsible for variations in elevations within the Mount Lofty Ranges.

Interpretations on the initiation of deformation to form the Mount Lofty and Flinders Ranges, includes a Palaeogene (65-23 Ma) origin (Webb 1957, Alley 1973, Wellman & Greenhalgh 1988, Tokarev 2005) and a Neogene (23-3 Ma) origin (Benson 1911, Sprigg 1946, Williams & Goode 1978, Sandiford 2003a, Quigley *et al.* 2006). Late Miocene to Early Pliocene coarse sedimentation in alluvial fan systems bounding the Flinders Ranges is inferred to mark the onset of range uplift (Callen & Tedford 1976, May 1992). A large part of the Mount Lofty Ranges was considered to be planated by the late Pliocene, as evident by the presence of remnant ferricrete surfaces and alluvial deposits capping the ranges in places (Bourman *et al.* 2010a) and forming a classic inverted topography. This suggests that much of the present day relief has formed as a result of neotectonic faulting since the late Pliocene and continues today.

Based on regional unconformities between Upper Miocene and Pliocene sequences, the neotectonic activity can be traced back at least to 5 Ma and the recognition of a number of range bounding reverse faults with significant Quaternary displacements; (Sprigg 1945, Williams 1973, Belperio 1995, Bourman *et al.* 2010a) suggest that half of the present elevation of the mountain ranges is a result of active stress regimes (Sandiford 2003a, Quigley *et al.* 2006).

The landscape evolution of the Mount Lofty and Flinders Ranges is influenced by active faulting (Sprigg 1945, Tokarev *et al.* 1999, Sandiford 2003a). The deformation of the ranges reflects low amplitude (~200-500 m) lithospheric flexuring, and range front reverse faulting (Sandiford 2003a, Celerier *et al.* 2005, Quigley *et al.* 2006). The western side of the southern Mount Lofty Ranges consists of discrete curvilinear fault scarps marked by a distinct range front, which displays a lack of significant range-front retreat (erosion). To the north of Adelaide these range-bounding faults are largely orientated N-S while further south the faults curve around to a more NE-SW strike forming a distinct horsetail splay structure (Buckman *et al.* 2009b).

Deeply weathered, gently undulating planation surfaces displaying remnants of an old palaeoplain are characteristics of the uplifted landscape within ~1-2 Ma (Fenner 1927, 1930). Recognised planation surfaces of various ages emphasise multiple episodes of landscape development (Bourman 1973, 1989). Distinct planation surfaces on the upthrown block, deeply incised by pre-existing river systems such as the Torrens River, often with an inherent degree of sinuosity, have created juvenile geomorphic features such as steep sided valleys incising previously planated surfaces and triangular facets on range fronts (Benson 1911, Fenner 1930, Sprigg 1945) and range bounding thrust faults are prominent features of the region (Twidale & Bourne 1975, Sandiford 2003b). Similarly, the eastern side of the northern Flinders Ranges consists of curvilinear fault scarps but without much exposure of fault zones.

Tensile stress induced normal faulting was considered to be the main tectonic mechanism by the early researchers (Benson 1911, Fenner 1930, Sprigg 1945) based on the sedimentary thickness of hanging walls (Lemon & McGowran 1989), which led to the interpretation of half-graben structures. Relative uplift associated with

normal faulting was proposed by Fenner (1930) and Sprigg (1945) as the mechanism of mountain building with respect to tensional stress-induced fracture patterns. But later, compressional reverse faulting during the Tertiary was recognised as the dominant fault mechanism by the majority of researchers following the identification of range-bounding thrust faults in outcrops (Fenner 1930, Glaessner 1953, Campana 1954, Cooper 1985, Wellman & Greenhalgh 1988, Bourman & Lindsay 1989, Benbow *et al.* 1995, Drexel & Preiss 1995, Love *et al.* 1995, Celerier *et al.* 2005). Tertiary compressional uplift gained more popularity than did the idea of lithospheric stretching followed by cooling and regional thermal subsidence (McKenzie 1978, Paul *et al.* 1999). Tokarev (2005) described faulting in three different stages accommodating both extension (normal faulting in the Tertiary) and compression (reverse faulting during the Quaternary), with a transition period between. Using slip rates inferred by limited field observations, vertical slip rates in the range of 20-150 m/Ma have been calculated (Sandiford 2003a), with the assumption that all range bounding faults in the Mount Lofty and Flinders Ranges are dominantly reverse faults caused by E-W compression. Unfortunately, none of the above explains what drives the consistently low level seismicity in this intraplate setting.

The degree of Palaeozoic reactivation within Neoproterozoic and Cambrian structures is displayed by the intensity and style of basement deformations. The reactivation of basement inliers and regional scale variation in deformation intensity is supposed to be primarily governed by thermal weakening of the crust. Moho temperature variations (of the upper mantle) and varying location of the brittle-ductile transition zone (thermal state of mid-upper crust) is mainly responsible for the thermal weakening (Paul 1998). Studies of Delamerian structures emphasise that the Neoproterozoic and Cambrian sediments were metamorphosed and intensely deformed to form the Southern Adelaide fold thrust belt (Flöttmann *et al.* 1994). This deformation is recognised as a west to northwest tapering orogenic wedge dominated by NNE and SSW trending fold axes (Clarke & Powell 1989, Jenkins 1990, Mancktelow 1990, Flöttmann *et al.* 1994). This evolution is also described as progressive localisation of convergent deformation (Sandiford *et al.* 1992). Structural trends in the Flinders Ranges reflect strain intensification accommodated by basement involved deformation and fold influenced weak deformation (Preiss 1986,

Li & Powell 1993). A detailed understanding of the Delamerian deformations is not considered in this study, but their location and nature has to be taken into consideration as appropriately, when considering hypotheses that suggests that neotectonic faults are merely reactivated Delamerian Faults.

2.9.1 Tectonics of the Mount Lofty and Flinders Ranges

Recognition of a series of block faults on the western side of the Mount Lofty Ranges by Benson (1911) is one of the earliest attempts to explain the Quaternary evolution of the ranges. It was presented with a model illustrating the main tectonic features using topographic maps and field observations. There is also a monoclinal (succession overturned) interpretation by Tate (1893) and an anticlinal interpretation by Howchin (1926) for deformation in Mount Lofty Ranges as stated by Sprigg (1946). Campana (1955) preferred to explain the origin of the Mt Lofty Ranges by compressional doming, which led to minor fault disruption on their margins. Complex basement flexuring produced reverse faults on the margins and normal faults within the ranges were the interpretation of Glaessner (1953) for the tectonic evolution of the Mount Lofty Ranges.

Gibson (1963) noted that the Clarendon/Ochre-Cove Fault displays a reverse habit, which was intersected by tunnelling operations during the construction of the Clarendon-Happy Valley pipeline. The Willunga and Milendella faults (on the west and east respectively) are given as examples of post-Miocene reverse faulting involving basement thrusting over the mid Pleistocene sequences. Shallow fault planes dipping towards the core of the ranges are characteristic features observed in both of them. Reverse faulting due to compression during most of late Pleistocene is confirmed in line with the traditional hypothesis of Tertiary compressional uplifting. An early uplift on the western side of the Mount Lofty and Flinders Ranges, compared to the east, is suggested based on the lithological variations of both sides (Belperio 1995) and the Murray Basin. There could have also been a slope towards the west during the Tertiary, according to the palaeochannel evidence (Tokarev 2005). Topographically the highest and the most active erosion in the Mount Lofty Ranges is associated with the Eden-Burnside Fault (Figure 2.8), which is on the

western side and is referred to as the uplift front. However, none provides descriptive information on particular field evidence that sheds light on the causes of the deformation.

Fenner (1930) proposed a two-stage tectonic model of uplift during the middle Eocene and early Pleistocene to account for the development of the Mount Lofty Ranges. The much proposed second phase Pleistocene uplift is contemporaneous with the eastern Australian 'Kosciuskan Orogeny' (Andrews 1933), which has more recently been termed Sprigg's Orogeny (Sandiford 2003a) in Southern Australia. The origin of Backstairs Passage (Benson 1911) which is the strait between the Fleurieu Peninsula and Kangaroo Island and the orientation of the Kangaroo Island, have been mentioned in the above models, but there is little consideration of the sigmoidal shape of the mountain range and the northern extension in the Flinders Ranges. However, the supposition of tensile block faulting and differential uplift since the late Tertiary, is accepted as leading to the present topography of the Mount Lofty and Flinders Ranges (Benson 1911, Fenner 1930, Sprigg 1945).

A study based on slickenside lineations and cleavage orientations in the Mount Lofty Ranges has shown some of them transected by thrusts and progressive rotations in fold axes (Mancktelow 1981). East trending slickensides on thrust planes parallel with mineral lineations and slaty cleavage led Mancktelow (1981) to propose that the curvature of the southern Mount Lofty Ranges is the result of compression against a cratonic margin, during the Delamerian Orogeny. The *en echelon* shaped mountain belt was also recognised as a crustal segmentation on a strain transfer zone (Tertiary Transfer Zone) in response to the present compressional continental stress (Tokarev 2005). The suggested Tertiary Transfer Zone (TTZ) obliquely crosses the Mount Lofty Ranges (Figure 2.8) and synchronises with the Tasman Fracture System connecting plate boundary and intraplate tectonics. The TTZ is in line with Jurassic-Cretaceous crustal extension and is parallel to a number of north-west trending ancient transform faults responsible for intra-continental crustal extension of the southern continental margin (Stagg *et al.* 1990, Willcox & Stagg 1990, Tokarev 2005).

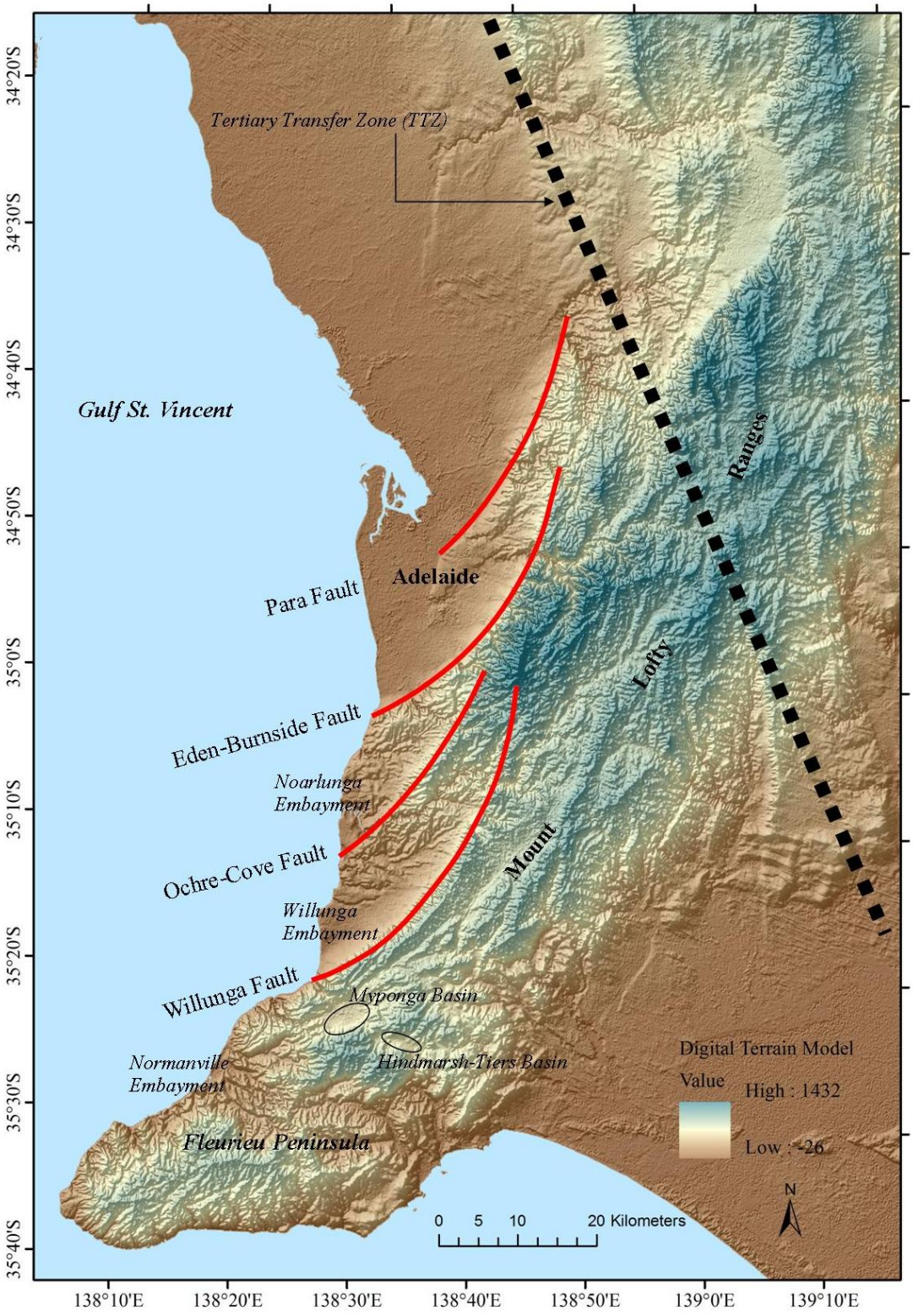

Figure 2.8 *Neotectonic setup of the Mount Lofty and Flinders Ranges (modified from Tokarev 2005)*

Sprigg (1946) proposed a three-stage deformational model for the Mount Lofty Ranges beginning with early to mid Palaeozoic monoclinal drag folding and block faulting followed by a long period of erosion. The middle stage is attributed to Late Palaeozoic to Mesozoic deformations, which took place along existing faults but moving in opposite directions. After a prolonged period of planation and tectonic quiescence, the last phase of deformation occurred since the Pliocene as the reactivation of ancient faults. This third stage of mountain building coincided with the Kosciuskan Orogeny and suggested that the Mount Lofty Ranges obtained its maximum local uplift during this period. Even though the model acknowledged the reactivation of older structures it does not provide sufficient information on the causes of deformation.

Tokarev (2005) presented a three-stage detailed tectonic model for the Mount Lofty Ranges based on local sea-level fluctuations, the assembly of flanking basins and geological, geomorphologic and tectonic data. Middle Eocene to middle Miocene crustal extension and segmentation by normal faulting was considered to be the first phase forming the adjacent basins. The second stage was one of landscape relaxation from the middle Miocene to earliest Pleistocene, which covers the transition of extensional tectonics to compressional. The third phase, which is still continuing, involves the compressional uplift of the mountains since the middle Pleistocene. This tectonic model accommodates different stages of mountain building within the Mount Lofty Ranges, but there are insufficient structural geological field observations in the Mount Lofty Ranges to support the hypothesis. Furthermore, the model does not give much attention to the evolution of the adjacent Flinders Ranges.

A threefold deformation model based on folding induced by plate boundary interactions was proposed by Sandiford & Quigley (2009a) and Sandiford *et al.* (2009b). A continental scale tilting, since the Late Miocene, due to plate subduction and ridge-push and slab-pull forces, has large wavelengths of 10000 km and amplitudes of ~300 m striking southwest and northeast. Lithospheric buckling due to intraplate stress is intermediate with 100 km wavelengths. Active faulting, which caused short wavelength deformations of 10 km, was considered to be the seismogenic mode. But this model does not take account of oblique stress fields

within South Australia or the travelling directional changes of the Indo-Australian Tectonic Plate. In addition, it treats the entire Australian continent as a homogeneous body rather than a complex mixture of rock types and structures that would behave differently under the variable stress conditions. Hence, it is over simplistic to consider the entire continent as being under compression as the stress regimes would be variable (Twidale & Bourne 2004), being partitioned against different geologic structures, thereby producing compression as well as extension.

A complex model developed by Marshak & Flottmann (1996) described Delamerian deformations within the present Mount Lofty and Flinders region. Accordingly, variations in fold axes orientations from E-W in the northern Flinders to N-S in the southern Flinders and back to E-W in the southern Mount Lofty Ranges suggest involvement of different processes to form the present topography. They divided the mountain belt into three sections with regard to the landscape formation. A dècollement involved deformation for the Flinders Ranges was suggested with detachment folds and fault propagation folds having axial trends approximately north-west (Clarke & Powell 1989, Marshak & Flöttmann 1996). In contrast, a two phase deformation (Offler & Fleming 1968) was attributed to the Mount Lofty section with folding and faulting controlled basement involved younger thrusts intersecting the older ones. Higher metamorphic grade units were observed within this section with tight folds and down dip lineations on south-east dipping thrusts. Reactivation on the Para, Eden-Burnside and Ochre-Cove faults (Figure 2.8) during the Cenozoic was considered, but excluded the well-exposed Willunga Fault. No strike-slip fault evidence has been recorded within the Flinders Ranges according to Marshak & Flottmann (1996). However, evidence of strike-slip movement on active fault segments, have since been recognised (Quigley *et al.* 2006, Quigley *et al.* 2007a, 2007b, Quigley *et al.* 2007c). The region between the Mount Lofty and Flinders curves is considered to be an intensely sheared zone with open folds. A thrust sense of shearing is observed, according to the kinematic indicators, which display east plunging, down dip mineral lineations. Deriving three separate modes of deformation for the sigmoidal shaped Mount Lofty and Flinders Ranges highlights the inhomogeneous shearing influenced by variable thicknesses of sediment sequences.

Pre-existing structures influenced left lateral shearing on a NW-SE trending mega shear couple (Figure 2.9) was considered to be the cause of deformation according to Coward (1976). Regional changes in the Palaeozoic fold axis (originally NE-SW trending) and cleavage orientations were used to determine the shear strain and orientations of isogons, which indicate a sinistral displacement during the Palaeozoic. According to Coward (1976) the maximum shear strain for this Palaeozoic ductile deformation occurs some 30 km north-east of Adelaide and overlaps with a zone of high-grade metamorphism indicating the presence of a high heat-flow. It is doubtful whether intense shear has created the anomalous heat or the shear zone has been aligned with a ductile zone initiated by an elevated heat flow. However, a source of heat could promote the local ductility irrespective of which occurred first. Accordingly, the Mount Lofty and Flinders Ranges could represent a deformation within the asthenosphere, with a larger scale shear zone extending to the mantle affecting the lithosphere (Coward 1976, Sutton 1976). As shear zones can be active over extensive periods of geological time (Coward 1976, Stewart 1976) a reactivation due to the local stress variations is possible under present conditions. High density basement at depth in some locations, and the presence of Palaeozoic granites and pegmatites could indicate the presence of high magmatic activity, hot spots or mantle plumes (von der Borch 1980). Observations on Late Proterozoic to early Palaeozoic progressive tectonic-sedimentary developments of a palaeo-rift passive margin suggest that the post Permian rifts of the region could be governed by heat induced tectonic activity (von der Borch 1980). It further states that the respective causes of rifting and crustal processes have been the same since Precambrian times.

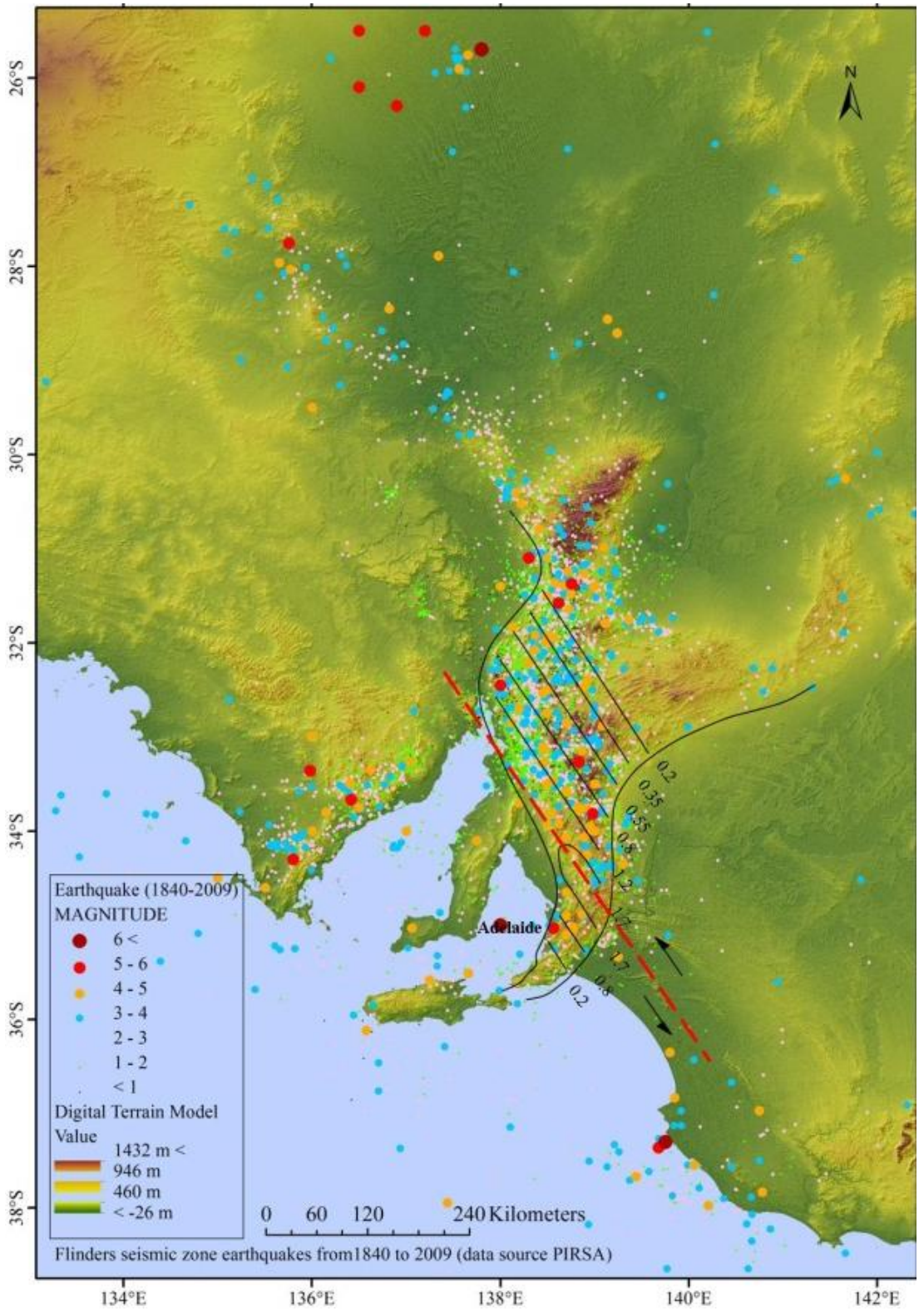

Figure 2.9 *Northwest directed Palaeozoic mega shear zone (red line) with left-lateral movements (Source: Coward 1976) overlying seismic data*

Crawford & Campbell's (1973) NW-SE trending early Ordovician dextral movements (Figure 2.10) attempt to explain the sigmoidal shape of the Mount Lofty and Flinders Ranges as a result of fault drag under the influence of two mega-shears. The northern dextral shear zone is responsible for dislocating the Willyama and Mount Painter blocks. The southern dextral shear zone has moved some 300 km creating extensive fault drag. This hypothesis was only supported by palaeomagnetic evidence and its validity was questioned by the borehole and seismic studies of Daily *et al*. (1973a). Larger scale folding against more stable blocks due to the lateral variations in basin geometry is also a possible explanation for the present shape of the Mount Lofty and Flinders Ranges (Daily *et al.* 1973a).

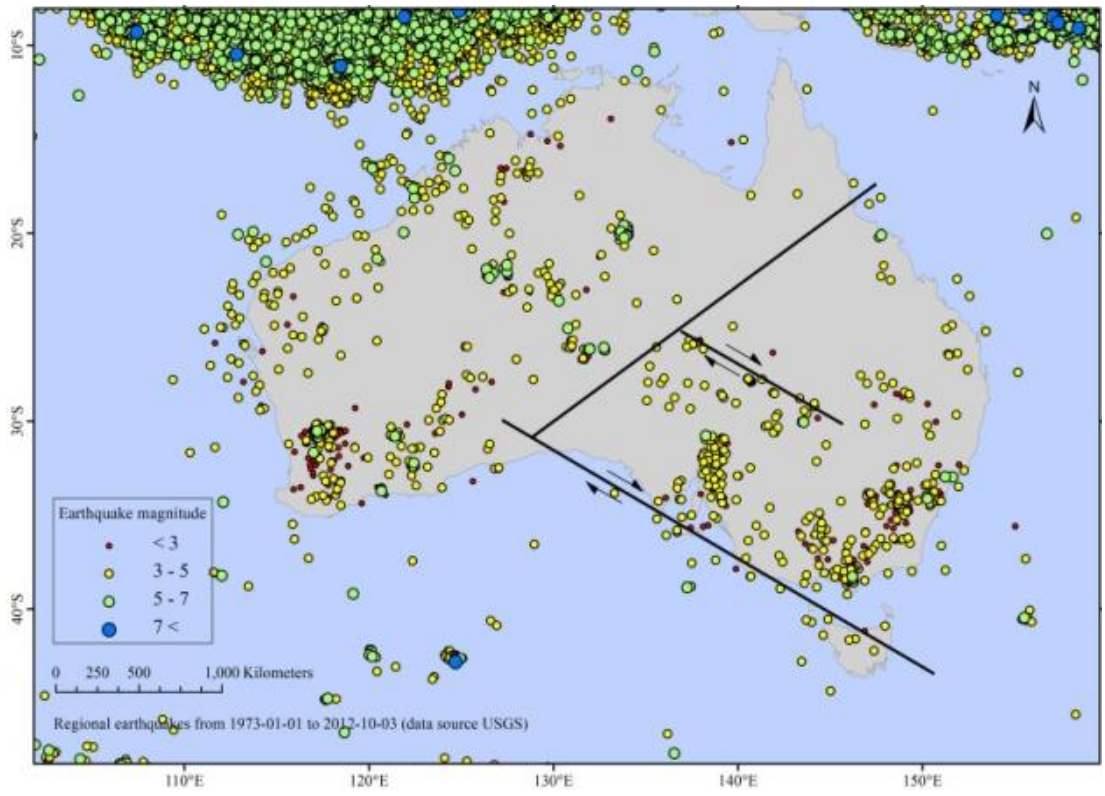

Figure 2.10 *Ordovician dextral shear zones (source Crawford & Campbell 1973) overlain with seismic data*

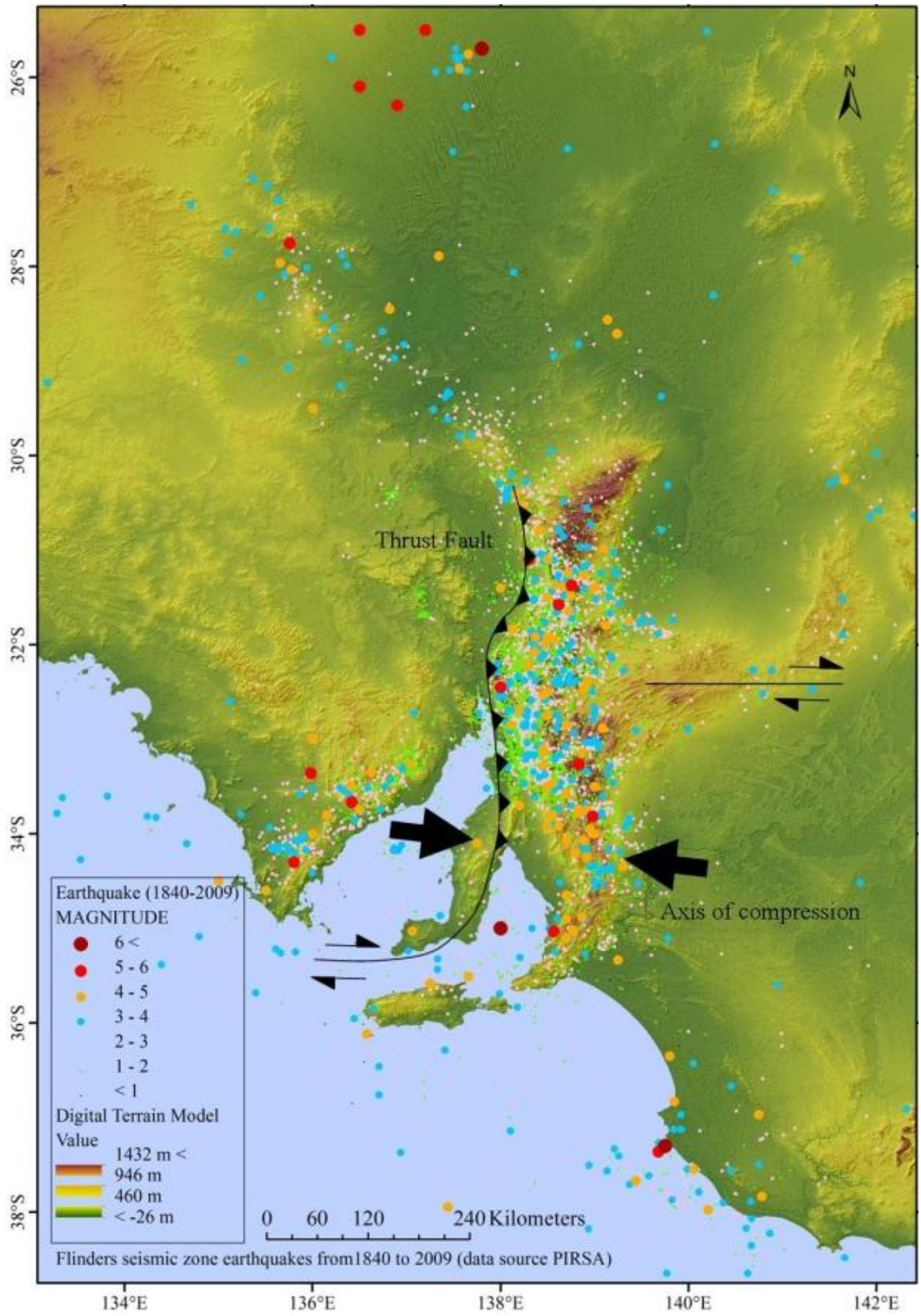

Figure 2.11 *East-west oriented dextral shear couple (source Clark & Powell 1989) overlain with seismic data*

Clark & Powell (1989) presented a dextral strike-slip model (Figure 2.11) supported by fault slickensides and stress data. The model is similar to the Ordovician dextral shear zone of Crawford & Campbell (1973) but is different in orientation. The model relates to Delamerian deformations and describes the present shape of the Mount Lofty and Flinders Ranges as a consequence of shearing between two east-west trending dextral strike-slip faults in the lower to mid Proterozoic basement. Evidence of transpressional deformation and orientation variations in fold axes within the mountain range imply that the shape would have been a result of a single compression event under the east-west oriented compressive stress. Crustal thickening and upright folding has been a result of compression under the influence of local stress. The northern Flinders Ranges have undergone considerable basement shortening to produce popup structures possibly due to a basement cover dècollement. A two-stage deformation was inferred by Clarke & Powell (1989) for the Mount Lofty Ranges based on east-west horizontal maximum compressive stress, unpublished fault orientations and slickenside data.

Harrington *et al.* (1973) introduced a model (Figure 2.12) based on oil and gas exploration data that incorporated sinistral as well as dextral pre-Tertiary movements, affiliated with a fracture zone triple junction located south of the Australian main-land, NW of Tasmania. Gambier (1) and Beaconsfield (2) fracture zones in Figure 2.12 are oriented WNW, whereas the Sorell fracture zone (3) has a more NW orientation merging with the Gambier and Beaconsfield fractures south of the present South Australian-Victorian state boundary. Sinistral shearing on Gambier and Beaconsfield was active during late Ordovician to middle Devonian times, shifting Tasmania to the west with a minimum slip of 1100 km. Even though clear evidence is not present, at least 900 km of dextral movement along the Gambier-Sorell fractures was inferred from the late Jurassic to Cretaceous times while Australia was attached to Antarctica. Left and right lateral movements on shear zones could have occurred in turn, as it may have been affected by changes in plate velocities and boundary forces. A convergent plate boundary was in existence at the current Mount Lofty and Flinders region when the intense folding and faulting took place during the Cambrian-Ordovician Delamerian Orogeny (Harrington *et al.* 1973).

However, the suggested Ordovician sinistral movement on the Gambier-Beaconsfield fracture zone contradicts the dextral-slip proposed by Crawford and Campbell (1973), even though the fracture orientations are identical.

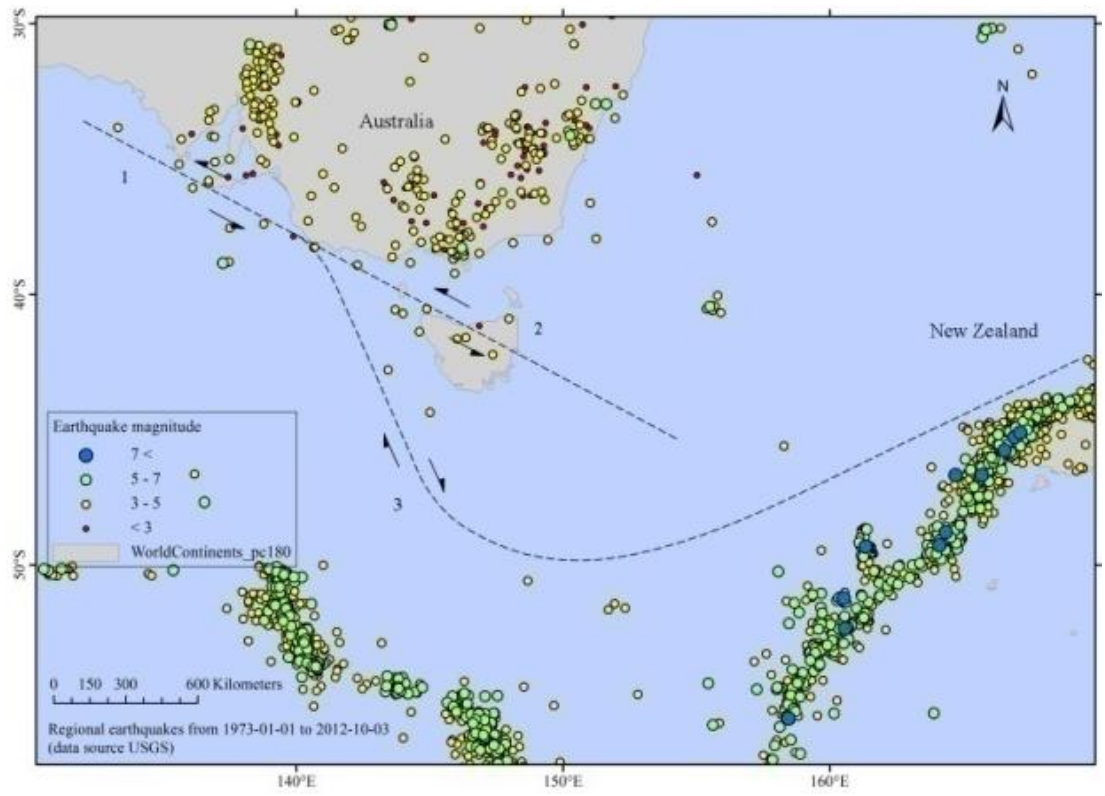

Figure 2.12 *Pre-Tertiary assembly of the southern fracture zones (source Harrington et al. 1973) overlain with seismic data*

A sub-plate tectonic model based on earthquake distributions was first presented by Cleary & Simpson (1971). They divided the Australian continent into three seismic zones (Figure 2.13) based on seismic records from ~1900 to 1966, and associate them with major oceanic fracture zones that extend to the Australian-Antarctic spreading ridge. These arcute lines of weaknesses delineate pre-existing zones of crustal weakness (Wilson 1965), such as the Torrens Hinge Zone within the Delamerian Orogen. Relative movements along the fracture zones act as transform faults, where those sub-plate boundaries were defined. A postulated subplate boundary with a NNW orientation and left-lateral shearing corresponds with the present Mount Lofty and Flinders Ranges. Accordingly, a reactivation, or the continuous differential movements on transform faults, is considered to be responsible for the present seismicity and geomorphic expression of the region. The

lack of seismic records along oceanic fracture zones only provides limited evidence for the differential movements of crustal mini-plates. However, this model cannot be disregarded as tectonic plates move extensive horizontal distances over geologic time (Sylvester 1988).

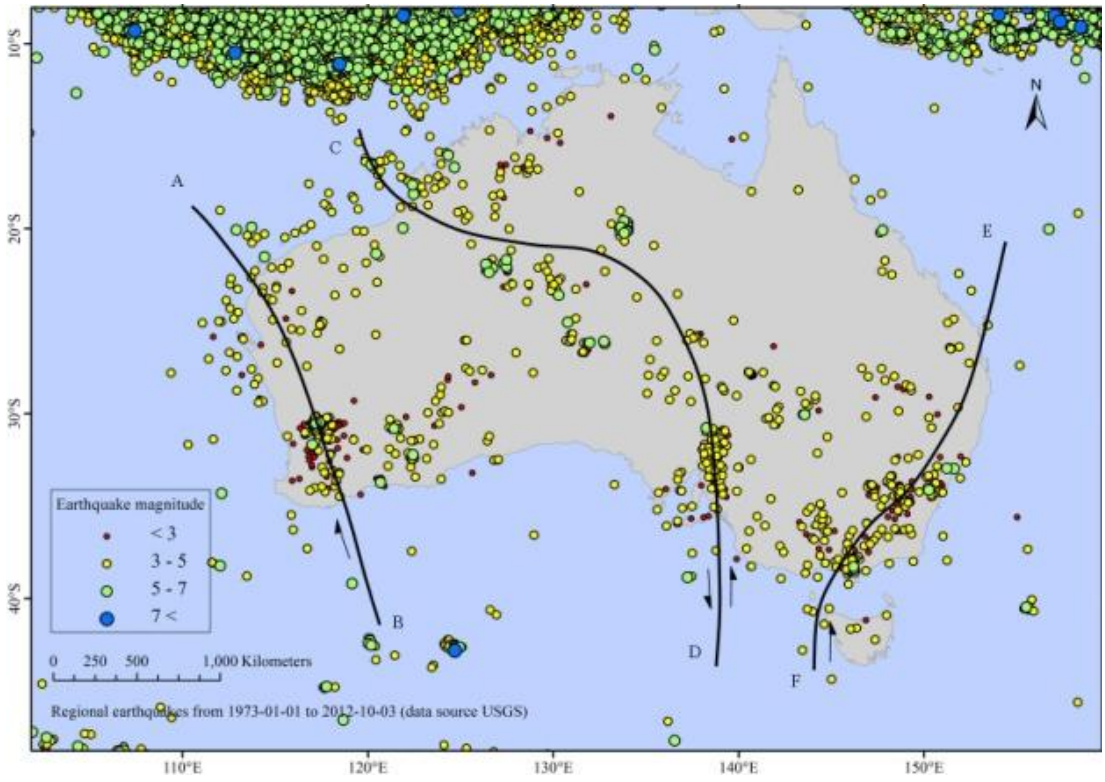

Figure 2.13 *Sub-plates within the Australian continent (source Cleary & Simpson 1971) overlain with the seismic records*

Stewart and Mount (1972) produced a tectonic model (Figure 2.14) based on South Australian earthquake epicentre trends and focal mechanisms within the limited period of 1967 to 1973. The model displays a network of fractures having right lateral motion representing major lines of weakness in the crust since the late Proterozoic. It explains complex variations of strike-slip faulting near Adelaide to dip-slip faulting in the Flinders Ranges (Stewart 1976). The proposed dextral shear zone is similar to the sinistral mega-shear of Coward (1976) and coincides with a region of high conductivity that possibly penetrates to the deep crust and the upper mantle. The lateral extent of the seismicity and the computed hypocentre depths also suggest the extension of the fractures beyond the lower crust. The influence of the mid-oceanic ridge transform faults on the crustal weak zones (Cleary *et al.* 1972) is

accepted in this hypothesis and the right lateral movement is shown to be controlled by the central Australian compressive stress regimes.

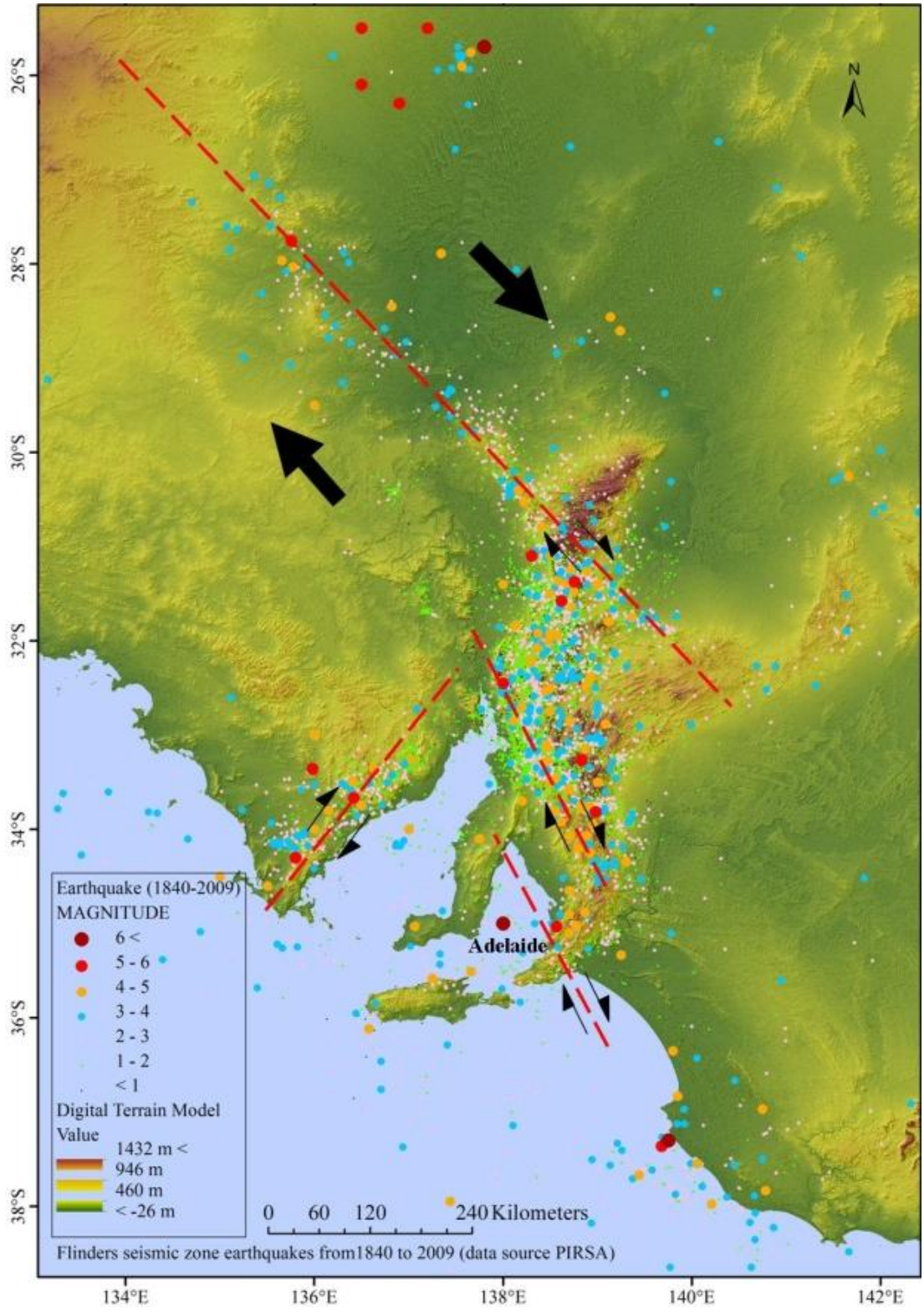

Figure 2.14 *Palaeozoic dextral shear zone (source Stewart & Mount 1972) with seismic data*

Dyksterhuis & Muller (2008) considered a two stage Sprigg's Orogeny based on the numerical modelling of the Australian continental stress regimes since 100 Ma. A ridge-push force governed strike slip dominant first stage is attributed to the ~23-11 Ma Pacific-Australian plate collision. A reverse reactivation of the existing structures due to compression was the second stage of deformation during ~11-6 Ma, in response to the collision along Papua New Guinea. A two fold increase in convergence along the Pacific-Australian boundary since ~6 Ma should theoretically explain the intraplate neotectonics and most probably with similar driving mechanisms to the ~23-11 Ma event. The study emphasised the influence of plate boundary forces on the interior deformations and localisation of such events depending on the pre-existing structures and crustal characteristics such as elevated temperature.

The various models described above provide a limited understanding of the possible processes responsible for the current topography of the Mount Lofty and Flinders Ranges. Most of the models are ambiguous about whether Delamerian activity or Quaternary mountain building is important in shaping the present topography. The lack of field evidence such as structural geological data, and corresponding interpretations leading towards logical hypothesis that would explain the possible driving mechanisms and seismicity is a limiting factor of most of the models. Neotectonic activity in South Australia has been discussed by many authors more recently and with a much broader approach (Sandiford *et al.* 1998b, Clark & Leonard 2003, Sandiford 2003a, Tokarev 2005, Sandiford & Quigley 2009a). Plate boundary forces, unusual stress patterns induced by them, influence of the heat anomaly, regional tilting of the Australian continent due to slab pull-push forces, and being driven through a geoid-high are taken into account as the main governing factors. However, the distinctive localised seismicity within the mountains and basins are yet to be adequately explained and a specific driving mechanism for intraplate mountain building in the Mount Lofty and the Flinders region is hard to recognise. Hence, an appropriate driving mechanism for the Mount Lofty and Flinders Ranges that represents its consistent seismicity and geomorphology is a timely requirement to improve the understanding of the processes involved.

2.10 Discussion

The seismicity record of the Flinders Seismic Zone reveals that the topography of the landscape may be controlled by local geology and active deformation. The presence of surface rupturing reverse faults over the last 100 ka suggests that South Australia has experienced many large earthquakes in the past, similar or larger than the 1954 Adelaide earthquake, and will continue to experience them into the future. Extrapolation of the seismicity record for the past is possible for South Australia, considering the overlap of historical seismicity and neotectonic faulting (Sandiford 2003a, Quigley *et al.* 2006).

Deformation due to fault movements within continents is a way of accommodating intraplate stress (Hillis *et al.* 2008). The Mount Lofty and Flinders Ranges of South Australia are a result of larger scale folding followed by differential fault movements (Flöttmann *et al.* 1994, Twidale & Bourne 2004). It is one of the most seismically active and geomorphologically rugged parts of the Australian continent (Sprigg 1945, Sandiford 2003a, Tokarev 2005). Consistent low levels of seismicity are one of the main pieces of evidence of active deformation within the Mount Lofty and Flinders Ranges. Naturally exposed fault contacts and deformation within the unconsolidated sediments confirm the continuation of deformation throughout the Cenozoic. Even though studies have determined that plate boundary forces and heat are influential components, the majority of the features in the region cannot be explained by the existing hypotheses. Most of them describe the tectonic behaviour of the Mount Lofty and Flinders Ranges related to Palaeozoic and Precambrian mountain building. They are ambiguous in relation to time and only a handful specifically addresses their Quaternary behaviour. This lack of understanding of what forces govern, and to what extent they determine, the neotectonic processes of southern South Australia, amplifies the risks associated from a natural hazardous perspective.

Plio-Quaternary faulting in the Mount Lofty and Flinders Ranges is attributed to the variations in far-field stresses associated with the Indo-Australian Plate boundary (Coblentz *et al.* 1995, Sandiford *et al.* 1995, Coblentz *et al.* 1998, Reynolds *et al.* 2003, Sandiford 2003a, Sandiford *et al.* 2004). Plate motion and obliquity between

maximum horizontal stresses across southern Australia also suggests that continental collisions play a major role in governing the patterns of deformation within the Australian continent. As the force changes in plate boundaries influence the stress orientations and magnitudes of plate interiors, a relationship could be established between plate boundary orogenic processes and intraplate tectonics. However, investigations of exposed Quaternary faults in the Flinders Ranges suggest that the seismicity does not depend exclusively on stresses, but is also influenced by local and regional geological features and the mode of deformation (Quigley *et al.* 2006).

Structural development of the Mount Lofty and Flinders Ranges involves extensional (Sprigg 1945, Cooper 1985), compressional (Sandiford 2003a) and a combination of extensional and compressional (Fenner 1930, Tokarev 2005) forces. There is clear evidence of post mid Pleistocene reverse faults and deformation associated with a compressional tectonic regime on both western and eastern sides of the ranges (May & Bourman 1984, Bourman & Lindsay 1989, Sandiford 2003) The rigid metamorphic core of the pre-Tertiary basement inhibited neotectonic folding and thus accounted for the absence of folds in both Tertiary extensional and Quaternary compressional environments (Tokarev 2005). Conversely, continuous lateral and vertical dislocations resulted widespread folding and faulting has been identified by Twidale & Bourne (2004), which the geometry and sense of motion is determined by pre-existing lineaments. Reverse sinistral movements and a steeply dipping network of faults recorded from segments of the Wilkatana Fault (Quigley *et al.* 2006) and the *en echelon* structures displaying sinistral transpressional behaviours on the Eden Burnside Fault (Bourman *et al.* 2010a) indicate that the regional neotectonic faulting could include both transpressional and compressional uplifting. Additionally, most of the present local stress vectors align obliquely to the identified neotectonic faults, suggesting that the faulting cannot be limited to dip-slip movement. This is in contrast to the present general understanding of the reverse faulting influenced compressional uplift for Cenozoic mountain building in the Mount Lofty and Flinders Ranges.

Neotectonic overprinting of Delamerian structures make the Mount Lofty and Flinders Ranges a structurally complex zone. Whether active faults represent new

structures developed in response to the current stress field (Tokarev 2005, Buckman *et al.* 2010) or the reactivation of older Delamerian faults have been reactivated (Love *et al.* 1995, Benbow *et al.* 1995a, Benbow *et al.* 1995b), is a contentious topic. To date, most interpretations suggest compressional reactivation of N to NE trending older Delamerian structures (Sprigg 1946, Ward 1966, Wellman & Greenhalgh 1988, Drexel & Preiss 1995, Preiss 1995, Benbow *et al.* 1995b, Flottmann & James 1997, Quigley *et al.* 2006, Hillis *et al.* 2008). Tertiary normal faulting could have followed the Delamerian weak zones for its crustal segmentation, leading to a possible reactivation of Tertiary normal faults to create Pleistocene reverse faulting. However, normal faults having single steep fault planes in contrast to the reverse faults existing as networks of sub-parallel high to low angle thrusts are characteristic features that differentiate the two regimes, highlighting their independence (Tokarev 2005).

Although definitive evidence or documented studies to support the following are lacking, the neotectonic faults could be differentiated from Delamerian faults given that there has been in the order of 20-30 km of erosion and unroofing of the Adelaidean rocks since the Delamerian Orogeny. Exposed Delamerian Faults have intense quartz veining or well developed micaceous shear zone foliations showing ductile deformation due to their formation in the middle-upper crustal regions under high temperature and pressure conditions. The neotectonic fault exposures should reveal brittle cataclastite dominated fault gouge material composed of a predominantly clay matrix devoid of quartz or micaceous fabrics with angular, tectonically brecciated lithic fragments (Bull 2007, McCalpin & Carver 2009). Conversely, it should be noted that shear zone fabrics and associated silicification can act to heal and strengthen the crust along fault zones, particularly in more ductile regimes. Hence, assumptions that existing neotectonic faults are reactivated Delamerian faults must be tested and validated.

Major geomorphological features not showing a close relationship with the pre-Tertiary basement fabric (Tokarev *et al.* 1999, Tokarev 2005) suggest that formation of the ranges was associated with local block faulting during the Tertiary and Quaternary. The absence of basement structures within the neotectonic structures denotes independence of neotectonic activities and the basement fabric. Attempts to

link the regional seismicity and the elevation of the Mount Lofty and Flinders Ranges through the spatial distribution of the older structures (Love *et al.* 1995) has not been supported by the exposed and observed neotectonic fault gouge zones, which do not show a reactivation of pre-existing structures.

Using observations of seismicity in combination with neotectonic features (Quigley *et al.* 2010), the Australian continent has been divided into four major seismic zones (Figure 2.2). However, the four zones do not sufficiently accommodate seismicity within central Australia for the recent records between 1973 January to 2012 October. Figure 2.6 shows that most of the seismic events were clustered in the regions where the stress fields are oblique to the NNE directed present plate movement. However, the continental scale stress regime does not show a significant relationship with the limited amount of recorded seismic data. The available models that describe modes of deformation for different segments of geologic time scale have been superimposed on the recent seismic data by section 2.6 to observe any relationships. The model of Clary & Simpson (1971) (Figure 2.13) best accommodate the seismic trends in a regional context. Coward (1976) (Figure 2.9) and Stewart & Mount (1972) (Figure 2.14) demonstrate that sinistral and dextral shear-couples best fit with the seismicity observed within the Mount Lofty and Flinders Ranges for the period from 1840 to 2009. However, detailed field evidence and further information is needed for scientific confirmation of the applicability of such models.

The intensity of neotectonic activity and historical seismicity within the mountain range reflects possible structural and thermal heterogeneities under the influence of regional stress fields dominated by far-field plate boundary forces (Quigley *et al.* 2006). Continental-scale heat anomaly maps do not show direct relationships with the available seismic data. There are discussions suggesting that a thermally weakened crust could have initiated localised zones of deformation within the Australian continent, but, the Southwest Seismic Zone resides on a comparatively lower region of the Australian Heat Anomaly (Figure 2.7). Hence, heat could not be the only source of localised mountain building as the anomalies extend beyond the spatial extent of the regions of deformation (Section 2.5). This reflects the anomalous

heat production from the underlying basement, but is not limited to the Neoproterozoic sediments (Paul 1998). Interestingly, it can be observed that, except for the western seismic zone, the majority of the Australian seismic zones are situated at the boundaries of the heat anomaly. However, it is difficult to establish a simple relationship between stress, heat and seismicity (Figure 2.15) for the Australian continent from the available information.

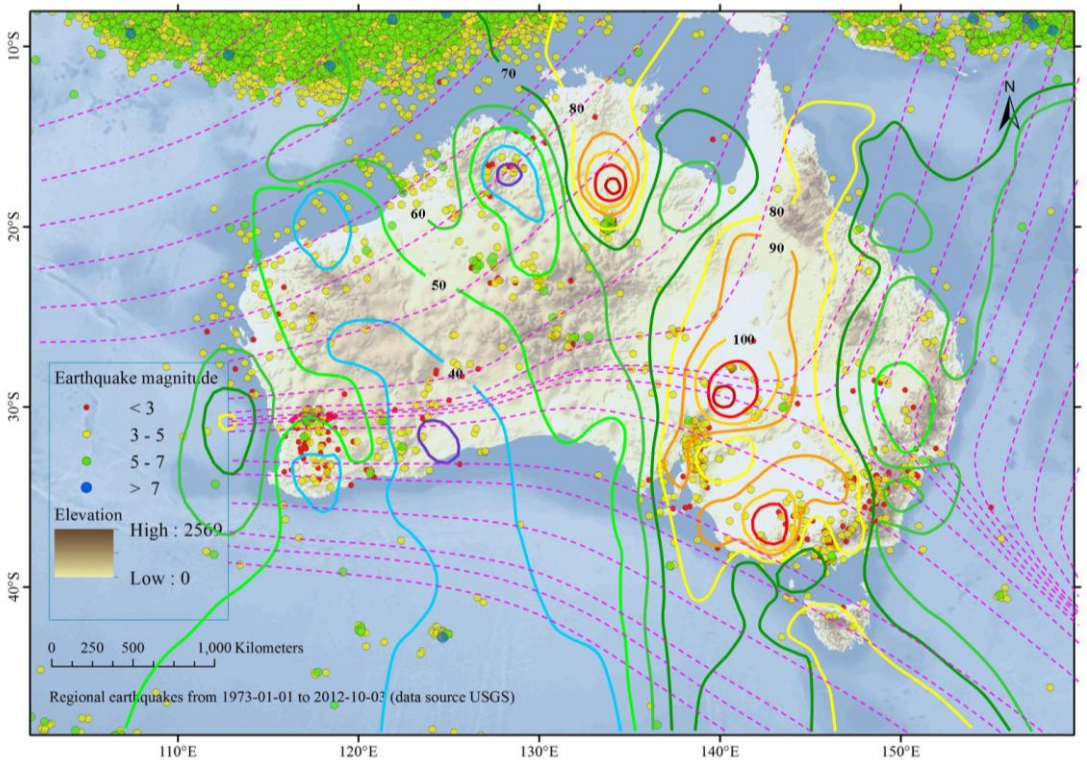

Figure 2.15 *A composite display of the seismic observations (1973 to 2012), Australian heat anomaly (mW/m^2) and maximum horizontal stress trajectories. (Combination of Figures 2.6 and 2.7)*

Neumann *et al*. (2000) described the inclined tendency of deformation along the mountain belt as a result of mutually facilitating heat flow and tectonic activity weakening of the Flinders Ranges crust. This idea is supported by the work of Paul (1998) and Celerier *et al.* (2005). Whether it is a coincidence or whether the thermally weakened crust has facilitated the anomalous deformation creating the Mount Lofty and Flinders Ranges, is a subject of interest, but it is difficult to see how broad-scale and diffuse crustal heat anomalies could be responsible for the narrow and abrupt deformation responsible for the Flinders/Mount Lofty Ranges. However, according to Wilson (1965), the thermally weakened zones within

continents are of transform fault origin as indicated by concurrence of continental and oceanic fracture zones. Shearing of these weak zones due to boundary forces has the tendency to produce sub-plates within continents reflected by mountain building and subsidence (Heirtzler *et al.* 1968, Cleary & Simpson 1971, Crawford & Campbell 1973, Coward 1976, Hillis *et al.* 2008).

The earth's crust is a heterogeneous mixture of rock types and complex structures as the elements which constitute the continents vary in composition and rheology (Hancock 1988). Hence, the stress is likely to vary as it partitions and negotiates within an inhomogeneous rock mass leading to complexity rather than simplicity of patterns (Twidale & Bourne 2004). As a result, models that describe deformation through continental scale compression may not comprehensively explain deformational features observed in southern South Australia. For an example, even though South Australia is regarded as being dominated by compressive stress regimes, there can be transtensional regions with normal faulting and these zones may be difficult to identify due to subsidence and consequent sediment infilling. The seismicity recorded beneath some of the Cenozoic basins adjacent to the Flinders Ranges such as the Torrens, Eyre, Frome and Murray Basins may be considered as such evidence, but requires further investigation. However, aeromagnetic and drilling data support the view that the Murray Basin has Delamerian structures underneath the Cenozoic sediments (Marshak & Flöttmann 1996)

A detailed field study of active faults provides an avenue for improving the understanding of neotectonic deformations (Hancock 1988). Knowing the individual behavioural patterns for separate fault segments within the Mount Lofty and Flinders Ranges could be used to derive a plausible explanation of the behaviour of the localised deformations. This could be further extended to explore possible driving mechanisms at a regional scale and their corresponding evolution through geologic time. The present study deploys field techniques to specifically understand the details of faulting in southern South Australia, which may be interpreted to determine possible driving mechanisms for their formation.

3 CHARACTERISTICS OF THE WILLUNGA FAULT AT SELLICKS BEACH

3.1 The general setting of the Willunga Fault

The Mount Lofty and Flinders Ranges extend some 800 km from the Fleurieu Peninsula in the south, to Maree in the North Flinders Ranges, and represent one of the most seismically active regions in Australia (Sandiford 2003a). These ranges attain elevations of up to ~1171 m in the Flinders Ranges and ~700m in the Mount Lofty Ranges, and form a distinctive *en echelon* or '*lazy S*' geomorphic expression (Figure 1.2). It has been well recognized that these mountains are juvenile geomorphic features (Bourman & Lindsay 1989, Bourman & Murray-Wallace 2002, Sandiford 2003a, 2003b, Celerier *et al.* 2005, Tokarev 2005, Hillis *et al.* 2008, Bourman *et al.* 2009) having been uplifted during the Cenozoic and do not exclusively represent the remnants of an ancient Palaeozoic mountain range. Hence, much of the current topography of the Mount Lofty and Flinders Ranges is considered as a result of the Cenozoic rejuvenated mountain building of the Sprigg Orogeny (Sandiford 2003a).

The Mount Lofty and Flinders Ranges are flanked by north-northeast striking range-bounding faults subjected to east-west compression (Sandiford 2003a, Celerier *et al.* 2005). The Willunga Fault is one of several neotectonic faults that border the western side of the southern Mount Lofty Ranges on Fleurieu Peninsula, South Australia (Belperio 1995). At Sellicks Beach, near Aldinga Bay, sections of this active fault have been exposed by coastal erosion and deep gully incision of the alluvial fan material (Figure 3.1), that has developed down-slope of the uplifted ranges to the east of the fault zone. Cambrian bedrock disrupts Neogene and Quaternary sediments at the intersection of the fault and coastal cliffs. Beneath the Quaternary terrestrial sediments are Eocene-Miocene limestones of the Port Willunga Formation, which have undergone significant tilting near the fault contact. Thrusting of lower Cambrian bedrock over the Quaternary alluvial fan sediments makes Willunga a reverse fault that shows rapid erosion of the eastern up-thrown block. Recent (Holocene) coastal erosion near Aldinga Bay has exposed this fault contact, which in other areas is usually covered by a thick blanket of Quaternary sediments.

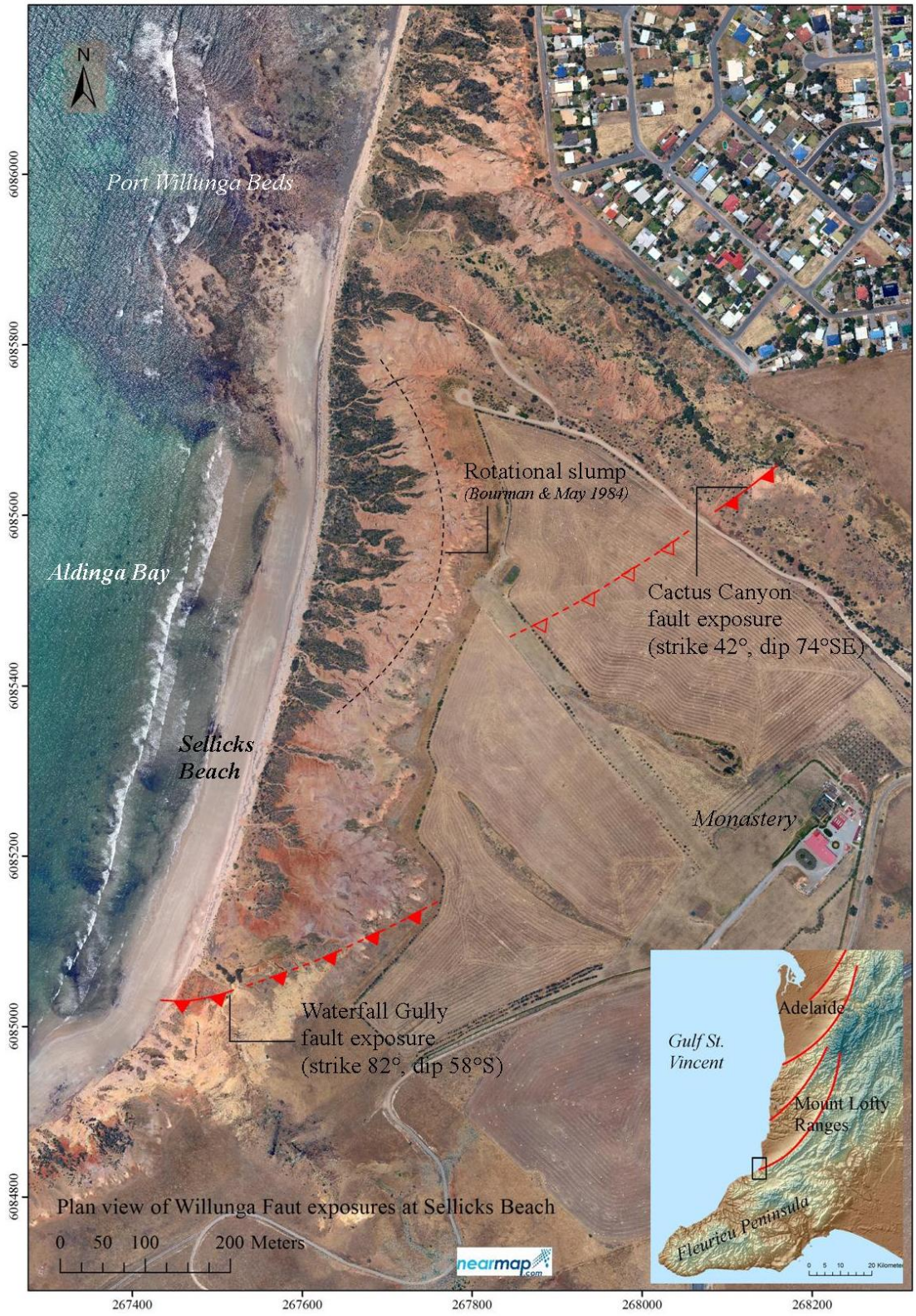

Figure 3.1 *Plan view of the Willunga Fault exposures at Sellicks Beach (see also Appendix I)*

Prominent features of the Sellicks region include deeply incised escarpment, range bounding thrust faults and an undulating surface expression (Sandiford 2003b). Exposures of dissected alluvial fans that are draped over and cut by the active range-bounding faults in this semi-arid environment, in combination with numerous Cenozoic marine incursions into Gulf St Vincent, make the Sellicks Beach site an excellent natural laboratory to study the extent and modes of intraplate deformation. Consequently, detailed field investigations were conducted at Sellicks Beach in order to collect comprehensive information associated with faulting, particularly focused on Quaternary movements. This chapter is a compilation of various techniques used to identify the characteristics of the Willunga Fault in the vicinity of Sellicks Beach. Some of these scientific findings were presented at a number of conferences during 2009-2012. The present investigation will improve the understanding of intraplate neotectonic mountain building of the Mount Lofty and the Flinders Ranges.

3.2 Cenozoic geology and stratigraphy of the Sellicks Beach

Unravelling the neotectonic record in South Australia may be achieved by obtaining a detailed chronology of the Cenozoic stratigraphy. These sedimentary units which are younger than ~65 Ma may have been displaced by faulting that has occurred since Australia rifted away from Antarctica and occupied an intra-plate tectonic setting. A rigorous stratigraphic and chronologic framework of Quaternary sediments has been developed for the range-bounding alluvial fans of the Mount Lofty Ranges (Ward 1966, May & Bourman 1984, Pillans & Bourman 1996, Bourman *et al.* 1997, Bourman *et al.* 1999, Bourman *et al.* 2000, Murray-Wallace & Bourman 2002, Banerjee *et al.* 2003, Bourman *et al.* 2010a). Recent stratigraphic work by Bourman *et al.* (2010 a, b) has provided much tighter age constraints for numerous, clearly identifiable marker horizons that in some cases can be traced across the range-bounding faults to determine vertical offsets. The available stratigraphic framework can be applied to exposures of neotectonic faults and Quaternary fans in the Mount Lofty and Flinders Ranges in order to develop a better regional understanding of the neotectonics and alluvial sedimentation on the range flanks.

The Willunga Embayment (Figure 2.8), which contains sediments dating at least from the mid Neogene, lies to the north of the intersection of the Willunga Fault with the coast. Sedimentation in the Willunga Embayment commenced in the early Eocene with deposition of non-marine to marginal marine sands and clays of the Maslin Sand (Daily *et al.* 1976, Cooper 1979, Lindsay & Alley 1995). A greater marine influence occurred during the late Tertiary and early Pleistocene in this region, with marine inundations producing distinctive sandy limestone units such as; Oligocene-Miocene Port Willunga Formation, Pliocene Hallet Cove Sandstone, earliest Pleistocene Burnham Limestone and the equivalents of the last interglacial Glanville Formation. On the surface, Post European Sediments blanket the region. The surface geology along the Willunga Fault involves Cenozoic sediments in contact with uplifted lower Cambrian bedrock, which consists of shales and limestone with banded calcareous shales, siltstones, sandstones and oolitic-dolomite (Belperio 1995). A brief description of the main stratigraphic units, which reflect the spatial and temporal movements of the Willunga Fault at the Sellicks region is, documented below.

3.2.1 Maslin Sands

The Maslin Sands accumulated during middle to late Eocene. The Quartzose, glauconitic and pyritic lithology of the sand represents a marginal-marine (near shore) deposits (Lindsay & Alley 1995). This is considered to be the first marine influence on the region as a result of subsidence of the St Vincent Basin accompanied by the tilting of the southern Australian continental shelf during global sea-level fall. The contact between the North Maslin Sand and the South Maslin Sand in the Willunga Embayment is transitional and conformable. However, in some areas near Adelaide and Moana, the North Maslin Sand is absent so that the South Maslin Sand directly overlies the pre-Tertiary basement (Miles 1952). An angular contact between the South and North Maslin Sands in the Noarlunga Embayment (Glaessner 1953), may have resulted from a low angle tilt of the hanging-wall block due to normal movements on the Ochre-Cove Fault (Tokarev 2005). Both the North Maslin Sand and South Maslin Sand are absent near the Willunga Fault contacts at Sellicks Beach.

The North Maslin Sand consists of medium to coarse grain cross-bedded quartz with intermittent pebbles, clay and silt lenses. This fluviolacustrine basal unit is also rich with terrestrial plant fossils of middle Eocene age (~42-40 Ma) and is often preserved in depressions where it unconformably overlies highly weathered pre-Tertiary basement (Lindsay & Alley 1995). The Mount Lofty Ranges were the main sediment source for the North Maslin Sand deposits in the St Vincent Basin, with W-SW directed small sinuous palaeostreams (Tokarev 2005) delivering the sediments. The South Maslin Sand contains sparse marine fossils of middle Eocene age (~39-38 Ma). Coarse sediments occur at the base, above which the lithology transitions to fine grained silt and muddy clay. It displays a thickness of ~6 m in the Adelaide region and increases southwards reaching over 30 m. Coarse sediments at the base of the South Maslin Sand may indicate a major pulse in the sediment supply, which could possibly have resulted in an extensive marine floodplain (Fairburn 1998). The angularity of the grains signifies that sedimentation occurred close to the source area. The rapid change in lithology can be taken as evidence of decreasing stream competence, possibly resulting from a new pulse of basin subsidence (Tokarev 2005).

3.2.2 Port Willunga Formation

The Oligocene-Miocene Port Willunga Formation (Lindsay & Alley 1995) is a limestone containing cross-bedded fossiliferous sandstone, mudstone and thin bands of clay. It reaches thicknesses of up to 150 m (Fairburn 1998), with early Oligocene faunas, marl, silt and chert bands occurring towards the middle of the unit, and silty sand layers towards the upper sections (Belperio 1995). Marine sedimentation was dominant during the late Eocene to middle Miocene with a possible hiatus at the Oligocene-Miocene boundary marked by an angular unconformity (disconformity) midway through the Port Willunga Formation exposed south of Aldinga Bay (Figure 3.3). Continuous marine sedimentation, in spite of considerable sea level fluctuations, is indicated by ~21 m thick limestone layers. The same Port Willunga Formation occurs in the inland basins of Myponga and Hindmarsh Tiers (Glaessner 1953, Glaessner & Wade 1958, Lindsay 1981). The variable thickness of the Port

Willunga Formation on the western side of the Mount Lofty Ranges has been interpreted as a result of sediment accommodation spaces mainly created by differential normal faulting during ~34-29 Ma (Tokarev 2005). A break in depositional succession represents a hiatus of ~18 My at Sellicks Beach and increases towards the north as ~32 at Maslin Bay and ~28 at Port Willunga. This disconformity (unconformity 2 of Figure 3.3a) midway through the Port Willunga Formation marks the Oligocene-Miocene boundary. Further south on the shoreline platform an unconformity between the Adelaidean Bedrock and the Port Willunga Formation can be observed (Figure 3.2).

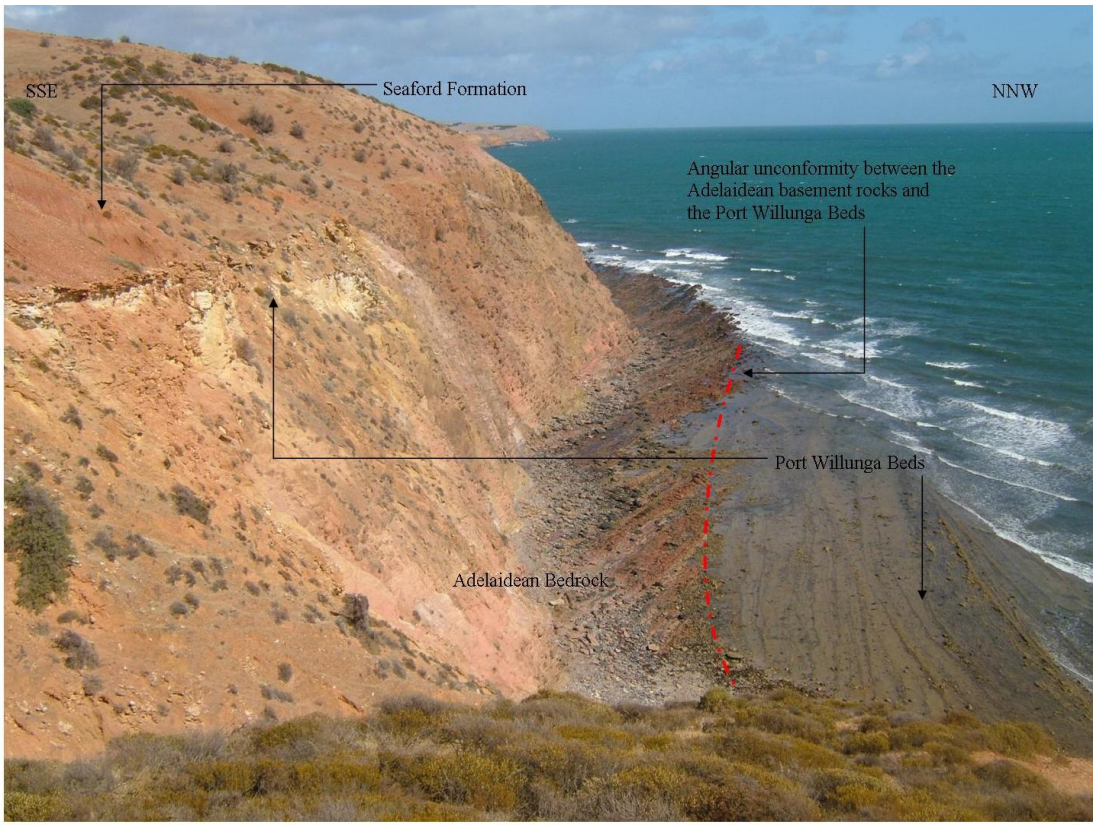

Figure 3.2 *Unconformity between the Adelaidean Bedrock and the Port Willunga Beds (dipping ~45°NW), south of the Willunga Fault. Location coordinates: 266280 E, 6084460 S*

As stated in Tokarev (2005), the Port Willunga Formation is a combination of the sedimentary units identified as Aldinga, Ruwarung, upper-Janjukian, Longfordian, Batesfordian - lower Balcombian and Munno Para Clay. The late Eocene to early Oligocene Aldinga Member occurs at the base of the Port Willunga Formation. The

unit is dominated by calcarenite with silt, clay, very fine-grained glauconitic quartz sands and abundant fossils, possibly deposited in near-shore environments with restricted access to the ocean (McGowran 1978b, Lindsay & Alley 1995). The Aldinga Unit is overlain by the Ruwarung Member, which consists of irregular nodules of fossiliferous chert in a fossiliferous mudstone matrix (Lindsay 1981). The depositional age of this unit has been dated as late Eocene to earliest Miocene, and is considered as the middle part of the Port Willunga Formation. The fossiliferous Upper-Janjukian Unit deposited during ~24-21 Ma resides on top of the Ruwarung Unit (Lindsay 1981). The glauconitic, sandy limestone/calcareous sandstone contain more clayey components than the Ruwarung Member (Lindsay 1981) and was deposited in a similar environment to that of the Aldinga Member. The early Miocene Longfordian Unit (~21-16 Ma) dominated by carbonates and sandy limestones, creates a conformable contact with the Upper Janjukian Unit, having similar lithologies. The early/middle Miocene (~16-13 Ma) Batesfordian - Lower Balcombian Unit (McGowran 1978a, 1978b, Lindsay 1981) of the Port Willunga Formation was deposited as a sandy limestone with quartzose, calcarenitic, sparsely glauconitic clayey limestone to calcarenitic clay and sandy clay (Lindsay 1981) possibly in a shallow water environment. The middle to early Miocene Munno Para Clay Member is the upper most section of the Port Willunga Formation, which was deposited in a restricted marine environment, mainly associated with sea level fluctuations (McGowran 1978a, Lindsay 1981). These fossiliferous limestones with grey and blue clays, but without coarse sediments were interpreted by Tokarev (2005), as indicators of low magnitude block movements in the western portion of the Mount Lofty Ranges, causing limited erosion on the low and undulating landscape.

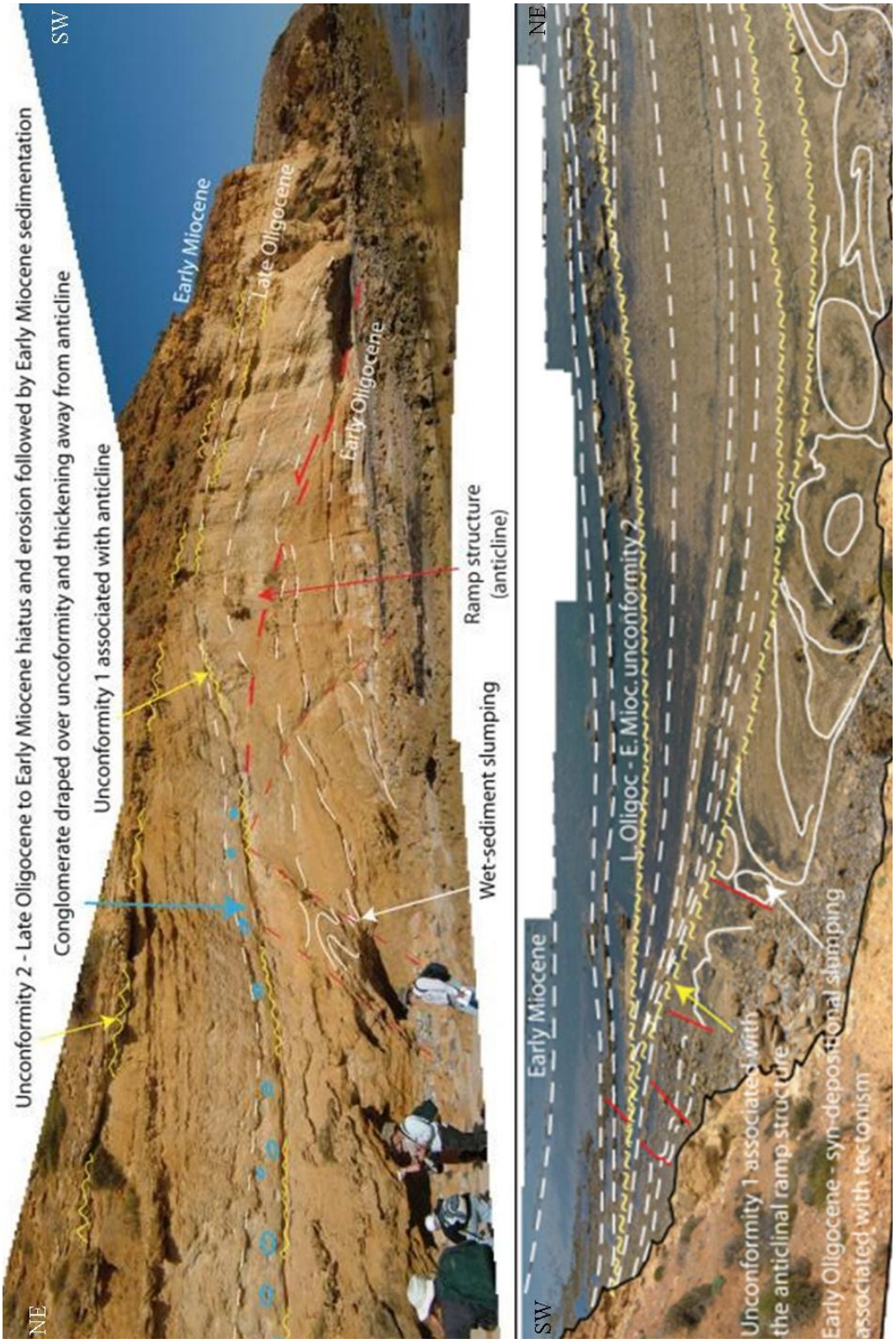

Figure 3.3 *An illustration of the unconformities within the Port Willunga Beds on (a) the cliff faces and (b) shoreline platform, south of the Willunga Fault contact. Location coordinates: 266650 E, 6084700 S*

3.2.3 Hallett Cove Sandstone

Hallett Cove Sandstone mainly outcrops in the present coastal zone of the Willunga Embayment to the Adelaide Plains, displaying fine-grained sands interbedded with bands of calcareous quartz sandstone or sandy limestones (Reynolds 1953). It also contains abundant marine fossils and at some locations interfingers with the upper parts of the fossiliferous shelly sand unit known as the Dry Creek Sand (Ludbrook 1961). Occasional pebbles and boulder clasts at the base of the Hallett Cove Sandstone has been recorded by Sprigg (1942), who described the unit as pale grey/brown coarsely quartzose calcareous sandstone with fossils. Deposition during the Pliocene (~5.5-2 Ma), in a shallow marginal marine environment with warm transgressive episodes (possibly before the late Neogene or Quaternary ice ages in the Pliocene, ~3 Ma) is inferred for this unit (McGowran 1978a, 1978b, Lindsay 1981).

Due to erosion, weathering and karstification, the distribution of the Hallett Cove Sandstone in the Adelaide region is uneven and the thickness of the unit varies from several centimetres to a maximum of ~12 m (Lindsay 1981). The irregular and insignificant thickness of the unit could also indicate that sediment supply during the late Pliocene was inconsistent. The Hallett Cove sandstone is not visible near the Willunga Fault contact at Waterfall Gully.

3.2.4 Burnham Limestone

The late Pliocene to early Pleistocene (~2.6 Ma), poorly fossiliferous, thin and crumbly Burnham Limestone (Firman 1976, Ludbrook 1983) resides on top of the Hallett Cove Sandstone in the stratigraphic sequence. The depositional ages of the Burnham Limestone samples from Kangaroo Island has been calculated as ~1.2 Ma (Belperio 1995), but as it straddles the Pleistocene/Pliocene boundary it is more likely to be 2.6 Ma old (Pillans & Bourman 1996). The unit is described as a white, pale grey, silty limestone and calcareous clay with sand and clasts derived from the underlying Hallett Cove Sandstone (Firman 1976). Deposition of the early Pleistocene Burnham Limestone possibly occurred in a shallow marginal-marine (Lindsay 1981, Ludbrook 1983) environment, marking the final episode of marine

sedimentation for the region (Firman 1976, Lindsay & Alley 1995). The soft, fossilliferous marl was deposited in a lagoonal environment (May 1992). The thickness of the unit varies from ~0.5 to 1 m in the Willunga Embayment (Firman 1976). The Burnham Limestone outcrops ~8 m above sea level on the coastal cliffs, disconformably overlying the Port Willunga Formation near the Sellicks Beach land-slump, few hundred metres north of the Waterfall Gully thrust fault contact. However, the unit could not be observed in the immediate neighbourhood south of the Willunga Fault exposure.

3.2.5 Seaford Formation

The earliest Pleistocene (~2.6-1.8 Ma) Seaford Formation (Ward 1966), consists of greenish-grey clayey fluviatile moderately to well bedded sands with orange mottles (Pillans & Bourman 1996). Fluvial sandy clays and consolidated sands inter bedded with pebble and gravel beds can be also observed. At Sellicks Beach the Burnham Limestone is overlain by the earliest Pleistocene Seaford Formation. This ~18 m thick unit interfingers with the Burnham Limestone near its base. It also coincides with the Matuyama Reversed Chron and the top of the Seaford Formation coincides with the base of the Jaramillo Normal Subchron (1070 ka).

3.2.6 Ochre-Cove Formation

The Seaford Formation is overlain by ~19 m of the middle Pleistocene Ochre Cove Formation (Ward 1966, Pillans & Bourman 1996) with an irregular erosion surface separating them. The Ochre Cove unit consists of red-orange, light-grey sandy clay with reddish-brown mottles and horizontally bedded alluvial sandstones (Ward 1966). The gravels and conglomerates within the Ochre Cove sediments were possibly deposited in warm and wet conditions of the middle Pleistocene (~0.8 Ma). It is prominently visible as a coarse-grained red-white mottled sandstone in the coastal cliffs (Fairburn 1998). May & Bourman (1984) noted that the Sellicks Beach sediments are dominated by the middle Pleistocene Ochre-Cove Formation, even though Fairburn (1998) does not report the existence of the sequence at Sellicks Beach.

The Ochre Cove Formation includes the Jaramillo Subchron (1070 to 970 ka) and the Brunhes/Matuyama Boundary (780 ka) (Pillans & Bourman 1996). Palaeomagnetism has used to reveal the tectonic disturbance of the strongly oxidized Ochre Cove Formation (Bourman & Pillans 1997) at Sellicks Beach and Cambrai due to reverse movements of the Willunga and Milendella Faults respectively.

3.2.7 Kurrajong Formation

Middle Pleistocene Kurrajong Formation (Ward 1966) underlies and merges with the lower boundary of the Ochre Cove Formation at Sellicks Beach. Yellowish-brown Kurrajong Formation is a lithified, brecciated unit, consisting of compact fanglomerates, gravels and clays which are commonly mottled with iron oxides and silica cement. Lithologies within the formation vary from talus deposits to alluvial fan deposits composed of clayey sandstone.

3.2.8 Ngaltinga Clay

Middle Pleistocene Ngaltinga Clay (Ward 1966, Firman 1967, Fairburn 1998) is visible at the top of the Ochre Cove Formation as a greenish-grey, olive-green sandy clay layer with ferruginous mottles. The origin of the Ngaltinga Clay has been variably explained as fluvial, with cross-bedding and gravel lenses (Phillips & Milnes 1988); aeolian (Ward 1966, Pillans & Bourman 2001) and by *in situ* weathering (Sheard & Bowman 1987). The Pleistocene (>0.5 Ma) age of this unit is discussed in detail by Pillans and Bourman (2001). Ngaltinga Clay is extensively developed in the Willunga Embayment with thicknesses commonly vary from ~14-10 m (Fairburn 1998).

3.2.9 Taringa Formation

Late Pleistocene Taringa Formation (Ward 1966) overlies the Ngaltinga Clay at Sellicks Beach, and represents an upper clay layer of the stratigraphic sequence. This greenish-grey clay shows columnar structure having angular clasts with calcium carbonates and considered to be a mudflow deposit or consolidated dune sand (Ward

1966). The Taringa Formation is very similar to Ngaltinga Clay and both of these formations contain the same heavy minerals (Ward 1966).

3.2.10 Calcrete unit

A thin calcareous unit of Pleistocene age (<0.5 Ma) overlies the Taringa Formation, and possibly covers the entire landscape (Reynolds 1953) due to its high preservation potential. Leaching and re-precipitation of calcium carbonate is a common process of soil development in semiarid environments, which produces calcrete. However, calcrete formation in coastal settings are hard to distinguished lithologically (Belperio 1988, Phillips & Milnes 1988).

A calcrete or lime-impregnated layer in the Sellicks region probably formed after marine retreat and during sea-level low stands, which exposed sedimentary surfaces of the nearby landscape. The carbonate blanketing Para and Eden-Burnside Faults was long recognised as a result of aeolian redistribution of marine, lagoonal and lacustrine carbonates of the St. Vincent Basin (Firman 1967, Selby & Lindsay 1982, Sheard & Bowman 1996).

3.2.11 Pooraka Formation

A distinctive red-brown sandy-silty clay deposit with inter-bedded layers of clay, sand and occasional lenses of gravels, pebbles, cobbles and boulders (Sheard & Bowman 1996) is known as the Pooraka Formation (Firman 1967, Belperio 1995). Bleached silty sand, reddish-brown clay with calcium carbonate nodules are observed within this unit, which overlies the calcrete layer at Sellicks Beach. The Pooraka Formation has a fluvial in origin and considered as equivalent of the Christies Beach Formation and the marine equivalent of Glanville Formation. The Pooraka Formation has been assigned a last interglacial age using optical luminescence dating (Bourman *et al.* 1997) and generally considered with an age range of ~132-118 ka (Bourman *et al.* 2010b). However, sections of this unit could be as young as late Pleistocene (~35-20 ka), due to its resurgence of alluvial and fluvial sedimentation possibly associated with marine isotope stage 3 (Williams 1973, Belperio 1995).

As stated in Tokarev (2005), the Pooraka Formation comprises the larger part of the extensive flangomerate deposits in the Murray Basin. This colluvial and high level alluvial deposit includes gravel and sand, clayey sand and clay with residual material from the weathered basement. It is considered as the result of an erosional response to a major uplift since middle Pleistocene, on the eastern side of the Mount Lofty and Flinders Ranges, (Tokarev 2005). Moderate to very high depositional rates were inferred from the depositional duration of the unit (~ 10,000 years) on the western flanks of the Mount Lofty Ranges (Belperio & Bateman 1986). This demonstrates the active erosion as a result of ongoing growth of the ranges in the late Pleistocene (Tokarev 2005).

3.2.12 Interstadial un-named Marine Isotope Stage 3 deposit

A large erosional hiatus of ~120 ka separates the last interglacial Pooraka Formation and the mid Holocene Waldeila Formation. However, a disconformable contact between a light-grey alluvium deposit that cuts into the Pooraka Formation at Sellicks Creek suggests a pulse of sedimentation prior to deposition of the Waldeila Formation (Bourman *et al.* 2010b). This fluvial unit with a limited distribution in southern South Australia has an inferred depositional age of ~50 to 30 ka (Bourman *et al.* 2010b). The fluvial unit between last interglacial Pooraka Fromation (~125 ka) and the mid Holocene Waldeila Formation (~6-4 ka) has been dated in the Burra Creek and in the trench of the River Murray as a Marine Isotope Stage 3 deposit. Pledge *et al.* (2002), reports the presence of this unit on both sides of the Mount Lofty Ranges, revealing the extent of the corresponding pluvial event.

3.2.13 Waldeila Formation

The Waldeila Formation (Ward 1965, 1966) overlies the Pooraka Formation at Sellicks Beach. It is identified as a dark grey alluvial unit forming low level terraces and floodplain deposits. Radiocarbon (Dury 1964, Bourman *et al.* 1997) and amino acid racemisation dating (Kimber & Milnes 1984) has determined the Waldeila Formation to be of mid Holocene age (~6-4 ka),whereas OSL ages of ~3.5 ka has been obtained a valley fill near Sellicks region (Bourman *et al.* 2010b). The Waldeila

Formation is regarded as the equivalent of the marine St. Kilda Formation and has an extensive distribution in the Noarlunga and Willunga Embayments. Nevertheless, Post European Sediment Aggradation (PESA) deposits and modern soils blanket most of the Waldeila Formation in Sellicks region at present.

3.3 Characteristics of faulting

Active faulting has had a marked influence on the landscape evolution of the Mount Lofty and Flinders Ranges (Sprigg 1945, Tokarev *et al.* 1999, Sandiford 2003a). The neotectonic Willunga Fault on the western flank of the ranges strikes inland towards the northeast and north over a distance of some 30 km. Some investigators regarded the Willunga Fault as a normal fault on the basis of the sedimentary unit thicknesses of the hanging wall (Lemon & McGowran 1989). However, the majority of the interpretations suggested that it is a high angle thrust fault (Sandiford 2003a), given that the range-bounding faults in the Mount Lofty and Flinders Ranges are likely to be reverse in nature as a result of E-W compression. Tokarev (2005) described the Willunga Fault as reflecting different stages of faulting, with extensional normal faulting and compressional reverse faulting regimes operating during the Neogene and Quaternary respectively. However, most of the interpretations are based on limited field observations, with no systematic collection of offset data and fault kinematics.

Steep east-dipping reverse faulting has been observed where Cambrian sedimentary rocks have been thrust against Quaternary sediments at Sellicks Beach (Sprigg 1945, Sandiford 2003a). The upward tilted middle-Pleistocene Ochre Cove Formation (May & Bourman 1984, Pillans & Bourman 1996, Bourman & Pillans 1997) near the Willunga Fault Zone is a significant feature that demonstrates tectonism during the Quaternary. Cactus Canyon and Waterfall Creek at Sellicks Beach are two locations where high angle reverse faulting is well exposed. From fault orientations and the spatial existence of the exposures, they can be considered either the main Willunga Fault, or major splays of the fault system. Despite the similar reverse motions displayed, Tokarev (2005) interpreted them as spatially disconnected. This suggests

that, rather than a single master fault, several reverse fault splays collectively form the differential topography of the Willunga Embayment.

Post-Eocene to pre-Pleistocene movements are implied by the disrupted stratigraphic sequences adjacent to Willunga Fault (Howchin 1911). Oligocene to early Miocene marine erosion has moulded the uniform summit surface of the Sellicks Hill. The western side of Mount Lofty Ranges was active during the initial middle-late Eocene crustal segmentation (Tokarev 2005), but the rates of this deformation are not available. According to Tokarev (2005), this was followed by landscape relaxation and a second phase of reverse compressional reactivation during the Quaternary, along the Neogene normal faults. Post-middle Pleistocene Quaternary compressional movements (May & Bourman 1984, Bournan & Lindsay 1989), accounts for vertical displacement rates of at least 50-70 m/Ma on the Willunga Fault according to Sandiford (2003a). The current study has recorded structural data on the exposed faults in Sellicks Beach region, with both location and kinematic information (Appendix I) used to determine the nature and rates of deformation.

A close approximation of the total displacement across the Willunga Fault can be computed from the elevation of the Port Willunga Beds across the Willunga Fault and along the western shoreline of Fleurieu Peninsula (Figure 3.4). For example, the Early Miocene Port Willunga beds, which are ~200 m below sea level in the Adelaide area, reach sea level just north of the Willunga Fault at Sellicks Beach and reach elevations up to ~240 m in the Myponga Basin (May & Bourman 1984), which is some 12 km south of the fault exposure. The same age sediments of the Port Willunga Beds occur ~30 m below and ~60 m above sea level elsewhere in the Willunga Embayment (Cooper 1979). Similarly, the Pleistocene Burnham Limestone (Pillans & Bourman 1996) varies in elevation from ~82 m below sea level at Port Adelaide, ~17 m above sea level at Marino, ~30 m at Hallett Cove, ~20 m at Maslin Beach, ~15 m at Port Willunga, ~8 m at Sellicks Beach (May & Bourman 1984) and the time-equivalent Port Ellen formation is ~60 m above sea level at Cape Jervis (Belperio 1995, Bourman *et al.* 1999).

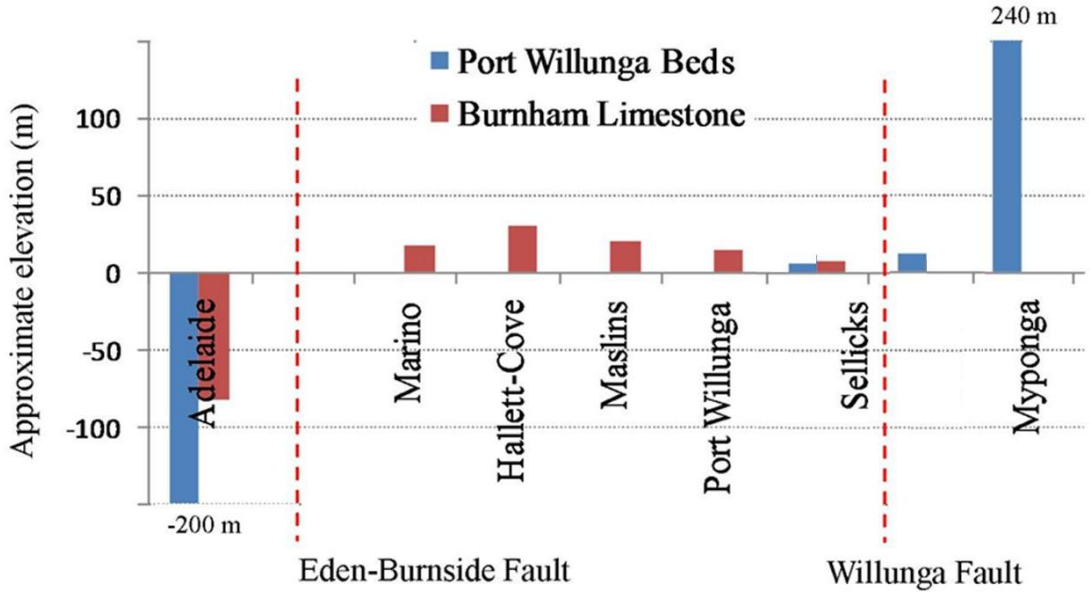

Figure 3.4 *Elevations of two of the prominent marine sedimentary units along west coast of the Fleurieu Peninsula expressing the dislocations due to active faulting (x axis not to scale)*

The distribution of Neogene units indicate the extent of deformation on the Sellicks Beach region due to the active Willunga Fault (Howchin 1911). The flat lying Ochre Cove Formation on the footwall has been draped and tilted upward towards the fault, indicating a reverse or thrust sense of motion after their deposition (Figure 3.8a). The Cambrian sedimentary rocks are unconformably overlain by Oligocene-Miocene units and Pleistocene gravels (Lemon & McGowran 1989, Quigley *et al.* 2010). After examining the progressive disconformities within the late Palaeocene to Pleistocene sedimentary units, Lemon and McGowran (1989), suggested at least an Oligocene origin for active faulting. Basement rocks in contact with younger terrestrial units, such as the Seaford, Ochre Cove, Ngaltinga, and Pooraka Formations, provide evidence of multiple deformational episodes during the Quaternary Figure 3.8b. Post middle Miocene uplift in the order of 100 m is estimated for the Mount Lofty and Flinders Ranges (Lindsay 1986, Bourman & Lindsay 1989). At a regional scale, from the available coastal stratigraphic marker units along the western side of the South Mount Lofty Ranges on Fleurieu Peninsula (Figure 3.4), it is possible to demonstrate more than 200 m of vertical offset on the Willunga Fault during the Cenozoic.

3.4 Investigation techniques and results

Detailed studies of the fault exposures at the Sellicks site provided essential baseline data to characterise the nature of local deformation and to establish a comprehensive framework in order to establish a better understanding of the driving mechanisms of intraplate crustal deformation in South Australia.

3.4.1 Sellicks geology and geomorphic implications

Although geological studies in the Willunga Embayment extend over more than a century, a detailed geology map of the Cenozoic sediments is lacking (Fairburn 1998). The amount of detailed information displayed on most of the available maps is restricted due to limitations of scale. To overcome this problem, a detailed geology map was constructed for the Sellicks area, based on this present work (Figure 3.6 & Appendix I), in which emphasis was placed on the Neogene and Quaternary geology near the Willunga Fault exposure. The map which has a scale of 1:1500 covers the Willunga Fault exposures and its neighbourhood, where the fault runs offshore at Aldinga Bay. The geology map was created using the ESRI ArcGIS program, with the help of field data and a NearMap satellite image, which provided background details.

An oblique view of the Willunga Fault exposure (Figure 3.7) indicates the dislocation of the stratigraphic units due to movements of the fault. The relative elevations of these units with regard to the past sea levels constrain the uplift or subsidence of the region. The map is useful to identify the change of Cenozoic units across the Willunga Fault and approximate the plausible fault movements from the known stratigraphic ages. Description on the different stratigraphic units is documented in section 3.2 with a summary on Figure 3.5. In order to avoid complexity, the details of geology and stratigraphical units are limited to the Cenozoic, unless considerations of older units are necessary for discussion.

Late Neogene and Quaternary stratigraphic units have been offset across the fault zones and dislocation of Miocene and earliest Pleistocene marine sediments on Fleurieu Peninsula can be attributed to ongoing tectonism (Bourman *et al.* 1999,

Bourman & Murray-Wallace 2002). The only Cenozoic marine unit present at the site is the Oligocene-Miocene Port Willunga Formation, which is overlain by terrestrial units. The Miocene Port Willunga Formation is exposed on the shoreline platform as a generally, flat-lying or gently undulating unit with the uppermost beds outcropping at elevations of around 10 m above present sea level (a.s.l), to the north of Aldinga Bay and on the footwall of Willunga Fault. The beds of the Port Willunga Formation are gently folded and are not apparent towards the fault contact, possibly due to compressional forces. Closer to the Willunga Fault, the Port Willunga Formation begins to dip gently to the south, disappearing beneath sea-level and is covered with a thick pile of Quaternary alluvial sediments that have accumulated adjacent to the fault. South of the fault zone the hanging wall consists of up-thrusted bedrock. Port Willunga Formation re-emerges as a series of north-dipping beds outcropping on the shoreline platform south of the fault. An unconformable contact between the Port Willunga Beds and underlying bedrock has been tilted up to ~45^{o} due to tectonic movements in the underlying bedrock. In the coastal cliffs and the wave cut platform the formation is steeply upturned due to tectonism.

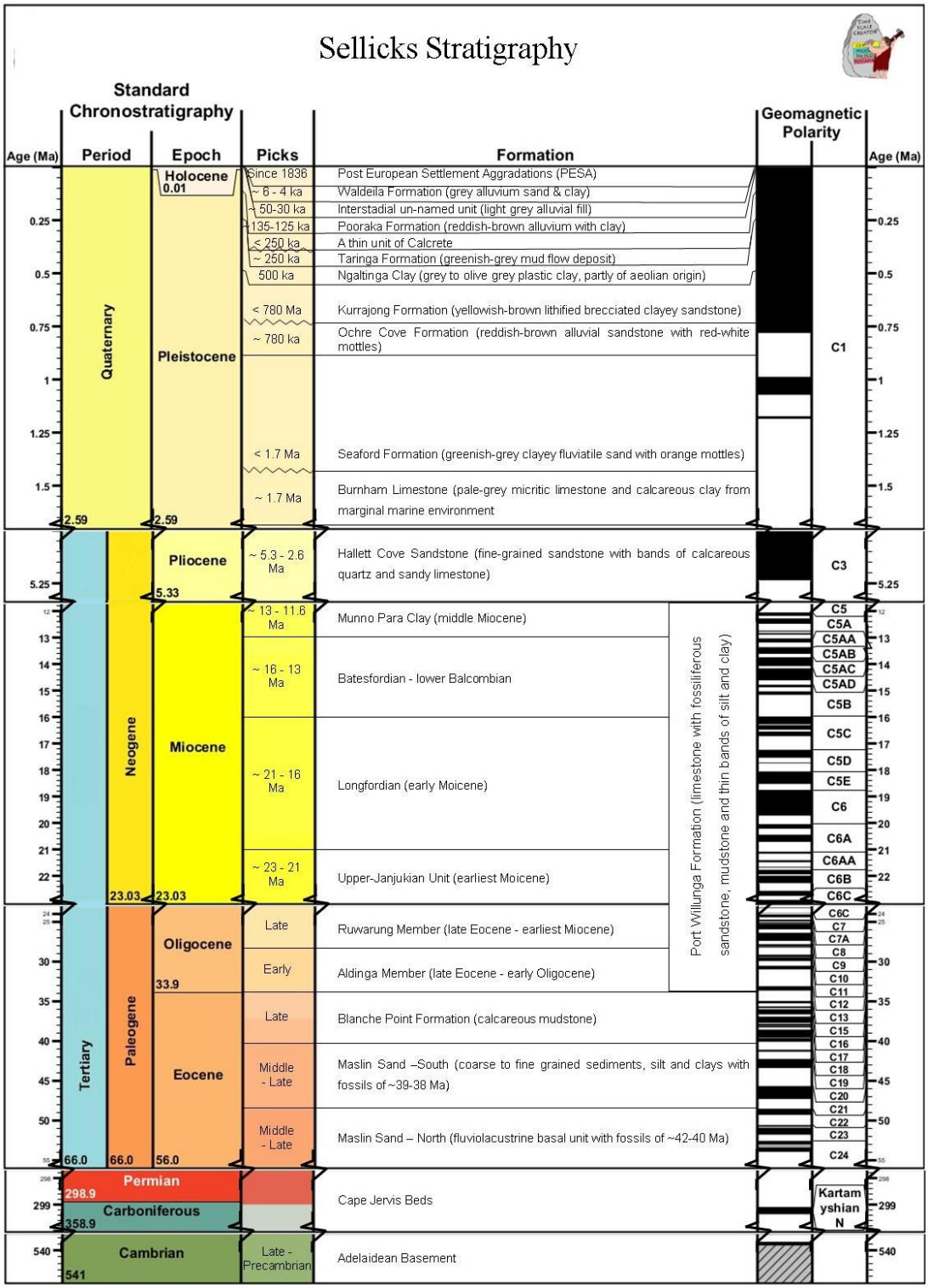

Figure 3.5 *Cenozoic stratigraphic sequences near the Willunga Fault at Sellicks region. Generated using the Timescale Creator program and the information from Ward 1966; May & Bourman 1984, Fairburn 1998, Pillans & Bourman 2001*

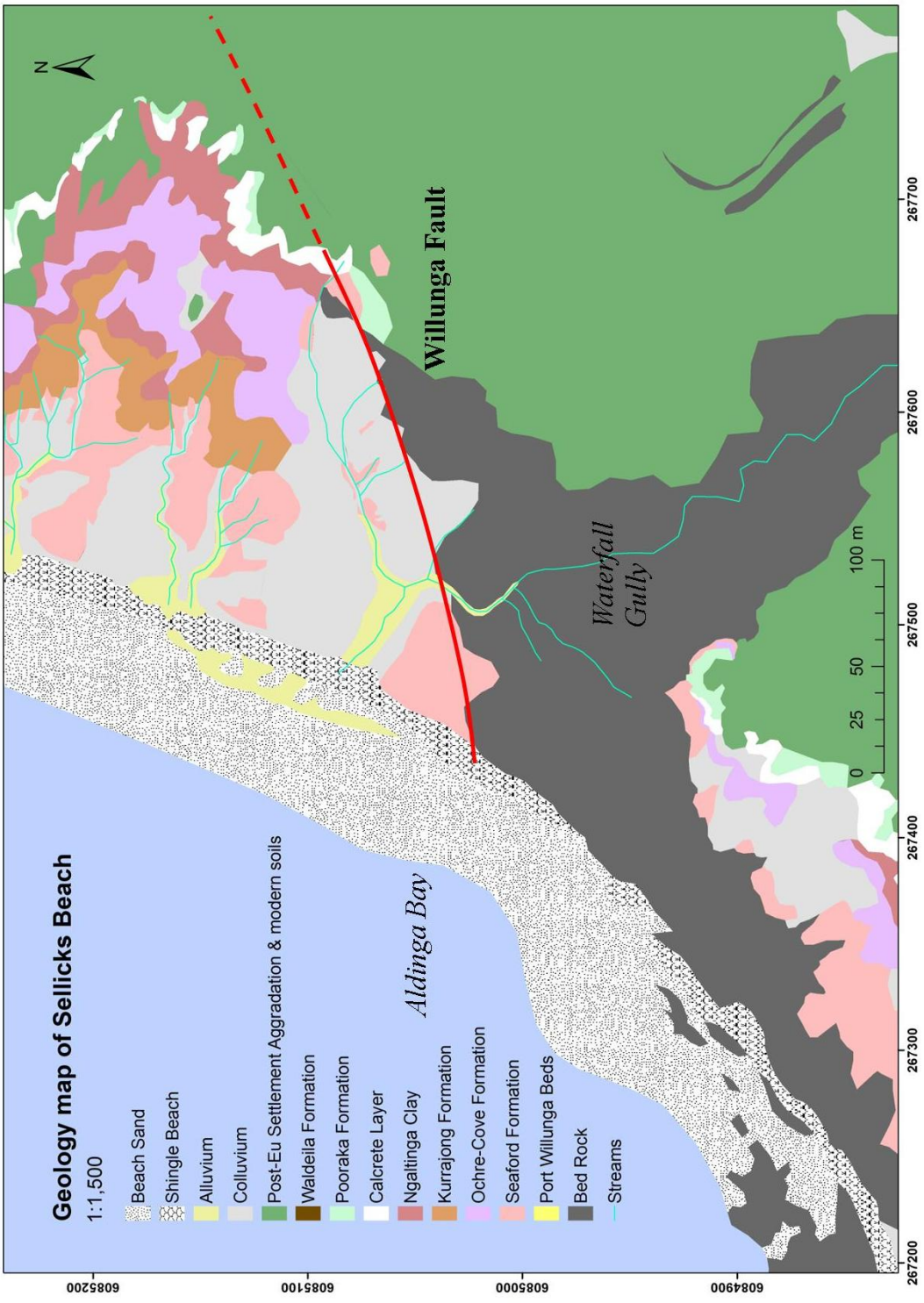

Figure 3.6 *Detailed geology map of Sellicks Beach (see also Appendix I)*

Figure 3.7 *An oblique view of the Willunga Fault showing stratigraphic dislocations*

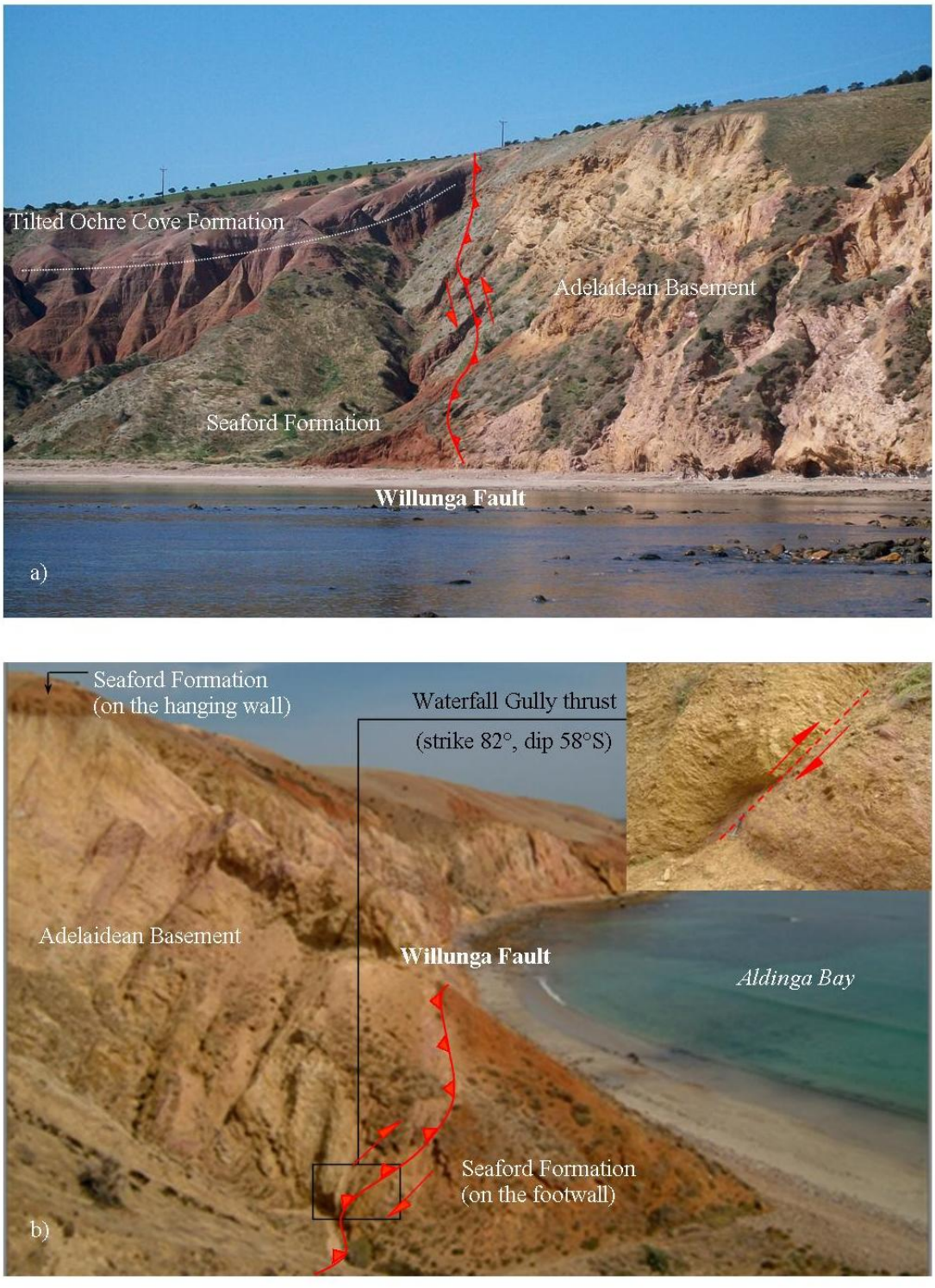

Figure 3.8 *Reverse fault at the Waterfall Gully, Sellicks Beach. a) Flat lying Pleistocene Ochre-Cove Formation on the footwall, tilted upwards as it reaches the fault contact at 267657 E, 6085098 S. b) Reverse fault outcrop in Waterfall Gully displaying Precambrian basement thrust over Quaternary Seaford Formation, at 267483 E, 6085036 S.*

May & Bourman (1984) documented tilted fanglomerates, due to movements on the Willunga Fault. Coarse sub-horizontal alluvial formations adjacent to the Willunga Fault, at Sellicks Beach, considered to be upper Pliocene to Pleistocene in age (Campana & Wilson 1953). The upper age limit for the most recent fault movement can be approximated at the lower depositional age of the oldest undisturbed sediments. On this basis, the Willunga Fault was active throughout the Pleistocene based on field observations of faulted Seaford Formation and tilted Ochre Cove Formation. It is not clear whether the Pooraka Formation has been deformed or if it is too unconsolidated to record the fault movements. However, gravel beds that appear to be similar to the Pooraka Formation have been warped into a gentle anticline, suggesting ongoing deformation (Figure 3.23). Furthermore, south of the Willunga Fault, the last interglacial shoreline platform has raised at ~4 m above present sea level (Murray-Wallace & Belperio 1991). It has developed prominent sea stacks on the shoreline platform (Figure 3.9) indicating an uplift of ~2 m since the last interglacial ~125 ka (Murray-Wallace & Bourman 2002).

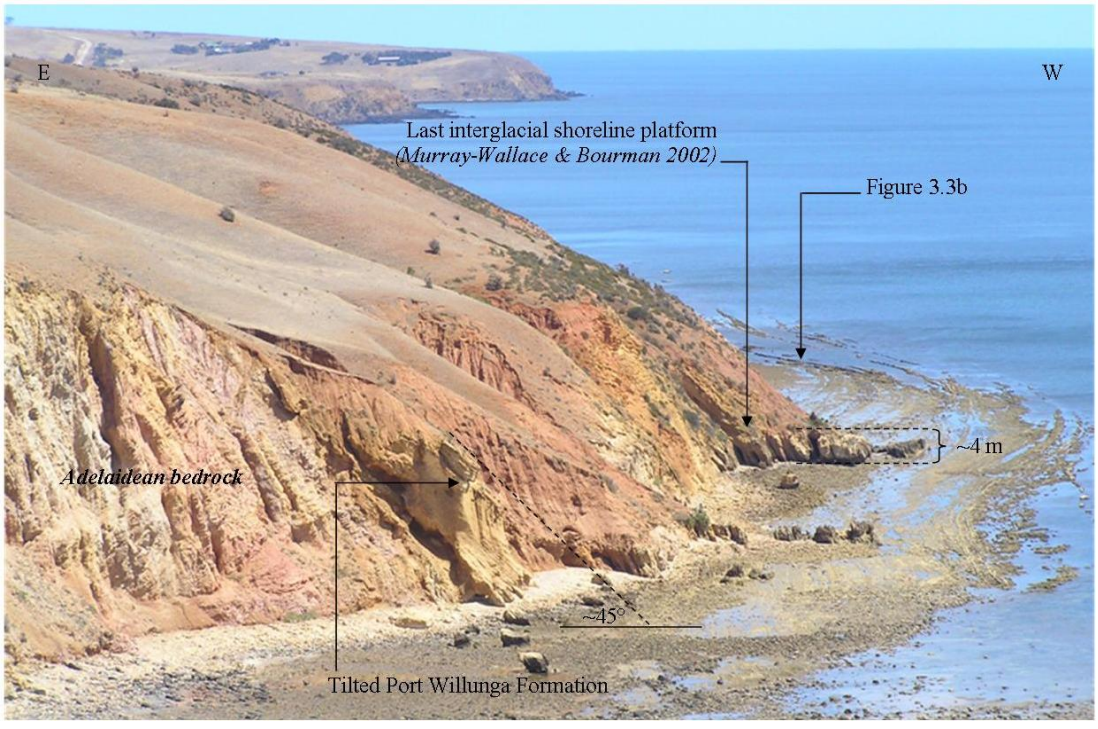

Figure 3.9 *The Port Willunga Formation exposed in the cliffs and shoreline platform, south of the Willunga Fault. The bevelled sea-stacks on the shoreline are overlain by last interglacial beach gravels and shells, residing ~4 m asl (source: Murray-Wallace & Bourman 2002)*

3.4.2 Structural data

Range-bounding faults on the western side of the Mount Lofty Ranges were sometimes considered to be normal, with Cenozoic sediments deposited on the downthrown block on a half-graben structure (Benson 1911, Fenner 1930, Sprigg 1945). The illusion of normal faulting can be observed, even at Sellicks Beach, closer to Aldinga Bay, where the embayment stratigraphy indicates down dip movement of the northwestern-block, which is covered with Pleistocene terrestrial sediments. However, further observations of fault outcrops have confirmed reverse or thrust movement where the hanging wall basement rocks have been thrown over a footwall of Quaternary units (Lemon & McGowran 1989, Clark & McCue 2003, Hillis *et al.* 2008). The exposed high angle thrusts of the Willunga Fault at Cactus Canyon and Waterfall Gully, surrounded with several low to high angle secondary thrusts (Appendix I), illustrates that the movements could be complex rather than simple dip-slip faulting.

Detailed structural mapping of fault exposures and the recording of kinematic indicators, such as slickensides, were undertaken to construct a better picture of the neotectonic activities in the Sellicks Beach region. Recording of the structural features were conducted according to the techniques outlined by Marrett and Allmendinger (1990) and Dumont *et al.* (2005) during several visits to the sites. They are presented in tabular format with location coordinates in Appendix I. The spatial coordinates for the structural geological features were recorded using a Garmin hand held GPS (model: GPS72 Personal Navigator) which has an accuracy of ~15 m (Garmin 2002). The structural data were plotted in stereonets to identify trends of faulting and links with the local geomorphology. The equal area stereoplots were constructed using the GEOrient and GEOCalculator programs of Holcombe (2009). Pole plots were contoured according to the floating circle contouring method.

3.4.2.1 Reverse faults

Major reverse faults (Figure 3.8 & Figure 3.11) were observed at Waterfall Gully (striking ENE-WSW) and Cactus Canyon (striking NE-SW), on the banks of the two creeks that flow towards the shoreline of Sellicks Beach near Aldinga Bay. The

remaining reverse faults were recorded on the hanging wall side of the identified Willunga Fault, with the majority striking ENE-WSW. The orientation of these secondary thrust faults implies they would have been a result of local N-S to NNW-SSE compression. These observations complement the NW-SE maximum horizontal stress orientations derived from a limited local stress-field data (Reynolds 2001), and differ from the widely accepted E-W regional compression for the Mount Lofty Ranges (Sandiford 2003a). Equal area (poles to the planes) stereoplot of the recorded reverse faults are given in the Figure 3.10.

3.4.2.2 Normal faults

Most of the normal faults were observed along the shoreline of Sellicks Beach (Figure 3.13). They were also visible on erosion gully banks and rarely on inland road cuttings. The majority of them have a strike direction of NNW-SSE, which is approximately orthogonal to the recorded reverse faults. Considering the trend of the normal faults, an ~E-W local extensional regime can proposed, instead of a compressional one. Equal area (poles to the planes) stereoplots of the recorded normal faults are given in the Figure 3.12.

3.4.2.3 Strike-slip Faults

Direct evidence for surface dislocations caused by the lateral movements of the Willunga Fault is hard to find. However, sub-horizontal slickensides (Figure 3.20) on some of the fault planes imply that their latest movements may not have been purely dip-slip. The neptunian-dykes observed within the unconsolidated sediments (Figure 3.15) could be considered as the openings due to the release of stress. The faults with sub-horizontal slickensides display a trend of NE-SW. Equal area (poles to the planes) stereoplots of the possible strike-slip faults are given in the Figure 3.14.

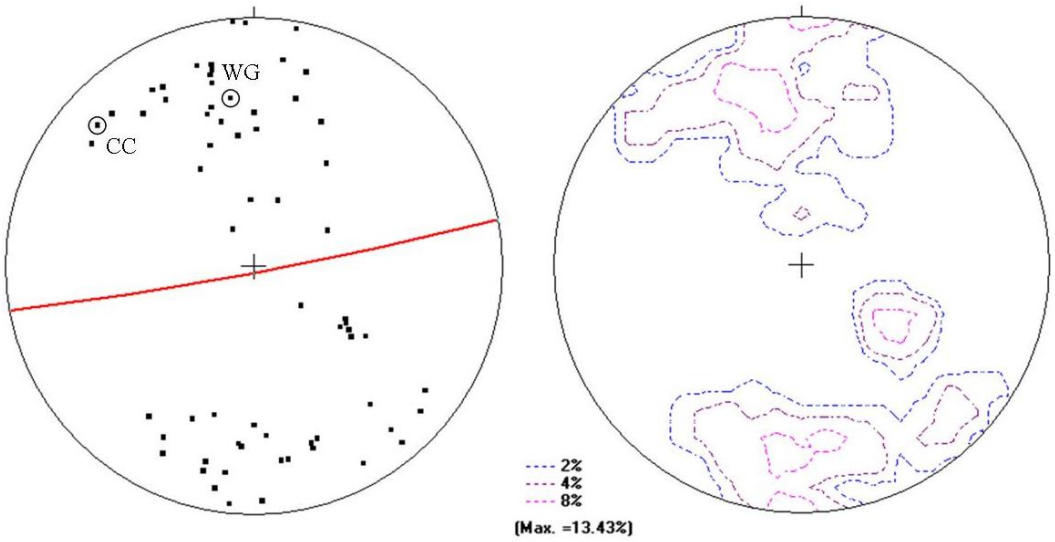

Figure 3.10 *Stereoplots of the reverse faults (CC- Cactus Canyon Fault, WG- Waterfall Gully Fault)*

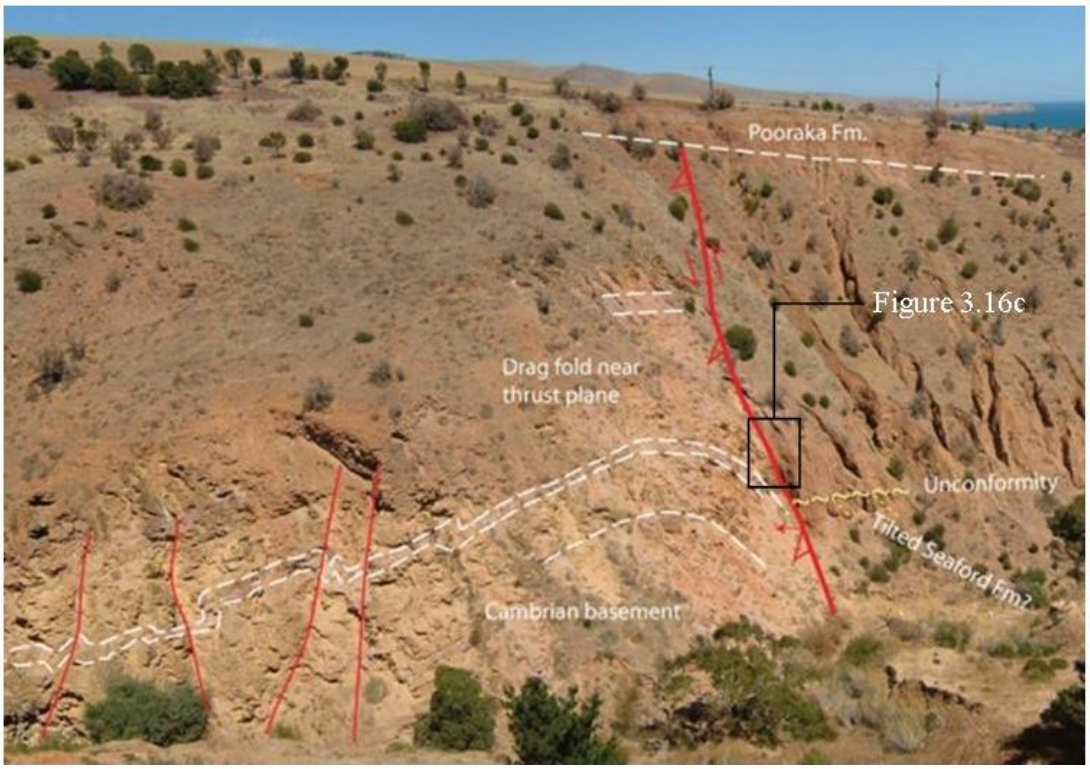

Figure 3.11 *The Cactus Canyon contact. Location coordinates 268135 E, 6085654 S (Photo taken towards SW)*

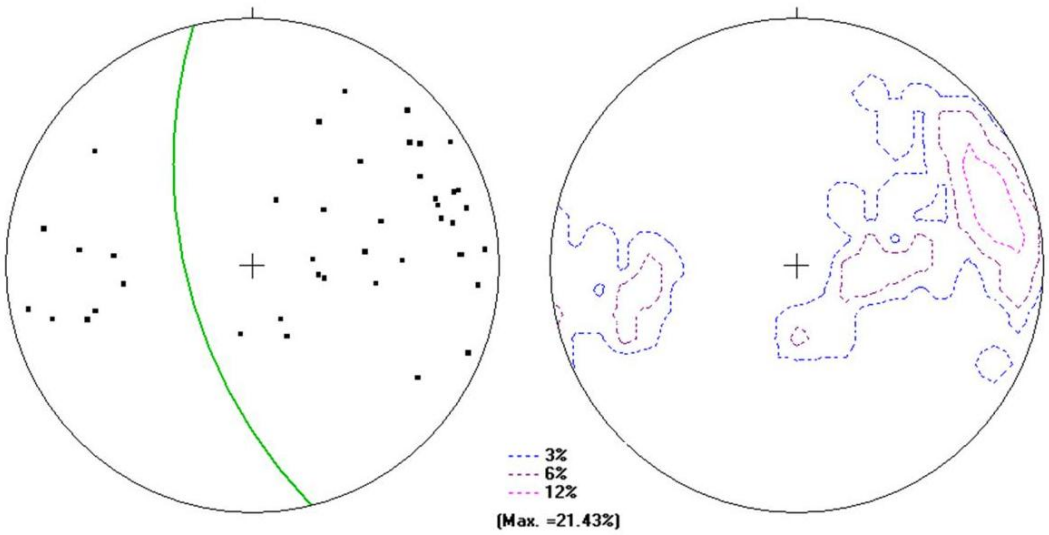

Figure 3.12 *Stereoplots of the normal faults*

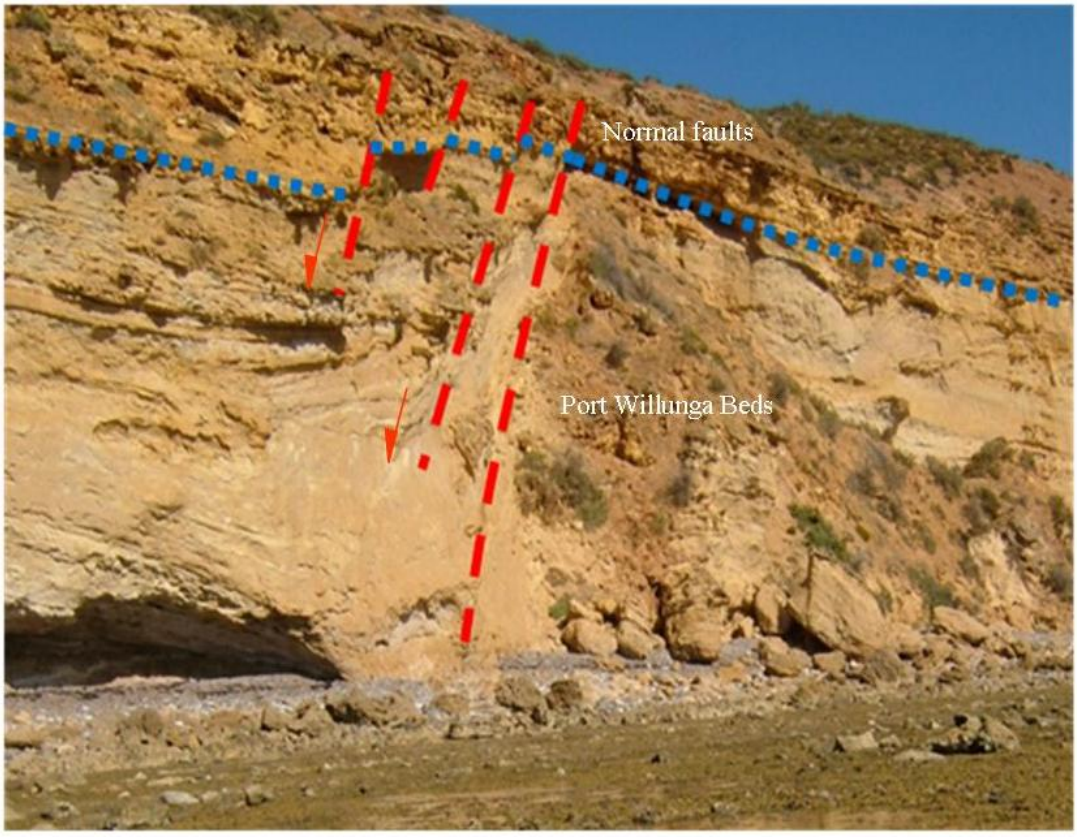

Figure 3.13 *Normal faults observed on eroded sea-cliffs of Tertiary Port Willunga Formation. Location coordinates: 266588 E,6084664 S*

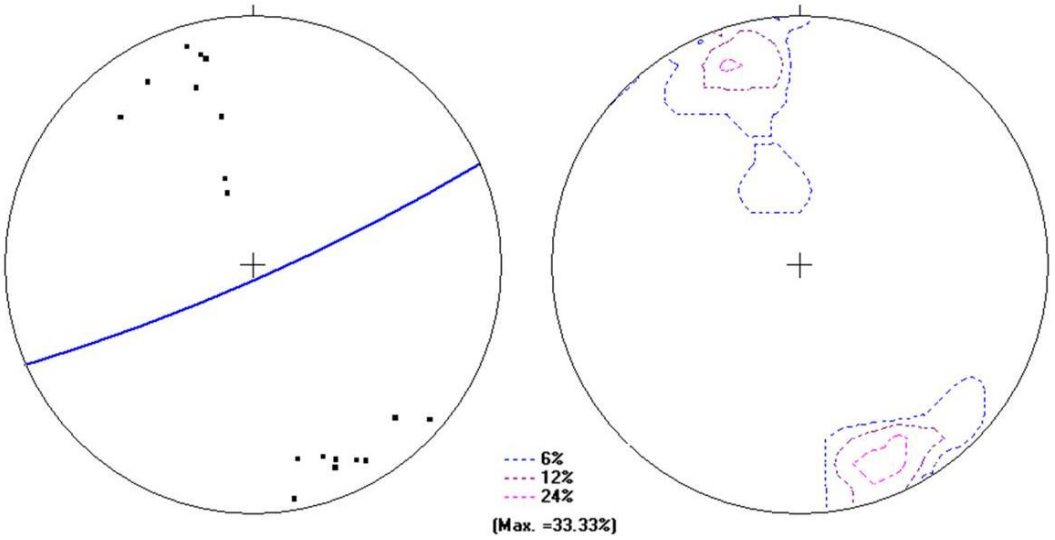

Figure 3.14 *Stereoplots of the strike-slip faults*

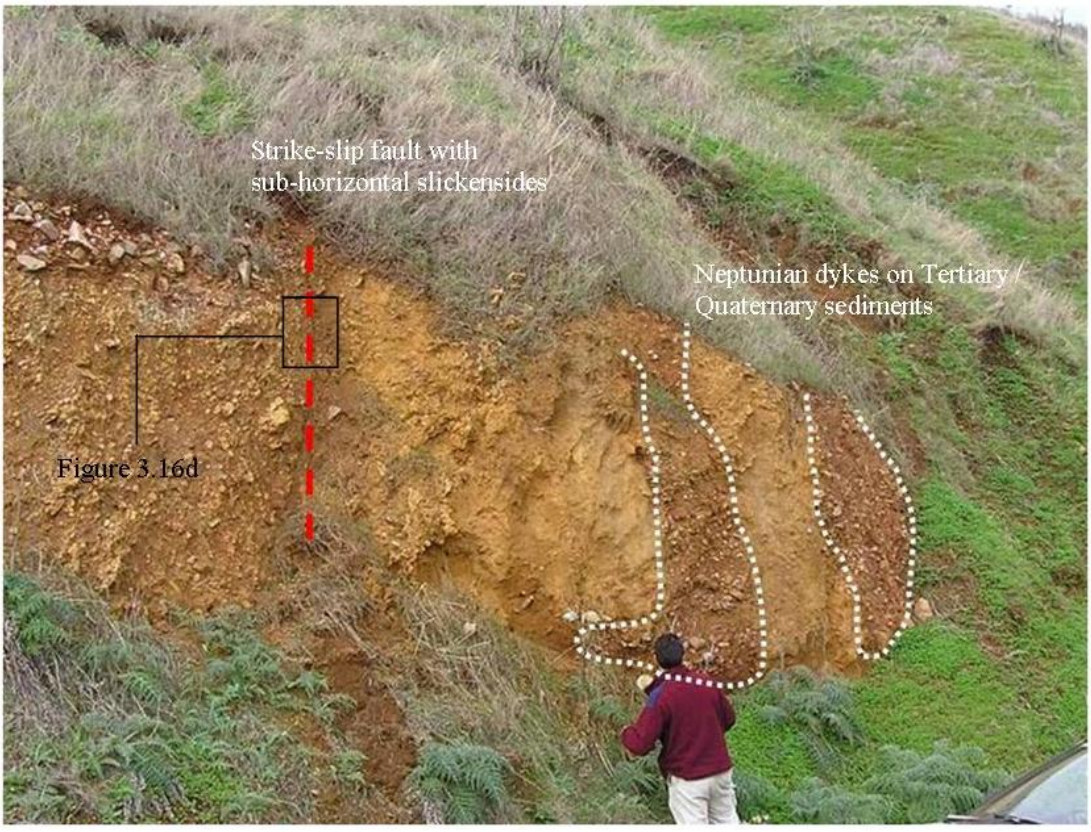

Figure 3.15 *A strike-slip fault with sub-horizontal slickensides showing left-lateral movements with neptunian dykes. Location coordinates: 267784 E, 6084802 S*

Types of fault	Reverse	Normal	Strike-slip
No of data points	69	45	18
Mean principal orientation	169/88	256/68	156/85
Principal eigenvector	2/349	22/76	5/336
Calculated girdle	079/81	348/86	066/84
Calculated beta axis	9-259	4-168	6-246

Table 3.1 *Summary of the structural data drawn on stereonets*

3.4.2.4 Bedding and Foliation

3.4.2.4.1 Port Willunga Formation

The bedding data of the tilted Port Willunga Formation was recorded mostly along the shoreline platform. The contoured pole population display a NNW-SSE compression with an ENE-WSW folding axis Figure 3.16. This is consistent with the compression direction indicated by the orientation of reverse faults shown in Figure 3.10 supporting the interpretation of a more NNW-SSE direction of maximum horizontal stresses, rather than E-W. Stereonet representation of the bedding readings of the Port Willunga Formation is as follows.

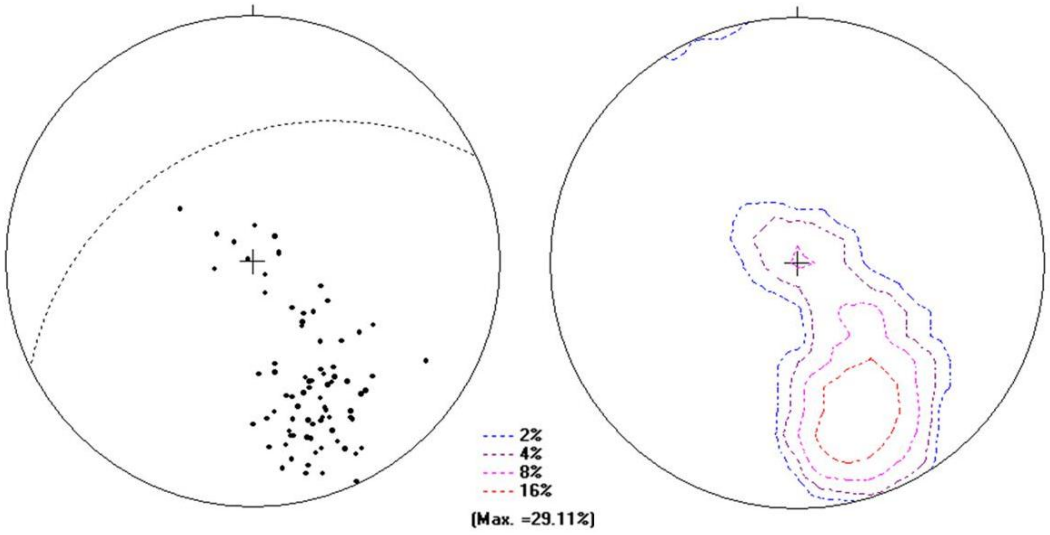

Figure 3.16 *Stereoplots of the Port Willunga Formation bedding*

Types of geological feature	Bedding on Port Willunga Formation
No of data points	83
Mean principal orientation	335/49
Principal eigenvector	41/155
Calculated girdle	069/85
Calculated beta axis	249-5

Table 3.2 *Structural information of the Port Willunga Formation bedding*

3.4.2.4.2 Precambrian basement rocks

Precambrian basement rocks in southern South Australia have experienced multiple episodes of deformation, including tight folding and faulting during the Delamerian Orogeny. Hence, the Precambrian basement structures may not significantly represent the neotectonic deformation in Sellicks region. Mainly, three sets of bedding planes dipping approximately towards SE, SW and NW can be extracted from the contoured pole population of the recorded structural data. The regional foliation in the basement is consistently vertical with a dip towards the NE and NW. A series of low angle foliations dipping towards the SE to SW also exists according to the stereoplot. The complexity of the observations could possibly be a result of experiencing significant refolding in the later stages of the Delamerian Orogeny. Stereonet representation of the pole plots for basement bedding and foliation are given in the Figure 3.17 and the Figure 3.18 respectively.

Types of geological feature	Bedding	Foliation
No of data points	87	115
Mean principal orientation	324/54	091/31
Principal eigenvector	36/144	59/271
Calculated girdle	064/76	325/71
Calculated beta axis	244-14	145-19

Table 3.3 *Structural information of the basement bedding and foliation*

Bedding of the basement

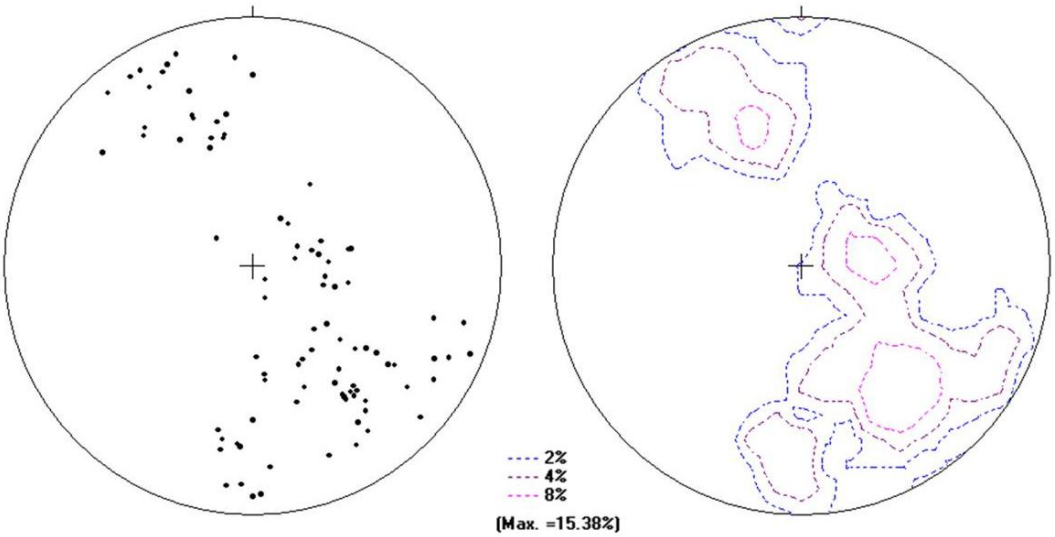

Figure 3.17 *Stereoplots of the basement bedding*

Foliation in the basement

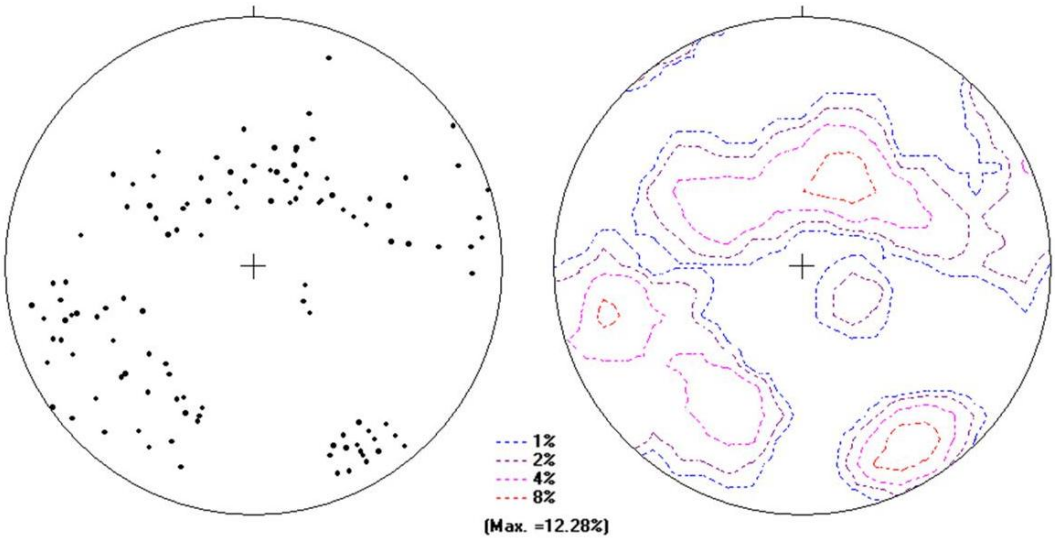

Figure 3.18 *Stereoplots of the basement foliation*

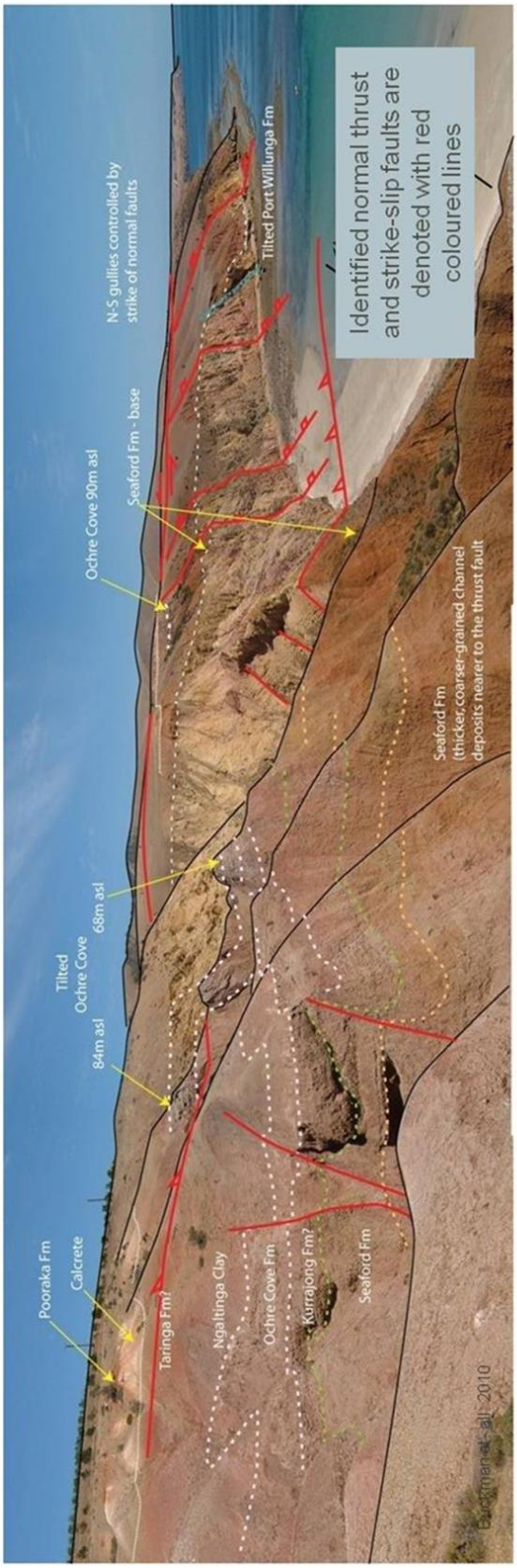

Figure 3.19 *Structural interpretation of the Sellicks Beach with evidence of neotectonism from Cenozoic stratigraphy (Source Buckman et al. 2010)*

3.4.3 Kinematic indicators

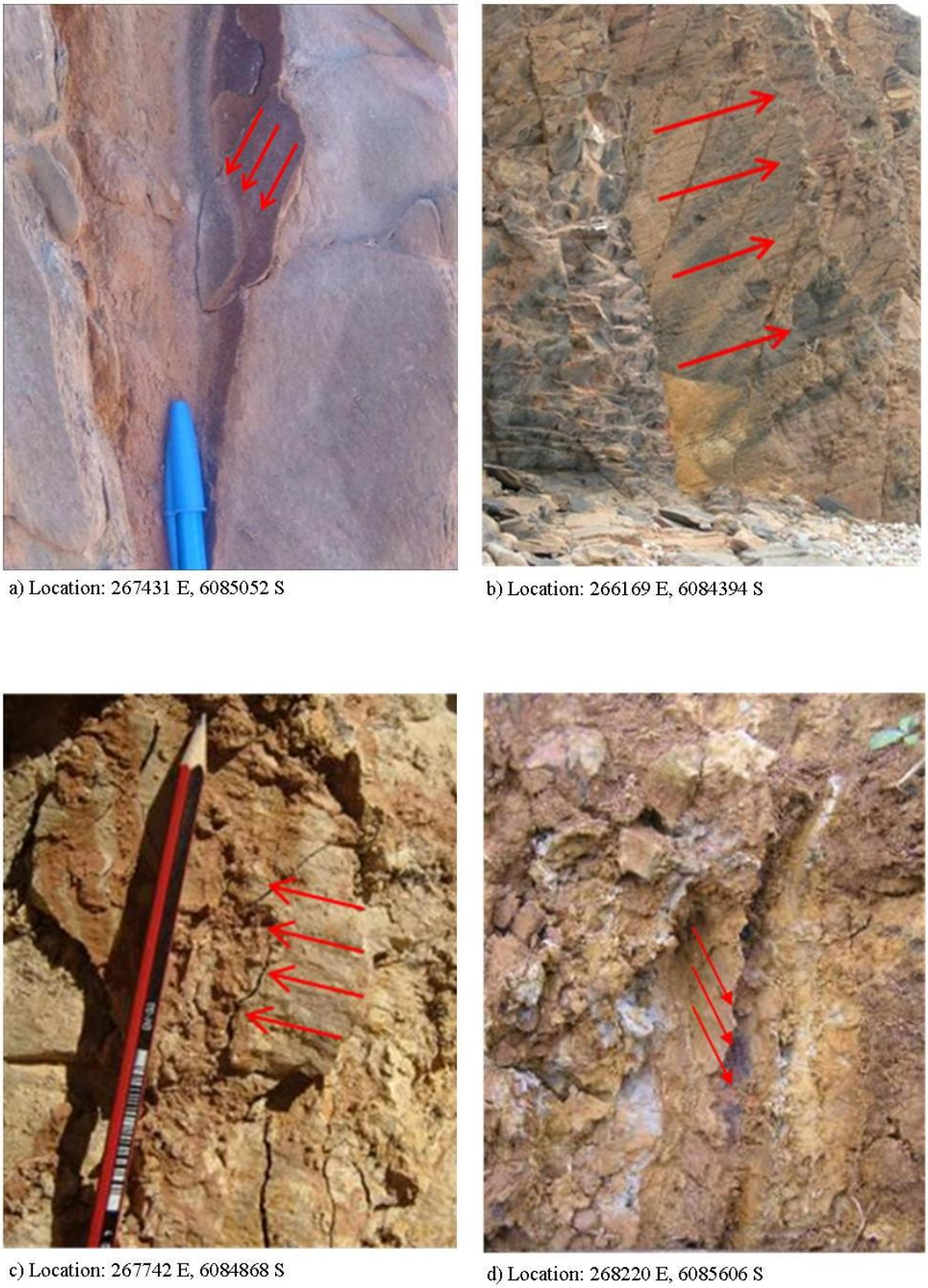

a) Location: 267431 E, 6085052 S

b) Location: 266169 E, 6084394 S

c) Location: 267742 E, 6084868 S

d) Location: 268220 E, 6085606 S

Figure 3.20 *Slickenside exposures showing evidence of horizontal movements at Sellicks Beach*

Slickenside information on the fault surfaces was recorded to determine the direction of the latest fault movements. For this purpose, the angle between the lineation and the strike line (rake) was measured in addition to the general dip and dip direction readings. GPS coordinates were noted at each location and some of the fault exposures have been photographed (Figure 3.20). Detailed information on the field records are given in Appendix I

3.4.3.1 Fault component diagram

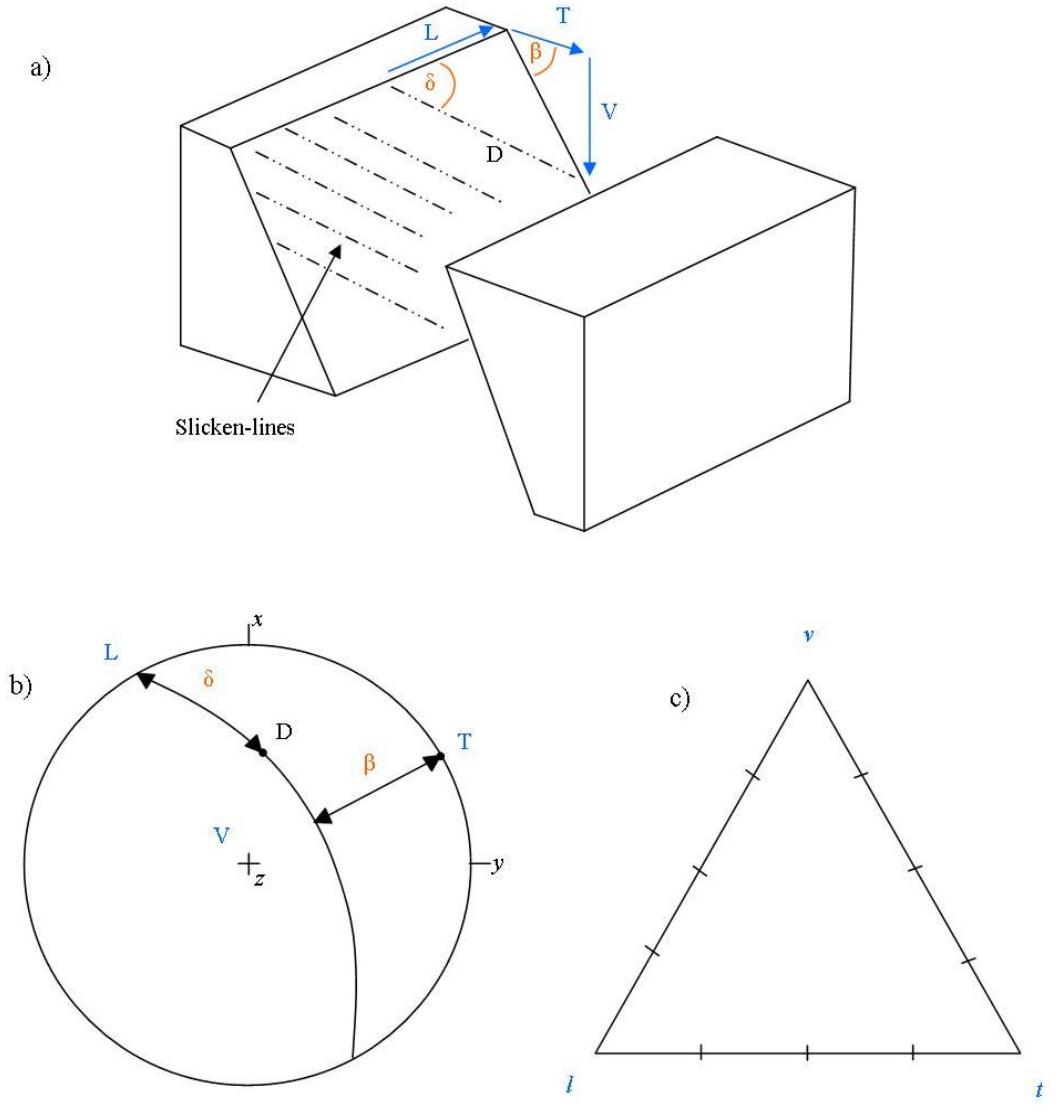

Figure 3.21 *Relationship between slip components, stereographic and tri-plot representation. a) Angular relationship between slip vectors, b) Stereographic representation of the slip components, c) Tri-plot representation of the slip vectors (source: Costa et al. 1997)*

Slickensides denote the slip vectors on the fault plane. By calculating the components of the slip vector in 3D space (i.e. in three perpendicular directions x, y, z) it is possible to determine the magnitudes of the vertical (z) and horizontal slip components (x, y) (Costa *et al.* 1997). The horizontal components, which are given by x and y, denote the lateral horizontal displacement (along the strike) and the transverse horizontal displacement (perpendicular to the strike, on the same horizontal plane). By assuming a unit vector, each of these three components can be drawn in a diagram making it possible to estimate the percentage contribution of each slip component to the absolute movement of a fault or a fault network (Costa *et al.* 1997). A fault component diagram is the graphical representation of the slip vectors and provides a way of quantifying movement of the fault in three directional components (Figure 3.21). Plotting those on a tri-plot can determine the dominant type of movement on a particular fault segment. The dip of the fault plane and the rake of slickensides are the inputs for this calculation, from which an interpretation can extend understanding of the total slip of a fault segment by knowing the offset along one of the components.

According to the Figure 3.21, L, T & V are the total slips in each direction;

Then,

$L = D.\cos \delta$
$T = D.\sin \delta.\cos \beta$
$V = D.\sin \delta.\sin \beta$

If we assume a total slip of unit length (D=1) the unit vectors in 3D (*x,y,z*) are given by (*l,t,v*) respectively;

$l = \cos \delta$
$t = \sin \delta.\cos \beta$
$v = \sin \delta.\sin \beta$
Where; $l^2 + t^2 + v^2 = 1$

The contribution of each of these components can be displayed via a fault component diagram to identify which is or what are the dominant fault behavioural patterns.

Where l, t and v denote the unit lengths of;

l – (Horizontal) lateral displacement
t – (Horizontal) transverse displacement
v – Vertical displacement

Field measurements of slickenside information from the Sellicks region can be distributed into respective fault components according to the above equations. Data table on Appendix I provides the results of computation with relevant spatial reference. The data was manipulated through the Microsoft Excel program, and the ternary diagram plotting software of Graham & Midgley (2000) was used to construct a fault component diagram.

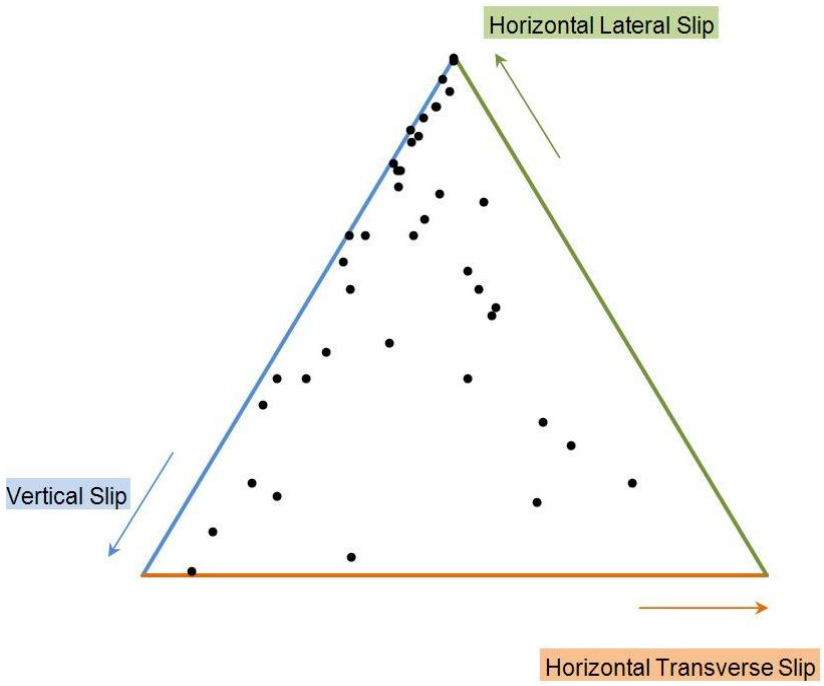

Figure 3.22 *Tri-plot representation of the slickenside data at Sellicks Beach* 3.16

According to the tri-plot (Figure 3.22), most of the data points are aligned towards the horizontal lateral (longitudinal) slip. It is being followed by the vertical slip and the horizontal transverse slip which has a handful of data points. Lack of horizontal transverse slip data denotes that the majority of the fault planes are steep so that the amount of shortening associated with the faulting was limited, in this particular region. The horizontal longitudinal slip, which is along the strike, shows dominant movements compared to the dip-slip component. This suggests that the recorded sub-horizontal slickensides may be a result of dominant lateral movements of the faults.

On average, one unit of oblique movement on the recorded faults would accompany displacements of ~0.7 on the horizontal longitudinal direction, ~0.3 on the horizontal

transverse direction and ~0.5 on the vertical plane. Hence, a fault slip ratio of 5:7:3 for vertical : horizontal lateral : horizontal transverse, can be approximated for the Sellicks region.

3.4.3.2 Compressional structures

The orientation of fold axes within Cenozoic sedimentary units records the orientation of compressional events subsequent to their deposition. This provides important long-term stress field data that is more consistent than one-off earthquake focal mechanism or bore-hole breakouts. Folded structures with an approximate NE-SW trending fold axis (Figure 3.23) were observed on the exposures of highly fractured bedrock and Cenozoic units. Compressional folding displayed on the Pleistocene Pooraka Formation on a sidewall of a road cutting, south-east of the Willunga Fault could only have occurred ~118 ka ago at the earliest, but is probably much younger. The observation of compressional structures within Quaternary sediments contradicts Tokarev (2005), who reported the absence of neotectonic folds as a result of the rigid pre-Tertiary basement.

Figure 3.23 *Compressional structures developed in Pooraka Formation showing ongoing deformation at Sellicks region. Location coordinates: 267665 E, 6084710 S*

Evidence of folding and faulting on basement structures could be seen at Sellicks region, on the cliffs south of the Willunga Fault contact as well as on the shoreline platform. The contribution of these older structures towards the neotectonic movements is uncertain, as some of them may be displaying the end results of multiple deformational episodes (Figure 3.24).

Figure 3.24 *Deformations within the basement fabric*

3.4.4 Topographic analysis using a LiDAR digital elevation model

The raw LiDAR strips were obtained from the Airborne Research Australia (ARA) in 2007. The data has a spatial resolution of ~5 cm and to obtain the smooth continuity among the stitched LiDAR strips, ~2 m vertical accuracy was maintained. The metadata-table of LiDAR strips are given in (Appendix I). ESRI's ArcGIS (version 10) was used as the main program to manipulate these high resolution images. Topographic contours at 10 m intervals were constructed using the LiDAR digital elevation model (DEM) to use as a base map for analysis purposes.

3.4.4.1 Stream profile analysis for knickpoints

Knickpoints are breaks in slope along the long profiles of valleys, some of which may be due to rejuvenation of the valley by progressive fault offsets. Several knickpoints were observed along the gullies across the Sellicks region. Mere field observations could not accurately determine which of those would have been created in conjunction with the nearby Willunga Fault. Topographic contours generated through the high resolution LiDAR image were used to determine the knickpoints and their spatial relationships with the fault trace. Potential knickpoints were identified from areas where the contours were very close and/or overlapped. Slopes greater than 60° (slope > 60°), were considered to be the knickpoints. A relatively higher value (60°) was selected as the minimum limit of the slope, in light of the steeply dipping Willunga Fault.

According to the above criteria, four locations (2 sets of slopes which are greater than 60°) were extracted from the LiDAR DEM as potential knickpoints (Figure 3.25). One of the identified slopes was a steep seacliff along the shoreline south of Aldinga Bay. Even though knickpoints may be generated from marine erosion, it is possible for a fault contact to facilitate and localise the process by creating a plane of weakness. The two sets of curvilinear faults, emanating from the main Willunga Fault as fault splays correspond with the identified knickpoints. As the knickpoints are on basement rock, they possibly represent progressive offsets produced by the repeated rupture events of the Willunga Fault.

The rate of knickpoint retreat may be associated with fault throw rates. In areas experiencing higher rates of uplift, the variations in channel width could largely explain the relationship between the knickpoint migration velocity and the rate of faulting (Whittaker & Boulton 2012). Erosion gullies developed due to stream channel incision is a common feature in the vicinity of the Willunga Fault in the Sellicks region. Most of them have a consistent flow direction of NW, and the depth increases rapidly due to the incision into bedrock within a few hundreds of meters along the path of the channel. The limited width of the channels observed through the LiDAR DEM could also infer higher rates of uplift. The knickpoints were identified as K1 to 4. Knickpoints K2 and K4 correspond with a gentle undulation of the

surface topography. Information extracted from the DEM on identified knickpoints are summarized in Table 3.4

Knickpoint	Elevation (a.s.l)	Upstream distance from fault contact	Height of the knickpoint	Channel width at the knickpoint
K1	~20 m	40 m	~18 m	~4.1 m
K2	~60 m	210 m	~10 m	~5.6 m
K3	~40 m	NA	>40 m	NA
K4	~70 m	NA	~8 m	~4.8 m

Table 3.4 *Knickpoint information extracted from the LiDAR digital elevation model*

3.4.4.2 Topographic cross sections

Several cross sections were produced using the LiDAR digital elevation model to extract the topographic features of the Sellicks region. These profiles were used to understand the relationship between the local topography and the active faulting. The representative cross section given in Figure 3.26 demonstrates the spatial distribution of the knickpoints and possible modes of faulting as reflected in disturbance of the local stratigraphy.

3.4.4.3 General approximation for stratigraphic offsets

Topographic contours generated through the LiDAR image were used to extract the approximate elevations of the stratigraphic sequences in the neighbourhood of the Willunga Fault contact at Waterfall Gully. The recently constructed 1:1500 geology map and a high resolution NearMap satellite image provided basemaps for this procedure (Appendix I). Approximate elevations displayed by the different stratigraphic units were recorded with respect to their bottom most exposure and are summarized in the Table 3.5

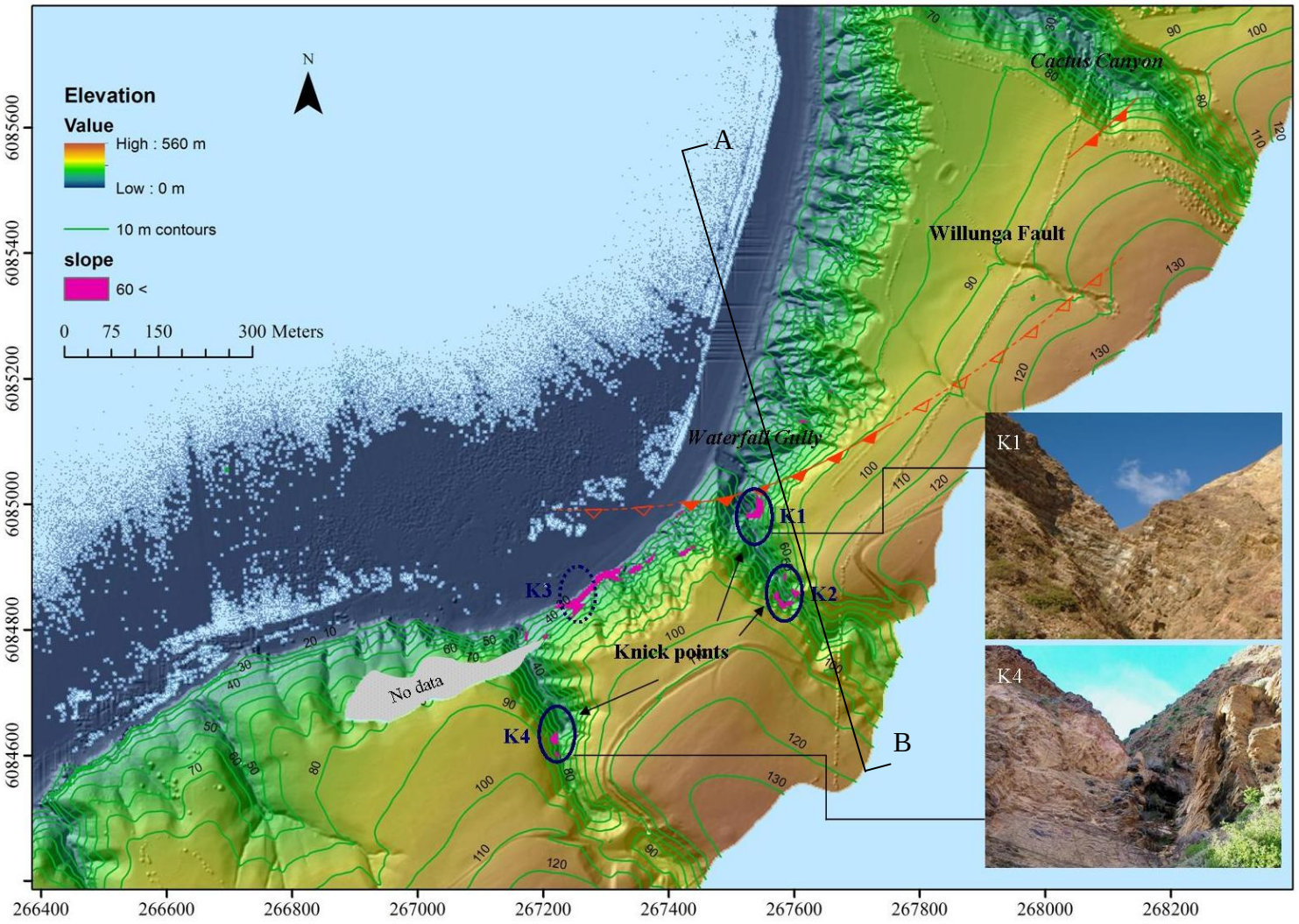

Figure 3.25 *Knickpoint retreat associated with the Willunga Fault*

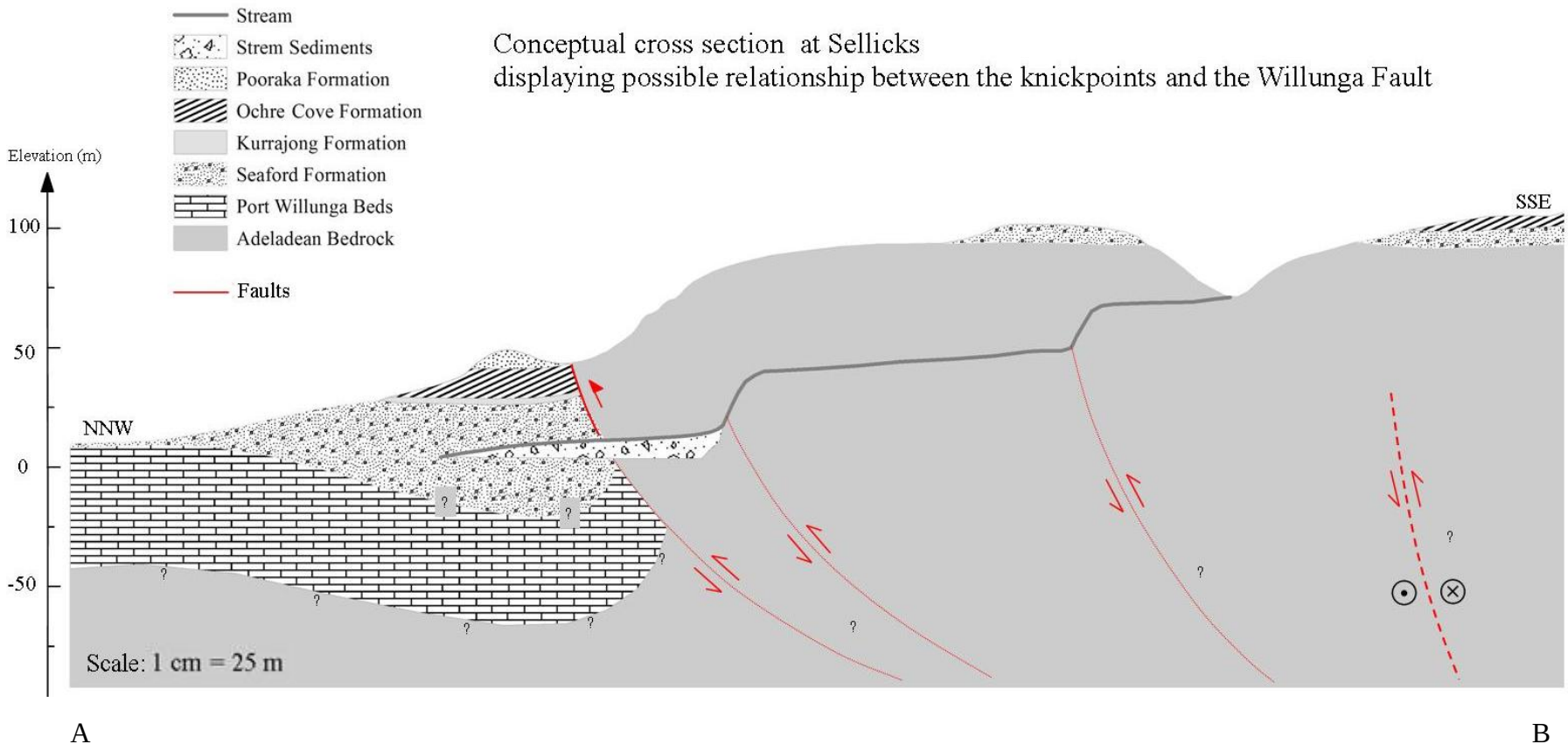

Figure 3.26 *Cross section along A-B (Figure 3.25) showing the possible relationship among the faults and knickpoints*

Footwall sequence (elevation a.s.l., where available)	Willunga Fault	Hanging wall sequence (elevation a.s.l., where available)
Top soil layer with grass (~1 m)		Top Soil layer with grass (~0.5 m)
Waldeila Formation (Holocene) 80 m		Waldeila Formation (Holocene) 92 m
Pooraka Formation (Holocene) 78 m		Poorka Formation (Holocene) 87 m
Calcrete Layer (Holocene) 75 m		Calcrete Layer (Holocene) 84 m
Taringa Formation (late Pleistocene) 60 m		Ngaltinga Clay (mid Pleistocene) 80 m
Ngaltinga Clay (mid Pleistocene) 58 m		Ochre-Cove Formation (mid Pleistocene) 70 m
Kurrajong formation (mid Pleistocene) 56 m		Seaford formation (early Pleistocene) 60 m
Ochre-Cove Formation (mid Pleistocene) 50 m		Highly weathered bedrock
Seaford Formation (early Pleistocene) 10 m		

Table 3.5 *Comparision of the stratigraphic units across the Willunga Fault*

3.4.5 Ground Penetrating Radar (GPR) surveying

A geophysical method was applied to facilitate further understanding of the spatial distribution of faults. Ground Penetrating Radar (GPR) was used to locate shallow depth subsurface faulting where the surface geomorphic expression is minimal. Furthermore, it was deployed with the aim of locating possible fault splay structures associated with the exposed Willunga Fault. The surveys were not completely satisfactory for identifying neotectonic faults within unconsolidated structures, possibly due to interferences from clay-rich ground conditions and equipment limitations. However, the profiles displayed a clear contrast where bedrock was in contact with the much younger unconsolidated material. Detailed descriptions of the survey with interpretations are presented in Chapter 6 and Appendix III.

3.5 An alternative mode of deformation for Willunga Fault Zone

The findings of this study can be summarized as follows.

1. The Willunga Fault is associated with many subsidiary faults displaying low angle thrusts, steep dipping reverse faults, normal faults and possible strike-slip faults. Most of the reverse faults have a strike direction of ENE-WSW, implying NNW-SSE local compression. The normal and reverse faults

largely align perpendicular to each other and the strike-slip faults are oblique to the reverse faults.

2. Bedding data recorded on the exposed Oligocene-Miocene Port Willunga Formation on south of the Willunga Fault display approximately NNW-SSE compression with an ENE-WSW folding axis
3. Sub-horizontal slickenside measurements reveal dominant oblique movements on the fault planes, emphasising the role of lateral movements involved in the deformational process
4. Structures within the unconsolidated sediments of the Quaternary age reflect ongoing deformation in the Sellicks region. Movements within the basement structures are also visible, but it is difficult to quantify their neotectonic contributions.
5. The knickpoints identified on the LiDAR image, curvilinearly aligns with the Willunga Fault exposure at the Waterfall Gully. They could also represent locations of progressive faulting in this locality.
6. The detailed geology map and the approximate elevations of the stratigraphic sequences near Waterfall Gully indicate the degree of displacement across the Willunga Fault.

In light of the above observations, the Willunga Fault and its subsidiary fault network, requires a new tectonic model to better explain the local deformation by accommodating characteristics of the region, beyond the conventional E-W compressional reverse faulting.

Strain ellipse models (Harding 1985, Burg 2011) are used to demonstrate the collective deformation resulting from different kinds of fault movements, mostly encountered in strike-slip zones. To determine the direction of the lateral movement, it was necessary to study different fault orientations with respect to the strain ellipse model. Accordingly, the alignment of reverse, normal and strike-slip faults in the Sellicks region best fit into a strain ellipse that represents NE-SW directed left-lateral movements (Figure 3.27). The proposed sinistral movement is in good agreement with roughness expressed on most of the sheared zones resulting from faulting, especially with slickensides.

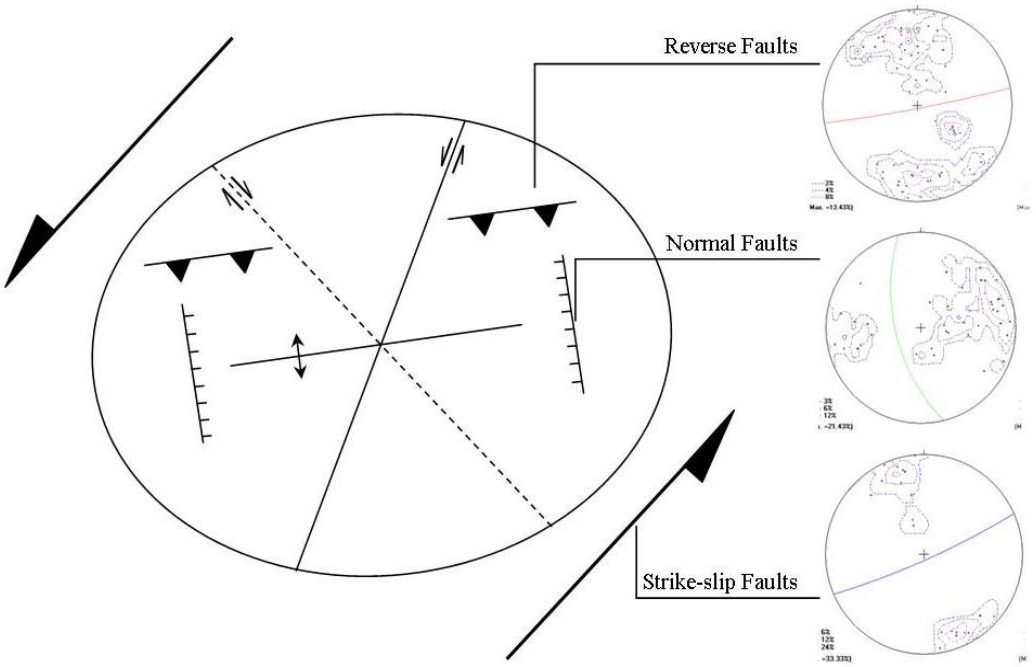

Figure 3.27 *Components of a strain ellipse illustrating the characteristics of left-lateral strike-slip movements (Source Harding 1985), with the stereoplots representing structural data trends from Sellicks region*

A strike-slip deformational mechanism accommodates the presence of oblique faulting and sub-horizontal slickensides in a region commonly attributed to reverse movements. The applicability of the suggested strike-slip tectonic model for the Sellicks region can be assessed as follows.

1. The topographic expression of the curvilinear nature of the Willunga Fault can be accommodated in a zone of NE-SW directed sinistral transpression, rather than by pure E-W compression.
2. High angle reverse faults displayed as horsetail-splay structures are likely represent splays of an unidentified subsurface strike-slip fault subjected to transpression. Accordingly, several oblique-reverse fault splays with *en echelon* step-over patterns collectively forms the differential topography of the Willunga Embayment explaining the undulating surface expression of the region.

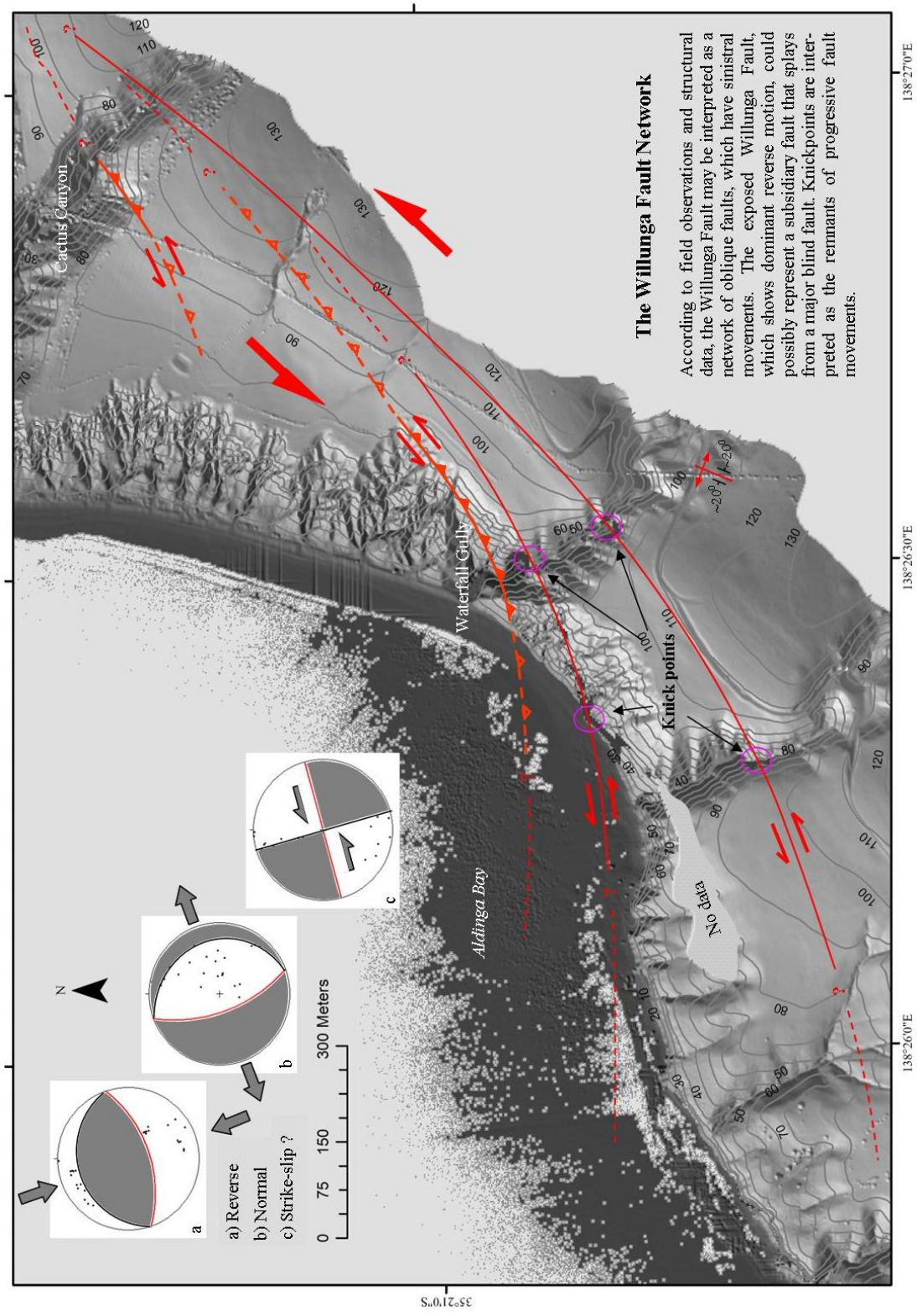

Figure 3.28 *The proposed sinistral strike-slip movements on Willunga Fault Zone*

3. Normal and reverse faults orthogonally disposed to each other would form localised zones of extension and compression as commonly observed in strike-slip systems.
4. High-angle reverse faults at Cactus Canyon and Waterfall Gully (striking 042 and 082 respectively) represent spatially disconnected fault splays in between the exposures.
5. A strike-slip model would better explain the dominant horizontal movements reflected by the slickensides and fault component analysis. Moreover, the curvilinear Willunga Fault being oblique to the current stress orientations could create sub-horizontal movements during the deformation.
6. A series of low angle thrusts and high angle reverse fault observations can be better explained by the development of positive flower structuring due to transpression. Hence, the alignment of knickpoints at Waterfall Gully (Figure 3.25) may well demonstrate the remnants of progressive fault movements. Furthermore, these faults may be merging into a single fault in the subsurface.
7. Most of the known reverse faulting tectonic offsets do not coincide with the fault scarps in the regional geomorphology. Oblique movements in strike-slip transpressional zones also do not necessarily result in significant surfacial evidence, particularly given the presence of unconsolidated surface sediments such as in the Sellicks region.
8. A strike-slip tectonic model would comprehensively accommodates most of the previous interpretations (Howchin 1911, Sprigg 1945, Sandiford 2003a, Tokarev 2005), which include both normal and reverse faulting during the deformational evolution of this region.

Vertical displacement rates of at least ~50-70 m/Ma have been experienced by the Willunga Fault (Sandiford 2003a), during post-middle Pleistocene compressional stages (May & Bourman 1984, Bourman & Lindsay 1989). Based on the proposition of strike-slip deformation, it is possible to calculate time-averaged horizontal slip rates, provided that vertical slip rates are a realistic estimation for the Sellicks locality.

As, vertical : horizontal lateral : horizontal transverse = 5:7:3
And, the time-averaged vertical slip rate = ~50-70 m/Ma
Hence, time-averaged horizontal lateral slip = ~70-98 m/Ma

The above ratio can be further extended for the vertical offsets of stratigraphic marker units across the Willunga Fault. Accordingly, mid Pleistocene Ochre Cove Formation demonstrates ~20 m of actual vertical offset (Table 3.5), while the slip calculations suggest ~28 m of lateral movements. The early Pleistocene Seaford Formation has been vertically offset by at least 50 m and possibly some 70 m dislocation along the strike as a result of the oblique movements on the Willunga Fault.

3.6 Discussion

The Willunga Fault has long been recognised as a single reverse fault, exposed at two distinct locations, namely Cactus Canyon and Waterfall Gully. This field-based study in the Sellicks region confirms the view of Tokarev (2005), that the Willunga Fault is associated with many subsidiary faults. The main thrust fault is well exposed on eroded sea cliffs and dominates the region as an oblique-reverse fault, while expressions of subsidiary faults are subtle but identifiable.

According to the present understanding of reverse faulting in this region, it is unusual to have normal and reverse faults perpendicular to each other, unless resulting from gravity settling of the reverse faults. A normal fault striking perpendicular to the cliff faces of the Sellicks Beach area could have been initiated due to undercutting of cliffs by wave action. Alternatively, erosion could have been facilitated along the weaker zones of fault planes. The latter has been given much recognition as the majority of the erosion gullies penetrating inland, follow the strike of the normal faults. High-angle normal and reverse faults having perpendicular strikes to each other have been recorded by Sprigg (1946), without spatial reference. The findings of this study corroborate their existence.

The sub-horizontal slickensides registered on some of the fault contacts emphasise that the Willunga Fault has experienced an oblique sense of motion during most of its Quaternary movements. It contains several subsidiary faults, which display *en echelon* step-over patterns with highly variable dips. Steeper dips near the centre of the fault zone with dips shallowing towards the margins, display positive flower-structuring patterns. In addition to the transpressional features observed above, ENE-WSW striking reverse faults, NNE-SSW striking normal faults and NE-SW striking possible strike-slip faults can be linked with a strain ellipse that represents sinistral strike-slip movements. The secondary fault observations can be considered as upward branches (fault splays) of a major subsurface fault given the sinistral strike-slip transpressional environment. This provides an identical setting to the Wilkatana Fault segments in the Flinders Ranges, explained by transpressional movements (Quigley *et al.* 2006).

Extensive alluvial fans form shields over the faults associated with the main scarps, and prevent direct observation of fault exposures. This may have resulted from the unconsolidated nature of the sediments, which prevented the preservation of surface indicators. An alternative explanation could be that thick sedimentation during the last major fan building event exceeded the fault offsets (Sandiford 2003a). On the other hand, inactive faults or faults dominated by lateral movements would also generate less vertical dislocations, as some of the Flinders Ranges sites (Quigley *et al.* 2006). Nevertheless, an understanding of the regional stratigraphy and the location of subsurface marker units can provide evidence of both fault behaviour and age constraints.

Dislocation of stratigraphic marker units across fault zones provides important constraints on the age and the amount of vertical fault movements. Contours generated through the LiDAR digital elevation model in conjunction with production of the detailed geology map and the use of high resolution NearMap images, facilitated the determination of elevations of the stratigraphic units across the Willunga Fault Zone (Table 3.5). The Oligocene-Miocene Port Willunga Formation provides evidence of the maximum extent of faulting, as it is flat lying to the north of

the fault and tilted to an almost vertical position across the fault zone. The absence of the Port Willunga Formation close to the Willunga Fault contact at Waterfall Gully is likely to be a result of uplift and erosion. The late Pleistocene Seaford Formation occurs almost at sea level on the footwall, while attaining elevations of more than ~50-60 m on the hanging wall.

Quaternary vertical displacement rates of at least ~50-70 m/Ma have been postulated for the Willunga Fault by Sandiford (2003a). Subsequently, this study provides ~70-98 m/Ma of horizontal displacement on the same fault, as indicated by records of slickensides. Oligocene-Miocene Port Willunga Formation has been vertically dislocated more than 200 m between the regions of Sellicks Beach and Myponga on Fleurieu Peninsula (Figure 3.26). This is considered to be the result of cumulative movements along the Willunga Fault Zone. Under the assumptions that faults are of strike-slip origin and experience uniform rates of dislocation, at least 300 m of left-lateral dislocation in-between the above locations can be estimated. However, the computed values could not be validated due to the absence of marker units to constrain the horizontal movements and poor preservation of surface evidence.

The vertical accuracy of the elevation model displayed good agreement with a previous GPS elevation measurement for the mid Pleistocene Ochre Cove Formation as demonstrated in Figure 3.26 and Table 3.5. However, stratigraphic units affected by earth-flows may complicate elevation determinations. The accurate identification of the units demands a good understanding of the lithology of the stratigraphic sequences, their depositional environments and successive members. Field measurements of the structural data could include spatial errors depending on the accuracy and capabilities of the GPS unit that records coordinates. This was clearly demonstrated on the map that displays structural measurements of the region (Appendix I), where measurements recorded within a few meters of radius were incorporated into a single location.

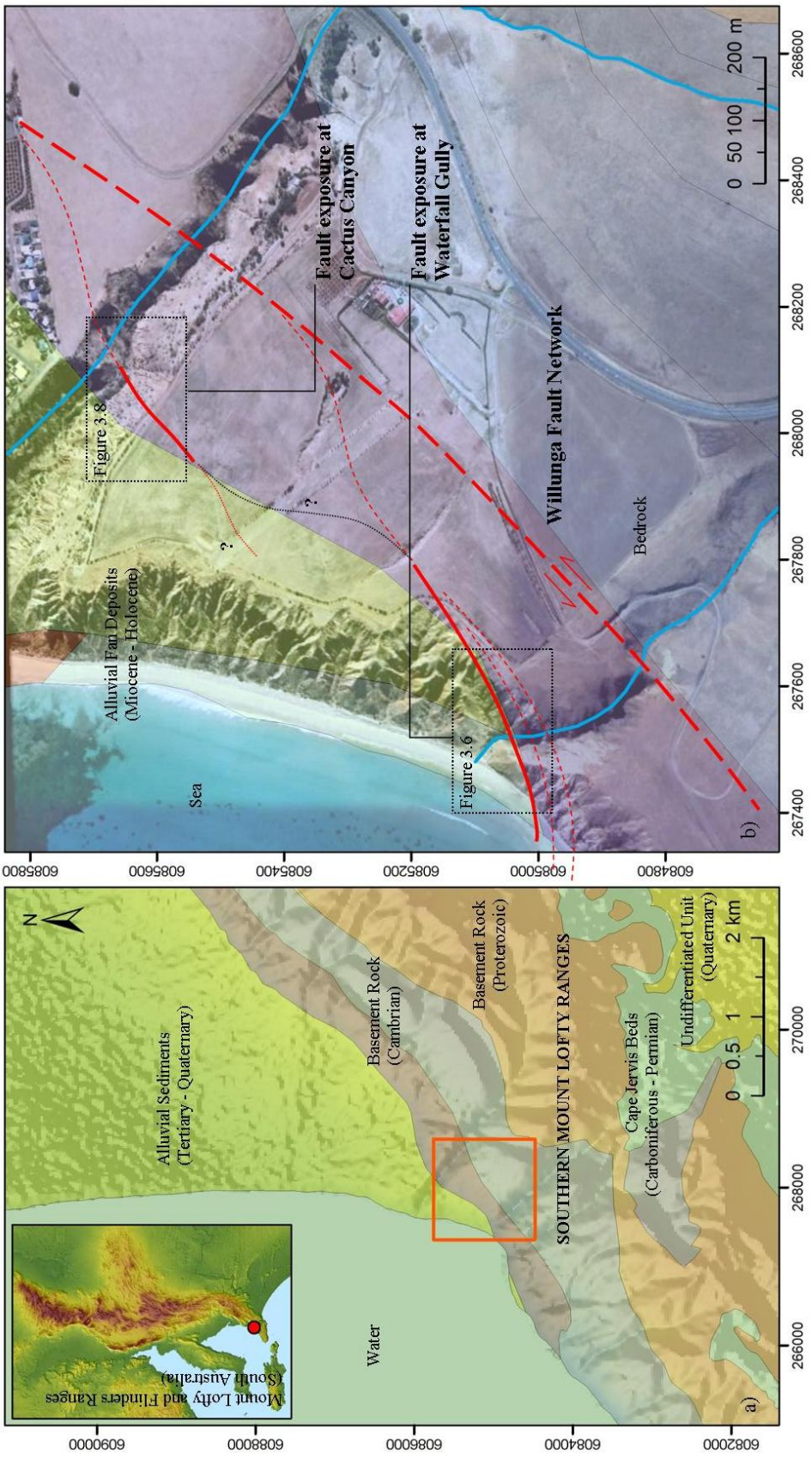

Figure 3.29 *Interpretation of the Willunga Fault at Sellicks in regional context*

Deeply incised erosion gullies reflect a rapidly changing landscape in Sellicks region. Two sets of basement knickpoints on erosion gullies south of the Willunga Fault were identified from the field observations, and established as having an inclination greater than 60° using the LiDAR digital elevation model. Their curvilinear existence with the present Willunga Fault (Figure 3.25) can be interpreted as resulting from headward propagation of knickpoints or the result of progressive faulting. These features are associated with a faint scarp, but further investigation is required to definitively establish this relationship. Nonetheless, this exercise demonstrates the usefulness of the LiDAR images as reconnaissance tools in identifying geomorphic features, which may highlight the presence of subsurface faults.

Continuous deformation within the region is expressed by ongoing low magnitude seismicity and the deformational features on Quaternary unconsolidated sediments such as neptunian dykes and compressional structures (Figure 3.15 Figure 3.23). The near surface faults and stratigraphic offsets suggest ongoing deformation since deposition of the late Pleistocene Pooraka Formation, but it could be as young as Holocene if the recent land slump (Bourman & May 1984) at Sellicks Beach has a seismic origin. Slumping and faulting within the basal section of the Port Willunga Formation is clearly truncated by an unconformity midway through the succession (Figure 3.3b). This suggests ongoing tectonism during deposition of the formation at least since the earliest Miocene. In some locations along the shore platform, the Port Willunga Formation is steeply inclined and even slightly overturned, indicating a major phase of regional deformation subsequent to its final deposition in the middle-late Miocene.

Transpressional uplift of the Sellicks region could have been facilitated by dislocations on multiple faults acting over a period of time in response to regional stress fields. The fact that most of the range-bounding faults are not being perpendicular to the current stress field favours the operation of oblique slip movements. Thrust fault measurements have shown more of an E-W orientation, indicating NNW-SSE regional compression, which is approximately perpendicular to

the generally acknowledged E-W compression. Sub-horizontal slickenside measurements within unconsolidated strata and in basement lithologies provide field evidence for substantial oblique movements. Basement fabrics could represent reactivated Delamerian structures, but they are regarded as being of neotectonic origin, because of the clay rich cataclastite nature of the fault gouge material.

The nature and amount of slip on the Willunga Fault favour the occurrence of both compressional and oblique-slip faulting, most likely representing a zone of transpression due to sinistral strike-slip movements. Detailed field studies on individual faults as conducted at Sellicks Beach, provide important evidence on the character of neotectonic faulting in Mount Lofty and Flinders Ranges.

4 PALEOSEISMOLOGY OF ACTIVE FAULTS IN THE MOUNT LOFTY AND FLINDERS RANGES

4.1 Introduction

The rupture frequency and amount of slip on active faults generally reveal the nature of deformation and consequent seismic hazards (Hancock 1988). Earthquake recurrence intervals are difficult to estimate in the intraplate Mount Lofty and Flinders Ranges due to the limited number of historic seismic records (Quigley *et al.* 2010). In order to understand the neotectonic trends and the long-term behaviour of faulting it is necessary to study the nature, timing, and displacement of prehistoric faulting. Thus detailed information on active faults based on field observations including structural, stratigraphic and geomorphological evidence is vital.

There may be hundreds or thousands of years between major earthquakes, particularly in intra-plate settings such as Australia (Clark 2010). However, evidence of ancient earthquakes can be extracted from the geological record, as most of the large earthquakes commonly leave a trace in the surrounding sedimentary structures (Clark & McPherson 2011). For example, the deposition of a colluvial wedge at the toe of a fault scarp following a fault rupture can reveal the amount of deformation experienced. The magnitudes of past earthquakes can be estimated by measuring the offset of a single event and tracing the horizontal distance of the fault scarp. For pre-historic events sediments may be dated using luminescence techniques to constrain the timing of previous rupture events (Quigley *et al.* 2006).

The study of the rupture history of a fault, based on evidence of stratigraphy, geology and landscape is known as ‘palaeoseismology’ (Azzaro *et al.* 2000, McCalpin & Carver 2009). Fault contacts have to be physically observed to extract the necessary information on local deformational characteristics. This commonly requires deploying destructive field investigation methods such as trenching, unless the fault contacts are naturally exposed. Trenching across fault lines facilitate the identification and reconstruction of stratigraphic units (Audemard *et al.* 1999). Sediment samples collected from the youngest disrupted units and the oldest non-disrupted (overlying) units can be used to place age constraints on a single rupture

event. Measuring the offset of progressively older units either side of a fault can help to determine the long-term slip rates resulting from several seismic events. Laboratory analyses of such samples for mineralogy, sediment content and grain-size, etc. can reveal additional information on the rupture environment. However, Quaternary slip rates on most of the faults are difficult to reconstruct due to the unconsolidated nature of many stratigraphic sequences, which are prone to erosion and reworking (Pizzi & Scisciani 2000).

4.2 Methods - Trenching

In this study, a trenching program was undertaken to explore some of the neotectonic faults in the Mount Lofty and Flinders Ranges. Later, it was synchronized with Geosciences Australia's trenching program implemented by Dr. Dan Clark and Dr. Andrew McPherson. The main objectives of this study were to identify stratigraphic offsets generated by near surface displacements within the soft Quaternary sediments and to collect appropriate samples for constraining the times of movement using luminescence (OSL) dating techniques. Trenching work was conducted in three separate visits to the Flinders and Mount Lofty Ranges. The first was the excavation of three trenches across the Paralana Fault near Moolawatana in July 2009. The second (May-2010) and third (Nov & Dec -2011) fieldwork campaigns visited the sites of Hoyleton, Tarlee, Burra, Gawler and Bethel (Figure 1.2).

Prior knowledge of the fault zones, analysis of geological maps, satellite images, digital elevation data and an understanding of the geomorphological and geological processes active within the locality were useful in determining the trench locations for this study. The absence of easily identifiable fault scarps, outcrops or trapezoidal facets within the locations of interest complicated the task, where, subtle geomorphic features and/or scarps and calcrete outcrops led the way to potential sites of near-surface fault ruptures. On the identified locations, the site was measured and gridded with pegs, the trench boundaries were established and the coordinates were recorded with a (Garmin GPS72-Personal Navigator) GPS.

The fieldwork was conducted adhering to the general codes of practice of safety and University of Wollongong safe fieldwork procedures. Appropriate personal protective gear was worn by the people on-site. The excavation was done using a backhoe, and the trench walls were not loaded with the excavated material to avoid wall collapse. Benches were created as appropriately to stabilize the walls of the excavation. However, it was not necessary to create a bench on the trench sides as the depth of excavation was just ~1 m at Moolawatana. Upon completion of work, the trenches were back-filled with the excavated material and site conditions were restored.

The trenches were surveyed, logged and photographed as necessary. Stratigraphic layers, geologic structures and fault contacts were the focus of observation and identification. Individual stratigraphic units exposed on the trench walls were classified and the structures were marked with flagging tape and nails with tags. OSL samples (Chapter 5) were extracted from the appropriate locations on the trench walls. Representative samples considered significant for future mineralogical analysis were collected from fault gouge and the surrounding stratigraphy.

4.3 Field observations and interpretations

The following sections compile the results of applying paleoseismology techniques at selected identified active faults in the Mount Lofty and Flinders Ranges. The trenching work has been illustratively documented for those faults with exposed fault contacts. Figures of the trench logs were generated with reference to the field notes of Dan Clark and Andrew McPherson. A summary of the trenching fieldwork is given in Table 4.1 and a summary of the active faults addressed within this chapter is given in Table 4.2.

4.3.1 Paralana Fault – Moolawatana

The Paralana Fault Zone extends over 150 km with sub-parallel faults and offsets separating the northern Flinders Ranges from the Frome Embayment (Brugger *et al.* 2005, Davey 2009, Thomas *et al.* 2012). The fault zone has been active since the Proterozoic with normal, reverse and strike-slip fault movements (Paul *et al.* 1999). The Paralana Fault Scarp is one of the steepest and most deeply dissected reliefs in Southern Australia (Sandiford 2003a). West dipping reverse faults were observed on the Paralana fans (Williams 1973), where Proterozoic basement has been thrust over Quaternary ferruginous sandstone and conglomerates (Bonilla & Lienkaemper 1990, Celerier *et al.* 2005, Quigley *et al.* 2006, Hillis *et al.* 2008). The western hanging wall is characterised by Neoproterozoic meta-sedimentary and igneous basement rocks that have been thrust over a mix of Cenozoic ferricreted or silcreted sandstones and conglomerates that were deposited into the Frome Embayment throughout the Cenozoic. The Cenozoic units within the footwall include the Eyre Formation and the late Miocene to early Pleistocene Willawortina Formation, which reaches thicknesses over 140 m starting at least 60 m below present sea level (Callen & Tedford 1976).

A left-lateral Delamerian movement on the north-east extension of the Paralana Fault was documented by Paul *et al.* (1999). The SE dipping basement involved deformation and popup geometries identified as flower structures. Fault propagation folding and north-south shortening has resulted in the formation of open anticlines on the basement, perpendicular to the principal fold axis (Paul *et al.* 1999). Shortening due to lateral fault movements were mostly accommodated by hanging wall anticlines producing flower structures along the fault. The left lateral transpressional movements due to north-south directed Delamerian shortening, could probably have been reactivated in the opposite direction at latter stages (Paul *et al.* 1999, Quigley *et al.* 2006).

A late Neogene fault movement, with a minimum average slip rate of 30 m/Ma is assigned to the Paralana fault, based on the thickness of the footwall consisting of the

Willawortina Formation (Sandiford 2003a). However, slip rates remain uncertain, due to the unavailability of definitive ages of displacement along most of the structures. Evidence of recent fault activity is observed at Lady Buxten Mine, as stated in Sandiford (2003a), with a 30° west dipping reverse fault. On another exposure at the foot of the scarp the fault has a dip of 45° with a hanging wall of Proterozoic metamorphic rocks thrusting over Palaeogene sediments of the Frome Embayment (Belperio 1995).

Variable neotectonic movements on reverse and thrust faults display Quaternary displacements exceeding ~150 m, while an increase in deformation is observed since terminal Miocene times (Paul *et al.* 1999). A late Mesozoic to early Tertiary origin for the Paralana Fault Scarp (Twidale & Bourne 1975) may not be a valid estimation because of the presence of youthful attributes including limited range-front retreat since the fault was initiated and steep range-front relief adjacent to the fault line. Furthermore, the Paralana Fault disrupts the Eyre Formation, emphasising that the faulting had occurred after the deposition of Eyre Formation.

Field observations

The Paralana Fault trenching site is located ~570 km to the north-northeast of the city of Adelaide, on the eastern side of the northern Flinders Ranges, bordering Lake Frome and Lake Callabonna. Trenching work was conducted at Moolawatana (Figure 4.1) from 15 to 18 July 2009. Three trenches PRLF-01, PRLF-02, and PRLF-03 were constructed parallel to each other and perpendicular to the fault trace (Figure 4.3). Only the trench PRLF- 03 was successful in locating the fault contact (Figure 4.2). PRLF- 01 exposed most of the angular, poorly sorted breccias obviously derived from the range front (youngest flanglomerates) overlying the fault, while PRLF- 02 only managed to intersect the fault at the NW end of the trench. The ~10 m long PRLF- 03 trench (Figure 4.4) was excavated with an orientation of NW-SE, almost perpendicular to the Paralana Fault trace. The average depth of the trench was ~1 m, with a maximum depth of 1.2 m.

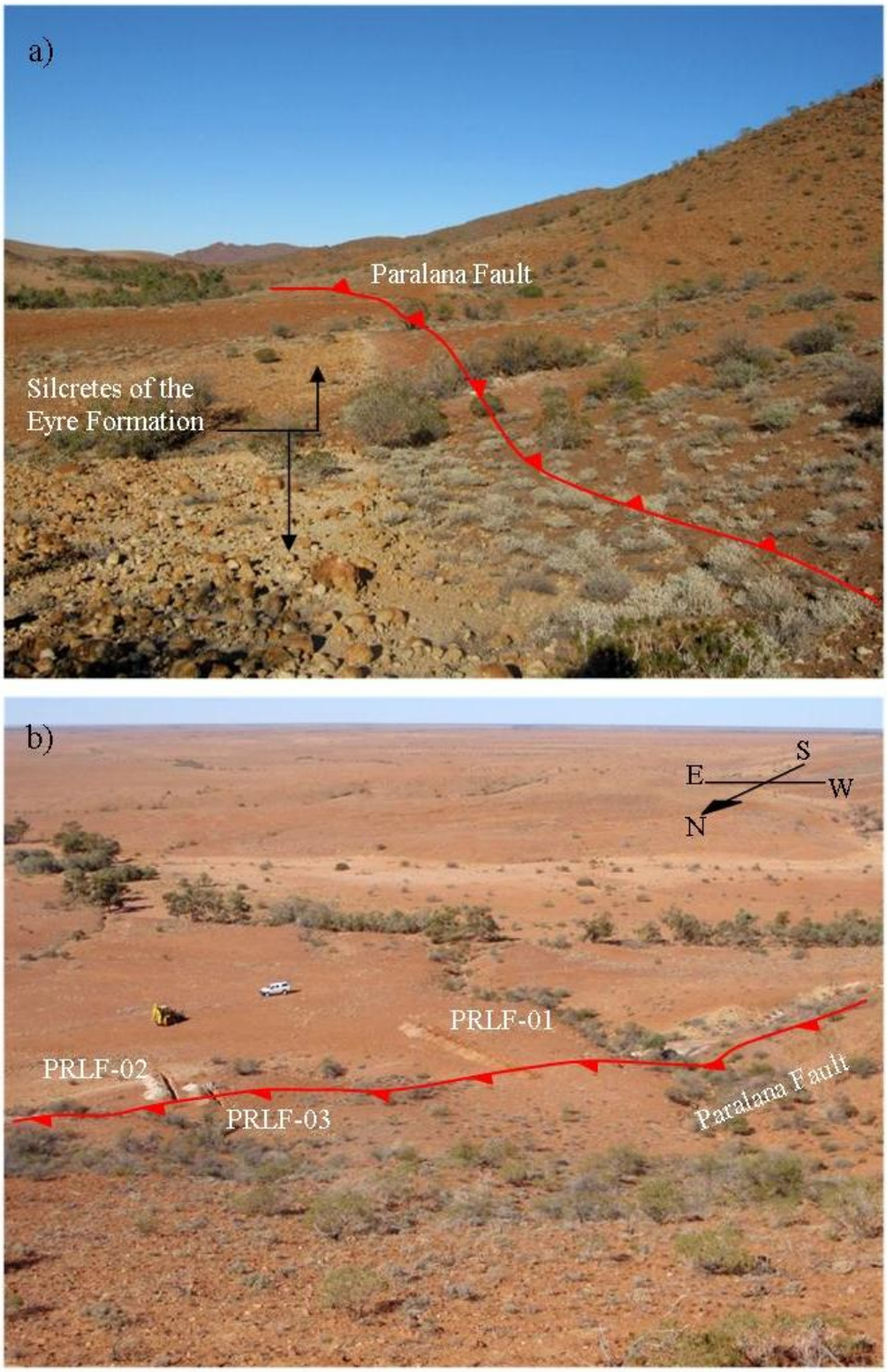

Figure 4.1 *Paralana Fault near Moolawatana a) Looking towards SW from 377225 E, 6688689 S, showing tilted silcretes of the Eyre Formation dragged up against the reverse fault b) Aerial view of the trenching site from top of the Paralana Escarpment. Prominent white colour outcrops of the Eyre Formation can be seen near the fault.*

A reverse fault contact striking at 029 and dipping at 52°W was identified within highly weathered and heavily sheared Proterozoic granite bedrock thrust over tilted silcretes of the Eyre Formation. The fault gouge material within the sheared contact has produced a clay-rich cataclastite containing abundant silcrete fragments. The fault contact is overlain by a coarse-grained, poorly sorted, angular reddish-brown ~0.5 m thick fanglomerate. The colluvial breccia is a part of the active hillslope, a clayey gravel layer with sand, which runs undisturbed across the fault contact. The hanging wall consists of yellowish-brown, grey coloured, highly to moderately weathered bedrock with calcite precipitated along its micro-fractures, and is possibly related to the deformation. It is difficult to recognise any other faults or structures within the bedrock due to its weathered nature. The footwall material is dominated by carbonate rich unconsolidated sandy gravels and cobbles. A colluvial wedge produced by the fault movement can be identified between the footwall sequence and a continuous gravel horizon, which runs across the fault. A single rupture event with a reverse sense of displacement could account for the observations of the exposed fault contact at this location.

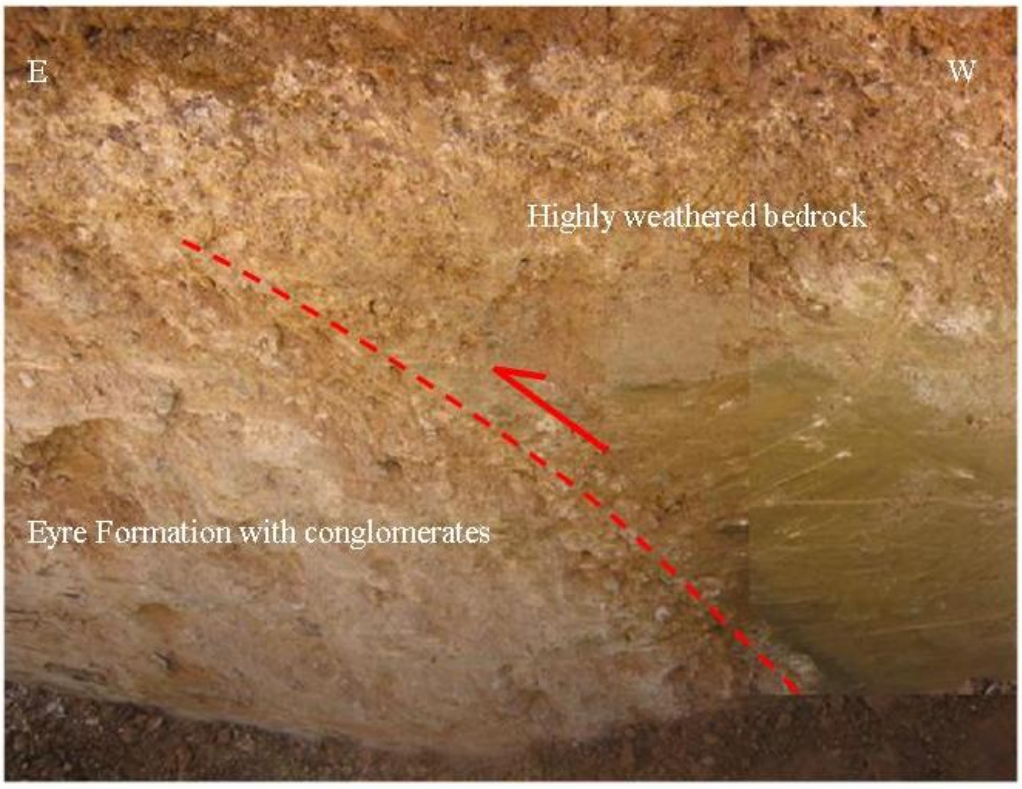

Figure 4.2 *Paralana Fault contact on trench PRLF-03. Strike 029 and Dip 52°W. Location coordinates: 377225 E, 6688689 S*

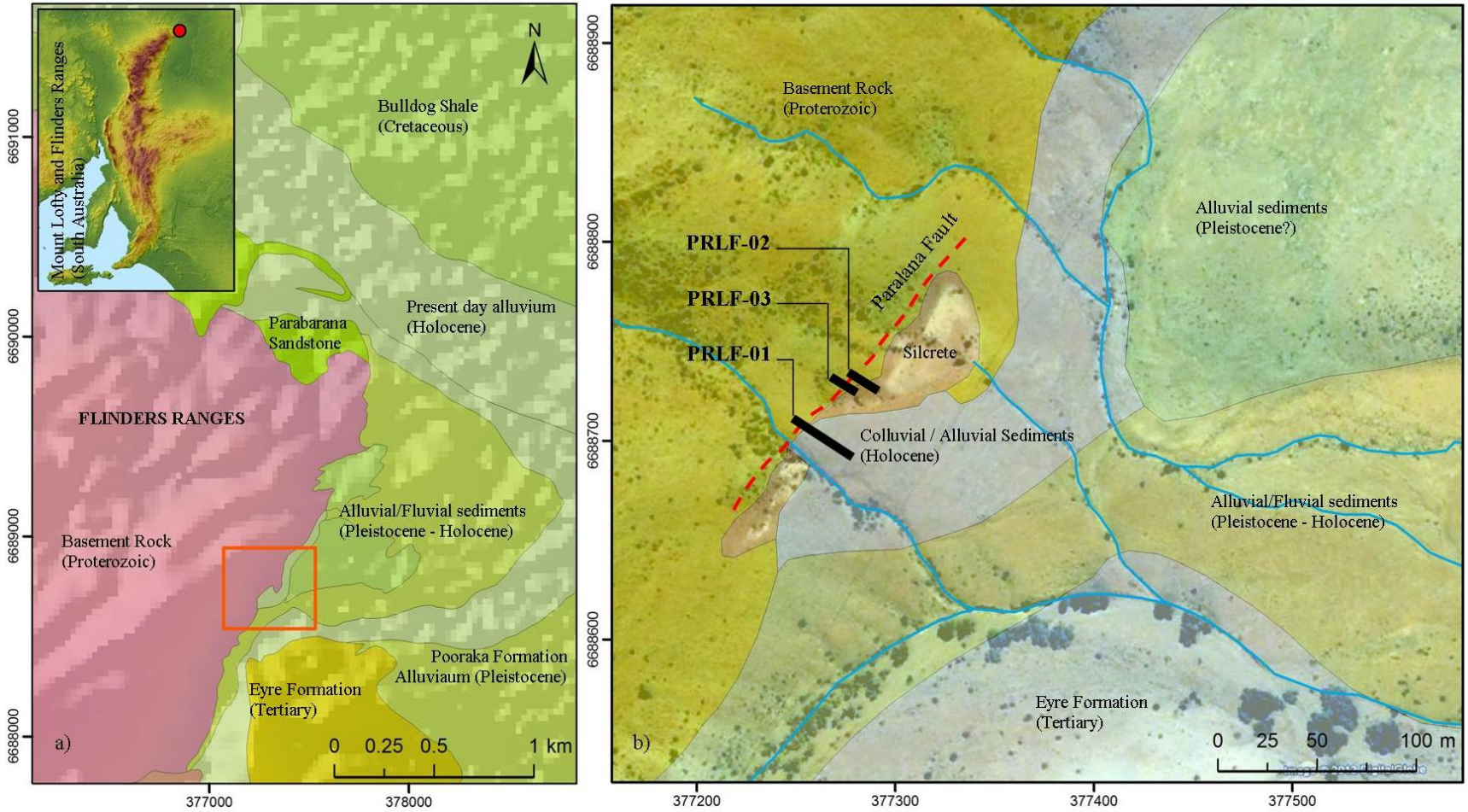

Figure 4.3 *Planview of the site near Moolawatana a) Regional geology map, b) Local geology and trench locations (Trenches not to scale)*

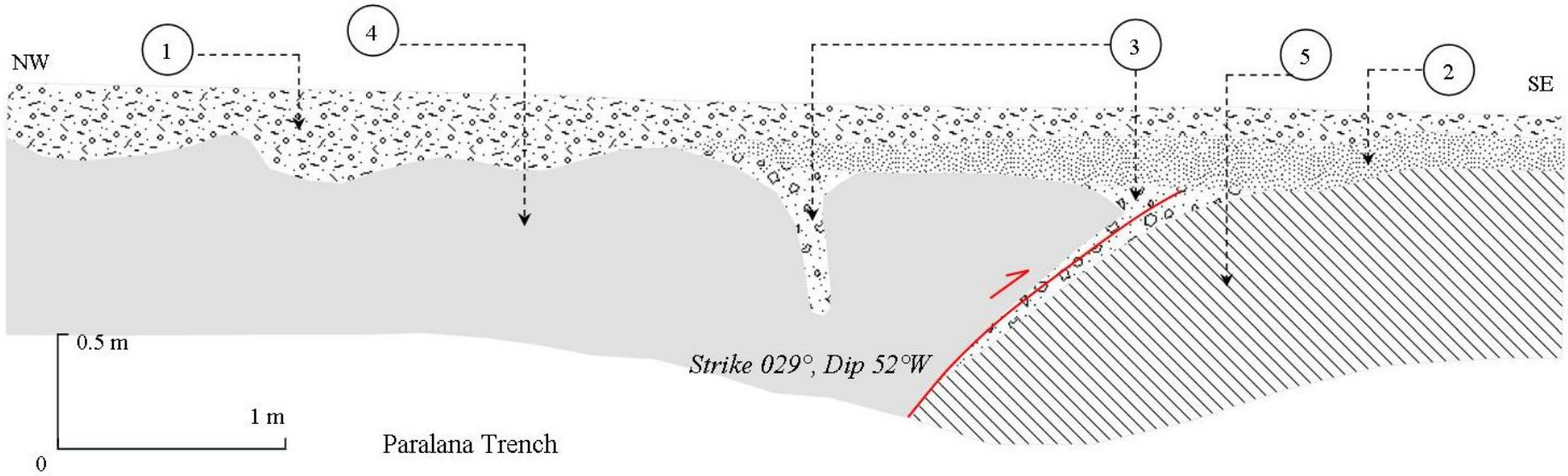

Figure 4.4 *Illustrative diagram of stratigraphic units on the Paralana Trench (PRLF-03).*

Unit descriptions follow the numbering sequence: 1) Topsoil layer – Reddish-brown to light-brown gravel layer, with medium to coarse grain sand, cobbles and pebbles. Contains occasional plant roots and silt lenses, 2) Hillslope colluvial layer – Reddish-brown to dark-brown silty gravel layer with abundant clay and sand with sub-angular particles of bedrock possibly resulted from a debris flow, 3) Veins of clay – Light-brown, pale yellow sandy clay unit with occasional bedrock particles, 4) Highly weathered bedrock – Yellowish brown, grey and light brown mixture of clay and sand. Consists of sub-vertical calcite veins and equally distributed slightly weathered brecciated bedrock. Veining and clay content increases towards the fault contact, 5) Thick layer of slightly-consolidated soil (Eyre formation?) – Pink, light-brown, pale-white sandy clay layer with reddish-brown mottles of clay and sand.

4.3.2 Alma Fault - Hoyleton

The Alma Fault is located within the middle section of the Mount Lofty and Flinders Ranges and strikes approximately north-south. Its southward extension may connect with the Para Fault (Alley 1973), possibly in the subsurface, as there is no surficial evidence. A single rupture event on the Alma Fault resulting in more than 1.8 m of reverse displacement along the fault plane has been observed near Hoyleton (Clark & McPherson 2011).

Field observations

The excavation work to expose the Alma Fault was conducted near Hoyleton, located ~100 km NNE of the city of Adelaide. This work was conducted from 27 April to 20 May 2010 in cooperation with Geosciences Australia. The two trenches are referred to as AF-01 and AF-02 (Figure 4.6). The fault was exposed only in AF-02 (Figure 4.5).

The east-west oriented AF-02 trench exposed a sequence of thrust faults involving bedrock at a location, which has limited surface expression. The fault strikes at 002 and dips at ~32^{o} E, and has thrust highly weathered Proterozoic bedrock over unconsolidated Cenozoic sediments. It segments towards the surface and divides into at least three low-angle thrusts, possibly representing multiple rupture events. The light yellowish coloured hanging wall of bedrock displays few parallel faults and sub-vertical extension fractures with similar orientations to the main fault (Figure 4.7). The footwall sequence of a reddish grey sandy clay layer has light-brown, reddish-brown and white mottles with well-developed calcrete patches and rhizomorphs, resembling the Ochre Cove Formation. Fault wedge material occurs on top of the footwall sequence and a thin layer of calcrete overlain by thin dark-brown soil layer covers the entire region, which is undisturbed across the reverse fault contact. The trench is located on a ridge crest and the thin top most soil layer appears to represent a partially stripped soil profile.

The trench AF-01 is located ~40 m north of AF-02, in a deposition dominated environment, possibly within a paleochannel. It contains a comparatively thick deposit similar to the Ochre Cove Formation. The thrust fault contacts could not be

located in AF-01, but a gentle warping within the sedimentary structures could be observed. The calcrete unit is absent within the depth of excavation and the top most dark brown-grey soil unit is likely to represent the Holocene Waldeila Formation.

Figure 4.5 *Alma Fault exposure near Hoyleton. Strike 002 and Dip 32°E. (Photo looking south)*

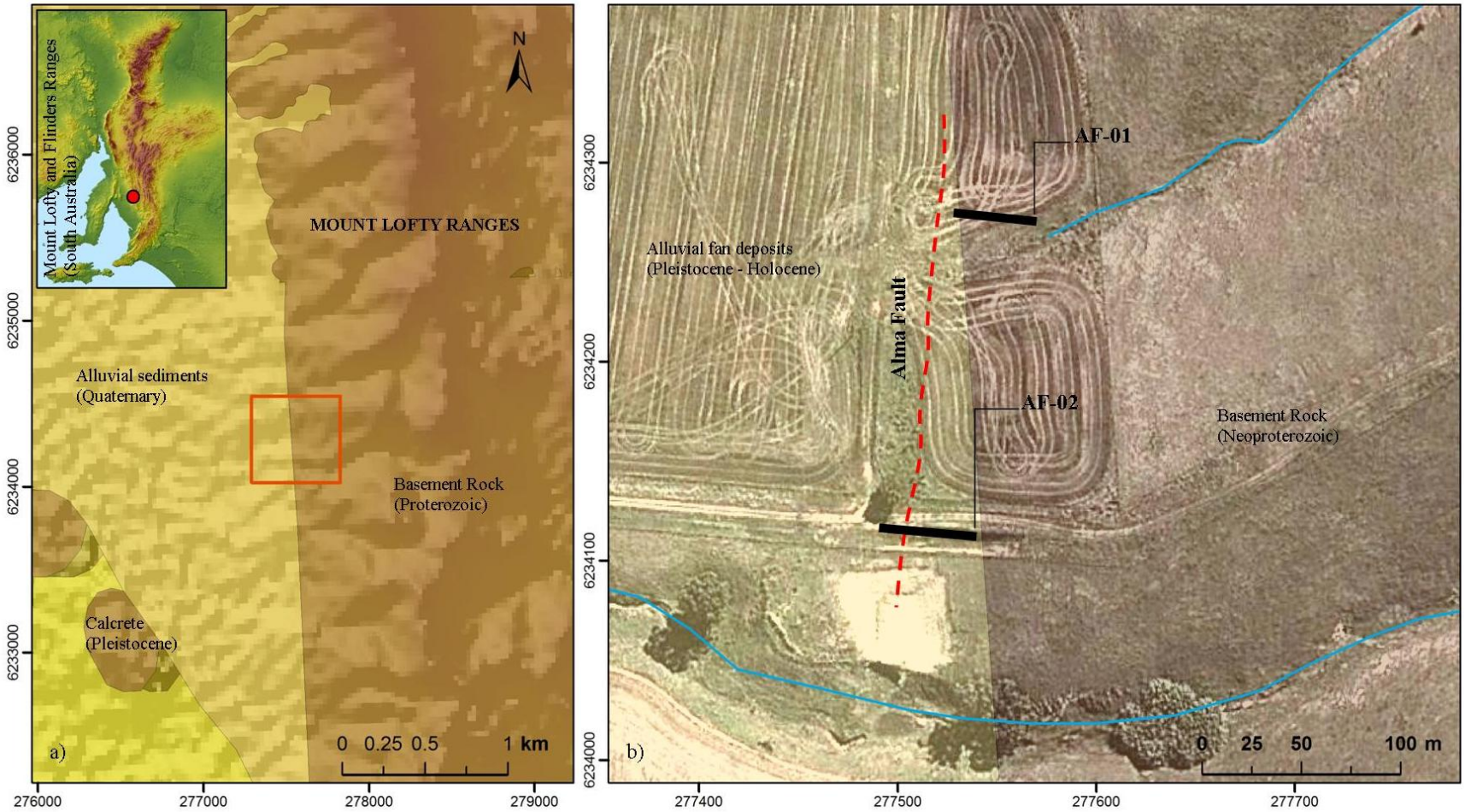

Figure 4.6 *Planview of the site near Hoyleton a) Regional geology map, b) Local geology and trench locations (Trenches not to scale)*

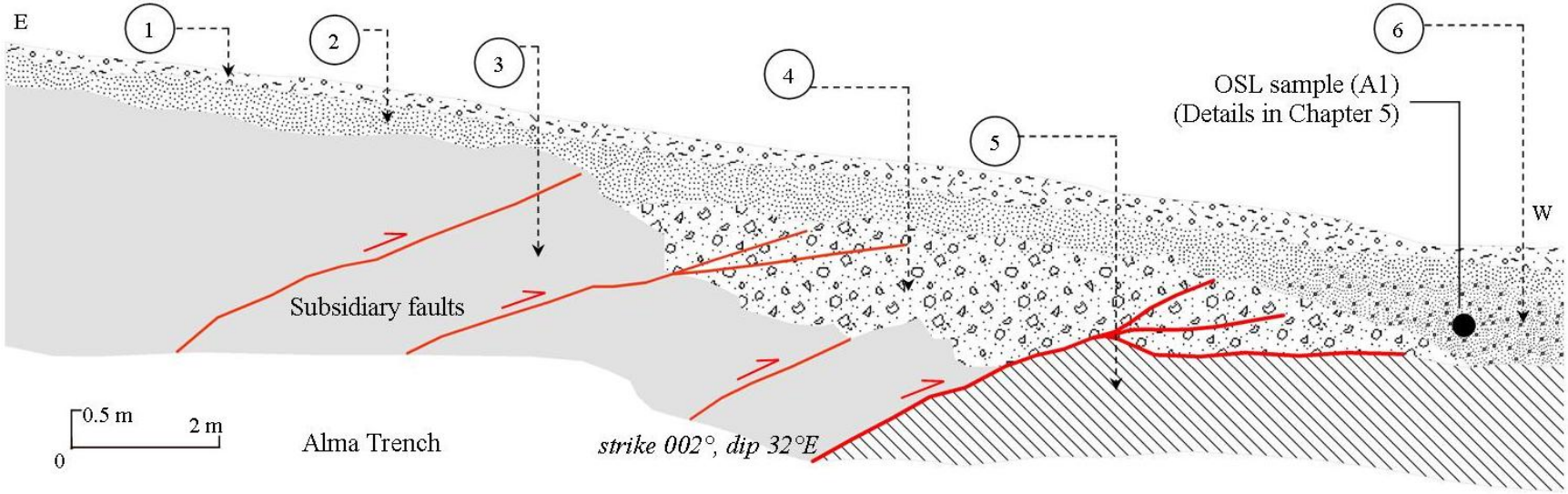

Figure 4.7 *Illustrative diagram of stratigraphic units on the Alma Trench (AF-02).*

Unit descriptions follow the numbering sequence 1) Topsoil layer – Dark-brown mixture of sand, silt and clay with gravel and abundant plant roots, 2) Layer of calcrete – Pale-white, slightly-pink fine to medium silty sand with occasional plant roots, 3) Weathered bedrock – Pale-yellow, light-brown, moderately to highly weathered bedrock with silt, quartz nodules and prominent sub-vertical extension fractures, 4) Colluvial wedge - Light-brown, pale-white, sandy clay layer with unsorted mixture of angular to sub-angular gravel and weathered bedrock particles, 5) Sandy clay layer (Ochre Cove Formation?) – Reddish-brown, brown sand and clay layer with white and dark-brown mottles, 6) Colluvial wedge 2 – Brown to yellowish-brown sandy clay layer with brecciated fragments of gravel and occasional lenses of peaty clay.

4.3.3 Burra Fault – Worlds End Creek

The Burra Fault is exposed within a steeply incised gully at Worlds End Creek and at a nearby erosion gully (Figure 4.9). At Worlds End Creek, the fault strikes NNW and dips towards the WSW (Quigley *et al.* 2006). Faint slickensides on parallel bedding structures display dip-slip motion, but do not show much surface expression. The hanging wall consists of highly weathered siltstones and tillites of Neoproterozoic Appila Tillite. The footwall material is fine-grained weathered alluvium marked by fluvial channels containing sand and carbonates (Quigley *et al.* 2006). A soil horizon ~0.4 m deep rests on the top of the sequence. Sub-vertical extensional fractures on the hanging wall are attributed to collapse following reverse faulting. A lag deposit of coarse weathered bedrock can be observed at the base of the hanging wall. The observations are interpreted as resulting from an individual rupture event with a reverse sense of motion involving a dip-slip offset of ~3.8 m. The earthquake records show that there had been a magnitude 5.1 seismic event with aftershock magnitude of 3.0, 2.3 and 3.5 in 1997, ~15 km SSE of Burra (McCue *et al.* 1997). However, evidence of recent activity along the fault or in the nearby landscape, could not be located within the study region.

Field observations

The Burra Fault exposure is located ~135 km northeast of Adelaide, on the eastern side of the northern Mount Lofty Ranges (Figure 4.10). The basement is faulted against the sediments that resemble Pooraka Formation, which has been confirmed by the OSL results of this study (Chapter 5). The faulting has occurred after deposition of the thick unit of Pooraka Formation, but the number of rupture events is difficult to calculate from the available field evidence. The 2 m deep trench excavated by Geosciences Australia during May 2010 did not intersect the main fault plane, even though it was only a few metres along strike (SE) of an erosion gully that exposes the Burra Fault contact (Figure 4.9). The line of strike determined from fault outcrops in two adjacent erosion gullies suggest that the trench may have missed the main fault surface by its position being east of the main fault. However, the trench does appear to have intersected a subsidiary fault plane at a depth of ~2 m (Figure 4.8) displaying highly weathered basement rock faulted against a unit of reddish-brown sandy clay with white mottles (possibly belonging to the Ochre Cove

Formation). The fault does not disrupt the carbonate rich clayey soil layer, which has an approximate thickness of 1 m. The fault contact displays a strike of 118° and a dip of 50° to the SW, whereas the nearby erosion gully, NW to the trench shows a strike of 146° with almost a vertical fault contact. The two exposures do not line up as a single strike direction according to the measurements, and possibly represent branches of the Burra Fault unless the dip and strike largely vary along the fault line.

Figure 4.8 *Burra Fault contact exposed in the trench BF-01. Strike 118° and dip 50° NE. Location coordinates 316936 E, 6259822 S*

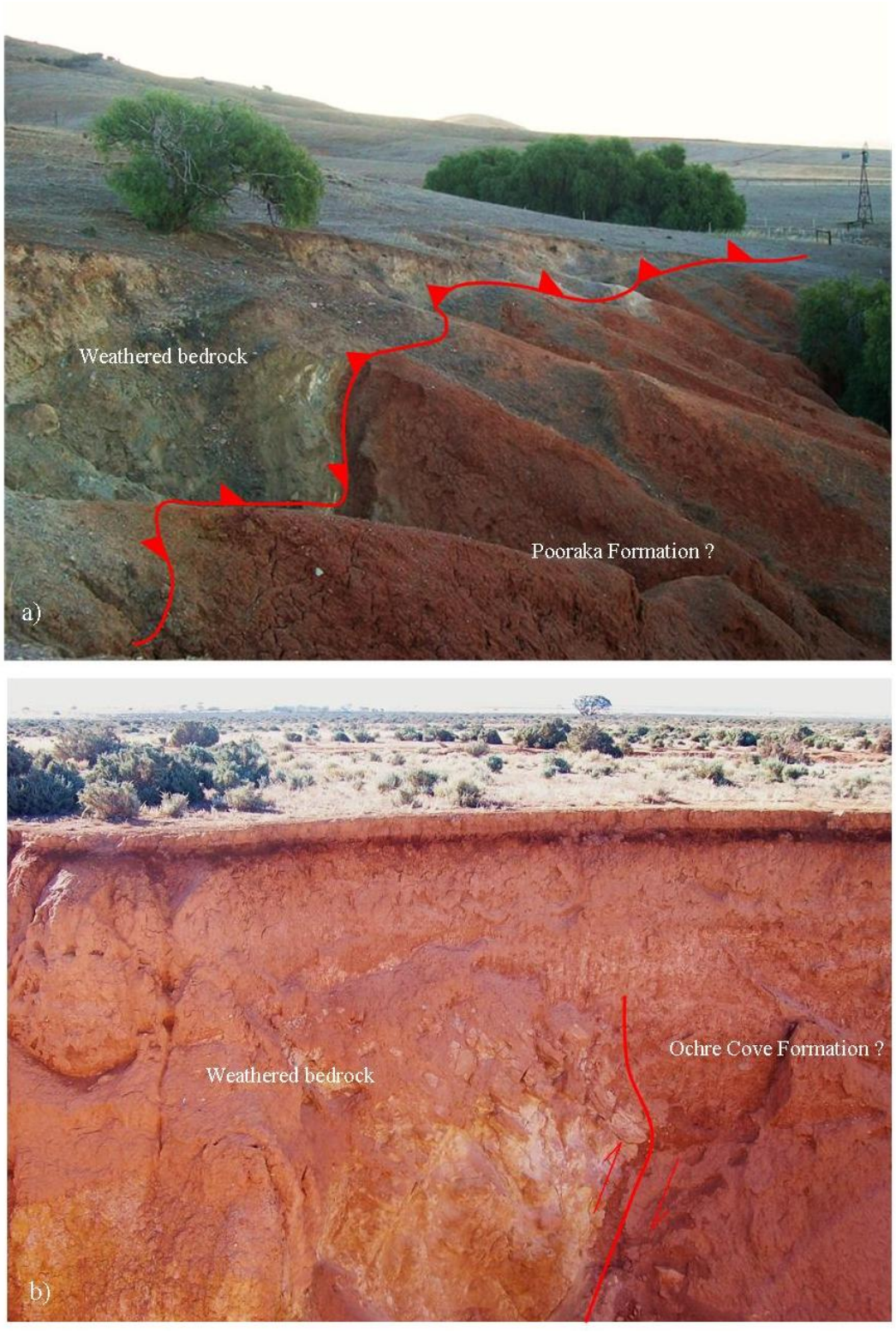

Figure 4.9 *Burra Fault exposure at Burra a) Fault exposure on a erosion gully near Worlds End. Photo taken looking towards WNW, location coordinates: 316928 E, 6259863 S, b) Fault exposure at Worlds End Creek adjacent to Worlds End Highway, South Australia, location coordinates: 320477 E, 6264051 S*

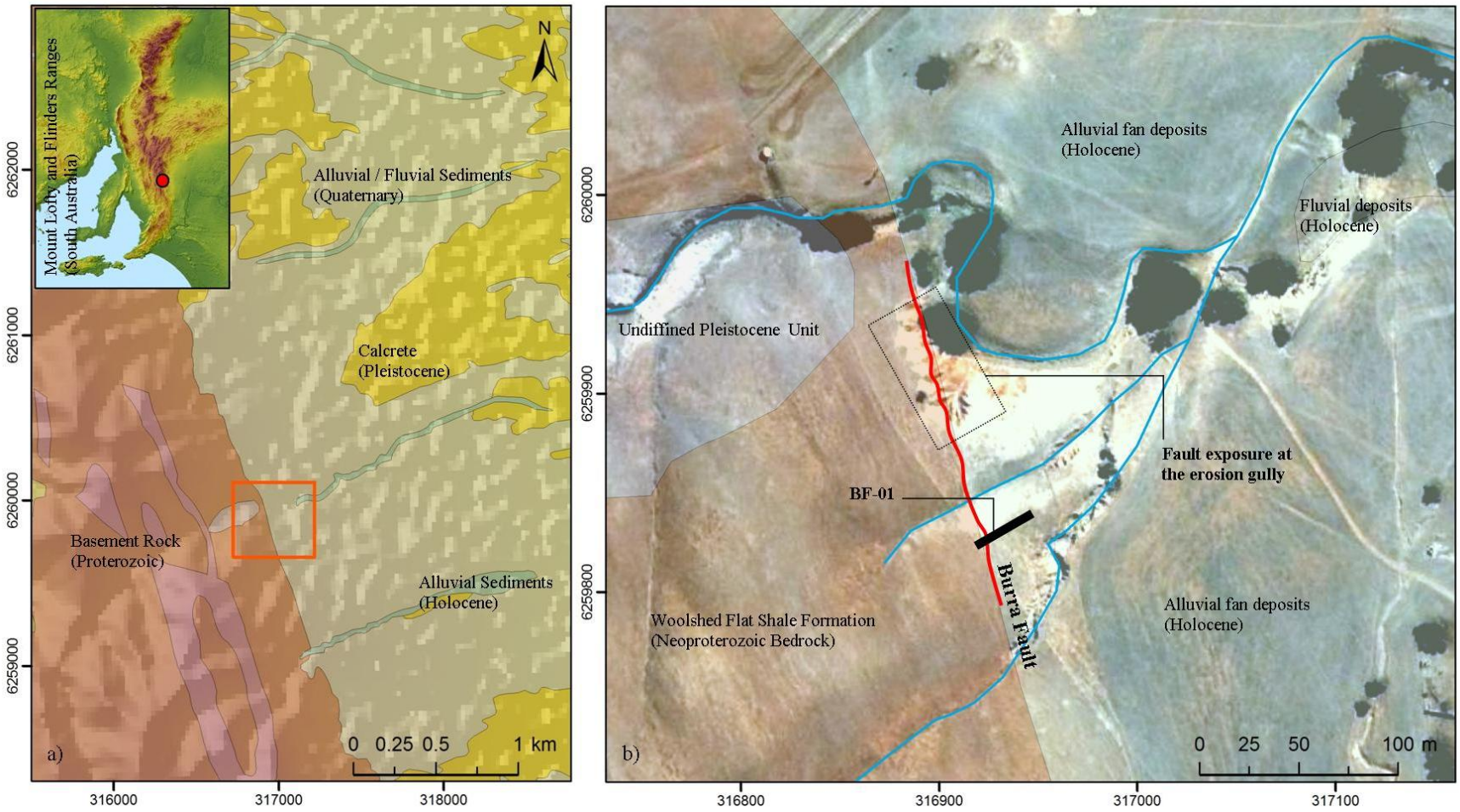

Figure 4.10 *Planview of the site near Burra a) Regional geology map, b) Local geology and trench locations (Trench not to scale)*

4.3.4 Williamstown-Meadows Fault – Tarlee & Bethel

The Williamstown–Meadows Fault is located towards the middle of the Mount Lofty Ranges. It is one of the longest faults identified in the ranges and was recognised as a combination of the Kitchener and Gilbert Range Faults by (Alley 1973). The Kitchener Fault may also have connections to the Stonyfell Fault (Sprigg 1946), making the Williamstown-Meadows Fault an amalgamation of three main faults. Generally SE dipping Williamstown-Meadows Fault expresses a reverse sense of movement with a changing strike, from northwest to north along the fault trace (Marshak & Flöttmann 1996). It is recognised as a reactivated basement fault, which serves as a zone of crustal weakness, possibly experiencing multiple episodes of deformation (Tokarev 2005). However, neotectonic activity along the Williamstown-Meadows Fault is clearly distinguishable based on the distribution of Tertiary sediment. Clark and McPherson (2011) suggested a single event surface rupture of at least 25 km, with a reverse displacement of ~1.8 m, but without specific age constraints. A magnitude 4.2 earthquake was recorded 30 km east of Kapunda in 1966 (Ma & Beroza 2008), in close proximity to the Tarlee and Bethel townships. However, there is no evidence of either a fault-generated scarp or a recent slip along the exposed contacts of the Williamstown-Meadows Fault related to this event.

Field observations - Tarlee

An exploration trench was excavated at Tarlee, ~73 km NNE to the city of Adelaide and the trench is referred as WMF-01T in this thesis (Figure 4.12). Subtle changes in topography and exposures in the banks of a creek revealing contacts between weathered bedrock and unconsolidated sediments near the Tarlee site provided evidence of fault activity. The east-west oriented ~38 m long trench at Tarlee (Figure 4.13) exposed a probable Quaternary displacement along the Williamstown-Meadows Fault. The low-angle thrust fault (Figure 4.11) with a strike of 354° and a dip of 26°E has an offset of ~1.6 m along the dipping plane, based on the displacement of a calcrete layer. At the base of the excavation, the low-angle thrust fault cuts through an unconsolidated soil stratum with red and white mottles resembling the Ochre Cove Formation.

The hanging wall stratigraphy from top to bottom of the excavation consists of a thin surface layer of a dark brown Holocene/recent soil layer, a thin light brown soil horizon on top of a thick calcrete layer of ~1 m underlain by a thin gravel layer, and ~0.5 m of a palaeosol on possible Ochre Cove (Hindmarsh Clay) at the bottom. The footwall sediment sequence includes a colluvial wedge beneath the recent dark brown soil layer. This has likely resulted from recent faulting and lies between the continuous topsoil horizon and a comparatively thick continuous layer of light-brown soil (Figure 4.13). Magnetic susceptibility values from the Tarlee trench have revealed slightly higher readings on the fault gouge material compared with readings on the hanging wall and footwall. The increase in the magnetic susceptibility values could possibly represent groundwater movement along the fault plane and precipitation of iron oxides.

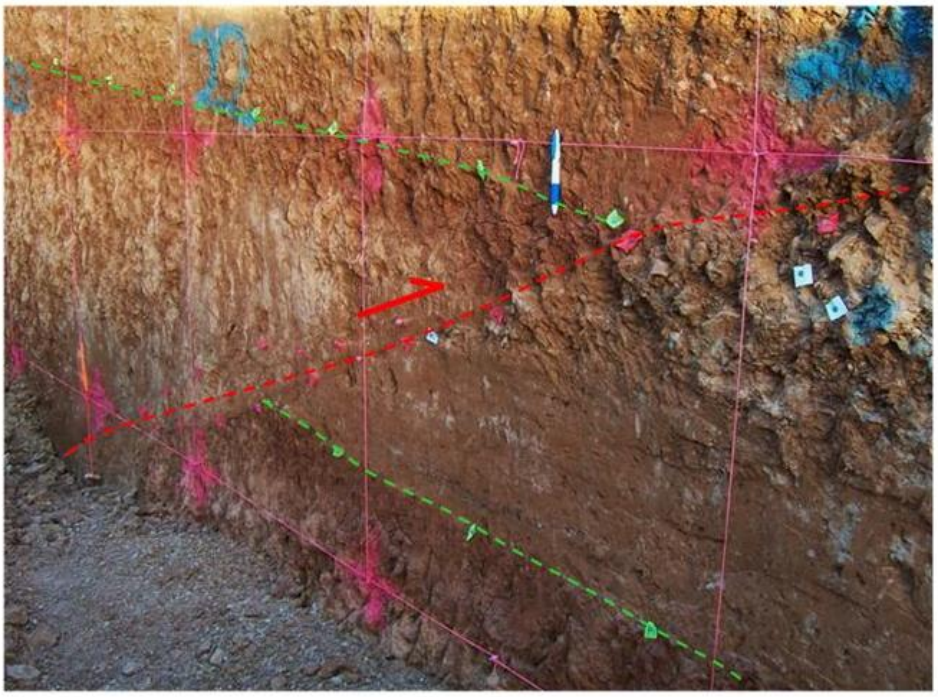

Figure 4.11 *Low-angle thrust fault of the Williamstown-Meadows Fault near Tarlee, showing ~ 354° strike and 26° of dip towards E. Offset of ~1.6 m along the dip is represented by the green colour dashed-lines. Photo facing SE of the trench WMF-01T, location coordinates: 296784 E, 6203073 S*

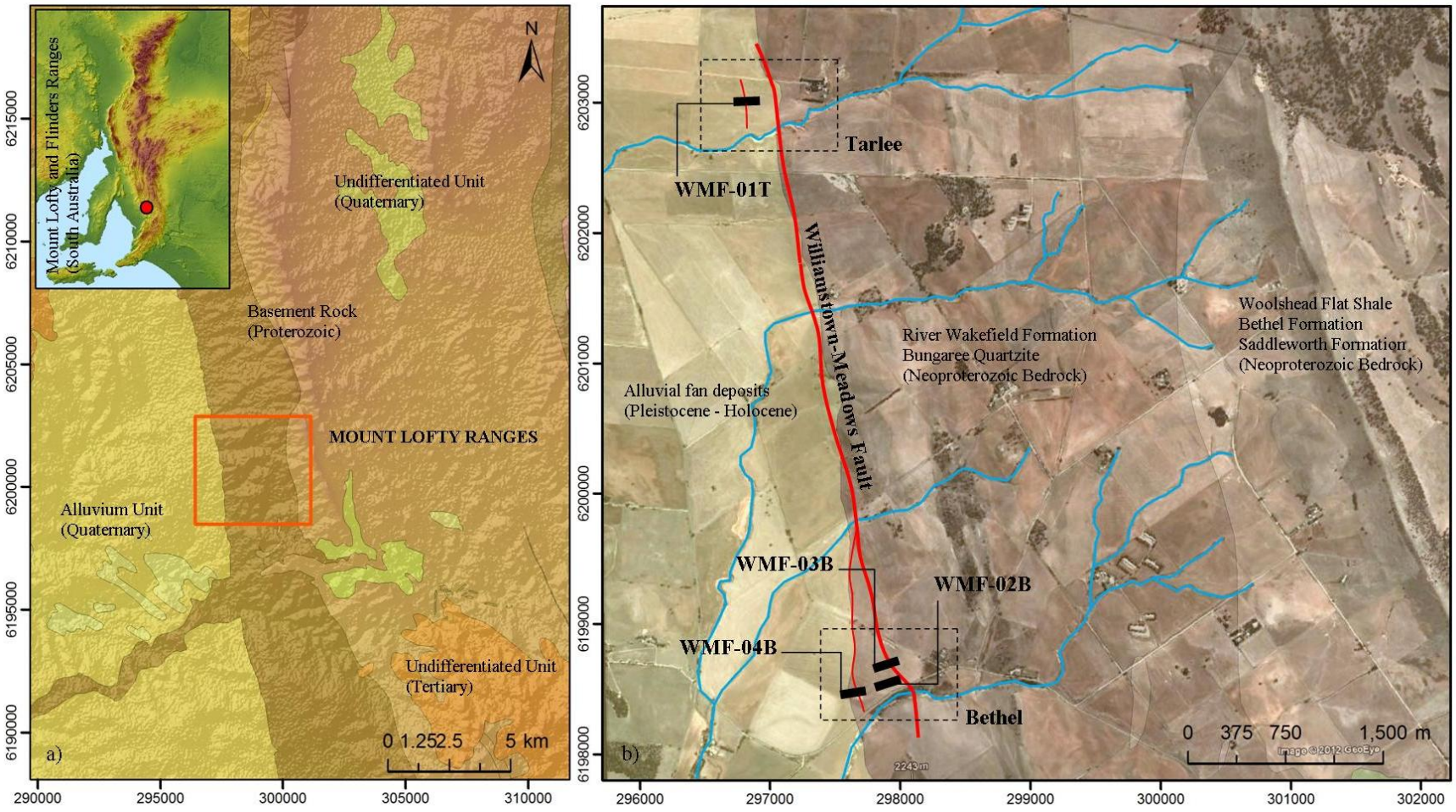

Figure 4.12 *Planview of the sites near Tarlee and Bethel a) Regional geology map, b) Local geology and trench locations (Trenches not to scale)*

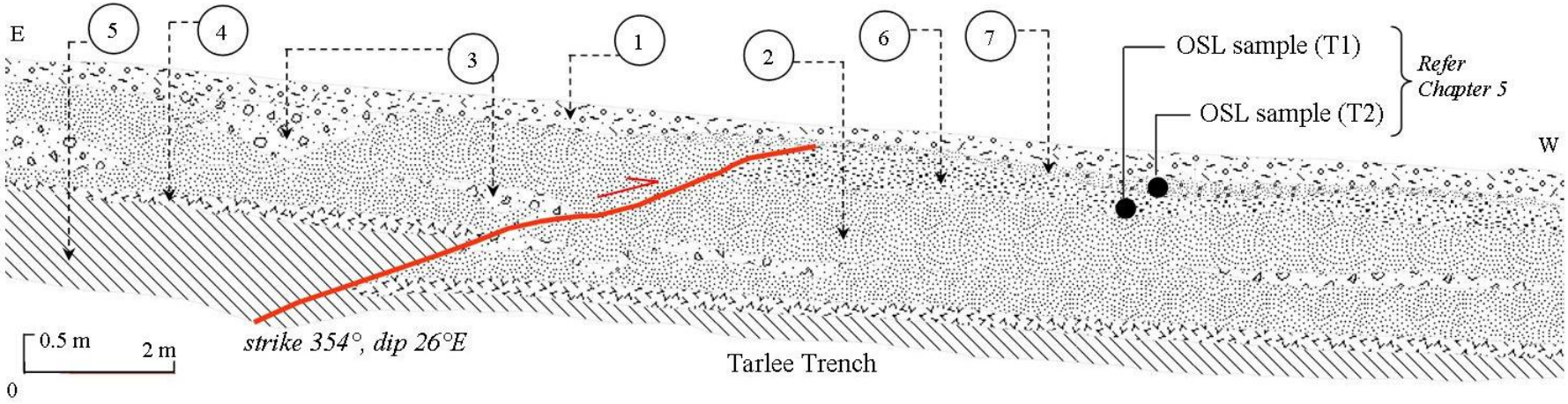

Figure 4.13 *Illustrative diagram of stratigraphic units on the Tarlee Trench (WMF-01T).*

Unit descriptions follow the numbering sequence: 1) Topsoil layer – Dark-brown and reddish-brown gravelly clay layer with lumps of sandy clay. This flat lying disturbed soil layer maintains an even thickness (~0.2 m on average) throughout the fault zone and it is rich with plant roots, 2) Calcrete unit– White and brownish-white fine grained silty sand layer. Thickness varies from 1.5 to 1.8m in the exposed trench. The fault has completely cut across this layer, leaving gravel lenses on both sides, 3) Gravel lenses – Equally distributed both on foot-wall and hanging-wall within the calcrete layer, 4) Thin layer of gravelly soil – Brown, soil layer with abundant gravels and silt, 5) Thick soil unit (Ochre Cove/Hindmarsh Clay?) – Light-brown, pale-yellow, sandy clay layer with orange, light-brown mottles, 6) Soil unit between the calcrete and the colluvial wedge – Light-brown to pink clayey coarse grained sand with gravel lenses. A comparatively uniform unit with an approximate thickness of 0.5 m, either a surface soil layer before the faulting or developed after the fault rupture (OSL-T1), 7) Colluvial wedge – Yellowish-brown, clayey fine grained sand layer having an unsorted matrix of gravels, cobbles and pebbles, possibly developed after the fault rupture, as the layer thickness increases away from the fault, from E to W on the exposed section of the trench. (OSL-T2)

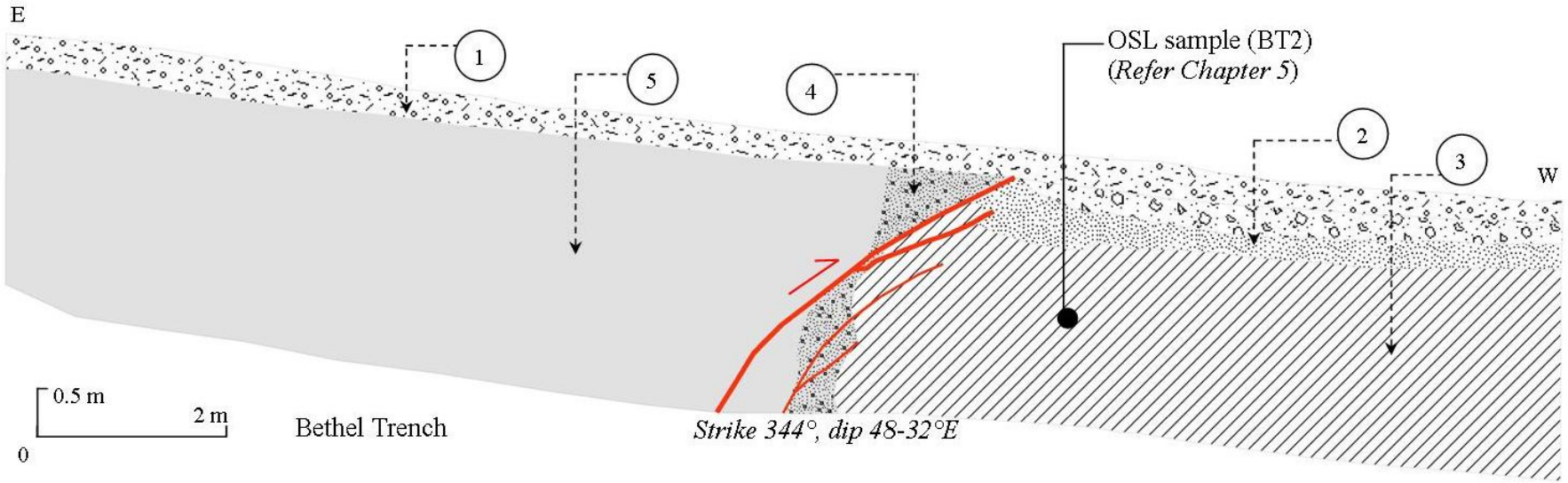

Figure 4.14 *Illustrative diagram of stratigraphic units on the Bethel Trench (WMF-03B).*

Unit descriptions follow the numbering sequence: 1) Topsoil layer – Dark-brown, brown, clayey thin soil layer with gravel and abundant plant roots. A very thin layer of calcrete has been developed underneath this (Holocene/recent) soil layer, which runs across the fault zone undisturbed, 2) Colluvial wedge - Light-brown, pale-yellow clayey sand with gravel and patches of carbonate rich soil, 3) Thick layer of clay - Reddish-brown, dark-brown, thick layer of clay with some silt and fine sand, 4) Fault gouge material – Yellow, pale-yellow, white and light-brown – sandy clay layer with highly weathered bedrock particles, 5) Weathered bedrock – Light-brown, light-grey, pale-yellow, highly weathered, highly fractured bedrock with quartz veins and clay filled sub-horizontal fracture sets almost parallel to the fault plane.

Field observations - Bethel

The Bethel trenching site was located ~68 km NNE of the city of Adelaide (Figure 4.12). The three east-west oriented trenches at Bethel are named as WMF-02B (Bethel-east), WMF-03B (Bethel-hill) and WMF-04B (Bethel-west) in this thesis. Gentle breaks in slope at the Bethel site and a bedrock knickpoint in a deeply incised creek, to the south of excavation site, provided evidence for ongoing deformation. Of the three trenches, WMF-03B (Figure 4.14) exposed a bedrock-involved thrust fault and WMF-04B, located ~500 m southwest of WMF-03B, exposed a low angle thrust within soft sediments (Figure 4.15b). The ~36 m long east-west oriented WMF-04B excavation displayed a fault contact with a strike of 000° and a dip of 13° towards the east. The fault dislocates a sandy clay layer with carbonate mottles for ~ 0.3 m along the dipping plane. WMF-02B did not encounter a fault contact but there was evidence of fracture sets oriented at 345° and dipping at 28°E. A vertical fissure filled with carbonate blocks, possibly resulting from settlement after thrusting was identified on the same fractures.

Approximately 28 m long, the Bethel-hill trench (WMF-03B) displayed a fault striking 344^0 with a varying dip of 48° - 32° towards east (Figure 4.15a). A displacement of about 0.75 m could be inferred at the main fault contact, whereas some upward branching could have possibly resulted from multiple rupture events. The hanging wall consists of grey coloured basement rock, increasingly weathered and fractured towards the fault contact. There are a few subsidiary faults and parallel fracture sets on the hanging wall. The footwall consists of a thick unit of reddish brown clay containing a few sand lenses. The fault contact is covered by a thin horizon of Holocene soil and a ~0.4 m colluvial wedge on top of the clay layer possibly related to the faulting. The subvertical extensional fractures on the hanging wall may have resulted from collapse after reverse faulting. The fault zone and bedrock fractures consist of strongly cemented breccias. Extensional fractures and subsidiary faults on the bedrock display both reactivation of older structures and new structures bisecting the older fabrics (Figure 4.16).

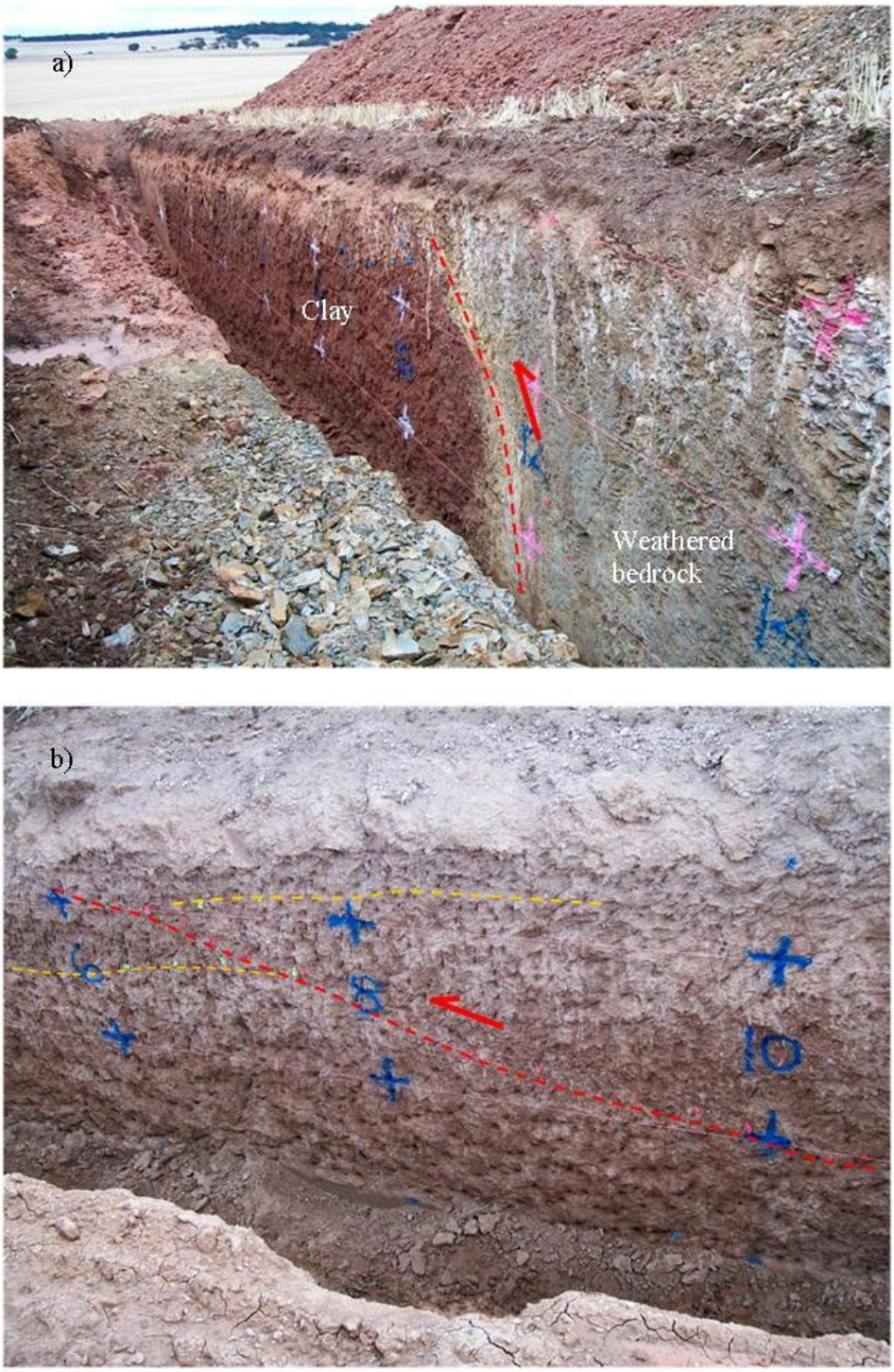

Figure 4.15 *Williamstown-Meadows Fault segments exposed near Bethel. a) High angle thrust fault from trench WMF-03B, recorded a strike of 344^0 and a varying dip of 48°-32° towards ENE. Photo taken facing northwest, location coordinates: 297912 E, 6198685 S, b) Low-angle thrust fault from trench WMF-04B displaying a strike of 000^0 and a dip of 13° E. The orange colour dashed line represents the offset of a gravel layer. Photo taken facing northwest, location coordinates: 297696 E, 6198460 S.*

Figure 4.16 *Bedrock structures showing neotectonics dissecting quartz veins possibly developed along the older fault contacts (trench WMF-03B)*

The orientations recorded from the structural fabrics exposed by trenching near Bethel display a gradual increase of dip from WSW towards ENE. These observations accord with a conceptual cross-section, which resembles positive flower structuring (Figure 4.18). Accordingly, WMF-04B represents the lowest thrust angle with 13°, whereas WMF-02B and WMF-01T record 28° and 30° respectively. The high-angle thrust in WMF-03B is the steepest fault in the assemblage, strongly suggesting the influence of transpressional dominant positive flower structuring. The orientation of fracture sets on WMF-02B aligns with the orientation of the Tarlee fault exposure. Based on these trenching observations Williamstown-Meadows Fault can branch into three main sets of faults, provided it is a continuous structure between the Tarlee and Bethal sites, (Figure 4.17).

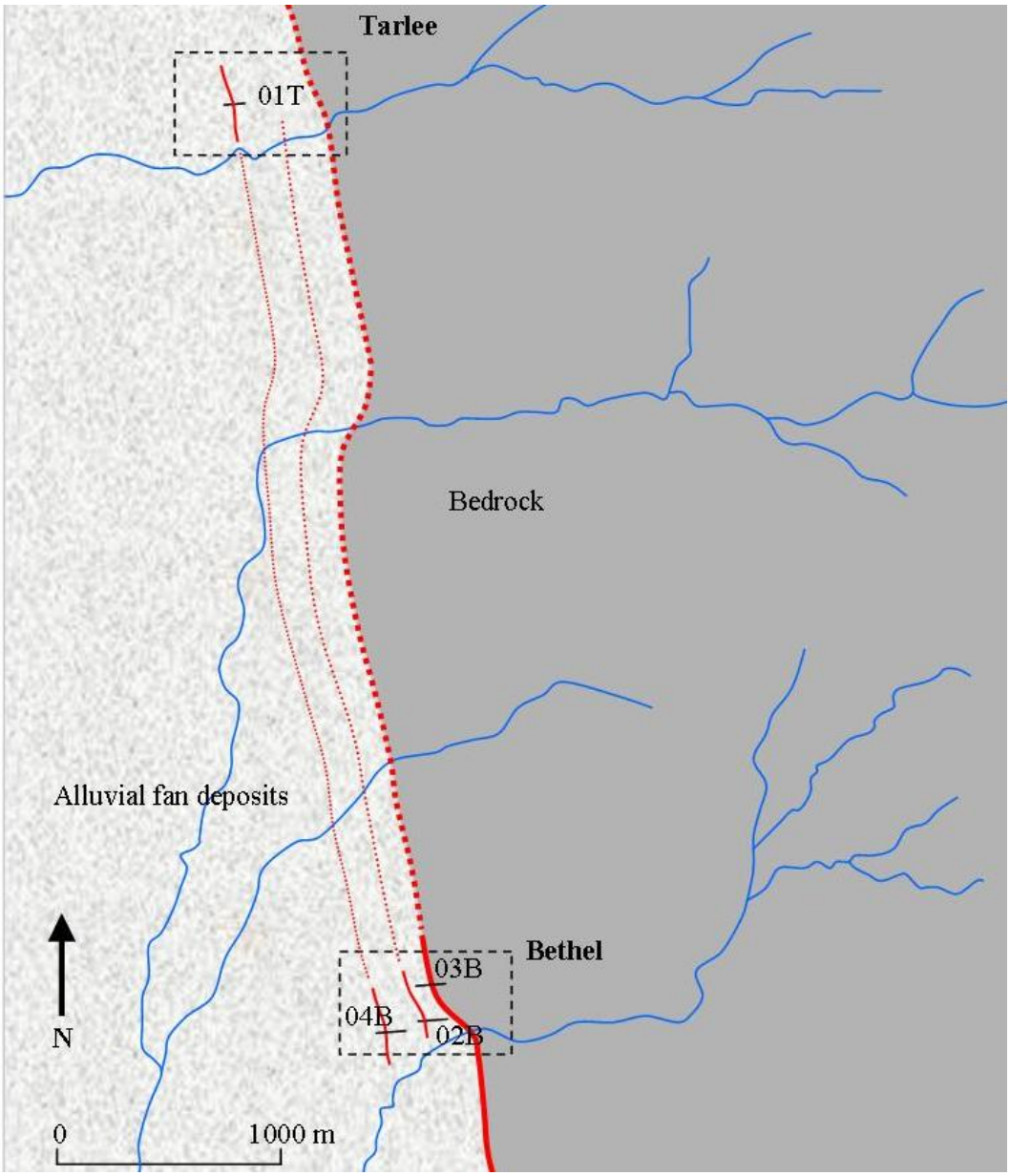

Figure 4.17 *Interpretations of possible branching of the Williamstown-Meadows Fault based on the observations near Tarlee and Bethel*

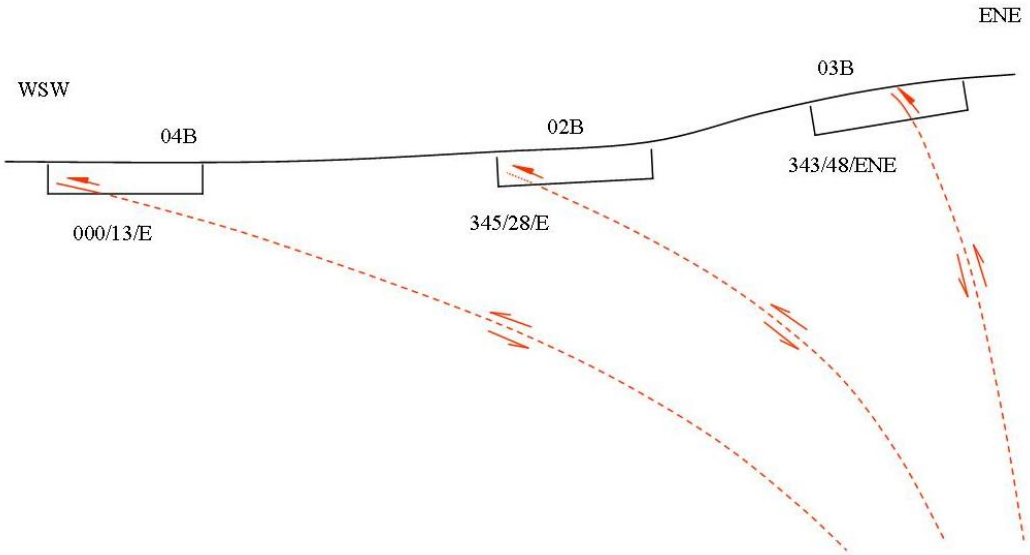

Figure 4.18 *Conceptual cross section of the segmentation experienced by the Williamstown-Meadows Fault near Bethel (Figure not to scale)*

4.3.5 Para Fault – Gawler East

The Para Fault is located on the western flanks of the Mount Lofty Ranges, and has a surface expression in an approximately 43 km long curvilinear scarp starting from Gawler. The elevation along the scarp decreases towards the south, and the fault runs offshore in subsurface through the western side of the city of Adelaide. The ENE trending Para Fault, has been interpreted as a normal fault dipping at 60°-80°W based on gravity data, and suggested to have been active during the Quaternary (Thomson 1969b). The proposition of a west dipping normal fault plane, contradicts the present understanding of east dipping range bounding reverse faults on the western flank of the Mount Lofty Ranges. However, Tokarev (2005) accommodated both normal and reverse faulting on the Para Fault, based on variations in the thickness of the Glanville Formation near Port Adelaide. The initial normal fault movements during the Tertiary would have provided increasing sediment accommodation space towards the fault, whereas Pleistocene block uplift increased the thickness of the sediments away from the fault. However, the increase in thickness of the Glanville Formation away from the fault indicates dragging up of both foot-wall and hanging-wall blocks due to the reverse movements of the Para Fault (Belperio & Bateman 1986, Belperio & Rice 1989, Sheard & Bowman 1996).

As stated in the field guide of McPherson & Clark (2011), a Delamerian-originated east dipping, wide ductile shear zone within the bedrock of the uplifted eastern side of the inferred Para Fault has been identified near Gawler. The same publication documents resistivity data showing a change in conductivity in certain regions of this locality, which may be an indication of groundwater in low conductive bedrock and the regolith. A series of *en echelon* fault splays towards the southern tip of the fault segment near Gawler, was postulated in a gravity study by Finlayson (1978). These splays were documented in geotechnical reports as west, main and east segments of the Para Fault, and included in the maps of Sheard & Bowman (1996). These seismic reflections at Gawler have also revealed possible east-dipping formations that could be interpreted as positive flower structures commonly observed in disrupted zones due to transpressional movements.

According to the borehole data, the movements in Para Fault have resulted at least 27 m of offset in the late Pleistocene Pooraka Formation (Sheard & Bowman 1996). Therefore, a time averaged fault slip rate of 0.2 – 0.8 mm/yr has been calculated for the last 35-125 ka (Drexel & Preiss 1995). Similar displacements on the underlying Pliocene Hallett Cove Sandstone, by the Para Fault (Glaessner & Wade 1958, Twidale & Bourne 2004), imply long-term slip rates smaller than those of the mid-Quaternary. A full-length rupture along the Para Fault has a potential recurrence time interval of 10,000 years. According to Fenner (1930), dirt scarps and the disrupted modern ground surface along the West Terrace of Adelaide can be related to recent fault activity of the Para Fault. However, considering the reverse faulting geometry of the Mount Lofty and Flinders Ranges, the 1954, magnitude 5.5 Adelaide earthquake may have registered a recent rupture event on the Para Fault at depth, instead of on the Eden-Burnside Fault.

Field observations

The trenching site at Gawler East was located ~32 km NNE of the Adelaide city (Figure 4.20). The two trenches of Geosciences Australia did not encounter a fault contact even though there is an indication of a subtle scarp-like feature in the surface topography (Figure 4.19). The trenches did not reveal stratigraphic evidence of fault-influenced deformation of either the Pooraka Formation (~120ka) or the Hindmarsh

Clay (300-500 ka). The most recent rupture on the Para Fault segment near Gawler, can be estimated beyond ~300 ka, with a bedrock offset of ~140 m (McPherson & Clark 2011).

Figure 4.19 *Trenches across Para Fault near Gawler a) South trench (PRF-01) photo taken looking towards E, location coordinates: 291745 E, 6161495 S, b) North trench (PRF-02) photo taken looking towards E, location coordinates: 291809 E, 6161768 S*

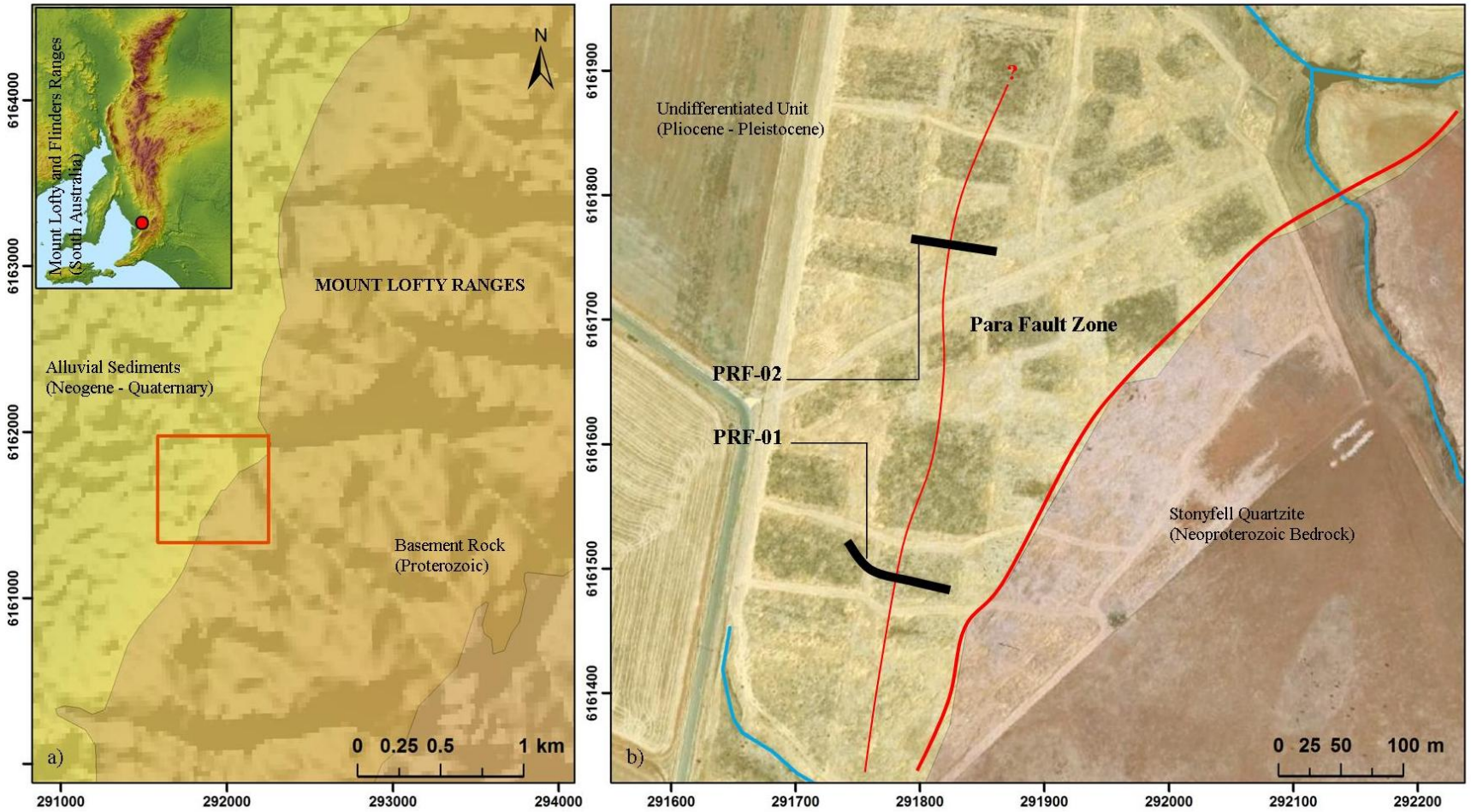

Figure 4.20 *Planview of the site near Gawler a) Regional geology map, b) Local geology and trench locations (Trenches not to scale)*

4.3.6 Milendella Fault - Cambrai

The Milendella Fault is located on the eastern flank of the Mount Lofty Ranges (Mills 1965). Given the clear evidence of recent tectonic dislocations, the Milendella Creek and its tributaries may have rapidly eroded and dissected the Milendella Fault Scarp, to leave limited remnants of a fault generated escarpment. A naturally exposed fault contact west of Cambrai accentuates the active compressional tectonic regime on the eastern flanks of the Mount Lofty Ranges (Bourman & Lindsay 1989, Sandiford 2003). The fault exposure on the stream bank near Cambrai records ~45° west dipping reverse movements, which may be considered as a possible reactivation of Palaeozoic thrust faults (Bourman & Lindsay 1989, Sandiford 2003a). Descriptions by Reid (2007) of another fault outcrop followed by a tectonically initiated bedrock knickpoint in the same locality, could possibly demonstrate progressive fault movements. A varying dip of 60-80°W has also been recorded by Coats & Thomson (1959) on segments of the Milendella Fault.

The hanging wall of the Milendella Fault consists of metamorphosed and brecciated Cambrian bedrock (Kanmantoo Group schist) and on the footwall, Middle Pleistocene fanglomerates of the ferruginous Ochre-Cove Formation. Quaternary sequences along the Milendella Fault are reported to have a thickness of ~30 m at this locality. Early Miocene limestone (Mannum Limestone) fragments have been dragged up along the fault (Bourman & Lindsay 1989, Bourman & Pillans 1997). A thin calcrete layer blanketing the footwall sequence is suggested to have derived from the dissolved and re-precipitated Tertiary limestones, which were dragged to the surface by faulting. Based on the disruptions to this calcrete layer it is possible that there were tectonic movements during the late Pleistocene, (Bourman & Lindsay 1989).

Post Miocene faulting at the Cambrai site (Twidale & Bourne 1975) could have been active up until the late-middle or early-late Pleistocene, based on the palaeomagnetic readings of 930-780 ka on the tectonically disrupted iron-rich Ochre Cove sediments (Pillans & Bourman 1996, Bourman & Pillans 1997). They demonstrated that the Ochre Cove sediments at Cambrai display a chaotic geomagnetic signature interpreted as indicating major tectonic disturbance following the imprint of the

weathering. At least ~300 m of present day topographic relief and ~60-90 m of displacement since the early Miocene due to the reverse movements of the Milendella Fault can be deduced from the offset of the Mannum Limestones (Mills 1965). This is further restrained to, at least ~30 m displacement of during the last ~1 Ma, with observations on the exposed fault contact (Bourman & Lindsay 1989, Sandiford 2003a). Moreover, a displacement of ~7 m from a single rupture event is inferred on the ~54 km long Milendella Fault Scarp by Clark & McPherson (2011).

Field observations

A natural exposure of the Milendella Fault contact can be observed in an erosion gully bank ~67 km ENE from Adelaide and ~4 km west of Cambrai township on the eastern flanks of the Mount Lofty Ranges (Figure 4.22). The fault contact records a strike of 188° and a dip of ~59° to the west, gradually decreasing as the fault reaches the surface (Figure 4.21).

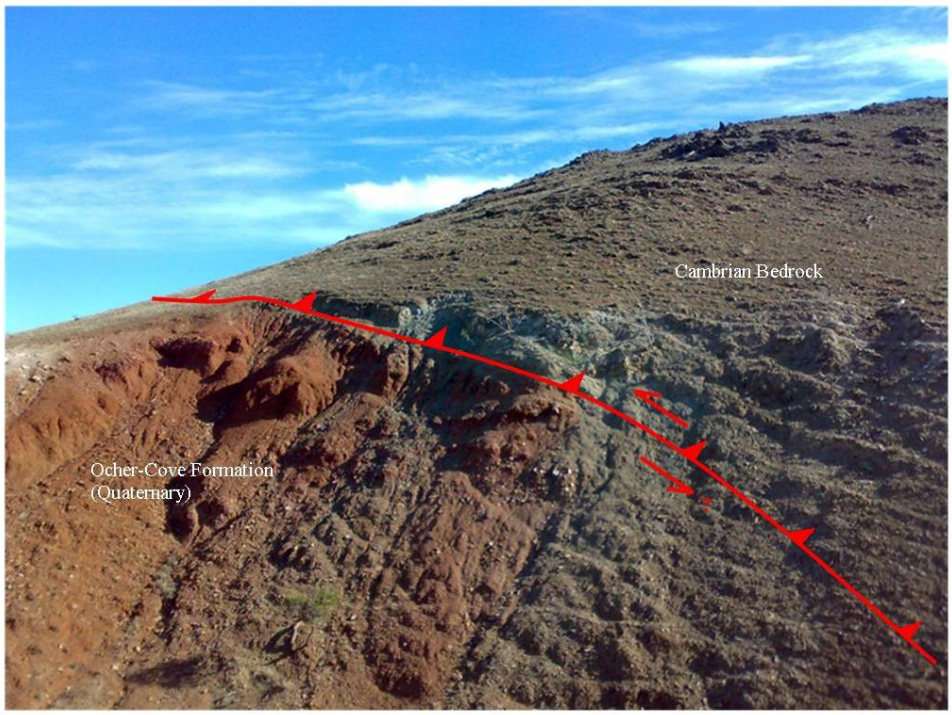

Figure 4.21 *Milendella Fault exposure near Cambrai, eastern flanks of the Mount Lofty Ranges. The view looking south along the strike of the fault. Location coordinates: 339080 E, 6163190 S*

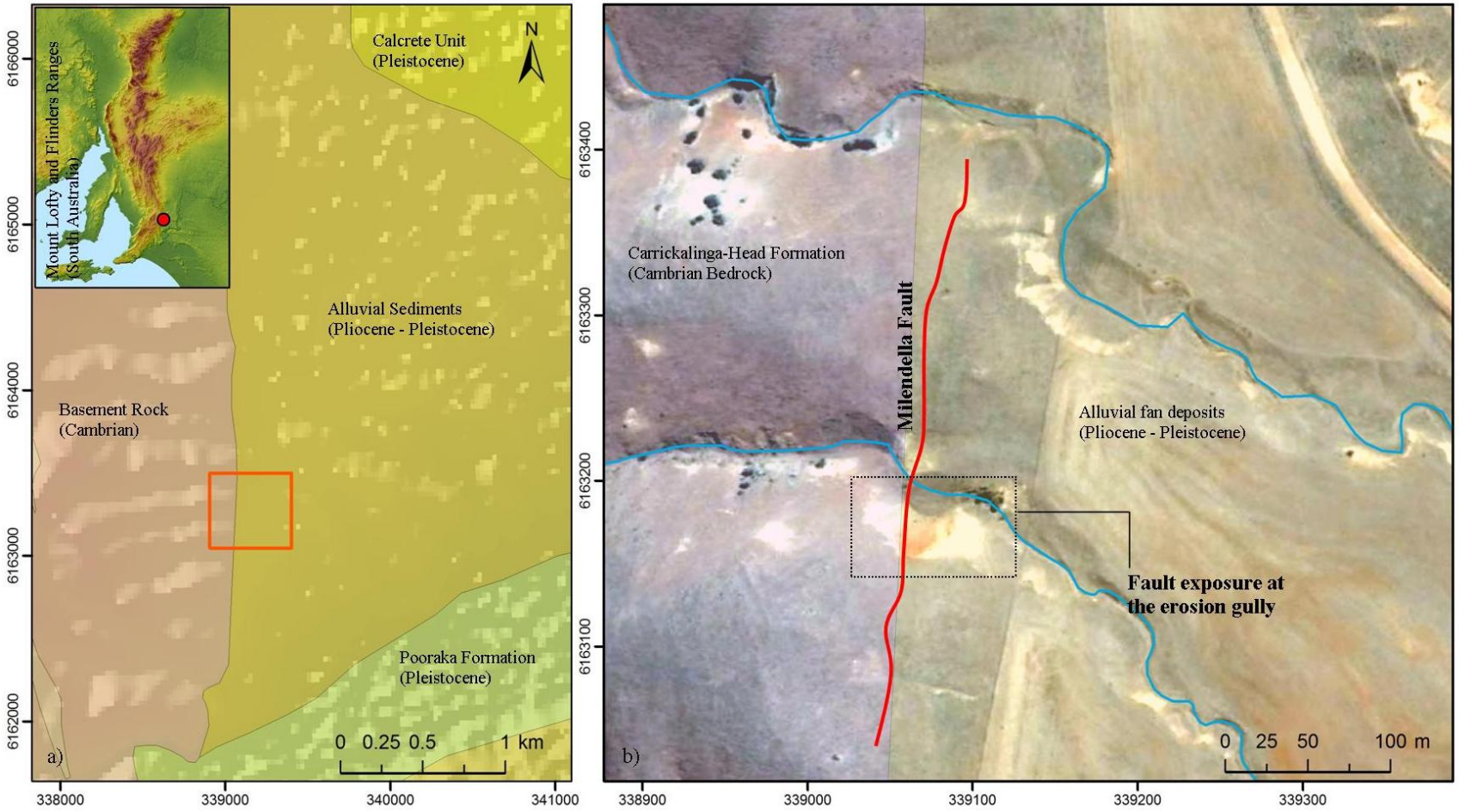

Figure 4.22 *Planview of the site near Cambrai a) Regional geology map, b) Local geology map*

4.3.7 Eden-Burnside Fault -Vista

The Eden-Burnside Fault is on the western side of the southern Mount Lofty Ranges and extends offshore near Marino. It is a combination of the Eden and Burnside Faults, where the Eden Fault forms the major escarpment and the Burnside Fault is primarily subsurface, largely covered with alluvial fans (Sprigg 1946). The Hope Valley Fault, which is northwest to the Eden-Burnside Fault (Sheard & Bowman 1996), could possibly be a fault splay radiating from Burnside segment. The Eden-Burnside Fault is identified as a fault network, displaying a complex series of movements (Fitzgerald 1978). It is exposed near Vista, to the east of the Highbury Quarry adjacent to the Anstey Hill Nature Reserve (Figure 4.23) ~15 km NEE of the Adelaide city. The fault exposure is also in close proximity to the Gun Emplacement, which is a prominent ferricrete terrace (Fitzgerald 1978, Bourman *et al.* 2010a). Clark and McPherson (2011) reported a ~5 km section of fault scarp preserved in ~120 ka sediments, south of Adelaide's eastern suburbs, which possibly relates to a single rupture event on the Eden-Burnside Fault.

The following descriptions are extracted from (Bourman *et al.* 2010a) and fieldwork conducted as a part of this study, unless stated otherwise. The Eden-Burnside Fault contact is exposed close to the unconformity of the Eocene North Maslin Sand with the weathered Adelaidean (Precambrian) Woolshed Flat Shale Formation (Figure 4.24). The gently folded high angle reverse fault tilts the North Maslin Sand steeply upwards at 60° to 80° at most of the locations. Distinct slickensides were identified on the weathered Woolshed Flat Shale Formation at the fault contact indicating vertical striations (Fitzgerald 1978) and oblique sinistral movements (Bourman *et al.* 2010a). The fault gouge material contains sandy clay, carbonates and iron oxides. Shear zone fabrics on an oriented sample of fault gouge indicates dominant reverse motion including elongated quartzite remains showing *en echelon* (Fisher *et al.* 1992) textures with left lateral movements for the most recent faulting (Bourman *et al.* 2010a).

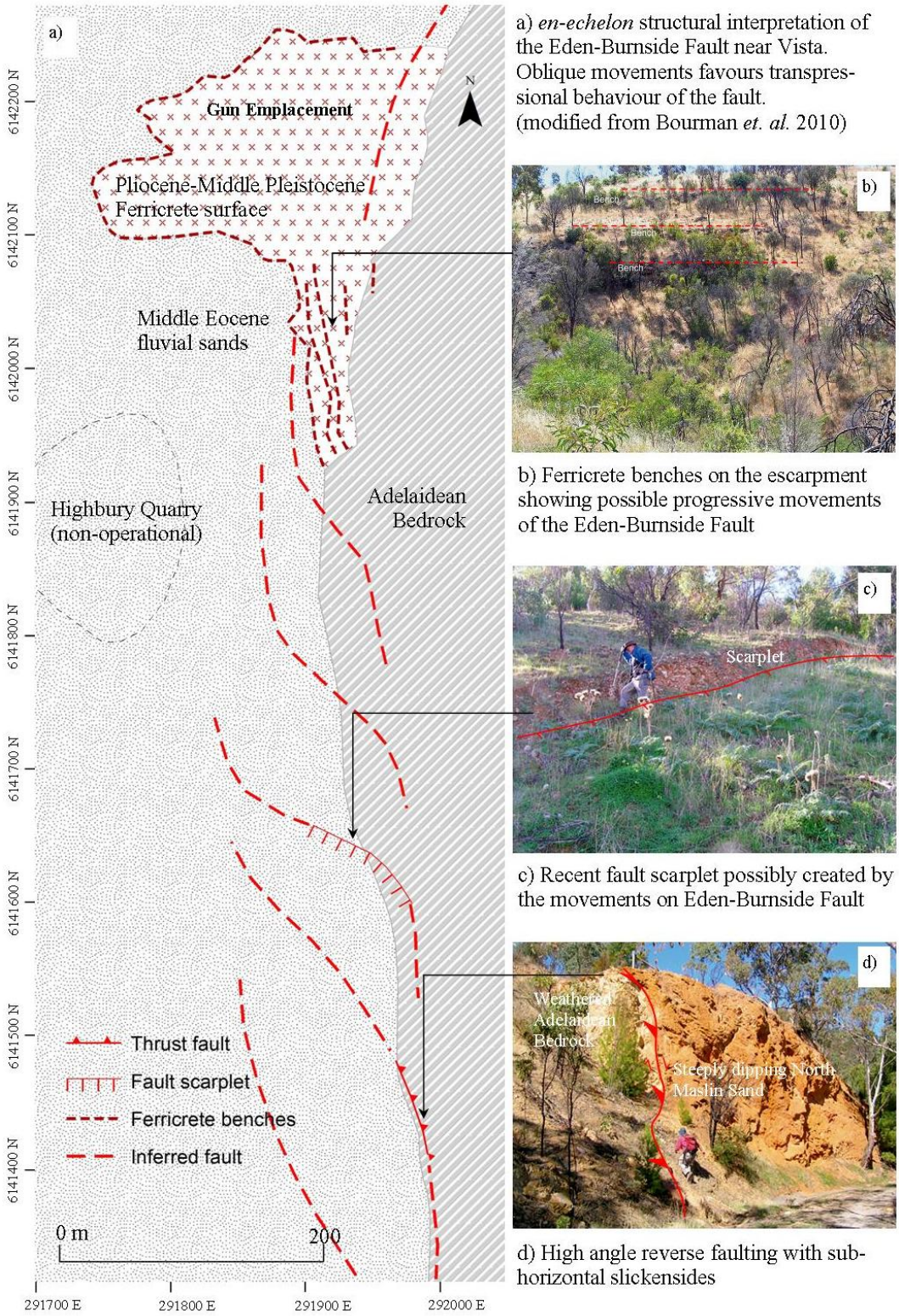

Figure 4.23 *Planview interpretations of the Eden-Burnside Fault near Vista (Bourman et al. 2010a)*

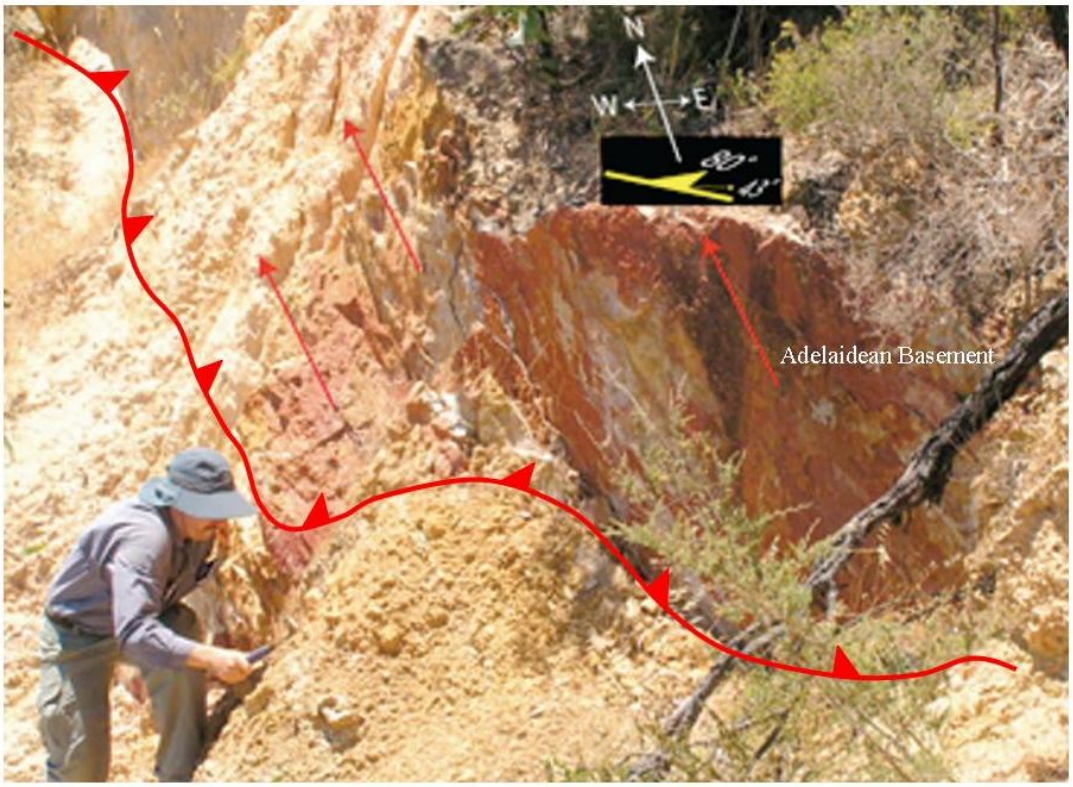

Figure 4.24 *Eden-Burnside Fault exposure at Anstey Hill Nature Reserve (Bourman et al 2010a)*

The remnants of a disrupted ferricrete surface by the successive movements of the Eden-Burnside Fault are observed uphill of the Gun Emplacement. The step-like arrangement of these benches is suggested to result from Pleistocene uplift, which led to erosion of overlying Eocene sands (Fitzgerald 1978). However, a recent surface rupture (Figure 4.23c) and the presence of differentially elevated ferricreted benches (Figure 4.23b) at this locality, were attributed a seismic origin and associated with progressive fault movements (Bourman *et al.* 2010a). The offset in topography north of the fault contact may have resulted from the 5.5 magnitude 1954 earthquake on the Eden-Burnside Fault; even though the epicentre was ~12 km away from this location. The ~1.5m high near vertical scarplet is considered to be very recent because of distinct deformational features such as slickensides, sheared lithified colluvial material and negligible upslope retreat of the scarp face. Horizontal slickensides observed on colluvial clays suggest predominantly strike-slip behaviour, oblique to the strike of the Eden-Burnside Fault. These observations suggest that the Eden-Burnside Fault has developed a transpressional behaviour resulting in *en echelon* structures at this locality. The strike of the fault changes across the Highbury

Quarry from NE-SW from south to a N-S orientation at the quarry and again to NE-SW towards the north. The dip direction of the fault varies from west to east along its strike. To the north of the fault exposure and at the recent fault scarp, the bedrock shows intense folding. This folding may be of Delamerian origin and could have influenced on the present movements along the Eden-Burnside Fault.

4.3.8 Wilkatana Fault - Barndioota

The Wilkatana Fault occurs along the western range front of the central Flinders Ranges, situated ~35 km north of Port Augusta. The fault is naturally exposed in the Wilkatana Creek to the east of Barndioota (Sandiford 2003a) and can be located on a Google Earth satellite image ~320 km NWN of the city of Adelaide. Most of the Wilkatana Fault is buried under hillslope and alluvial sediments, but a few segments are exposed towards the southern end of the fault trace. Approximately 6.1 m of offset has been reported due to reverse movements towards the E, with a strike of north-south on exposed contacts (Quigley *et al.* 2007b). An approximately 45° east-dipping reverse fault, which displays limited surface expression, has been observed on another section near the Depot Creek Fan. Sandiford (2003a) recorded ~2-3 m reverse offsets on sections of the Wilkatana Fault, with respect to the footwall sedimentary sequences of late Pleistocene age. Williams (1973) suggested that there has been some 50 m of Quaternary displacement, but without providing detailed filed evidence.

The following information was taken from the work of Mark Quigley unless stated otherwise (Quigley *et al.* 2006, Quigley *et al.* 2007a, Quigley *et al.* 2007c). The Wilkatana Fault comprises a network of moderately to steeply east-dipping reverse faults (Figure 4.25) striking NNW. The dip varies from 45° to 80° along the strike, and the length of the fault has been estimated to be approximately 13.8 km (Quigley *et al.* 2007b). The hanging wall of the Wilkatana Fault consists of Neoproterozoic Emeroo Quartzite, which thrusts over footwall Quaternary units of loosely consolidated talus, breccias and fluvial gravels of the Pooraka Formation of late Pleistocene age (Sandiford 2003a). Reverse oblique-slip due to east-west compression is compatible with the regional maximum horizontal compressive stress vectors. A reverse sinistral motion is recorded on hanging wall slickensides, with

features such as steeply dipping, north striking subsidiary reverse faults splaying off from the main fault trace. Knickpoints are identified as the indicators of progressive fault activity and their headword propagation has created some steeply incised creeks. Fault exposures in close proximity to the range front have been interpreted as evidence of recent movements on the Wilkatana Fault segments. In this context, differentially elevated fluvial gravel terraces (Eyre Gravel) found on the northern Wilkatana Fans might also be related to progressive fault movements.

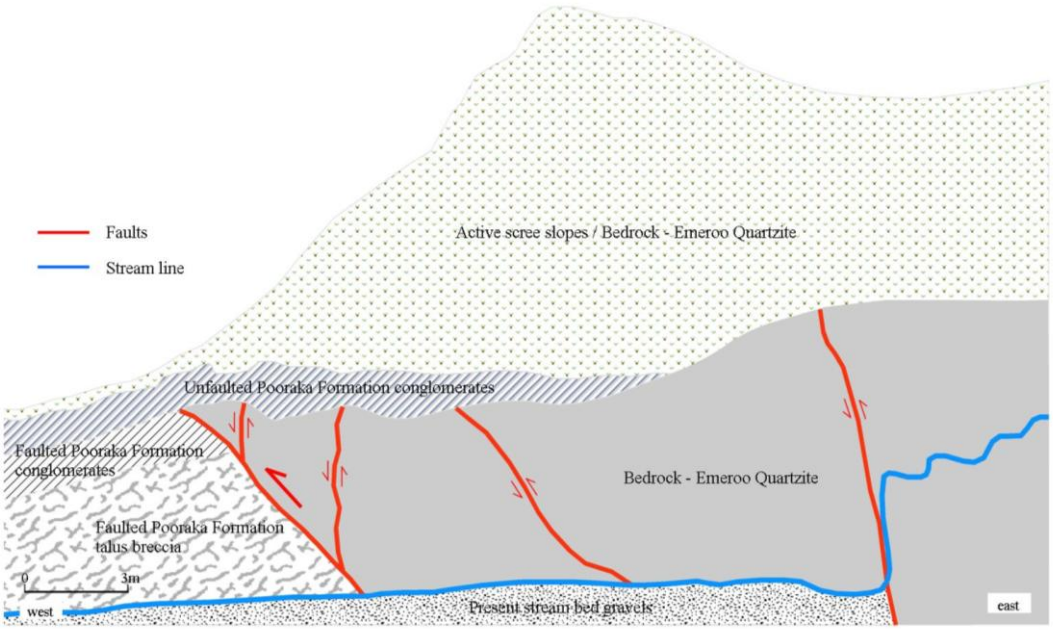

Figure 4.25 *Cross sectional interpretation of the Wilkatana Fault*

The Flinders Ranges have been subject to significant surface rupturing since at least ~80 ka (Quigley *et al.* 2006). Optically Stimulated Luminescence Dating of faulted and post-faulting strata has also registered two possible rupture events since ~67 ka. It has been inferred that the youngest event lead to a ~3.8 m displacement and generated a scarp of ~2 m on the northern section of the Wilkatana Fault, which is consistent with the reverse oblique movements shown by slickensides. Even more recent faulting has been determined (32-29 ka), with a displacement of ~4 m on another segment of the same fault. Hence, a cumulative displacement of ~12 m has been inferred for the time ~67-12 ka. Considering the displacement of Neogene and Quaternary sediments, long term minimum slip rates of 20-30 m/Ma can be attributed to the western bounding faults of the Flinders Ranges (Sandiford 2003a).

Trench	Length (m)	Location	Coordinates				Fault contact	OSL sample name	Comments
			Start		*End*				
			E	S	E	S			
PRLF- 01	34	Moolawatana	377237	6688713	377274	6688692	-	MW 100, 104, 105 & 109	OSL samples were collected from the nearby erosion gullies
PRLF- 02	15	Moolawatana	377276	6688743	377282	6688737	-		
PRLF- 03	10	Moolawatana	377267	6688740	377275	6688736	029 – 52 W		
	Following information from Dan Clark and Andrew McPherson's 2010/11 field notes								
AF-01	40	Hoyleton	277692	6234239	277646	6234239	-	-	Could not locate a fault
AF-02	28	Hoyleton	277678	6234135	277647	6234137	002 – 35 E	A1	-
BF-01	36	Burra	316921	6259814	316966	6259845	118 – 50 NE	B1	OSL sample from erosion gully
WMF-01T	38	Tarlee	296806	6203074	296768	6203075	354 – 26 E	T1 & T2	-
WMF-02B	28	Bethel-east	297967	6198574	297838	6198562	345 – 28 E	BT3A, BT3B	Only fracture sets
WMF-03B	28	Bethel-hill	297934	6198684	297827	6198683	344 – 40 ENE	BT2	-
WMF-04B	40	Bethel-west	297797	6198467	297670	6198456	000 – 13 E	BT1	-
PRF-01	38	Gawler	291918	6161495	291787	6161546	-	-	Could not locate a fault
PRF-02	48	Gawler	291909	6161728	291811	6161731	-	-	Could not locate a fault

Table 4.1 *Summary of the trenching fieldwork*

Fault Name	Figure	Strike	Dip	Motion	Striations	Slip rates	Comments
Willunga (WLF)	3.6	NE to N	70-80 E	Reverse Oblique?	Reverse + left lateral	50-70 m/Ma	Shows transpressional behaviour with compressional structures. Fault splays with sinistral movements
Eden-Burnside (EBF)	4.24	NE to N	80-90 E & W	Oblique	Reverse + left lateral	-	Well developed *en echelon* structures, transpressional behaviour
Milendella (MF)	4.21	N	~45 W	Reverse	-	60-90 m/ (Miocene)	At least 30 m displacement during last 1 Ma
Paralana (PRLF)	4.2	N - NE	30-45 W	Reverse + oblique	-	30 m/Ma	Popup structures, flower structures. Possible left lateral movements during the Delamerian deformations
Williamstown-Medows (WMF)	4.11,15	N	~26-48 E	Reverse	-	-	Upward branching of faults near Bethel
Alma (Wolin et al.)	4.5	N	~35 E	Reverse	-	-	Series of parallel faults on the hanging wall, Upward segmentation of the main fault
Burra (BF)	4.8,9	N- NW	W - SW	High-angle reverse	-	-	Naturally exposed at 316928 E, 6259863 S
Para (PF)	-	N - NE	60-80 W?	Reverse	-	0.2-0.8 mm/Ma	Series of *en echelon* fault splays
Wilkatana (WLKF)	-	N- NW	45-80 E	Reverse + oblique	Reverse + left lateral	~50 m/ (Quaternary)	Fault splays displaying upward branching

Table 4.2 *Summary of the neotectonic fault characteristics revealed by the present study*

4.4 Limitations of paleoseismic investigations

Lack of geomorphic expression on fault scarps is a major constraint that restricts neotectonic investigations in the Mount Lofty and Flinders Ranges. Locating subtle geomorphic features, evidence in erosion gullies and published regional geology maps led the way to determine appropriate sites for field investigations. High resolution LiDAR images or satellite images were not available for all of the trenching sites and detecting the subtle topographic variations across large alluvial fans was difficult. In spite of the systematic approach of field location selection, there were some trenches, which failed to expose fault contacts such as Gawler, Hoyelton and Moolawatana. Among the trenches with exposed fault contacts, it was often difficult to find preserved fault striations, possibly due to the unconsolidated nature of the subsurface sediments. As subsurface gravelly material was prone to collapse at locations like Moolawatana, cleaning of the trench walls did not always provide a straightforward expression of the subsurface stratigraphy. Hence, it was essential not to disturb the unique footprints of faulting, which reveals important information on the nature of fault movements.

Accessibility, cultivation activities and local weather changes restricted site selection and the time of field investigation. Large spatial distribution of the planned trenching sites, extending into very remote locations, time restrictions and mobility issues with the heavy equipment did not allow field investigations in every site. As a result, the Wilkatana Fault could not be visited and trenching was prioritized to cover most of the sites where there were no natural fault exposures. It would have been ideal to conduct GPR surveying on these sites before trenching took place, but equipment availability problems and time restrictions did not favour this plan. Finally, the complex nature of segmentation and deformation on observed fault contacts restricted the information required to ascertain the lengths and distribution of the fault lines. Hence, magnitude of the rupture events could not be calculated, even though stratigraphic offset information was available.

4.5 Discussion

The nature and amount of displacement, recurrence intervals, slip rates and the spatial distribution of most of the active faults in the Mount Lofty and Flinders Ranges are poorly constrained. However, there is clear evidence that major neotectonic faults have sliced through majority of the landscape resulting in uplift, erosion and exposure of the basement geology in this region. Palaeoseismic studies help to reconstruct the nature and amounts of a fault displacements (McCalpin & Carver 2009), and the trenching exercise revealed characteristics of prominent neotectonic faults in the Mount Lofty and Flinders Ranges. A summary of the field activities are given in Table 4.1and Table 4.2.

The complex nature of deformation in the Mount Lofty and Flinders Ranges can be listed as follows;

1) Fault networks have developed through branching of major faults with variable dips varying from low to high angles. Eg: Eden-Burnside, Williamstown-Meadows, Willunga and Wilkatana faults.
2) Often only subtle surface expressions are associated with active faults in the middle of the Mount Lofty and Flinders Ranges. Eg: Alma, Burra and Williamstown-Meadows faults near Hoyleton, Burra, Tarlee and Bethel
3) Multiple rupture events and recurrent movements on older faults may be responsible for resurfacing the basement rocks on the Williamstown-Meadows Fault (trench WMF-03B) near Bethel, Alma Fault (trench AF-02) near Hoyleton and the Willunga Fault (Chapter 3) near Sellicks.
4) Variable sediment characteristics observed on the trench walls may indicate changes to the sediment supply and source regions, which, most probably resulted from fault activity.
5) Deeply incised erosion gullies can be observed at sites near Burra, Tarlee, Bethel, Gawler and Sellicks. Tarlee, Bethel and Sellicks associated with knickpoints, possibly originating from progressive faulting.
6) Triangularly faceted spurs can be observed on most of the scarps nearby the Paralana, Milendella, Alma, Burra and Willunga faults.
7) Slickenside measurements display left-lateral oblique movements on fault contacts such as on the Wilkatana, Eden-Burnside and Willunga faults.

8) Alternative dip-directions along the strike of the Eden-Burnside Fault near Anstey Hill is unlikely to result only from compression.
9) *En echelon* fault segments along the Eden-Burnside Fault near Vista and the Willunga Fault at Sellicks Beach, demonstrate regions of transpression.

Deeply incised gullies, some with knickpoints, are common features in this region, and they facilitated to locate suitable sites for field investigations. The level of incision achieved within a limited downstream distance on gullies near the sites of Burra, Tarlee, Bethel and Sellicks is a reflection of erosion resulting from tectonic uplifting. Knickpoints, which form waterfalls along deeply incised creeks and remain close to their generative scarps, suggest a youthful origin for the tectonic scarps (Sandiford 2003a). At field sites near Tarlee, Bethel and Willunga, prominent knickpoints are linked to major reverse faults, in which cases basement material has been thrust over younger sediments.

Changes in sedimentation characteristics such as from debris flow to conglomerate deposition and vice-versa are taken as indicators of tectonic changes within source regions (Quigley *et al.* 2007b). Walls of the trenches display unconsolidated soil strata with varying thicknesses separated by thin layers or lenses of gravel and brecciated particles of weathered bedrock. These changes may be associated with different episodes of neotectonic faulting, which would probably reflect the recurrence of rupture events. Remnants of several dislocated ferricrete terraces spanning ~25 m on the Eden-Burnside Fault Escarpment have been interpreted as a result of recurrent tectonic activity, disrupting the colluvial capping and uplifted the terraces into distinctively elevated benches (Bourman *et al.* 2010a). Differentially elevated gravel terraces identified in the northern Wilkatana Fans of the Flinders Ranges have been attributed to variations in fluvial deposition (Quigley *et al.* 2007a, 2007b). However, considering the similarities in nature of deformation experienced by the Wilkatana and Eden-Burnside faults, the alluvial terraces could have also resulted from uplift followed by tectonic dislocation. Repeated cycles of extension and compression during the Delamerian and Tertiary may have created the weak zones of older bedrock fabrics (Jenkins 1990, Tokarev 2005). Evidence of structures developed under the present stress regime, dissecting quartz veins developed along

the older discontinuities, could be observed on the hanging wall of a trench near Bethel (WMF-03B). Most of these older structures were dipping NNE, whereas the younger features were dipping ESE, reflecting the discrepancies between the characteristics of deformation.

The Williamstown-Meadows Fault near Tarlee, dips at ~26°E (Figure 4.11), whereas near Bethel it has dips of 13°E, 28°E and ~32-48°ENE have been registered in three separate trenches. Conceptually, the assembly of gradual increasing dips from WSW to ENE on three separate and approximately parallel fault segments near Bethel (Figure 4.15) can be regarded as branches of the same fault. It is hypothesised that the faults merge to a single fault at depth, and are interpreted as positive flower structuring developed on a region subjected to transpression. A gradual decrease of dip and upward branching into several strands was observed, as the primary Alma Fault contact reaches the shallow subsurface near Hoyleton. Additionally, a series of sub-horizontal thrusts on the hanging-wall could also represent strands of the Alma Fault and multiple rupture events. Similar upward branching at the Wilkatana Fault has been recorded by Quigley *et al*. (2007a) and the illustrative cross section can be extended to resemble a positive flower structure.

The alternative dip-directions recorded along the strike of the Eden-Burnside Fault near Vista indicate influential forces beyond simple compression. Steeply dipping *en echelon* fault segments at this locality have been interpreted as resulting from oblique-sinistral movements, possibly resulting from transpression (Bourman *et al.* 2010a). Similar dip variations along the strike of the Wilkatana Fault segments were also recorded with possible oblique-sinistral movements (Quigley *et al.* 2007a). The curvilinear Willunga Fault at Sellicks (Chapter 3) also demonstrated varying dips on its Cactus Canyon and Waterfall Gully exposures (Buckman *et al.* 2009b, Buckman *et al.* 2010). A gravity survey towards the southern end of the Para Fault reveals series of parallel *en echelon* fault splays near Adelaide (Finlayson 1978), providing evidence of the *en echelon* behaviour of faults on the western flanks of the Mount Lofty and Flinders Ranges.

Dislocations caused by low angle thrust faults were largely observed within the soft sediments of shallow subsurface (trenches WMF-01T and WMF-04B). A surface

rupture on unconsolidated material would have a limited lifespan and limited recognizable surface expression as the dip angle gets lower. This may be a plausible explanation for Williamstown-Meadows Fault to leave only subtle surface evidence at the excavation site near Tarlee, even after confronting a dip slip of ~1.6 m possibly resulted from a single rupture event. Triangularly faceted ridge-spurs, which are characteristic of strike-slip and normal fault zones (Sylvester 1988) can be observed on many of the fault scarps in the Mount Lofty and Flinders Ranges, although the scarps are considered to be developed through compressional reverse faulting.

Preservation of a fault scarplet may depend primarily on the local geology, the amount of fault displacement, the thickness of the sediments deposited during subsequent fan building events, rates of degradation due to locally enhanced erosion, and the nature of faulting (Sandiford 2003a, Quigley *et al.* 2007a, 2007b). The bedrock involved in faults such as the Williamstown-Meadows (Figure 4.15a), Burra (Figure 4.9), Alma (Figure 4.5), Paralana (Figure 4.2) and Willunga (Figure 3.8) demonstrates limited surface expression. Their presence in the shallow subsurface, blanketed with thin layers of unconsolidated soil strata could have resulted from high rates of erosion, unless it has resulted from lateral fault movements.

Strike-slip fault scarps generally have limited surface expression and become obvious only at places where the surface has been disrupted (Sylvester 1988). Similarly, the evidence of faulting becomes difficult to decipher even within short distances from their natural exposures at places near Burra, Cambrai, Vista and Sellicks. These localities do not reveal direct evidence for heavy sedimentation of Quaternary/Pleistocene alluvium or colluvial flows from seismic shaking, to blanket the fault offsets (Quigley *et al.* 2007a). The absence of heavy sedimentation and long-lasting and recognizable fault scarps suggests that the nature of faulting is different from the generally accepted explanation of reverse faulting.

Surface evidence for horizontal movements along fault lines was difficult to determine. However, observations of sub-horizontal slickensides on fault segments of Eden-Burnside (Bourman *et al.* 2010a), Wilkatana (Quigley *et al.* 2007a), and Willunga (Chapter 3) faults reveal left-lateral movements, additionally to the well known reverse faulting. Evidence of oblique shearing on fault planes was largely

observed on naturally exposed fault contacts, while trenches did not display slickenside information on exposed fault planes. The impacts of excessive disturbances on subsurface structures by heavy machinery during excavation are demonstrated by extremely sheared trench walls. These processes may be responsible for destroying much of the shearing evidence within the unconsolidated fault contacts. However, a detailed field study on each individual fault, such as the work documented in Chapter 3, can provide additional information on fault kinematics.

The trenches at Gawler did not expose stratigraphic evidence of faulting, even though there was a subtle fault scarp, in line with the inferred strike of the Para Fault. Faults interpreted through geophysical surveying (Thomson 1969a, McPherson & Clark 2011) could not be observed within the unconsolidated thick sediment layers of, possibly Ochre Cove Formation, even though the South Australian Geology Map indicates a bedrock involved fault contact further east of the trenching location (Figure 4.20). Similarly, two trenches excavated near Sellicks across the Willunga Fault (Reid 2007), did not reveal evidence of faulting within hundred meters from its natural exposures on erosion gullies. Branching of the faults, inconsistent dip angles, rapidly varying strike directions, heavy erosion rates and thick sedimentation could be some of the causes hindering recognition of the subsurface dislocations. Additionally, lateral displacement on fault planes could also be responsible for limited offsets in subsurface stratigraphy as well as subdued surface fault scarps.

The nature and rate of faulting on a particular fault may change over geologic time. Height of a fault scarp generally indicates the minimum vertical displacement of a fault (Peltzer & Tapponnier 1988, Sylvester 1988). However, the height of a scarplet, may vary along the strike of the fault depending on the dip-slip component and the degree of partitioning within the fault network. Considering the complex nature of faulting on some of the observed active faults in the Mount Lofty and Flinders Ranges, it is difficult to establish realistic slip rates on individual faults, except at specific locations. Apart from clearly understanding the spatial distribution of fault networks and details on the nature and amounts of displacement, it is essential to constrain the age component related to dislocations to ascertain recurrence intervals and slip rates.

5 GEOCHRONOLOGY OF ACTIVE FAULTS

5.1 Introduction

Cenozoic stratigraphic relationships and age constraints are important in understanding active tectonic processes (Schmidt *et al.* 2012). Offsets in stratigraphic marker units are helpful to determine regional fault activity (Hancock 1988). Obtaining burial age constraints on sediments deformed by faulting can generate approximate ages for seismic rupture events along a particular fault. By these means, different amounts of offsets in stratigraphic layers provide information to quantify recurrence intervals, slip-rates and approximate magnitudes of palaeo-earthquakes (Hancock 1988, Hutton *et al.* 1994). Vertical dislocations of several hundred metres on the Oligocene-Miocene Port Willunga Beds between Adelaide and Myponga, have been reported (May & Bourman 1984). As most of the movements on faults result from large earthquakes, it is apparent that Adelaide would have experienced many 10's or even 100's of large (>5.0) magnitude earthquakes over the past 10-20 million years. However, intraplate tectonics are typically much less pronounced than those on plate boundaries and are commonly punctuated by long periods of stability. Consequently, dating techniques do not always reach back far enough into the past to constrain the timing of faulting and uplift.

The approximate age ranges of the Quaternary dating techniques commonly used are given in Figure 5.1. Age limits depend on factors unique to each method, the nature of the material being dated, and ambient conditions (Walker 2005). Reliability, accuracy and precision of ages obtained through dating depend on the ability to directly date minerals or elements in sediment or in bedrock (Watchman & Twidale 2002). Researchers have had success in tectonically active regions such as California, with radiocarbon, amino acid racemisation and optical luminescence dating techniques, by obtaining ages for colluvial wedges that have eroded from active fault scarps, thus indirectly dating the successive timing of fault ruptures (DeLong & Arnold 2007). Recently, the radioactive Be^{10} nuclide has been used to determine rates of erosion and exposure ages (Bierman & Nichols 2004) of bedrock materials to constrain the timing of the most recent uplift. Quigley *et al.* (2007a, 2007b) successfully determined the rates of uplift and erosion on some of the active fault segments in the Flinders Ranges using these techniques.

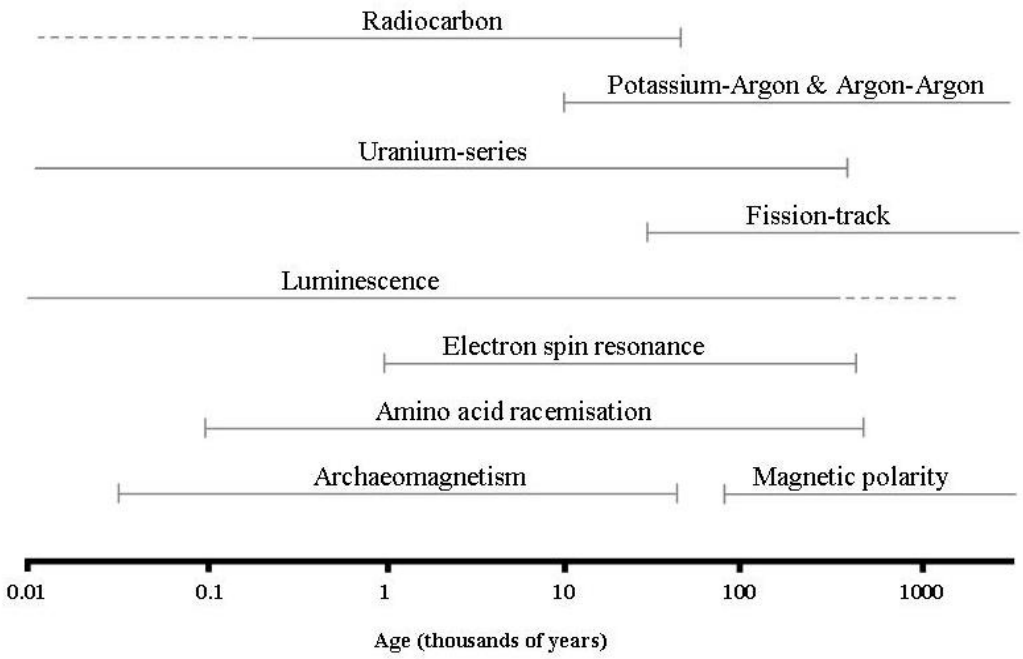

Figure 5.1 *Approximate age-ranges of some of the Quaternary dating techniques commonly in use (modified after Aitken 1998)*

Luminescence dating is capable of providing age constraints from a few years to hundreds of thousands of years, and is useful to directly estimate the burial age of Quaternary sediments (Aitken 1994, Roberts 1997, Berger 1998, Lian & Roberts 2006). It has been used to calculate accurate depositional ages for Quaternary sediments associated with palaeo-earthquakes in Australia (Hutton *et al.* 1994), as well as other geographic regions (Singhvi *et al.* 1994, van der Pluijm *et al.* 2001, Feathers 2003). The charges trapped within defected crystal structures of silicate minerals (such as quartz and feldspar) are of interest in luminescence methods (Aitken 1998, Jacobs *et al.* 2003) to determine the time since the sediments (grains) were last exposed to sunlight. Burial ages can be evaluated by irradiating the accumulated electrons within the defects of the crystal lattice of silicate minerals such as quartz and feldspar, using specific light waves, and measuring the emitted energy (Huntley *et al.* 1985, Aitken 1998). More recent advancements in OSL, such as the single-grain method, can provide even more accurate age estimates (Duller 2003, Jacobs *et al.* 2003, 2006).

5.2 Optically Stimulated Luminescence (OSL) dating

Thermo-luminescence (TL) (Daniels *et al.* 1953) is considered as the beginning of luminescence dating. Optically stimulated luminescence (OSL) is a branch of luminescence dating. Developments in optical luminescence (Shelkoplyas & Morozov 1965) for dating unheated sediments (Huntley *et al.* 1985) evolved, as TL was most reliable for dating heated sediments. Single-grain OSL (Roberts *et al.* 1998) and the introduction of the single-aliquot regeneration (SAR) procedure (Murray & Roberts 1998, Murray & Wintle 2000) are significant advancements in this technique. Quartz and potassium-rich feldspar grains are ideal for optical luminescence dating, while calcite, zircon and sodium-rich feldspars are also regarded as appropriate (Wintle 2008). Quartz grains are preferred over feldspars in general, but the selection depends on the abundance of the mineral, applicability to a particular age range and site-specific conditions (Lian & Scott 2007a, 2007b).

5.2.1 Methods

Electrons of an atom are ideally arranged within energy bands separated by forbidden zones. Exposure to radiation derived from the surrounding sediments in the form of alpha, beta and gamma rays from the decay of U, Th, K and Rb, can provide sufficient energy to excite the electrons to reach higher energy levels producing electron-hole pairs. Cosmic rays and internal radiation derived from U and Th inclusions within the crystal lattice may also facilitate this process (Aitken 1985). When the electrons encounter a defect in the crystal lattice, they are trapped within the forbidden zone (Aitken 1985, 1998). Under stimulation of light, these trapped electrons may reach the conduction band, and recombine with a hole-trap, by emitting a particular luminescence signal (Aitken 1998). In the laboratory, the luminescence signal is detected by a photo-multiplier and used to calculate the radiation dose that the material has absorbed.

Exposure of the material to sunlight or intense heat can destroy the luminescence signal by removing the radiation acquired since its burial, known as "resetting the time clock". Assuming that the mineral grains were sufficiently exposed to sunlight before they were buried, the amount of radiation absorbed reflects the time period

that sediment remained subsurface. The age is determined by using Equation 5.1, which compares the total radiation absorbed by the sample since resetting of the clock (De) and the rate of radiation supply from the environmental (Dr).

$$\text{Optical age } (ka) = \frac{\mathrm{D_e}(Gy)}{\mathrm{D_r}(Gy\ ka^{-1})} \qquad \textit{Equation 5.1}$$

The calculation of D_e and D_r values is a two-stage process, which involves systematic and random errors, known as uncertainties related to a particular sample. The relative error associated with a sample is calculated using Equation 5.2 (Aitken 1985). The standard error of an optical age calculation is given when the relative error is multiplied by the calculated age.

$$\text{Relative error} = \sqrt{\left(\frac{\text{Total uncertainty on } \mathrm{D_e}}{\mathrm{D_e}}\right)^2 + \left(\frac{\text{Total uncertainty on } \mathrm{D_r}}{\mathrm{D_r}}\right)^2} \qquad \textit{Equation 5.2}$$

5.2.2 Sample collection

Sediments were collected in 63 mm diameter, ~20-30 cm long stainless-steel tubes at selected locations, following the general procedures for collecting OSL samples (Wallinga 2002). At each sample location, surface sediments were cleaned, and the outer most portion removed before inserting the standard OSL tube to collect the light-sensitive sample. The tube was then removed, along with the sample that contained the light sensitive OSL signal, and both ends were covered with opaque (black) caps and sealed with duct-tape. To prevent mixing of the sampled material, any space between the sample and the end of the tube was filled with clean paper, prior to sealing the tube with opaque end-caps. OSL tubes were labelled and the samples were carefully stored for transportation. Field notes and photographs were taken for identification purposes as well as to illustrate the field context of the OSL samples. Coordinates of the sample locations were recorded using a Garmin GPS. Information on sample locations is presented in Table 5.1.

Sample Name	Location	Location Coordinates		Associated Fault	Approximate Distance from Fault (m)	Approximate Depth (m)
		E	S			
MW100	Moolawatana	378534	6688660	Paralana	1250	0.30
MW104	Moolawatana	377387	6688614	Paralana	900	0.55
MW105	Moolawatana	378218	6688590	Paralana	950	0.55
MW109	Moolawatana	378150	6688622	Paralana	150	0.50
A1	Hoyleton	277478	6234139	Alma	3	0.75
B1	Burra	316928	6259863	Burra	2	1.0
T1	Tarlee	296768	6203075	Williamstown- Meadows	6	0.6
T2	Tarlee	296768	6203075	Williamstown- Meadows	6	0.3
BT1	Bethel	297725	6198462	Williamstown- Meadows	1.5	0.8
BT2	Bethel	297696	6198460	Williamstown- Meadows	2	1.75
BT3A	Bethel	297912	6198685	Williamstown- Meadows	8	1.3
BT3B	Bethel	297912	6198685	Williamstown- Meadows	7	1.3

Table 5.1 *Overview of OSL samples*

Twelve OSL samples were collected from five study sites (Moolawatana, Hoyleton, Burra, Tarlee and Bethel) in the Mount Lofty and Flinders Ranges. The sampling strategy targeted the stratigraphically younger undisturbed layers and youngest ruptured sediments associated with identified faults. Extra samples were collected in re-sealable bags for water content measurements and mineralogical analysis, if required.

5.2.3 Sample preparation

OSL samples carefully collected in opaque tubes were prepared under subdued red light (Aitken 1998). Laboratory procedures mainly involve wet-lab processing for sample preparation and luminescence measurement. Processing of the samples was carried out at the OSL lab facility of the School of Earth & Environmental Sciences, University of Wollongong. Four samples were sent for further analysis at the OSL lab facility of Institute for Geology and Palaeontology, University of Innsbruck, Austria. All samples were prepared adhering to the standard laboratory procedures (Aitken 1998) and laboratory work was performed under subdued red light. Appropriate lighting conditions were arranged by covering the fluorescent tubes and light emitting diode head-torches with primary red filter paper (Lamothe 1995). All the samples were stored in properly labelled black-coloured sample bags after removal from the OSL tubes. All the equipment used was also appropriately labelled to reflect sample identity. The main segments involved with wet-lab processing are documented in the following sections, and were conducted adhering to the safety standards and laboratory procedures of the University of Wollongong. The intention was to isolate 90-125 µm and 180-212 µm size fractions of quartz and feldspar grains for the luminescence signal measurements.

1) Unpacking: OSL sample tubes were opened and at least 2 cm of sediment from both ends were removed to avoid possible contamination with light. Approximately 5 cm of material from each end of the tube was separated for environmental dose rate (Dr) calculations. From the remaining, half of the sample was then taken for preparations, while the other was carefully stored for future reference (if required).

2) HCl treatment: the samples were mixed with distilled water and 10% HCl was added and retained to react with dissolved carbonates.

3) H_2O_2 treatment: when the reaction with HCl terminated, the samples were rinsed with tap water followed by distilled water. Then they were mixed with 15% H_2O_2 to remove the organic matter by oxidation.

4) Drying: the samples were washed with tap water followed by distilled water and were oven dried at 500 C.

5) Sieving: dry samples were sieved on a sieve stack that consists of 90, 125, 150, 180, 212 and 300 µm sieves, using a mechanical sieve shaker. Sample fractions, 180-212 µm were separated for single-grain analysis and 90-125 µm for standard single-aliquot analysis. Each sieve was carefully cleaned by soaking in an ultrasound bath and oven dried, before reuse.

6) Density separation: heavy minerals (density > 2.70 g/cm^3) were removed from the 180-212 µm sample fraction, by mixing with a sodium poly-tungstate (SPT) solution having a density of 2.70 g/cm^3, and filtering through standard filter papers. Mixing the sample with 2.62 g/cm^3 SPT and filtering further separated quartz (density 2.62 - 2.70 g/cm^3) from feldspars.

7) HF treatment: extracted quartz grains were etched with 48% hydrofluoric (HF) acid, to dissolve any residual feldspar grains present, as well as to remove the outer 0.02 mm of the alpha irradiated surface from quartz grains.

8) HCL treatment: samples were washed with concentrated HCl to remove any dissolved fluoride precipitates.

9) Drying and sieving: samples were oven dried at 600° C, and sieved again to ensure an accurately extraction of 180-212 µm and 90-125 µm sample fractions.

10) Purified quartz samples were labelled and stored carefully for measurement of the luminescence signal.

5.2.4 Sample analysis

Quartz grains were mounted on to discs for analysis in the TL/OSL reader. Stainless steel discs with silkospray silicon adhesive covering an area of 0.3 mm were used for the single-aliquots, whereas gold-coated aluminium discs were used for the single grains. Standard SAR tests were conducted on selected samples, including a recycling ratio test, recuperation test (Murray & Wintle 2000) and OSL-IR depletion ratio test (Duller 2003), in addition to a modified SAR procedure (Murray & Wintle 2000). Appropriate measurement and data analysis procedures were conducted, based on the dose recovery tests to obtain reliable estimates of the equivalent dose. Post depositional mixing and beta dose rate heterogeneities were accommodated by applying corrections to the affected samples. The values that best reflected the sediment burial ages were considered as the OSL ages of the respective samples. Refer to Appendix II for further details on sample analysis and age calculations.

5.2.4.1 Equivalent dose determination (D_e)

D_e is estimated through a sensitivity-corrected dose response curve in a conventional single-aliquot regenerative (SAR) procedure (Murray & Wintle 2000, Jacobs *et al.* 2003a, Jacobs *et al.* 2003b, Ma & Beroza 2008). A minimum of three cycles of measurements of OSL intensity against laboratory generated doses is (Figure 5.2) recorded as regenerative dose measurements (Jacobs & Roberts 2007). A sample is also given a zero dose and subjected to identical steps to detect changes of traps from light insensitive to light sensitive due to successive heating. This is followed by another regenerative dose to check the appropriateness of the sensitivity correction (Murray & Wintle 2000). The total dose naturally received by the aliquot is determined using the sensitivity corrected dose responsive curve and the OSL intensity of the natural dose.

The single-aliquot method measures the signal from multiple grains, whereas in single-grain OSL the luminescence signal is measured from individual grains. Single-grain OSL has the ability to assess the degree of mixing within a deposit, the adequacy of clock resetting, and the ability to reject grains with abnormal physical properties from the sample to achieve more accurate age estimates (Jacobs & Roberts 2007). The resulting individual D_e values are often plotted on a radial-plot (Figure

5.2) (Galbraith *et al.* 1999), which demonstrates the equivalent dose distribution of the sample with trends and precision of measurements (Galbraith 1988, 1990). D_e values along a radial line, from the standard estimate axis to the log arc, have received the same equivalent doses. The precision increases from left to right of the single-grain radial plots.

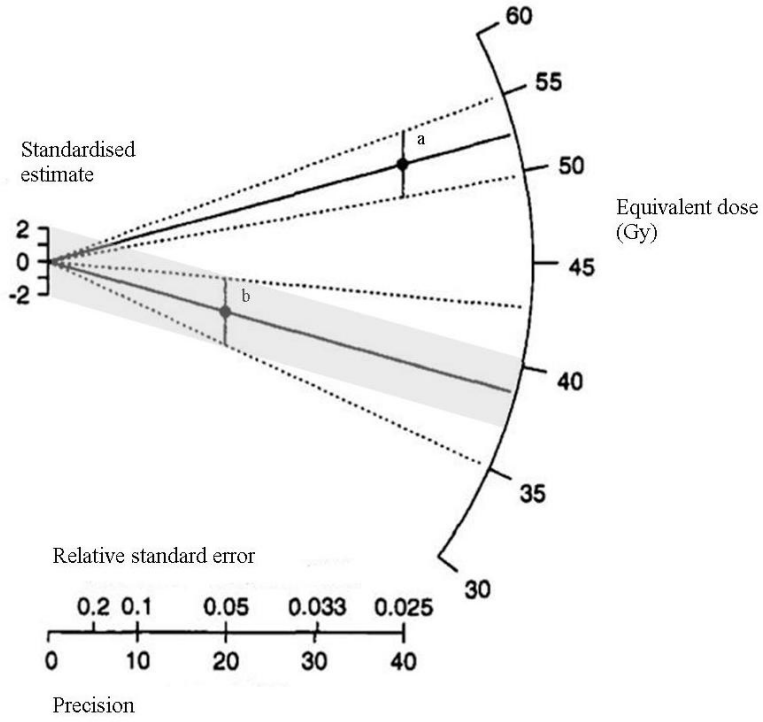

Figure 5.2 *Radial-plot illustration of two hypothetical grains (a & b) having different equivalent doses on a palaeodose scale centered at 45 Gy. The equivalent dose (De) values are represented in logarithmic scale and the horizontal axis displays the relative standard error and precision. A grey band from the standardised estimates represents the 95% confidence interval. (Source: Galbraith et al. 1999)*

Dose recovery and other experiments were conducted on single-aliquot (~50 grains) and single-grain levels for samples from Mount Lofty Ranges, and the detailed results are summarized in the Appendix II. In summary, the most accurate and precise results were obtained with a pre-heat (PH) of 160ºC for 10 s prior to measurement of the natural (L_N) and each regenerative dose (L_x), and a preheat of 160 ºC for 5 s (PH 2) prior to measurement of the test dose (T_N and T_x). With these specifications, measured/given dose ratios of 0.98 ± 0.01 and 1.06 ± 0.03 were obtained for single-aliquot and single-grain, respectively. Additional experiments with higher pre-heat combinations resulted in significant underestimation of the given dose. Therefore, all further OSL measurements were conducted with a PH 1 of

160 ºC for 10 s and a PH2 of 160 ºC for 5 s. In order to test the suitability of the samples from Moolawatana for OSL dating with quartz, 1000 single quartz grains of 180-212 µm grain size were measured for sample MW 105 following a modified SAR procedure (Murray & Wintle 2000), and applying regenerative and test dose pre-heats of 180°C for 10 s and 160°C for 5 s, respectively. Standard tests of SAR (single-aliquot regeneration) suitability were applied, including a recycling ratio test, recuperation test (Murray & Wintle 2000), and an OSL-IR depletion ratio test (Duller 2003).

Depending on the differences in luminescence intensities, radial-plots may display three main patterns (Jacobs & Roberts 2007). These patterns may reflect the dominant depositional or post-depositional processes experienced in the sampling environment. However, it is essential to be aware of the geomorphic and sedimentary forming processes and stratigraphy of the sampling sites to properly extract and interpret the information displayed on a radial-plot (Murray & Roberts 1998).

1) An ideal distribution, having most of the grains within the grey band representing the 95% confidence interval, may be displayed by a fully bleached sample which remained undisturbed.
2) A solid base line with continuous spreading can be observed in samples containing partially bleached grains. Here, it is assumed that the lowest population of D_e values represents the most bleached grains and indicates the last time that the sediments were exposed to sunlight.
3) Multiple dose populations are displayed in sediments confronted with variable beta-dose rates or a mixture of well-bleached grains from multiple samples. The cluster representing the greatest proportion of grains is considered to indicate the latest resetting event, provided that burial doses can be meaningfully resolved.

Upon obtaining the results, an appropriate age model is used to define a single D_e value, to be used in the age estimation. An age model is a statistical procedure used to determine a reliable and representative equivalent dose value for a particular sample that has several D_e values from individual aliquots or grains (Galbraith *et al.*

1999, Galbraith & Roberts 2012). The choice of an appropriate age model depends on the stratigraphical context of the sample. This selection is particularly critical for single-grain OSL, and there is a need to consider burial histories and independent age controls within the site context to obtain the best statistical fit. According to Galbraith and Roberts (2012), age models can be summarized as follows, where central (CAM), minimum (MAM) and finite mixture (FMM) models are most commonly used.

1) Common age model: Estimates a weighted average De from sediments well bleached during deposition. Error calculations and overdispersion estimates are made using appropriate statistical equations (Galbraith *et al.* 1999) on the sediments, which have not experienced sediment mixing.
2) Central age model (CAM): A weighted mean is calculated for the sample population (Galbraith *et al.* 1999) and better handles the overdispersion between independent estimates of De (Galbraith & Roberts 2012). CAM is best applicable for sediments well bleached prior to deposition.
3) Minimum age model (MAM): This model estimates a De value for the most recent bleaching event, assuming that the log De values from the lower truncation point of a normal distribution correspond to the fully bleached grains. The model avoids the influence of poorly bleached grains and therefore, is suitable for samples having a mixture of fully and partially bleached grains with a large overdispersion (Galbraith *et al.* 1999).
4) Maximum age model: This model estimates a De value from the earliest depositional event represented by the fully bleached grains using a statistical approach similar to the minimum age model. This model is most suitable for sediments that were fully bleached during the initial deposition and were subjected to consecutive mixing with younger sediments (Galbraith *et al.* 1999) or sediments that experienced partial bleaching after deposition (Galbraith & Roberts 2012).
5) Finite mixture model (FMM): This model is only applicable for single grain OSL measurements and is ideal for sediments showing multiple populations on radial plots, or with an overdispersion value >20% (Roberts *et al.* 2000). The model statistically distinguishes different De populations within a sample

(Jacobs *et al.* 2006), and when FMM fails to extract discrete populations, a potential age range may be determined using minimum and maximum age models (Olley *et al.* 2004).

5.2.4.2 Environmental dose rate determination (D_r)

A portion of sediments was taken from the OSL tube, dried and pulverized to measure the environmental dose rates. Environmental radiation is responsible for the electron movements within a quartz crystal lattice, where the rate of emission is considered to be proportional to the rate at which the energy is absorbed. The environmental radiation experienced by a sample is a combination of alpha (α), beta (β), gamma (γ) and cosmic rays due to ^{238}U, ^{235}U, ^{232}Th, including their decay products and ^{40}K. The total environmental dose rate is given by the sum of alpha (D_α), beta (D_β), gamma (D_γ) and cosmic-ray (D_c) dose rates, as represented by the Equation 5.3. A constant (0.9) has been derived to accommodate the effects of etching and grain size variations (Aitken 1998).

$$D_r = 0.9D_\beta + D_\gamma + D_c + D_\alpha \qquad \textit{Equation 5.3}$$

The decay of uranium (U), thorium (Th) and potassium (^{40}K) are the main sources of ionising radiation, and their presence is regarded as constant due to their large half-lives. The grains themselves can internally generate α and β radiation, which is not limited to external sources. However, internal radiation generated within quartz is considered insignificant, as it typically contains negligible amounts of radioactive elements (Aitken 1998), and specifically for Australia (Bowler *et al.* 2003). The contribution of each radiation component towards the total radiation can be summarized as follows:

- Alpha particles: The decay of U and Th produces α-particles. They are rich in energy, but only penetrate ~0.025 mm, making a negligible external contribution (Aitken 1985, 1998).
- Beta particles: The decay of 238 & 235U, 323Th and 40K largely produces β-particles (Aitken 1985). These particles can penetrate a ~2 mm range and

considerably contributes for the environmental radiation. The β dose rate can be measured with a beta-counter and needs to be adjusted for HF etching (Bell & Zimmerman 1978) and grain size (Mejdahl 1979).

- Gamma particles: The decay of U, Th and K produces ɣ-rays, which penetrate depths up to ~30 cm through sediments. Measurements of the gamma dose rate either can be obtained directly with an *in situ* gamma spectrometer or be indirectly calculated in the laboratory.
- Cosmic rays: Even though cosmic rays can achieve higher penetration depths compared to α, β and ɣ radiation, their contribution towards the environmental dose rate is limited (Aitken 1985, Prescott & Hutton 1994). The geomagnetic latitude and altitude of the site, and the type of overburden and sampling depth have to be considered when calculating the cosmic ray contribution to the environmental dose rate (Prescott & Hutton 1994).

Water attenuates the environmental radiation, and therefore, it is necessary to determine the dose rate attenuation due to the impact of moisture on each sample. A portion of each sample was used to determine the water content, which is calculated as a percentage (Equation 5.4) by weighing a specific sample, before and after drying. Assuming that the value obtained from Equation 5.4 represents the long-term moisture content of the sediments of interest, the calculated beta, gamma and cosmic ray dose rates have to be adjusted for the effects of moisture content (Aitken & Xie 1990).

$$\text{Water content} = \frac{\text{wet mass} - \text{dry mass}}{\text{dry mass}} \times 100\% \qquad \textit{Equation 5.4}$$

For the samples from the Northern Flinders Ranges, a GM-25-5 beta counter (Mejdahl 1979, Bøtter-Jensen & Mejdahl 1988, Aitken 2010) in the OSL Laboratory of the University of Wollongong was used to measure the bulk beta dose rate for each sample and adjusted for beta attenuation based on grain size (Mejdahl 1979). Gamma dose rates were measured by thick-source alpha counting (TSAC). The conversion factors of Aidamiec and Aitken (1998) were also used for the beta and gamma dose rate calculations. The cosmic dose rate was calculated according to Prescott and Hutton (1994). For the samples from the Mt. Lofty Ranges the U, Th

and K concentrations were determined on sub-samples of dried, homogenised and powdered samples by IC-PMS measurements by the Activation Laboratories Ltd, Ancaster, Canada. Elemental concentrations were converted to dry dose rates using conversion factors (Stokes *et al.* 2003) and adjusted for the water content, expressed as % of dry mass of the sample using the dose correction factors of Aidamiec and Aitken (1998).

5.3 Results and interpretations

Four samples from Moolawatana in the northern Flinders Ranges, and four samples from Hoyleton, Burra and Tarlee localities in the Mount Lofty Ranges were processed with the aim of determining age constraints for some of the more recent palaeo-earthquakes. Given their different geographic origins, geological settings and general characteristics of sediments, as well as the different analytical pathways in different laboratories (University of Wollongong and University of Innsbruck), the results are presented separately, with respect to individual sample locations. Field descriptions of sediment exposed in trench walls and natural exposures associated with palaeo-faulting were documented in Chapter 4.

5.3.1 Mount Lofty Ranges

Four samples were taken for OSL analysis from shallow (<2.5 m depth) trenches near Hoyleton (A1) and Tarlee (T1 and T2) localities. The Burra sample (B1) was collected from a natural exposure of the fault at Worlds End Creek (section 4.3.3). These samples are associated with the Alma, Williamstown-Meadows and Burra faults, respectively. In general, the sampled sediment varies from coarse-grained, angular hill-slope deposits to whitish, coarse gravelly deposits immediately overlying a calcrete.

The environmental dose rates for the four samples from the Mount Lofty Ranges are summarized in Appendix II. They range from 2.72 ± 0.14 Gy/ka at Tarlee (T2) to 4.28 ± 0.21 Gy/ka at Alma (A1). A total of 1000 quartz grains between 180-212 µm was measured for each of the four samples and details of the measurements are provided in the Appendix II. Between 11 (B1) and 96 (T2) grains passed all applied

selection criteria and were accepted for D_e determination. The resulting D_e distributions are complex. Therefore, implications for the application of an appropriate age model, stratigraphic context and distance with respect to the fault line under investigation are very important and are discussed separately for the three sampled locations

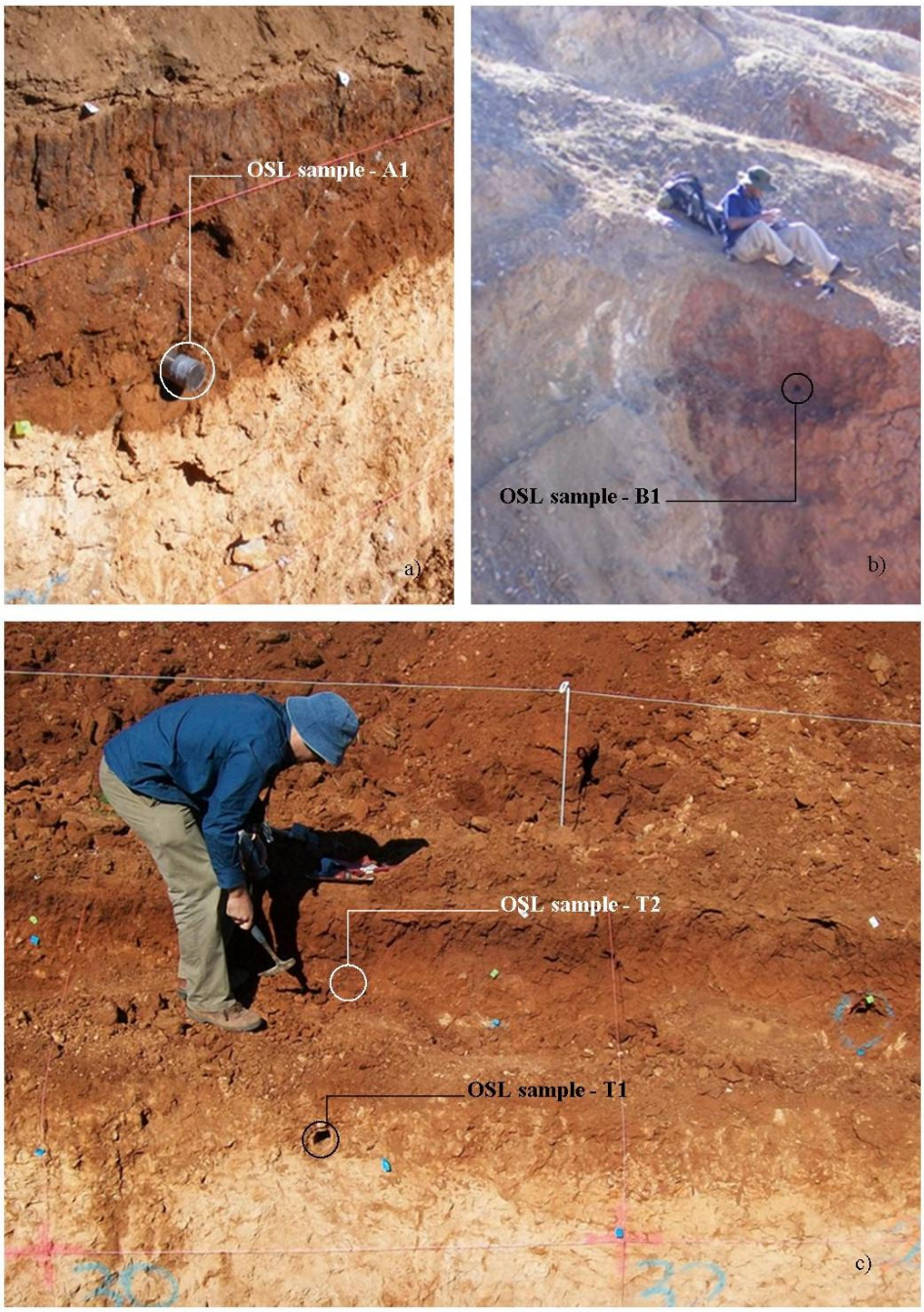

Figure 5.3 *Sample locations in the Mount Lofty Ranges a) Hoyleton, b) Burra, c) Tarlee (refer Table 5.1 for details)*

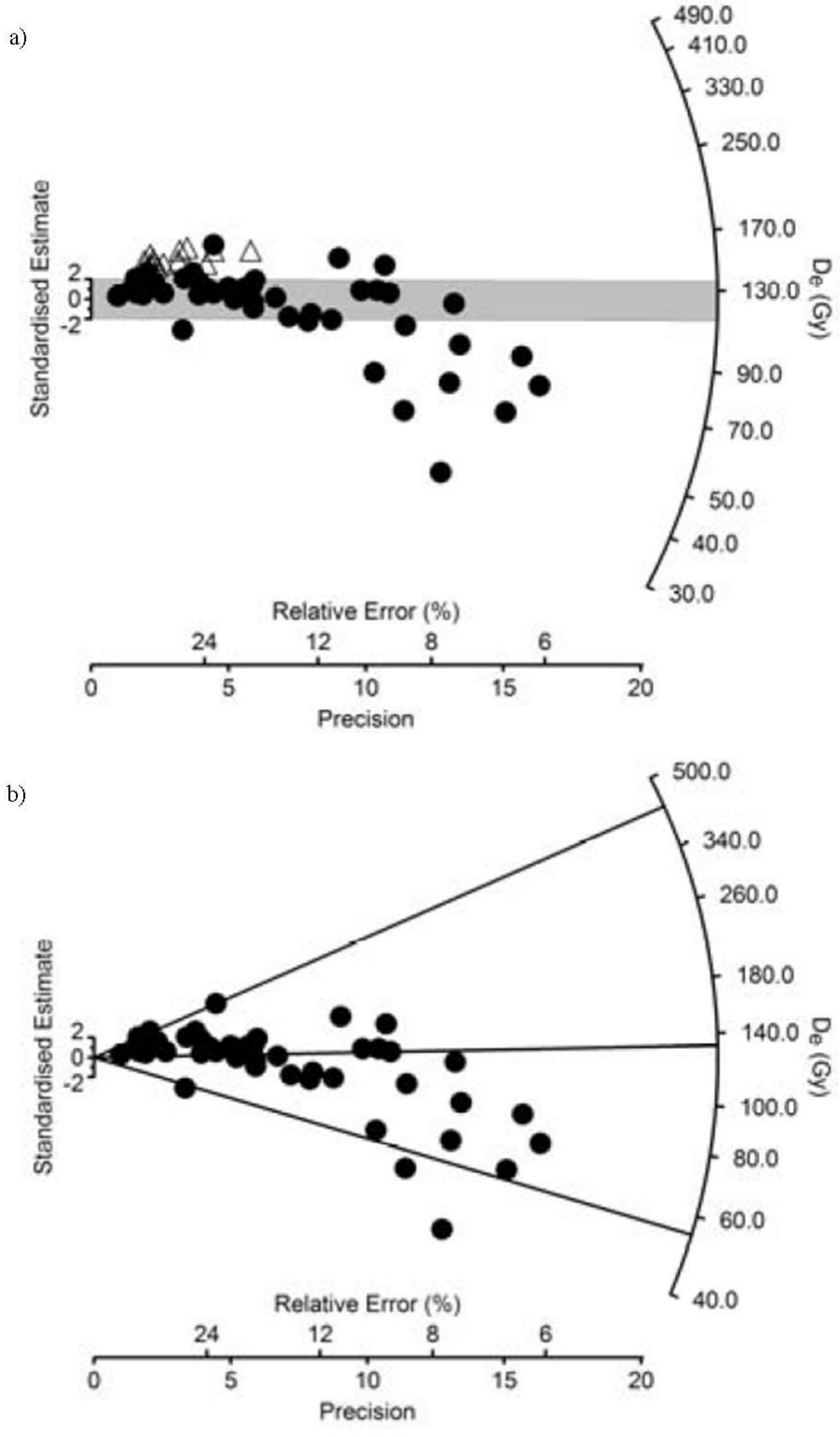

Figure 5.4 *Single-grain D_e distributions for the Alma sample (A1). Radial plots show entire single-grain De data set with (a) 2 sigma uncertainty range in grey, for CAM D_e estimates, black dots - accepted grains, triangles - extrapolated grains, (b) D_e distribution with FMM - 3 component fit results. For further details see Appendix II*

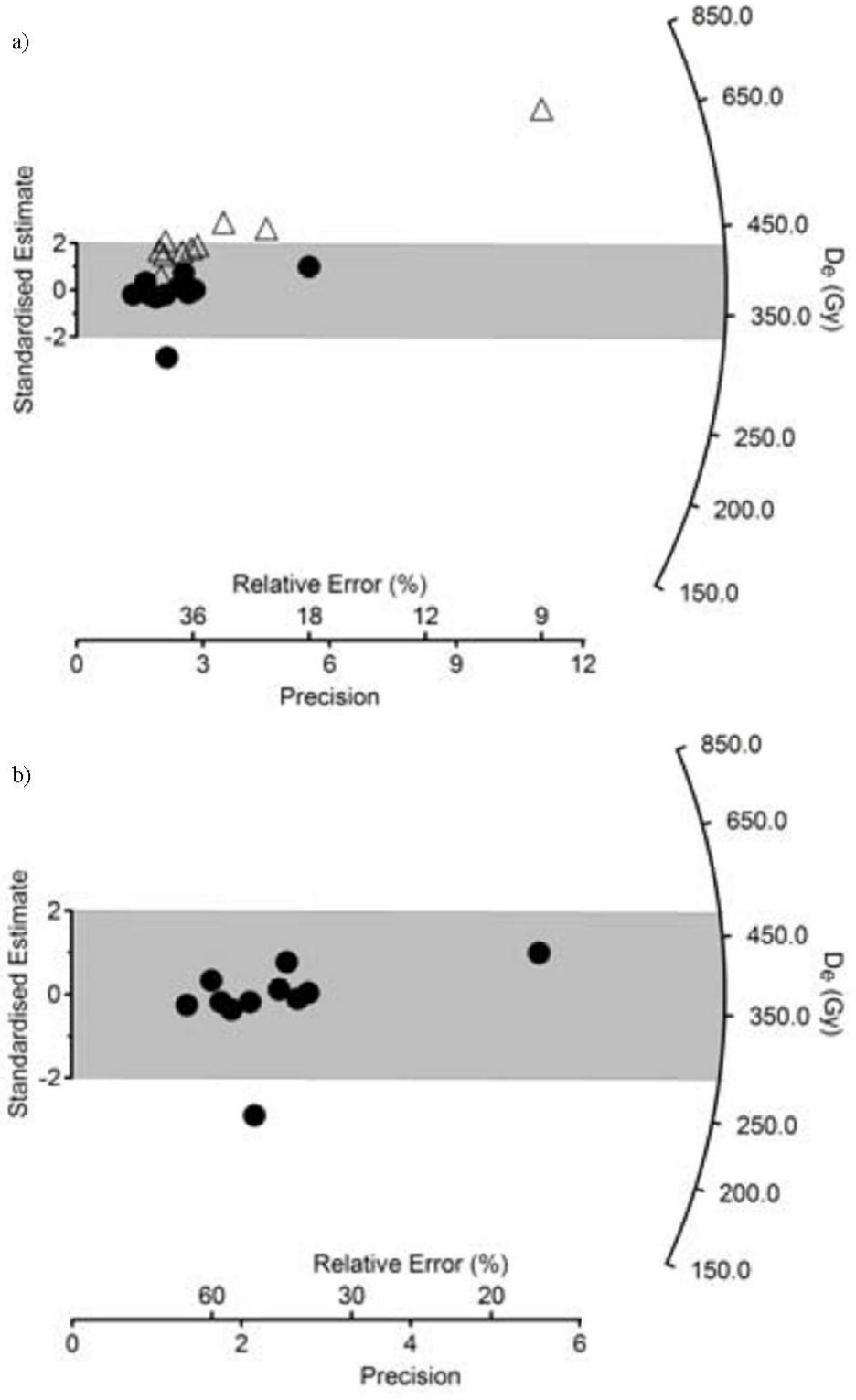

Figure 5.5 *Single-grain D_e distributions for the Burra sample (B1). Radial plots show entire single-grain De data set with 2 sigma uncertainty range in grey, for CAM D_e estimates, (a) black dots - accepted grains, triangles - extrapolated grains, (b) D_e distribution with CAM results. For further details see Appendix II*

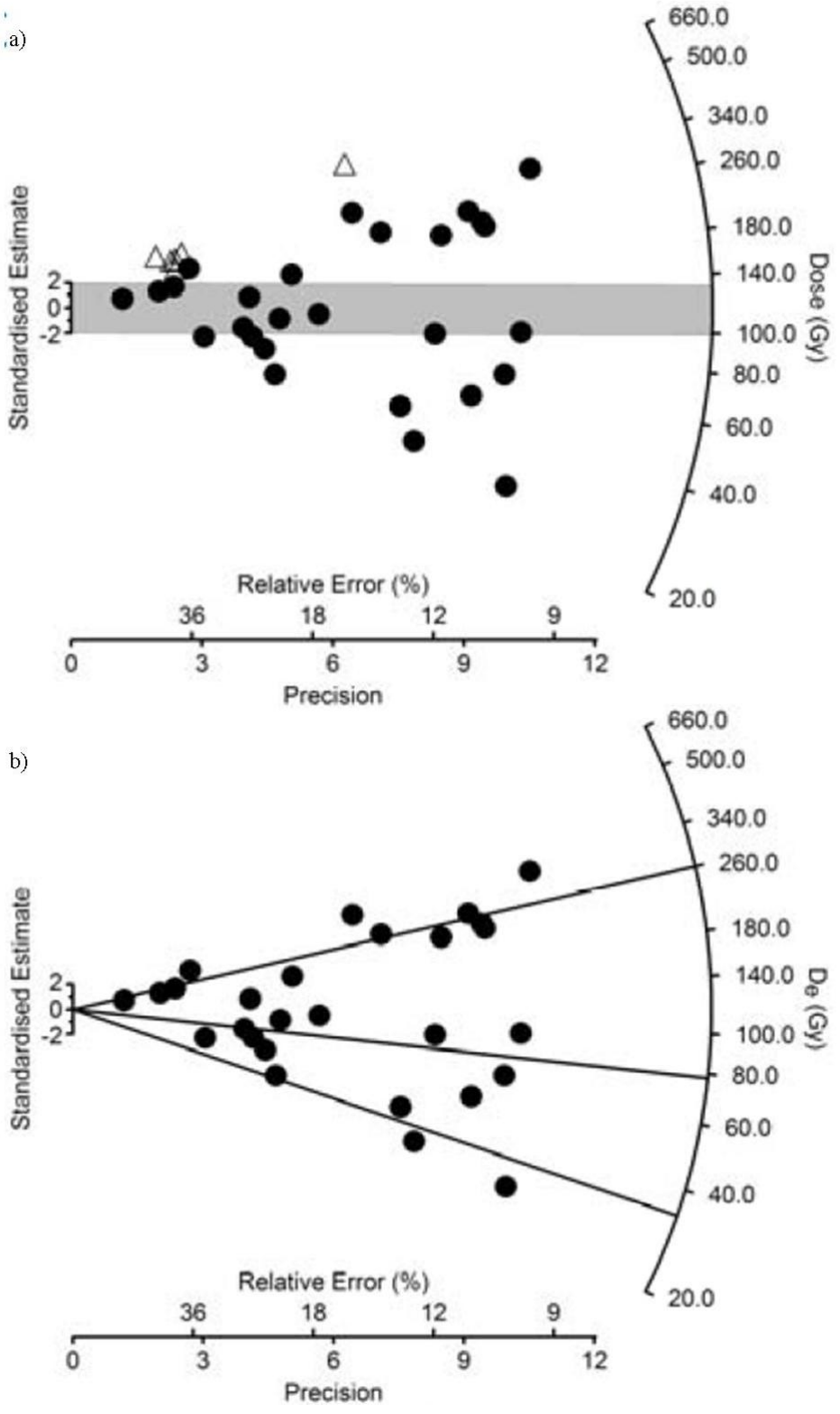

Figure 5.6 *Single-grain D_e distributions for the Tarlee sample (T1). Radial plots show entire single-grain De data set with (a) 2 sigma uncertainty range in grey, for CAM D_e estimates, black dots - accepted grains, triangles - extrapolated grains, (b) D_e distribution with FMM - 3 component fit results. For further details see Appendix II*

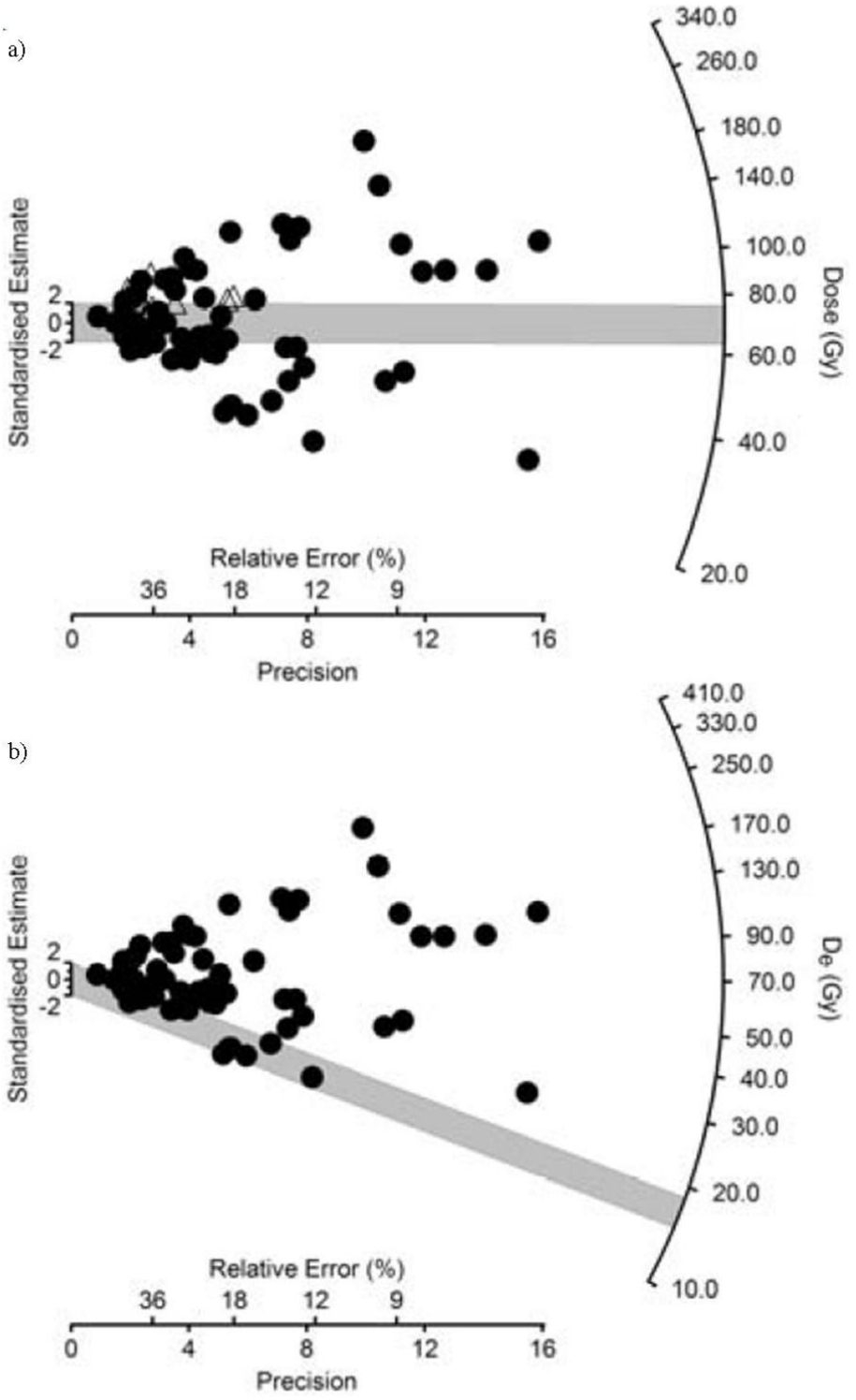

Figure 5.7 *Single-grain D_e distributions for the Tarlee sample (T2). Radial plots show entire single-grain De data set with (a) 2 sigma uncertainty range in grey, for CAM D_e estimates, black dots - accepted grains, triangles - extrapolated grains, (b) D_e distribution with MAM age modelling results. For further details see Appendix II*

5.3.1.1 Alma Fault – Hoyleton

An OSL sample (A1) was collected in association with the Alma Fault at a locality near Hoyleton (section 4.3.2). The sample was collected from the base of a sedimentary unit, which resembles the last interglacial Pooraka Formation (Bourman *et al.* 1997). The Alma Fault does not disrupt this sedimentary unit in the sampled trench. Thus, the OSL age should provide a maximum age for the last fault rupture event.

The distribution of the accepted D_e values is complex (Figure 5.4) and encompasses a wide range with a relatively high overdispersion of 47%. As there is a slight asymmetry towards younger values, and the FMM (Finite mixture model) was used for the determination of representative D_e's. Three components displayed the best overall fit of the distribution. These components correspond to D_e values of 55.5 ± 6.0, 133.3 ± 7.1 and 423.9 ± 44.2 Gy. The second component (133.3 ± 7.1) contains 57.4 % of the accepted grains and is considered to be the major component. This major component corresponds with an age of 31.2 ± 2.3 ka, while the minor components correspond to 13.0 ± 1.6 and 99.1 ± 11.6 ka, respectively.

Based on the results, the depositional age for sample A1 should be about 31.2 ± 2.3 ka and is significantly younger than expected. Older grains expressed by the minor component, 99.1 ± 11.6 ka, may reflect the integration of partially bleached grains from an older underlying formation, which could probably coincide with the Pooraka Formation. In contrast, the post-depositional intrusion of younger grains may be interpreted as the result of recent soil formation and bioturbation, and would also reflect the relatively shallow depth of this sample. Provided the interpretation is accurate, the last rupture of the Alma Fault near Hoyleton probably occurred about or before ~31 ka.

5.3.1.2 Burra Fault – Worlds End Creek

The Burra OSL sample (B1) was been collected from the banks of the Worlds End Creek near Burra, which intersects the Burra Fault (section 4.3.3). The sample was taken from the centre of a thick sedimentary unit, possibly the Pooraka Formation.

These reddish beds as well as the fault contact are almost vertically inclined, arguing for a comparatively long and/or dynamic local faulting history.

The distribution of the D_e values and its interpretation is not straightforward (Figure 5.5a), as large numbers of grains (D_e values) could only be obtained via linear extrapolation of the dose response curve. The extrapolated grains with high equivalent dose values reflect very old grains and are commonly not included in further age calculations. Without these grains the distribution is much better constrained (Figure 5.5b) and exhibits only a single younger outlier. Therefore, the Central Age Model (CAM) was been applied and the resulting D_e of 376.3 ± 42.5 Gy corresponds to an age of 89.1 ± 11.1 ka.

These results generally confirm the expected Pooraka Formation age of the faulted sediments. Consequently, the observed faulting should have occurred within the last ~90 ka. Given the vertical nature of the fault contact, multiple rupture and deformation events are likely to have occurred in this locality. However, as many of the measured D_e values were extrapolated and have not been incorporated into the age model, a lot of the grains were assumed to be saturated. Hence, the actual depositional age for this sample may be much older than first suspected, and the CAM value of ~90 ka should be carefully considered as a minimum age for the both the deposition and all post-depositional fault activity.

5.3.1.3 Williamstown-Meadows Fault – Tarlee

In contrast to the samples from Hoyleton and Burra, two samples were available from a single trench near Tarlee, in association with the Williamstown-Meadows Fault (section 4.3.4). Here, the lower sample (T1) was collected from immediately above a distinct and disrupted calcrete layer. Therefore, it represents the sediments deposited before the fault rupture. The upper sample (T2) comes from a colluvial wedge, which was likely generated from erosion of the fault scarp immediately after the rupture event. The difference between T1 and T2 therefore constrains the timing of fault rupture at Tarlee.

The distribution of the accepted D_e values for both T1 and T2 covers a wide spectrum with very high overdispersions of 80 and 96% respectively. In the case of T1, the D_e values (Figure 5.6) visually seem to belong to individual populations mixed within the sample. Therefore, the FMM (Finite mixture model) was applied to the observed D_e distribution and the resulting best fit of the three components gave values of 34.3 ± 5.6, 77.8 ± 8.6 and 262.1 ± 21.4 Gy. The last component (262.1 ± 21.4) seems to be the dominant population having 44.9% of the grains, whereas the second component encompasses 37.4% of the grains. These populations correspond to ages of 76.7 ± 7.7 and 22.7 ± 2.8 ka, respectively. Given its slightly higher percentage of grains, the former age is interpreted to reflect an estimate of the depositional age for the dated sedimentary unit. However, considering the comparatively high proportion of grains falling into the second largest component, the formation of this paleosol may also have an age as young as 22.7 ± 2.8 ka. This scenario would indicate that the calcrete paleosol may have formed within the older pre-existing host sediment of Pooraka age, as reflected in the FMM components. In contrast, the younger age of 10.0 ± 1.7 ka could represent a population of grains, which were introduced into the sediment possibly due to bioturbation processes.

In contrast to T1, the D_e values of T2 (Figure 5.7) visually seem to be distributed much more continuously, indicating a high degree of mixing and/or partial bleaching. Therefore, both the MAM (Minimum age model) and the FMM (Finite mixture model) have been applied and the MAM resulted in an age of 6.2 ± 1.0 ka. The FMM shows the best fit of four components at 15.7 ± 2.0, 40.4 ± 2.7, 111.3 ± 10.0 and 302.1 ± 24.2 Gy, correspond to the ages of 5.8 ± 0.8, 14.8 ± 1.3, 40.9 ± 4.3, and 110.0 ± 10.9 ka, respectively. The second component contains 46.2% of the grains, which is the largest proportion of this population. The third and fourth components are both intermediate components with ~20% of the grains, while the first component is being relatively minor. Based on these results, the most likely depositional age for T2 should be around 14-15 ka. Assuming that the depositional process associated with the sedimentary unit of T2 is spatially and temporally closely related to the fault activity, the rupture event would date to 14.8 ± 1.3 ka. This scenario is corroborated by the above discussed alternative ages for the subsequently ruptured paleosol

horizon dated with T1 to be ~76 or 22 ka. In both T1 and T2, the minor youngest components seem to reflect intrusive grains from overlaying strata and/or the surface.

5.3.2 Northern Flinders Ranges

As documented in section 4.3.1, the Paralana Fault in the northeastern Flinders Ranges was investigated near Moolawatana. The fault was mapped and described in detail, based on the trench observations. The offset of the Tertiary Eyre Formation and weathered bedrock clearly reflected the degree of displacement. These faulted units were overlain by an undisturbed unit of reddish, coarse colluvial-alluvial deposits regarded as an equivalent of the Pleistocene Pooraka Formation (Sheard 2009). The Pooraka Formation has a reported last interglacial age (~132-118 ka) in the Mount Lofty Ranges (Bourman *et al.* 1997, Bourman *et al.* 2010b), but there is no absolute chronology established for the formation in Moolawatana region. Therefore, the sampling strategy at Moolawatana was directed at better constraining local depositional ages for this unit, and thereby inferring a minimum age for the last activity of the Paralana Fault.

Environmental dose rates (D_r)

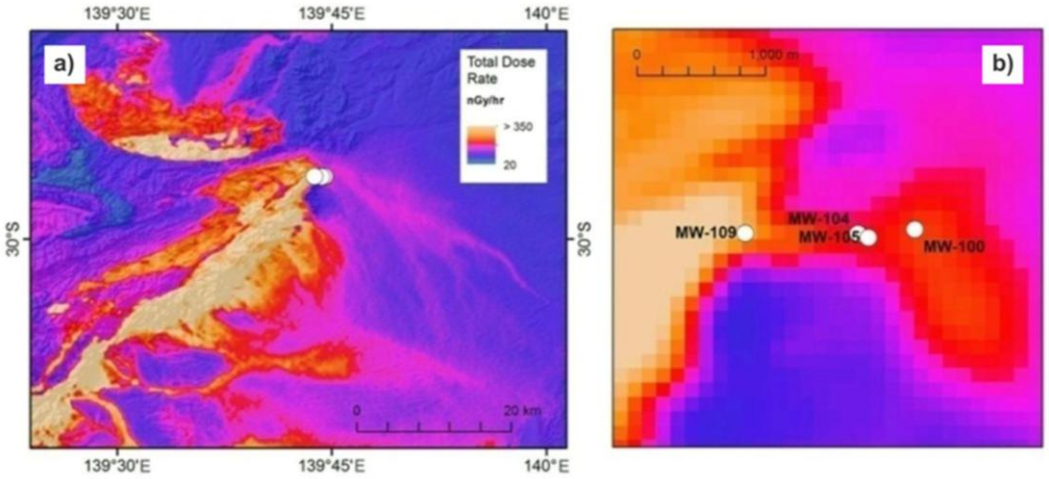

Figure 5.8 *Spatial pattern of total dose rate as calculated from airborne measurement of radio-elements (K, U, Th). a) Total dose rate in the Northern Flinders Ranges showing zones of very high doses in the ranges and along the major creeks and alluvial fans. (Source: Minty et al. 2009). b) OSL sample locations (white dots) coincide with high total dose rates in the immediate vicinity of Moolawatana, which exhibits high doses in relation to bedrock in the ranges (left) and along the creek.*

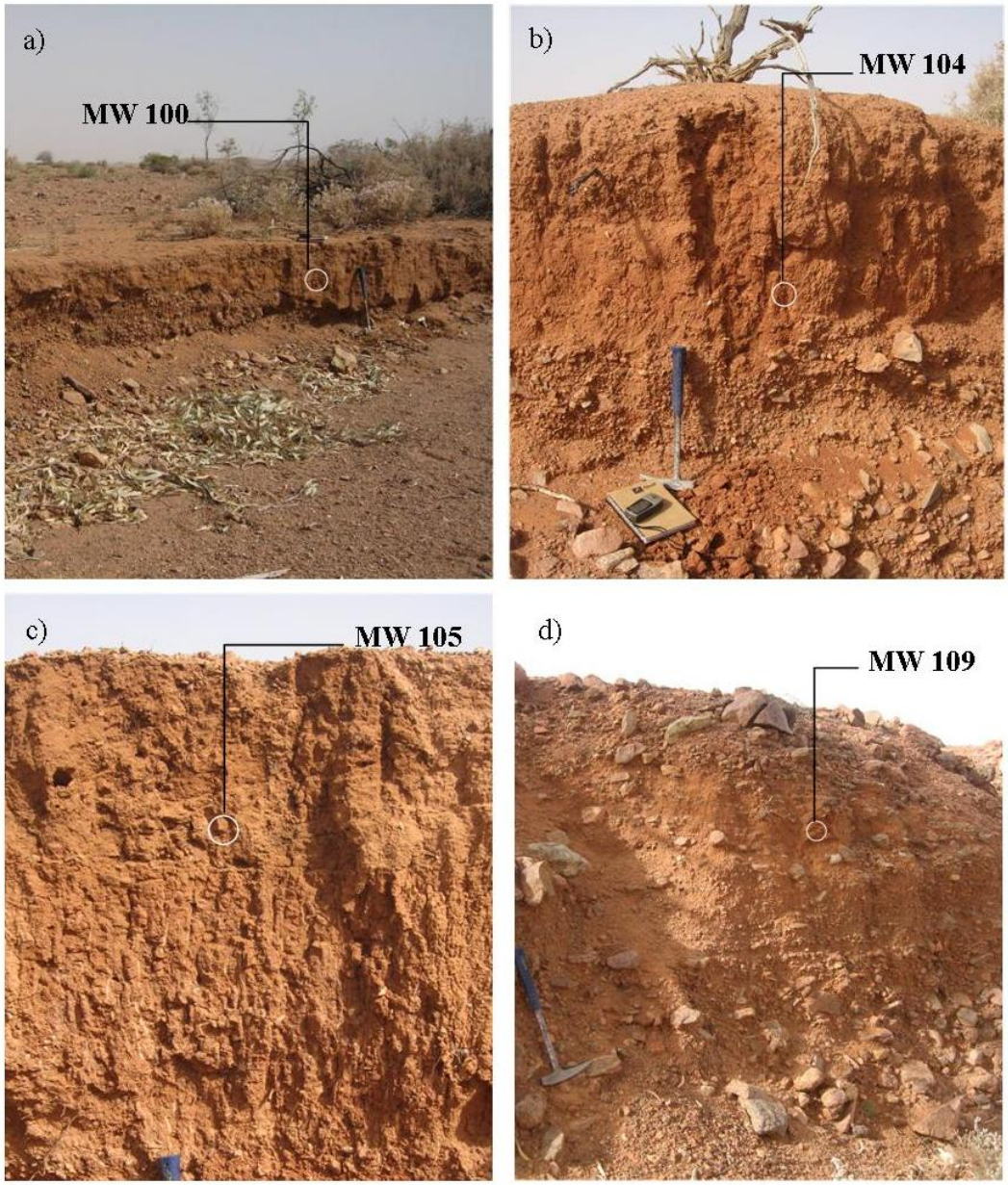

Figure 5.9 *Sample locations at northern Flinders Ranges a) MW100, b) MW104, c) MW105, d) MW109 (refer Table 5.1 for details)*

Extraordinarily high total dose rates in and around the northern Flinders Ranges (Figure 5.8a), were confirmed by the preliminary inspection of the spatial pattern and intensity of total dose rates calculated from airborne measurement of radioactive elements (K, U, Th). Sample locations near Moolawatana (Figure 5.8b) correspond with a zone of high environmental dose rates; the estimated airborne total dose rates due to terrestrial and cosmic radiation, are averaged in 100x100 m^2 pixels, range between ~200-300 nGy/hr, and corresponding to ~1.8 to 2.6 Gy/ka (Table 1 – Appendix II).

The total environmental dose rate was also recorded directly from pulverized sediments for each sample. The measured water content was used to calculate dose rate attenuation by moisture, with 50% and 100% uncertainties accommodating variations in the moisture content. The resulting total environmental dose rates range between 6.8 Gy/ka and 8.9 Gy/ka and are summarized in Table 1 of Appendix II. When compared to other luminescence studies in adjacent regions (Nanson *et al.* 1998, Cohen *et al.* 2011), the values from Moolawatana exceed the previously reported highest environmental dose rates by factors of 2-8.

Equivalent dose values (D_e) and their interpretation

Of the 1000 single quartz grains of 180-212 μm grain size measured for sample MW 105, 81 grains had appropriate OSL signals and produced finite equivalent dose (De) estimates. The corresponding D_e values displayed a skewed distribution with an overdispersion value of 150% (Figure 5.10). The plot suggests that the sample is modern, as 67% of the accepted grains have D_e values consistently within 0 to 2σ. However, it also highlights the presence of a significant proportion of partially bleached grains, which is a typical characteristic for fluvial or alluvial samples (Olley *et al.* 1999, Arnold *et al.* 2007).

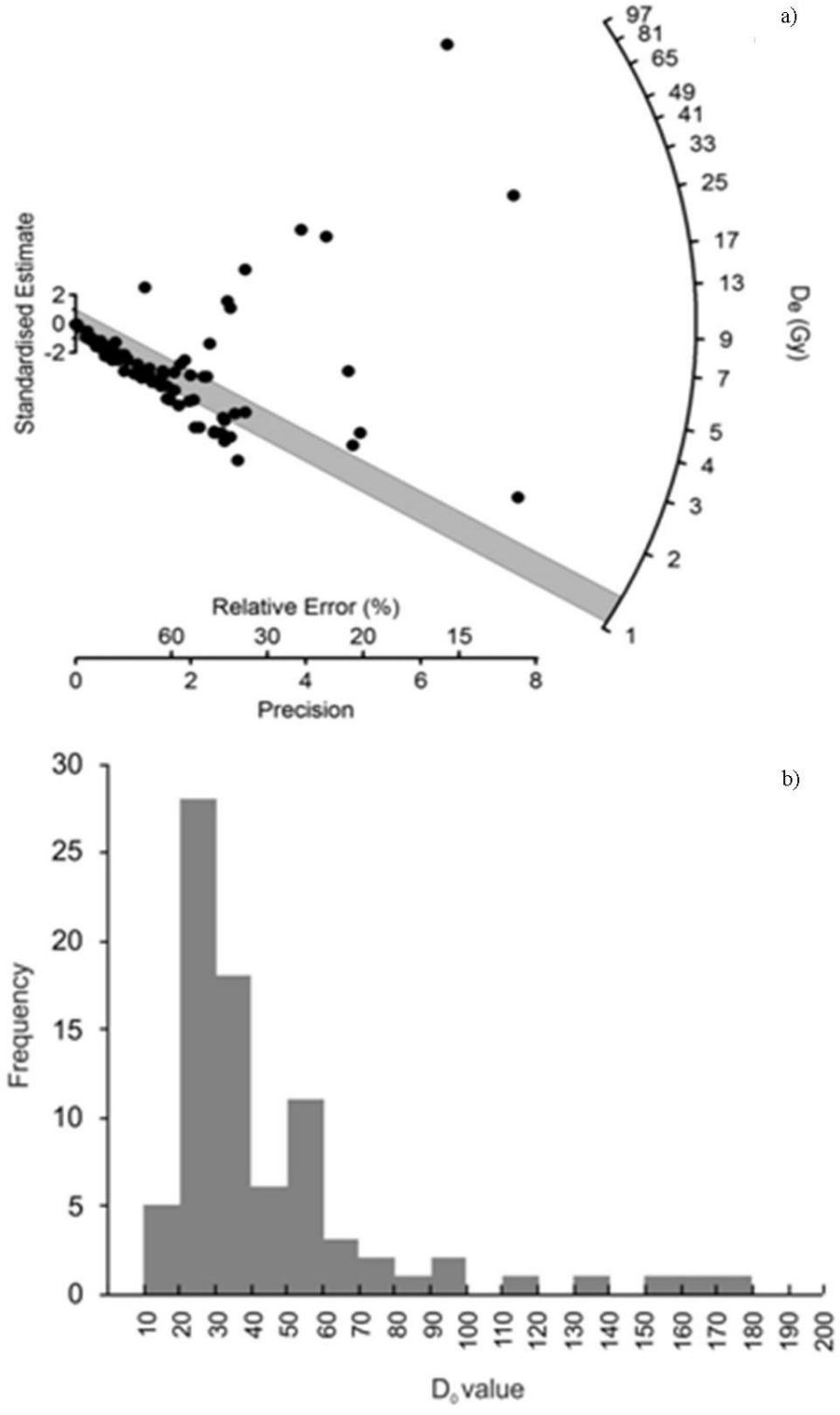

Figure 5.10 *Plots of single grain data from sample MW 105. a) Radialplot of accepted D_e distribution. b) Histogram of D_o values from the same sample.*

The D_0 value is a dose that characterises the rate of onset of saturation with dose for a single saturating exponential function (Preusser *et al.* 2009). Maximum, minimum, median and mean D_0 values are summarized in Table 5.2, and all D_0 values show a skewed distribution with only a few D_0 values (~6%) exceeding ~100 Gy (Figure 5.10). Wintle and Murray (2006), suggested that D_e estimates exceeding 2 x D_0 fall in the saturated portion of the dose-response curve. For the grains of sample MW 105, the mean 2 x D_o value is 89 Gy and the maximum value 340 Gy. Using the above established environmental dose rates for all four Moolawatana samples, on average, the individual sand grains would saturate after ~10-13 ka, and only a very few grains would saturate after ~39-50 ka.

	D_0 (Gy)	2*D_0 (Gy)	Saturation Age Equivalent (ka) for sample MW 105	Max. Saturation Age Equivalent (ka) for all samples
Mean	44	89	13	10
Medean	32	65	9.5	7.3
Maximum	170	340	49.6	38.2
Minimum	16	32	4.7	3.6

Table 5.2 *D_o values for sample MW 105 and corresponding saturation age equivalents for the samples MW100, MW104, MW105 and MW109 at Moolawatana*

5.3.2.1 Paralana Fault - Moolawatana

Given the very low percentage of grains with appropriately high saturation doses, and the suggested last interglacial age estimates for the Pooraka Formation (Bourman *et al.* 1997), quartz grains in the sample MW105 do not provide an appropriate dosimeter for OSL dating at Moolawatana. Hence, alternative methods (e.g. Feldspar OSL) will have to be assessed for their suitability. For the purpose of constraining the last rupture event of the Paralana Fault at Moolawatana, the previously published ages of the Pooraka Formation (Bourman *et al.* 1997) are therefore the only available chronological data to be carefully considered as an age estimation for the last fault activity. Hence, assuming that the material blanketing the Paralana Fault contact near Moolawatana is Pooraka Formation, the latest rupture event of the fault may be

~120-130 ka, based on correlation with the same sediments in the Mount Lofty Ranges. However, Bourman *et al.* (1997) also suggests that the Pooraka Formation might extend over a greater age, not limited to the Last Interglacial, as the recent and ongoing tectonism in the Flinders Ranges could have triggered erosion and deposition of Pooraka type sediments over longer time periods.

5.4 Discussion

This chapter documents the first OSL based chronological constraints for some of the active fault in the Mount Lofty and Flinders Ranges. Corresponding OSL sampling locations, faults exposures in trenches and erosion gullies were documented in Chapter 4. The resulting age estimates were used to infer possible timing of the associated palaeo-earthquakes, and to understand the degree of sediment mixing in each locality. Age constraints for the rupture events associated with Alma, Burra and Tarlee faults were successfully determined. The timing of the last rupture event for the Paralana Fault was not straight forward as the results of the samples taken from the northern Flinders Ranges near Moolawatana, did not return acceptable ages. High environmental dose rates and the associated fast saturation of the quartz minerals militated against obtaining accurate age estimations. Considering the stratigraphic relationship of the samples to the Paralana Fault, in association with the present understanding of the age of the Pooraka Formation, it can be assumed that the most recent rupture event probably occurred earlier than the Last Interglacial. However, it also to be considered possible resurgence of alluvial and fluvial sedimentation within the Pooraka Formation, giving much younger Pleistocene ages (~35-20 ka) for sections of this unit (Williams 1973, Belperio 1995). Quigley *et al*. (2006) has reported ~71-56 ka for the Pooraka Formation debris flows and ~32-29 ka on Pooraka Formation conglomerates from north Wilkatana of the Flinders Ranges. Bourman *et al.* (2010b) also demonstrated that there is a reasonably widespread, Marine Isotope Stage 3 alluvial unit (~50-30 ka), in places containing bones of the extinct marsupial megafauna Diprotodon. This younger unit superficially resembles the Pooraka Formation, for which it may be mistaken.

The samples analysed from the Mount Lofty Ranges are characterised by generally bright to very-bright OSL signals of 10^3 to 10^5 photon counts in the initial signal channels. However, the build-up of background signals was observed for several of the quartz grains, which otherwise passed the applied rejection criteria, and may therefore complicate D_e determination. To overcome this complication and to test the influence of the observed background on D_e determination the early background subtraction method (EBG) was applied to the data obtained from the single-grain dose recovery test at low preheats (i.e. PH 1 of 160 ºC for 10 s and a PH2 of 160 ºC for 5 s), and 0.02 s of the decay curve were used as natural OSL signal intervals. This experiment increased sample overdispersion and resulted in an improvement of the measured/given dose ratio. Therefore, EBG subtraction was applied to the analysis of all further OSL measurements and data. Despite the high overdispersion and complexity in the D_e distributions, four samples from the Mount Lofty Ranges produced realistic ages for the timing of the (last) rupture event of the investigated faults.

The observed D_e heterogeneity of the samples may be related to the degree of beta heterogeneity as these samples stemmed from highly heterogeneous and often poorly sorted coarse hill-slope deposits of varying lithologies, containing varying amounts of calcium carbonates. Dose rate heterogeneity could not be accounted for within the framework of this study. Therefore, the use of *in-situ* gamma spectrometry is recommended to avoid these uncertainties in future studies. The observed large overdispersions inherent in all the samples can be attributed to depositional (e.g. partial bleaching) and post-depositional processes (e.g. mixing). However, the application of the FMM (Finite mixture model) to identify different grain populations in the samples, using the single-grain approach, provided a base for the analysis of these complex D_e distributions. As a result, interpretation of a minimum age of ~31 ka for the most recent rupture at the Alma Fault is acceptable. The FMM analysis for the two samples from Tarlee led the establishment of a rupture age of ~15 ka for the Williamstown-Meadows Fault. However, the maximum age of ~90 ka for the Burra Fault seems still ambiguous, given the large number of extrapolated grains.

A summary of the age estimates is given in (Table 5.3). Given the complexity of the D_e distributions on the radial plots, two separate developments can be postulated. Accordingly, the ages obtained for fault rupture events are assigned a youngest possible and an oldest possible scenario. The youngest possible age represents rapidly degrading environments, where the fault scarps produce scree material at a rapid rate. Inversely, the oldest possible scenario would represent slow landscape changes. Considering the evidence of anomalously incised stream profiles and sub-angular unsorted sediments as matrices of fan material, which reflect dynamic environments near Burra, Tarlee, Bethel and Moolawatana, the youngest possible age approximation is preferred. However, the slower process cannot be simply ignored, taking into account consistently lower magnitude seismicity events reflected in ongoing deformations within the region.

Associated Fault	**Timing of the last rupture**		**Sample name**
	Youngest	**Oldest**	
Alma	≥ 30 ka	> ~100	A1
Burra	≤ 90 ka	-	B1
Williamstown – Meadows	~ 15 ka	~22 ka	T1, T2
Paralana	> ~35 ka	> ~125 ka	MW100, MW104, MW105, MW109

Table 5.3 *Summary of the timing of the last rupture events as discussed in the text*

6 A GROUND PENETRATING RADAR APPROACH TO IDENTIFY SUBSURFACE FAULTS

6.1 Introduction

Localised erosion and canyon formation have exposed a few of the many suspected neotectonic faults in the Mount Lofty and Flinders Ranges. Limited exposure of fault contacts and the lack of surface expression of faulting (Sandiford 2003a) have produced ambiguity on the extent of Quaternary faulting in this region (Belperio 1995). Nonetheless, from available literature and the field observations documented in previous chapters, it is possible to deduce that identified major faults broaden beyond simple single faults to fault networks having several subsidiary faults. Most of these are overlain by veneers of alluvial and colluvial material and should be recognisable through analysis of subsurface structures.

Several approaches that facilitate subsurface structure analysis include trenching, drilling, gravity surveying or soil density contrasts (Selby & Lindsay 1982) as well as other traditional palaeo-faulting investigation methods. Ground Penetrating Radar (GPR) is one of the best approaches in terms of time, money, accuracy and effectiveness. GPR is a non-invasive geophysical investigation tool suitable for imaging the shallow subsurface. It can be a swift tool for neotectonic fieldwork, covering large aerial extents, when used in collaboration with remote sensing techniques. The main purpose of the GPR surveying was, to record, analyse and validate data across known faults, in order to interpret the subsurface structures and stratigraphic sequences at selected locations in the Mount Lofty and Finders Ranges.

A total of six sites, namely, Sellicks, Gawler, Vista, Hoyelton, Tarlee, and Bethel were selected for GPR studies in the Mount Lofty Ranges region (Figure 1.2). These sites feature the Willunga, Para, Eden-Burnside, Alma, and Williamstown-Meadows faults respectively. Fieldwork was carried out using the newly purchased MALA GPR unit of the School of Earth and Environmental Sciences, University of Wollongong. Two-dimensional GPR surveying was conducted at the six sites using 100 MHz, 250 MHz and 500 MHz antennae with varying resolutions and depths of penetration characteristics. Results of this study reveal the applicability of GPR as a primary field investigative tool, as it improves the effectiveness of trench location,

which, in turn, should expedite the characterisation of neotectonic faulting in the Mount Lofty and Flinders Ranges. Furthermore, the results reveal the usefulness of GPR as a primary tool for detecting subsurface fault splays, and in particularly identifying previously unknown faults.

6.2 Ground Penetrating Radar (GPR)

Ground penetrating radar (GPR) is a well established technique for detecting subsurface features at shallow depths (Benson 1995, Smith & Jol 1995, Cagnoli & Russell 2000, Dagallier *et al.* 2000, Chow *et al.* 2001, Lanbo & Yong 2001, Aranha *et al.* 2002, Anderson *et al.* 2003, Rashed *et al.* 2003, Rossetti 2003, Denis *et al.* 2009, Dougherty 2009, Jol 2009, Stevens *et al.* 2009, Taylor 2010). It is a non-destructive geophysical investigation method, which can provide a clear image of deformational structures (Rashed *et al.* 2003) and sedimentary sequences (Smith & Jol 1995, Cooke & Gladwin 1999). Previous studies by many researchers have successfully identified shallow subsurface fractures and faults using ground penetrating radar in a variety of geological settings (Benson 1995, Smith & Jol 1995, Toshioka *et al.* 1995, Chow *et al.* 2001, Rashed *et al.* 2003, Switzer *et al.* 2006).

6.2.1 Methodology

A GPR survey consists of data acquisition, processing, interpretation and ground-truthing or validation of the observed results. Most of the following information on GPR methodology is taken from Jol (2009) unless stated otherwise. The transmitting antenna of the GPR emits an electromagnetic signal within the microwave bandwidth in the form of a radar wave to the ground under investigation and then acquired as a reflected signal. As it penetrates through the subsurface, electromagnetic energy gets scattered and only a portion of the wave is reflected back to the surface (Fisher *et al.* 1996, Neal 2004). The reasons for scattering could be stratigraphical in-homogeneities, such as layers having different physical or chemical properties, or sediments with varying water contents and mineralogies (Jol *et al.* 2003). The receiver antenna captures the reflected radar signal and passes the signal through to the control unit where it is stored as raw data in the form of a radargram (Figure 6.1). The result is a continuous high resolution profile that can be observed through a

display device attached to the GPR equipment or on a computer. Analysis of the waveforms on a radargram using post-processing tools helps to construct an image of subsurface stratigraphic variations and objects within the survey region.

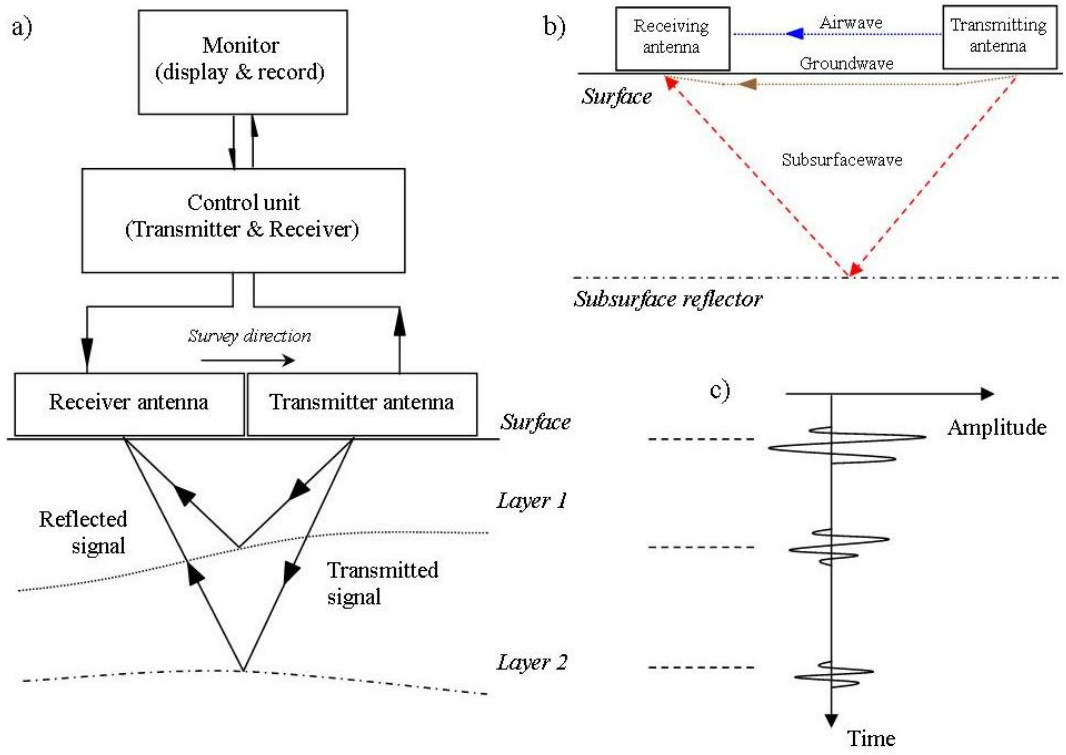

Figure 6.1 *Block diagram illustrating the basics of GPR a) System components and subsurface reflector configuration for data acquisition at an individual survey point (Neal 2004), b) The airwave, ground wave and reflected wave travel paths between transmitting and receiving antennae (Fisher et al. 1996), c) Schematic diagram of the idealised GPR record for the configuration displayed by a)*

Proper understanding of radar wave velocities within the subsurface is essential in order to determine the apparent depths revealed by the signal variations on the acquired profile. Accurate *in-situ* field velocities were calculated through a calibration process by using a known object buried at a measured depth and observing the two way travel time of the radar wave. The wave velocity primarily depends on the dielectric constant of the subsurface sediments, but it is also influenced by the magnetic permeability and electrical conductivity of the medium (Annan 2009). There are standard data tables with dielectric constants for known

types of sediments (Davis & Annan 1989) for general purposes (Appendix III). Of the controllable parameters, antenna frequency governs the depth of penetration. High frequency antennae produce radar pulses of shorter wavelengths, which attenuate strongly, resulting in rapid dissipation of its wave energy. Hence, the reflected and recorded wave on the radargram should contain a high amount of fine detail (also known as high resolution) but with less depth of penetration. The amount of detail collected through an antenna of a specific frequency could be optimized by adjusting the signal velocity, sampling frequency, time window, point interval, number of samples, number of stacks and options available via the user interface. The parameter manipulation capability varies with the brand of the equipment.

Using the GPR, a fault zone can be recognised (Rashed *et al.* 2003, Rossetti 2003, Villamor & Berryman 2006, Taylor 2010) from stratigraphic layer offsets and fault gouge material, which has unique characteristics created by shearing compared to the adjoining fault blocks. A fault zone may be subjected to high heat levels due to intense movements along faults. This may create weak zones, which are susceptible to weathering and which may act as conduits for ground water. The fault gouge material could contain mineralogy different from the surrounding material as a result of the above processes. A difference in dielectric properties within a fault zone creates unique reflections on radar signals, which are recognizable from a GPR survey.

6.2.2 The GPR Instrument

A typical GPR system consists of transmitter and receiver antennae separately or housed in a single unit (transceiver), connected to a control unit and a display unit. The antenna frequency primarily determines the depth of penetration of the radar waves. Higher antenna frequencies gives better resolution, but with a reduced depth of exploration. For this particular study the depth of penetration and resolution were important factors because of the varying thicknesses of the sediment cover over the neotectonic faults.

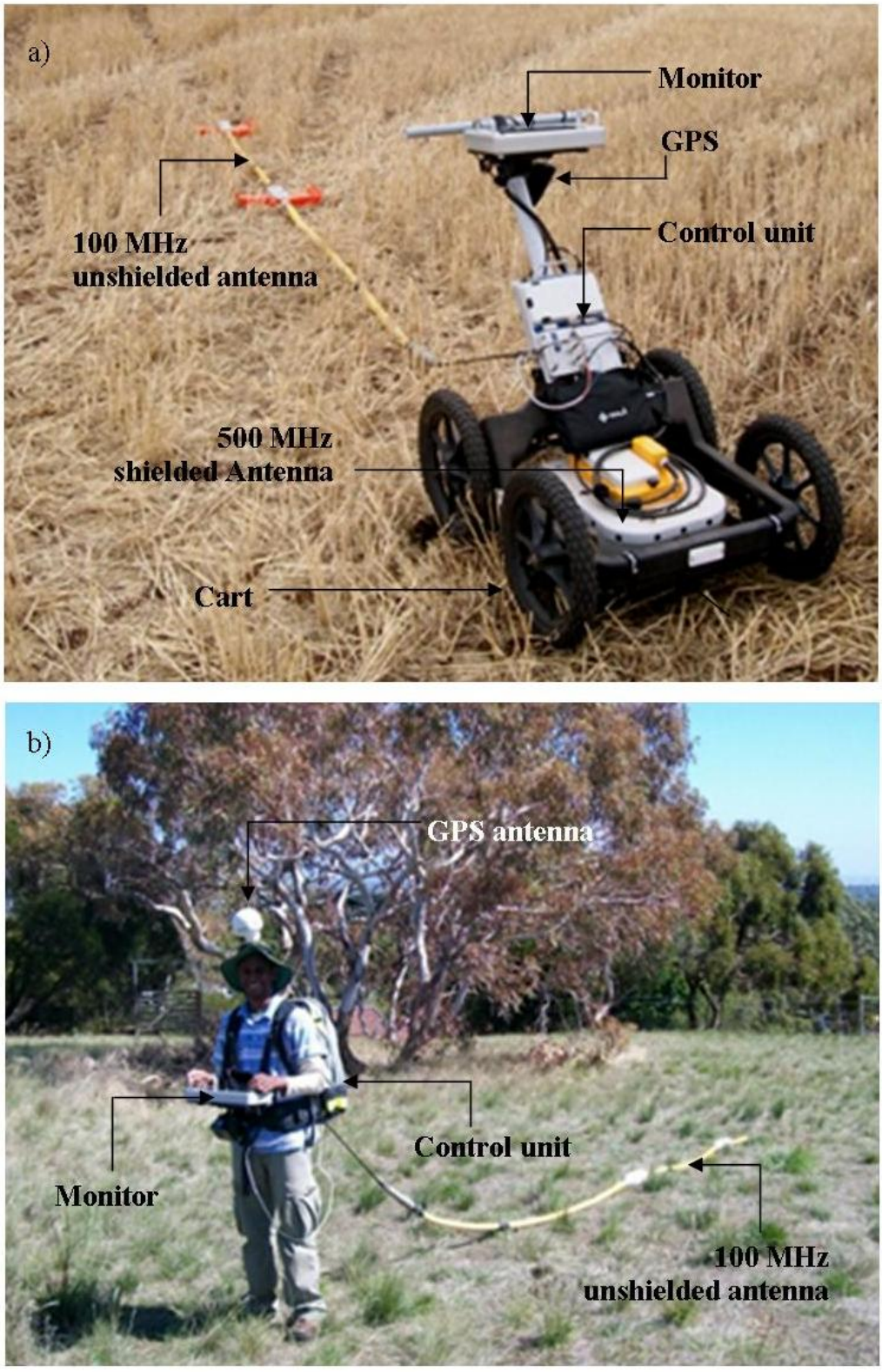

Figure 6.2 *Components of the MALA ground penetrating radar unit a) Housed in the cart at Bethel site, b) Housed in the backpack at Gun Emplacement in Anstey Hill Nature Reserve near Vista*

A MALA branded ProEX GPR unit, which consists of a monitor, control unit and an antenna, was used in this particular study (Figure 6.2). Garmin handheld GPS receiver and a MALA branded beacon corrected GPS unit were used simultaneously in order to acquire spatial coordinates on survey traverses. Depending on terrain conditions either the cart or the backpack was used to house the control unit and the monitor. Whenever possible, shielded antennae were accommodated within the cart, while the unshielded low frequency antenna was towed along the ground. An odometer attached to the cart-wheel or the hip-chain with the backpack was deployed for distance measurements and triggering.

6.2.2.1 The Antennae

Two of the MALA branded shielded antennae having frequencies of 250 MHz and 500 MHz with an un-shielded 100 MHz rough terrain antenna (RTA) were available with the GPR unit. Each antenna was powered by a separate Lithium-Iron rechargeable battery attached on top of its body, which sustained an average day's fieldwork from a single charge. The 100 MHz unshielded antenna was assembled on a 6.5 m flexible structure with the transmitter-receiver separation of 2.2 m (Figure 6.2). For the 250 MHz and 500 MHz antennae, the transmitter and the receiver were assembled within a single shielded console (Figure 6.3b). Under ideal conditions, the 100 MHz rough terrain antenna is capable of reaching a depth of approximately 20 m, but only half of that provided good resolution with the particular field conditions encountered in this study. The 250 and 500 MHz shielded antennae are capable of reaching maximum depths of 10 m and 6 m respectively under ideal conditions (Table 6.1).

The 100 MHz rough terrain antenna was subjected to twist while being towed due to its flexible arrangement causing the transmitter and receiver to assume different alignments with the ground. A plastic plate was designed to rectify this issue, and it was successfully deployed during the fieldwork (Figure 6.4).

Antenna	Theoretical max. depth of penetration	Achieved depth of penetration in field	Transmitter Receiver separation (m)	Frequency range for Bandpass filtering (MHz)
100 MHz unshielded	20 m +	~ 10 m	2.20	25 - 175
250 MHz shielded	10 m	~ 5 m	0.31	62 - 438
500 MHz shielded	6 m	~ 2 m	0.18	125 - 875

Table 6.1 *GPR antenna data table (data source: equipment specifications)*

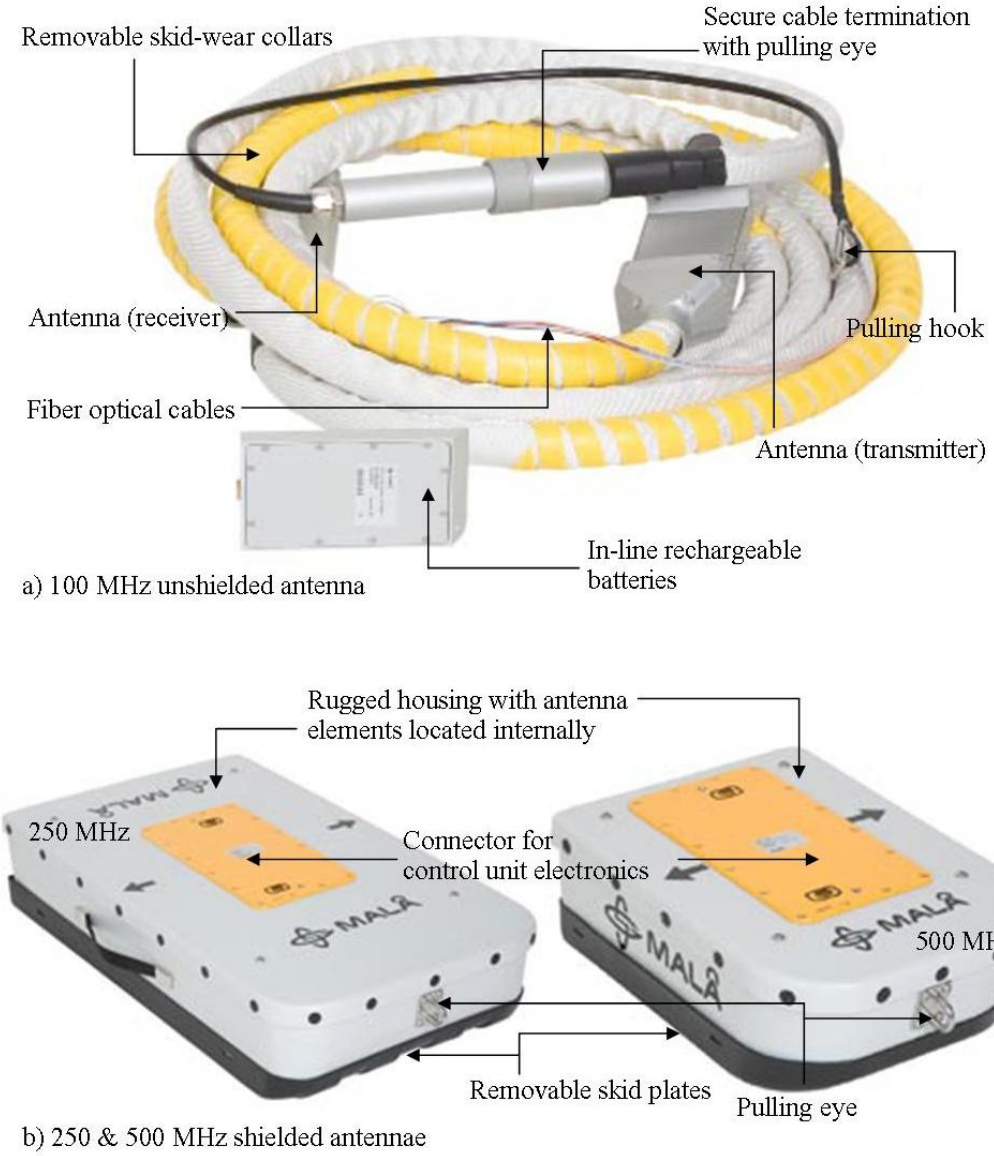

Figure 6.3 *MALA GPR Antennae used for the surveying (image source: equipment specifications)*

Figure 6.4 *Skid-plate assembly for safety and to avoid the rotation of 100 MHz unshielded antenna*

6.2.2.2 Control Unit

The GPR assembly has a MALA professional explorer (ProEx) system as the control unit (Figure 6.5). It is considered to be the most versatile control unit in the MALA range of products and has been designed on a high standard technical platform. The control unit communicates with the monitor through an ethernet cable, with the antennae using three separate fibre-optic cables. It is powered by a Lithium-Iron rechargeable battery attached to the unit. Depending on the requirement, a distance triggering device such as an odometer or a hip-chain can be attached directly to the serial port. The firmware running on the control unit communicates with the MALA geosciences RAMAC Ground Vision (version 2) software on the monitor, enabling the manipulation of acquisition parameters according to the antenna and field conditions.

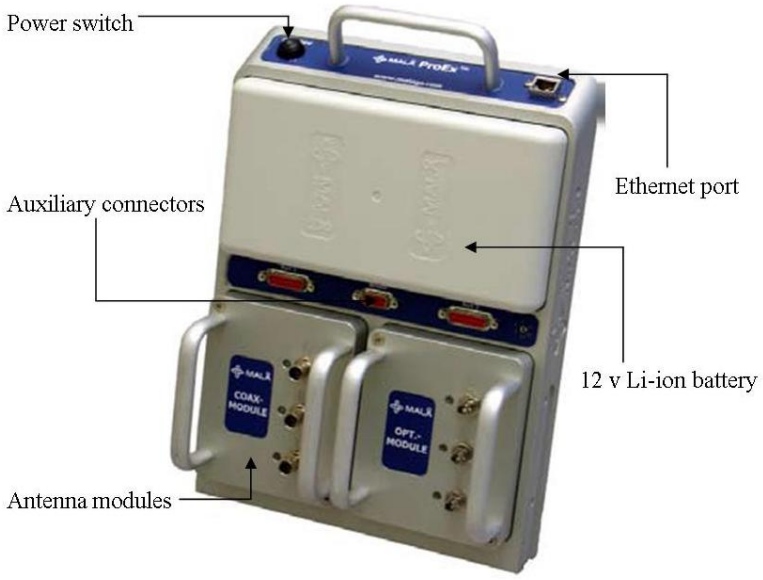

Figure 6.5 *Control unit of the MALA GPR (image source: equipment specifications)*

6.2.2.3 Monitor

The MALA ProEx RAMAC xvii monitor is an energy efficient, high performance unit operated by a dual function turn-push button with a user-friendly interface provided by the GroundVision software. It operates on a Linux based platform with the MALA geosciences RAMAC Ground Vision (version *2*) software. It is powered by a separate Lithium-Iron rechargeable battery connected to the power inlet. The internal memory of the monitor has a data recording capacity of up to 900 Mb. It provides connectivity through USB, Ethernet, serial and parallel ports. The monitor and control unit communicates through the Ethernet interface and a GPS can be attached through the serial interface. The monitor records the reflected wave (from the receiver antenna transferred through the control unit) as a profile with spatial coordinates streamed from the GPS unit. Recorded data is instantaneously displayed on the monitor as a radargram. A single radargram is a combination of seven separate files, which contain different segments of information such as elevation, surface markers, etc. (Appendix III).

The radargrams or the recorded profiles on the monitor can be post-processed on a computer by transferring them to an external memory device using the USB interface. The functionality of the monitor can be replaced with a mobile computing

device, which has the GroundVision program installed. Calibration and changes to the surveying parameters can be applied to the equipment through the monitor from its user-friendly interface, which operates by the dual turn-push button. General operational instructions for the monitor are available from the MALA Geosciences operating manual v 1.3.

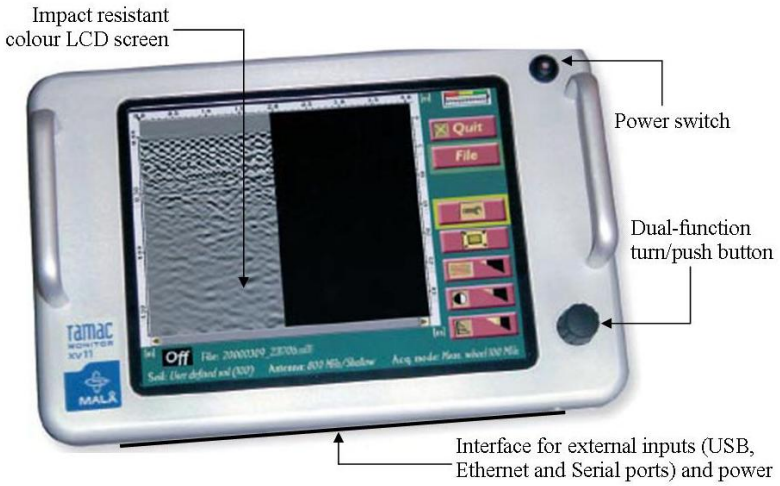

Figure 6.6 *ProEx RAMAC xvii monitor (image source: equipment specifications)*

6.3 Data acquisition

The GPR surveying was performed on the western flanks of the Mount Lofty Ranges, covering sites at Sellicks, Tarlee, Bethel, Hoyelton, Gawler and the Gun Emplacement (near Vista). The exercise was conducted in two stages (from 28-March to 10-April, and 15 to 21 December 2011) and collected a total of 167 GPR profiles extending over a length of 20 km, across the sites identified with subsurface deformation related to neotectonic faulting. GPR transects were oriented orthogonal to the suspected fault lines based on the morphology of the scarp. Traverses were measured with a 50 m tape, and the beginning and end points were surveyed with a Garmin GPS system.

The majority of the sites of investigation were paddocks with thin covers of vegetation, and the majority of the soils were of alluvial origin consisting of an unconsolidated mixture of clay and sand. Sites visited under this study being less populated and experiencing semi-arid weather conditions encountered negligible adverse effects from the environment. However, due care was taken to minimise

environmental effects and to avoid artificial disturbances such as power lines, steel structures, vehicles and mobile phones, which might create noise on the recorded profiles.

GoogleMaps satellite images and information reconnaissance surveying, conducted during previous field visits, were used to determine the survey locations and transect directions on potential fault scarps. Information from Clark & McPherson (2010, 2011) on Geosciences Australia's neotectonic trenching sites assisted in constraining the fault zones and the surveying locations.

6.3.1 Parameter selection

The acquisition parameters were site dependent and were configured independently for each site, mainly based on the level of information required, coupled antenna and subsurface conditions. To obtain the most appropriate field parameters and optimum functionality of the GPR, several test runs with *in situ* trial and error methods were undertaken on each location before a traverse began. Some transects were repeated several times with the same or different antennae with varying acquisition parameters to obtain a better balance of penetration depth and resolution detail. The GPR was used in its reflection mode using single channel data acquisition throughout the survey. Traverse parameters and location details are given in (Appendix III).

The filters applied during data acquisition influence only the displayed profile through the monitor, but not the original raw data. The measurements displayed on the monitor while traversing were the length of traverse on the x-axis and the depth of penetration on the y-axis. Once the profile is saved the y-axis becomes the two-way travel time in nano-seconds, while the x-axis displays the same as previously. The study was conducted in a semi-arid environment during dry seasons. The sites had not experienced rain for at least three weeks prior to the surveys, and the weather during most of the surveying days was fine and sunny. Hence, the influence of subsurface moisture content for GPR surveying was regarded as negligible. Furthermore, the ground water table was beyond the depths of interest as the sites were located at reasonable elevations.

6.3.2 Method of triggering

For data acquisition, distance-triggering and time-triggering were the available options for firing of radar waves, and the former was used throughout this survey. The odometer attached to the cart or the hip-chain (when the unit was housed in the backpack) was the mechanism used for distance triggering. Instead of the manual marking at the desired intervals, the odometer or the hip chain, attached to the unit, were programmed to trigger according to the parameters set. The triggering device could be connected either through the antenna or directly to the control unit via a serial port. Regular calibration of the odometer and hip-chain using a measuring tape was practised to maintain the accuracy of distance measurements. The radar profiles in this study were generated through continuous profiling and the equipment was pushed or pulled at a constant speed.

6.3.3 Spatial reference

A beacon-corrected MALA branded real-time GPS unit with sub-centimetre accuracy level was attached to the GPR for location coordinates and elevation data acquisition. The GPS was connected through the serial port of the monitor to continuously record the positional data throughout each traverse. A hand held Garmin GPS unit was separately deployed to collect the spatial as well as elevation data along the traverse as a backup option. As most of the survey locations were on flat open terrains, the accuracy level of the elevation records are considered relatively high with ideal satellite reception. However, due care was taken to achieve the highest possible precision levels in GPS measurements by maintaining a low dilution of precision, given the reliance of the post-processing topographic corrections on these measurements. Before taking the measurements, the GPS was left stable on open ground for at least five minutes each time it was first switched on to establish proper communication with the satellites in order to obtain accurate location coordinates.

6.3.4 Ground-truthing

Ground-truthing is essential for accurate interpretation and display of radargrams in a GPR study. It also helps to evaluate and validate the accuracy of depth calculations during the interpretations, with respect to the corresponding subsurface depths. By obtaining ground-truthing information for a location, it can be extended to determine the thicknesses of the stratigraphic sequences based on the GPR reflectors for that region. Natural exposures, auguring and trenching are a few common methods of ground-truthing.

Ground-truthing information and generally established stratigraphic sequences were available for most of the sites, as a result of recent trenching undertaken by the Geosciences Australia. Additionally, field studies at places such as Sellicks and Vista provided accurate and comprehensive subsurface stratigraphic information. 76 mm auger holes up to depths of 2 m facilitated the GPR traverses that extended beyond the limits of the trenches at Bethel (Figure 6.7). The detailed stratigraphic sequences and geological information on some of the sites are given in Chapters 3 and 4.

Figure 6.7 *Ground-truthing using 2 m deep auger holes at Bethel*

6.4 Data processing

Data processing in GPR surveys is carried out to improve the raw-data quality for interpretation purposes (Cassidy 2009), and to acquire accurate data replication of the subsurface conditions. It requires elimination of noise and other distortions while enhancing poor reflections on real signals. In general, the processing parameters were determined by considering the data acquisition configurations and the subsurface geology. The degree of data processing required is very much site dependent, but it could also depend on the quality and amount of details required in the interpretation. Post-processing allows for adjustment of most of the parameters, which can highlight contrasts in the subsurface features. However, the signal velocity has to be established at the time of surveying in keeping with the onsite surface conditions. It is advisable to conduct a minimum amount of post-processing, as over-processing may destroy the original signals. However, advanced post-processing methods were not used in this study as the prime objective was to identify the subsurface faults, but not acquire a detailed characterisation of the subsurface properties.

Processing of the raw data of this study was undertaken through the DECO-Geophysics RadExplorer program (version 1.4), which was provided with the MALA GPR unit. The available routines for processing on RadExplorer 1.4 are discussed in the following sections to elucidate profile enhancements achieved through post-processing. The flow of processing routines on the RadExplorer software was followed according to the sequence of appearance within the program, mainly in reference to the RadExplorer 1.4 user manual. Display and module parameter windows were used to adjust the viewing and processing parameters for each routine. The completed processing routines and parameters are automatically recorded into a flow within the RadExplorer program, which can be saved as a separate file with the .fl extension. This file can be reused and the parameters can be reviewed, if required, to perform the same processing steps with other profiles.

6.4.1 DC Removal

DC removal is a routine that eliminates any direct current signal that causes DC biased behaviour (electronic drift) of the reflection signal. This brings the data to mean zero axes in which the positive and negative amplitudes of the GPR trace (a sine wave) are re-established (Cassidy 2009) by rectifying the trace that is bent towards one polarity. This is also known as De-wow filtering and is one of the basic and important routines in the post-processing of GPR profiles. RadExplorer allows the selection of start and end time of the DC removal functionality, and the modes with which it can be operated are mean, median or alpha trimmed. Most of the profiles in this study were processed under the median mode as it gave comparatively higher clarity level to the profiles.

6.4.2 Time adjustment

Variations in the ground clearance (antenna and ground surface air gap) during traversing can alter the initial arrival time (time zero point) of air-ground waves. This affects the two-way travel time (y-axis) including the depth scale of the radargram. Hence, a common zero level representing the actual ground surface should be obtained (Cassidy 2009). The input parameters for this routine are transmitter-receiver antennae separation, direct wave adjustment velocity and the first break in nanoseconds. The direct wave velocity on the ground air interface is considered to be 30 (cm/ns) whereas the antenna separation depends on the type of antenna that has been used (Table 6.1). This routine is also known as time-zero correction.

6.4.3 Trace-edit

The trace-edit routine can be regarded as an editing tool that helps to extract the desired radargram. The trace-edit module provides two basic functions for removing the invalid or unwanted traces (kill traces) and the removal of unnecessary data from the top and bottom of the profile (vertical crop). Removing the distorted signals improves the clarity of the features, while cropping enhances the display of the radargram. The traces can be removed individually or as a range in the RadExplorer program and the cropping can be done as horizontal bands from top and bottom of the profiles by inserting the time values in nanoseconds.

6.4.4 Spatial interpolation

Variations in antenna moving speeds while surveying on rough terrain, changes in slope or the use of time triggering may generate variations in the trace intervals. Spatial interpolation allows adjustment of the distance between the trace intervals. Data is recalculated to a constant horizontal scale by interpolation with the option of varying the original distances. This routine is also known as rubber-band interpolation (Cassidy 2009) or distance normalisation (Rashed *et al.* 2003). The input module parameter for the routine is the desired distance between the traces in metres. It is advisable to use this routine if the processing involves trace editing.

6.4.5 Background removal

Background removal can be considered as a type of a spatial-filter (Cassidy 2009). This routine removes the noise component present within the profile. The background noise can be observed in profiles as continuous horizontal banding, which are also known as "multiples" (Dougherty 2009) and could be erroneously interpreted as horizontal strata. Most of the time, the instrument itself could be a source of noise, in which case a mean trace value is subtracted from the entire profile to eliminate the effect. This is an important processing step especially for environments where shallow subsurface layers prevent the deep reflections from reaching the receiver antenna by making significance resonance on the reflection signals. By applying background removal, deep fuzzy reflectors can be sharpened. However, it may also diminish the sub-horizontal boundary reflectors (MALA-Geosciences 2009) and continuous horizontal reflectors (Cassidy 2009) such as real horizontal stratigraphy.

6.4.6 2D spatial filtering

The application of filters improves the visual quality of data and enhance certain features of interest by removing noise (Cassidy 2009). 2D spatial filtering is a combination of temporal and spatial filtering (Cassidy 2009), which could be applied on individual traces (along the y-axis) or multiple traces across the x-axis simultaneously. 2D mean, median and alpha-trimmed mean are the three types

available on the RadExplorer program with options available for filter size and filter mode. Usage of the subtraction mode in 2D spatial filtering can operate similarly to the background removal routine (Section 6.4.5).

6.4.7 Amplitude correction

Amplitude correction is a gain control routine, which increases the signal amplitude to enhance the visibility of features in a radargram. In RadExplorer program there are four types of amplitude correction functions available: spherical divergence, automatic gain control, traces equalisation and time variant scaling. These can be applied either individually or as a combination. However, noise and unwanted data should be eliminated through the aforementioned processing steps prior to applying this tool. Moreover, due care has to be taken not to over-gain as it would make the recognition of subtle signatures more difficult.

The spherical divergence option makes a correction for the energy loss of wave in the subsurface, which is proportionate to the square of the distance travelled. The correction is applied as a linear gain function that proportionally increases with the two-way travel time to compensate for the energy decay with increasing depth (Jol *et al.* 2003). This is also known as Spreading and Exponential Correction (Cassidy 2009).

Automatic gain control (AGC) equalises the amplitudes of every trace individually and enhances the deeper weak signals. Operator length can be inserted in nanoseconds to specify the window length for gain calculations. It is important to set the appropriate window length, which is generally recommended to include between 3-10 % of the total sample length (Cassidy 2009). The type of AGC coefficient can be chosen from mean or root-mean-square options. The position where the AGC coefficient is applied on to a trace is selected from center, leading or trailing options.

Trace equalisation influences each individual trace by reducing the amplitude variations within adjacent traces. For this a balancing coefficient should be calculated by mean, root mean square value or maximum. The starting and ending times of analysis windows can also be adjusted.

Time-variant scaling is a user-defined function having varying gains by manually inserting each coefficient for different times of each trace. A linear interpolation method is deployed to obtain the gain coefficients in-between the manually inserted values.

6.4.8 Predictive deconvolution

Deconvolution increases the resolution of the radargram by compressing the recorded wavelets. The start and end times of the analysis can be inserted through the routine input parameter window. Prediction gap, deconvolution operator length and white noise levels are three options that can be controlled within this process. The wavelet compression rate can be adjusted through the prediction gap or the deconvolution interval value. In general, the lower the prediction gap the higher the compression. However, higher compression also increases noise levels. The range of the deconvolution operator is controlled by the deconvolution operator length. Dilution of multiple reflections and antenna ringing can occur for higher values of the deconvolution operator length. The white noise level values become significant only for the shorter prediction gaps. Application of the deconvolution routine can also increase noise levels within the profile. Hence, deconvolution is generally followed by band-pass filtering to eliminate the generated undesirable noise.

6.4.9 Bandpass filtering

The loss of signal strength with increasing depth due to physical phenomena such as geometric spreading, attenuation and scattering can increase the noise component within a radargram. This adversely affects the quality of a GPR survey data by masking the deep reflectors (MALA-Geosciences 2009). Frequency filtering is one way to eradicate such noise, and improve the visual quality of data to assist interpretation. The objective is to enhance the clarity of data by removing the frequencies that hinder the identification of genuine subsurface characteristics.

A bandpass filter is a basic frequency filter having a combination of high and low pass filters, which operate on individual traces. It limits the trace frequencies to a specific range that includes the antenna frequency and removes frequencies beyond (both above and below) the specified range (Rashed *et al.* 2003). In the RadExplorer

program, low cut, low pass, high pass and high cut frequency values can be inserted through the module parameter tab, which interactively displays the trapezoidal filter shape on its frequency space diagram. In general, the values for the pass region are calculated with a bandwidth of 1.5 times, symmetrically disposed on either side of the peak antenna frequency (Cassidy 2009). Table 6.1 gives the bandwidth details for bandpass filtering with respect to the antennae used in this particular study.

6.4.10 Slot F-K migration

The visibility of deep reflections associated with stratigraphic layering may be weakened by the presence of hyperbolic reflectors in a profile. Using migration functions, hyperbolic diffractions are converted to point sources, and steep dipping reflectors are restored into more accurate subsurface positions (Rashed *et al.* 2003). This improves the location, shape and orientation of reflecting boundaries, giving a spatially realistic image of the subsurface. Wave propagation velocity within the subsurface medium is the input parameter as the migration velocity for the slot F-K migration routine in the RadExplorer program. Wave propagation velocity can be obtained by hyperbolic fitting on the profile, with the assumption of a constant velocity throughout the medium.

6.4.11 Reflection strength

With the reflection strength routine the radar traces are converted into instantaneous amplitudes to observe significant contrasts in amplitude variations. This helps to determine the high and low amplitude segments of a signal by clearly demarcating the reflecting boundaries within the radargram. The RadExplorer program does not allow input parameters for this routine, and it is not recommended to further process a radargram once this routine is applied.

6.4.12 Topography

Topographic variations of the survey path are not recorded within the radargram. The topography routine re-assembles the traces relative to each other according to the surface topography along the GPR traverse. This is an important processing step for accurate data interpretation as it gives a realistic view of the subsurface features by the observed changes in relief, apparent depth and reflection orientations within the radargram. The height data can be inserted in absolute or relative values as the

program converts them into static corrections based on the maximum elevation. Heights are linearly interpolated using the known points for the elevations that were not recorded during the GPR firings. The effectiveness of the topographic correction depends on the accuracy of surveying. No further processing is recommended after the topographic correction is carried out. Topography correction in the RadExplorer program requires knowledge of the wave propagation velocity within the subsurface of interest. The elevations can be inserted either manually or by using an elevation file in space-separated-tabular-text format. As the MALA GPR unit used for this study provides an interface to connect a GPS, the elevation data were recorded as a separate file (with the .cor extension) and saved within the GPR unit with the radargram files (Appendix III) An accurate sub-surface velocity could be obtained by ground-truthing, common midpoint surveying or by hyperbola fitting (Cassidy 2009).

6.5 Interpretations

A post-processed radargram can be presented in different output styles and unique colour schemes to achieve a reasonable contrast when displaying the interested subsurface features (Figure 6.8). A greyscale scheme was chosen for this exercise due to the clarity of the display (Figure 6.8d). Interpretation of the subsurface features on a processed radar profile is termed as ‘modelling’ in the RadExplorer program. In modelling, polygons are created and labelled to demarcate different stratigraphic sequences. Stratigraphic units obtained from the trenching logs, natural exposures and augering profiles were used for depth calibration and ground velocity determination with several test profiles. Parameters such as wave velocity and dielectric constant can be inserted and named. The y-axis of the completed velocity model can be converted from two-way travel time to the depth scale as the final step of the interpretation. In a processed GPR profile, the topmost (possibly two) bandings represent the direct waves travelling from the transmitter to the receiver antennae, within air and ground. The subsurface features are represented by reflections and diffractions on the radar wave, expressed through the rest of the profile.

Identification of faults depends on the scale of the structure and contrasts between offset layers. Buried objects or subsurface contacts are generally represented as dark clouds on the profile due to their strong reflective properties. In general, hyperbolas represent the point reflectors and lines represent the planar reflectors (Goodman & Piro 2013). Subsurface faulting could also be represented by the hyperbolas, as the radar signals tend to scatter at faults, and continuous layered tomography indicates folding in general. The diffractions undergone by the radar signals are generally visible as hyperbolas. The shape of the hyperbola contains the wave propagation velocity information within a particular stratum. The wider the hyperbolic reflector, the faster is the wave propagation speed. Hence, the hyperbolic reflector information is important in determining accurate velocities for the migration and time-depth conversions of a radar profile. Under the circumstances where hyperbolic reflections are subtle, the layer offset could also used for subsurface interpretations.

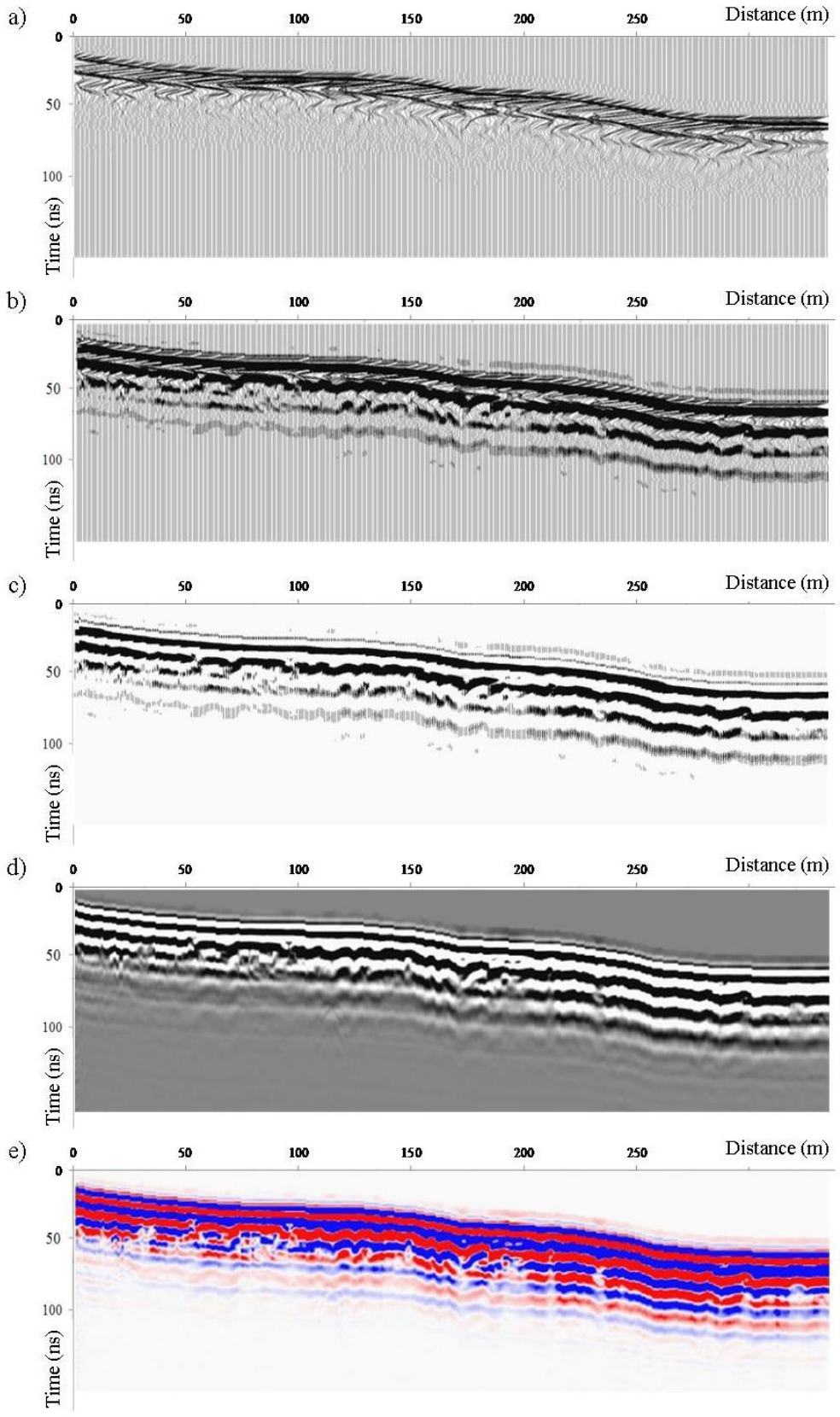

Figure 6.8 *Comparison of different output styles available with the RadExplorer program*

6.6 Results

Representative samples from each site with corresponding illustrations, are presented below. A summary of the selected profiles is given in Table 6.2, and details of the GPR field traverses are given in Appendix III.

6.6.1 Sellicks – Willunga Fault

The radargram related to Sellicks, and its interpretations are presented in Figure 6.9. The traverse extended in a northwesterly direction across the Willunga Fault on land belonging to a Monastery (Figure 3.1). The profile shows a limited depth of penetration of the radar signal, and information is gathered only up to a depth of ~4 m, which is below the capabilities of a 100 MHz unshielded antenna. The top-most bands denote the air-surface interface, followed by a thin layer of alluvial sediments, possibly the Holocene Waldeila Formation. A slight variation in the reflected signal towards the middle of the radargram, could be the fault zone that has weathered bedrock in contact with Cenozoic sediments. Two southeast dipping thrust faults are identified (WLF1 & WLF2) at ~130 m and ~210 m distances along the profile. These are inferred as possible extensions of the Cactus Canyon and Waterfall Gully faults, or unidentified branches of the Willunga Fault.

6.6.2 Hoyelton - Alma Fault

The east-west trending GPR profile across the Alma Fault is given in Figure 6.10. The black and white strong banding denotes the shape of the unconsolidated sediments mimicking the trench-logs. Underneath is highly weathered bedrock. At the western extremity, a subtle reflection from a different layer of clay can be observed. Few hyperbolic reflections are present on the profile within a distance of ~10 m to 30 m from the start of the traverse. This could be related either to fault gouge material on the faults or the effect of tree roots on the 100 MHz unshielded antenna. The feature (H), which is apparent to a depth beyond ~4 m is more likely to be caused by tree roots rather than the reflections from the fault contact. In line with the trenching information and the features of the radargram, three possible thrust faults can be identified (AF1, AF2, AF3). These are possibly branches of the Alma Fault or fractures generated as a result of the compressional fault movements.

However, there is limited surface expression of a fault at this locality, apart from a slight topographic change from north to south.

6.6.3 Tarlee - Williamstown-Meadows Fault

The trench at Tarlee was established on a cultivated land, intersecting the Williamstown-Meadows Fault. The top-most layers, exposed to cultivation were clay-rich soil stratums. The trench exposed an east dipping thrust fault displaying at least ~2 m of recent slip movements, which the GPR profile has been identified as (WMFT1) about the 60-70 m profile length. Towards the eastern end of the profile (~0-20 m profile length) layer offsets of the radargram reveals possibly another fault (WMFT2). There is an indication of slight compression on the unconsolidated subsurface, which the warped structure is clearly recognisable in the GPR profile (Figure 6.11).

6.6.4 Bethel – Williamstown Meadows Fault

The GPR traverse at Bethel was conducted from west to east, parallel to a trench, which exposed bedrock thrust against younger unconsolidated sediments. The fault contact (WMFB1) is clearly visible on the radargram with unique reflection patterns (Figure 6.12), and the fault zone was identified as an east dipping high angle thrust. The bright banding at the top of the profile represents a strong air-surface interface masking the details of the shallow subsurface. A separate GPR traverse was conducted along the bottom of the trench to provide further information on the possible extent of the fault. However, this did not yield informative results.

6.6.5 Gawler - Para Fault

The west to east GPR profiling at Gawler (Figure 6.13) was affected by power lines (H) that extend across the site along the strike of the inferred Para Fault. The strong hyperbolic reflector reveals the influence of the power lines on the 100 MHz unshielded antenna. However, subsurface structures were imaged up to a depth of ~2 m. From the reflection differences and layer offsets, it is possible to infer the presence of three east- dipping thrust faults (PF1, PF2, and PF3). Nevertheless, a ~30 m trench excavated towards the western end of the traverse failed to locate any of the faults.

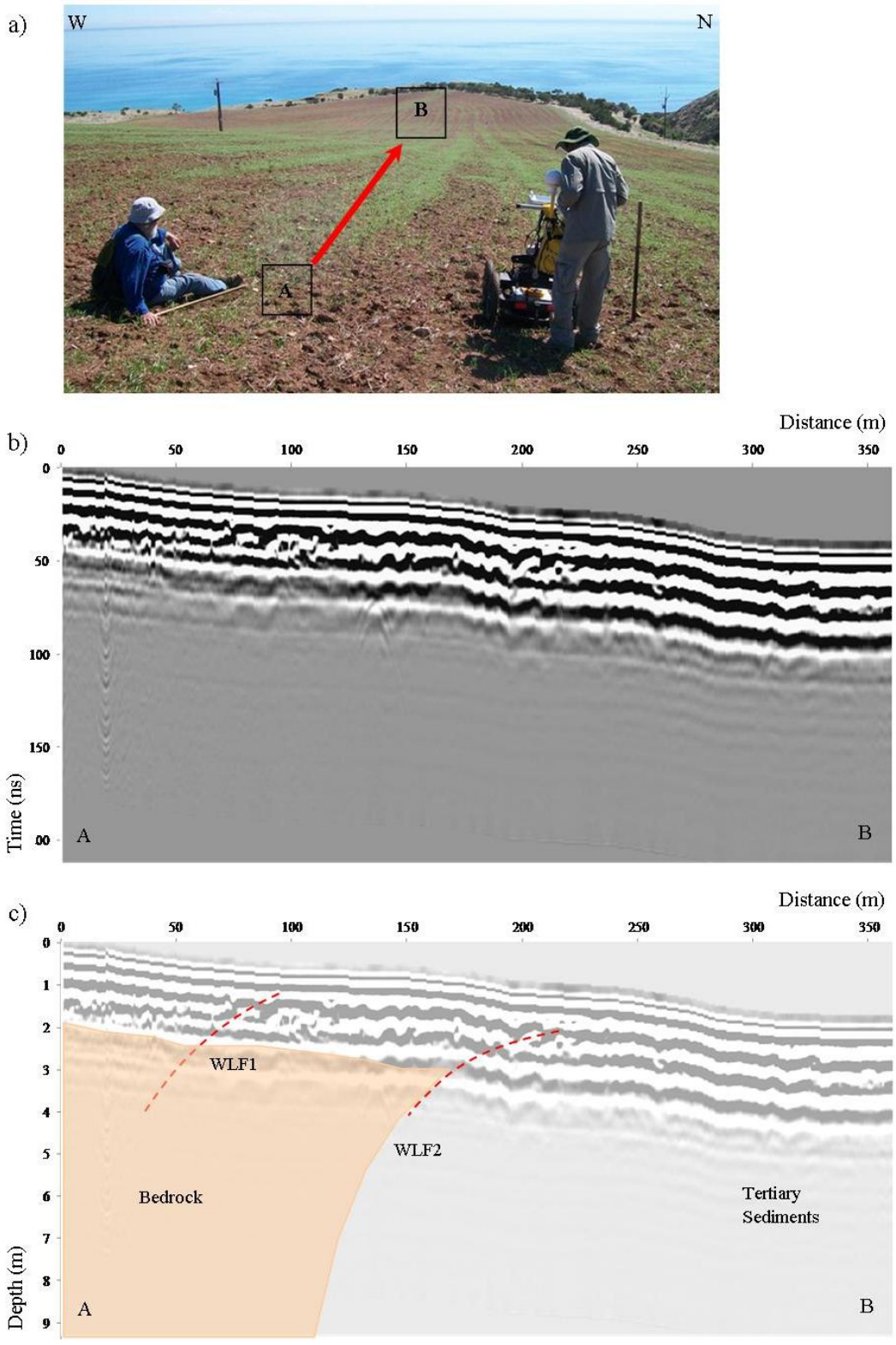

Figure 6.9 *GPR profiles with the 100 MHz antenna at Sellicks a) Field photograph, b) Processed radargram, c) Interpretation*

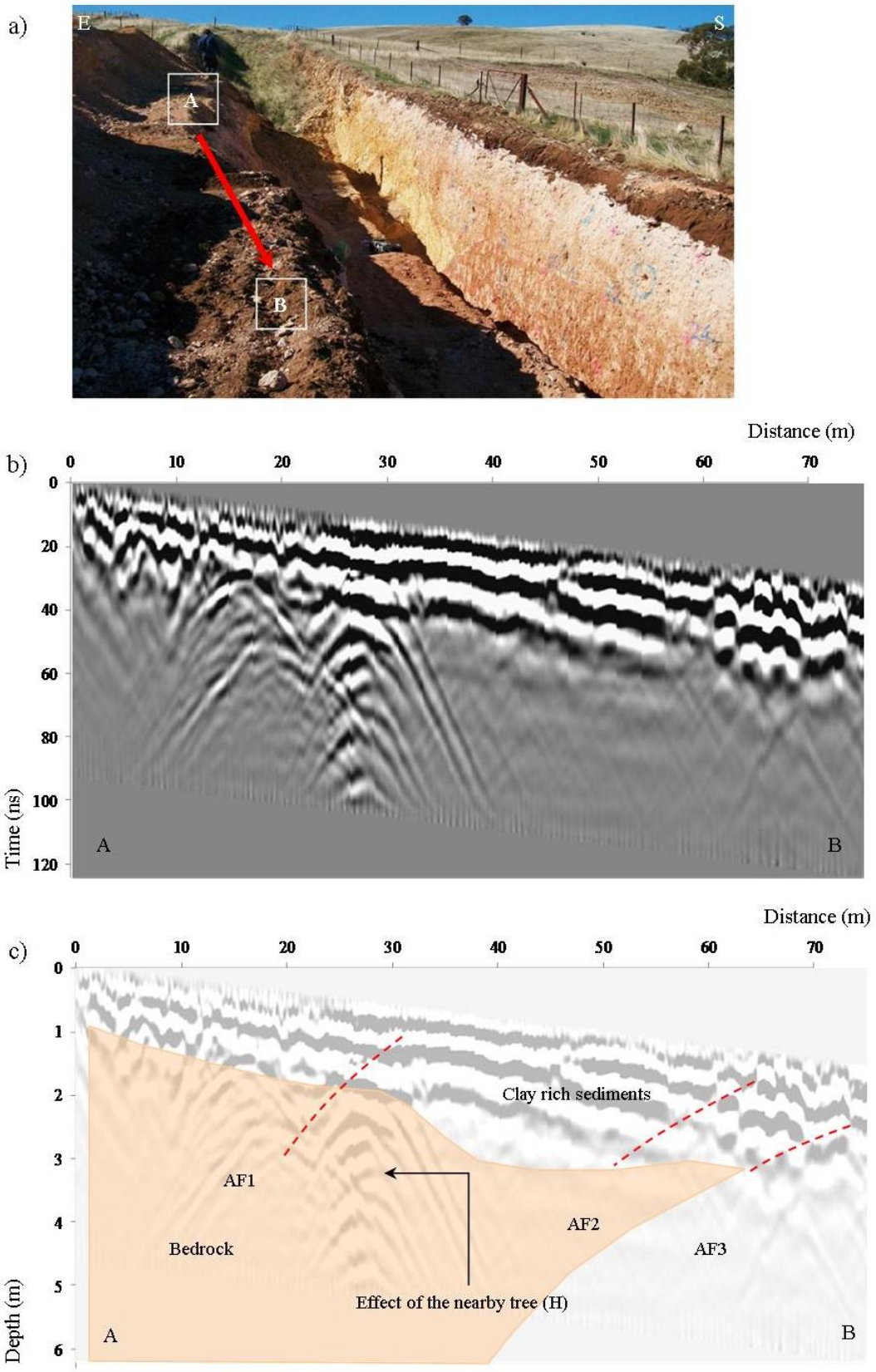

Figure 6.10 *GPR profiles with the 100 MHz antenna at Alma a) Field photograph, b) Processed radargram, c) Interpretation*

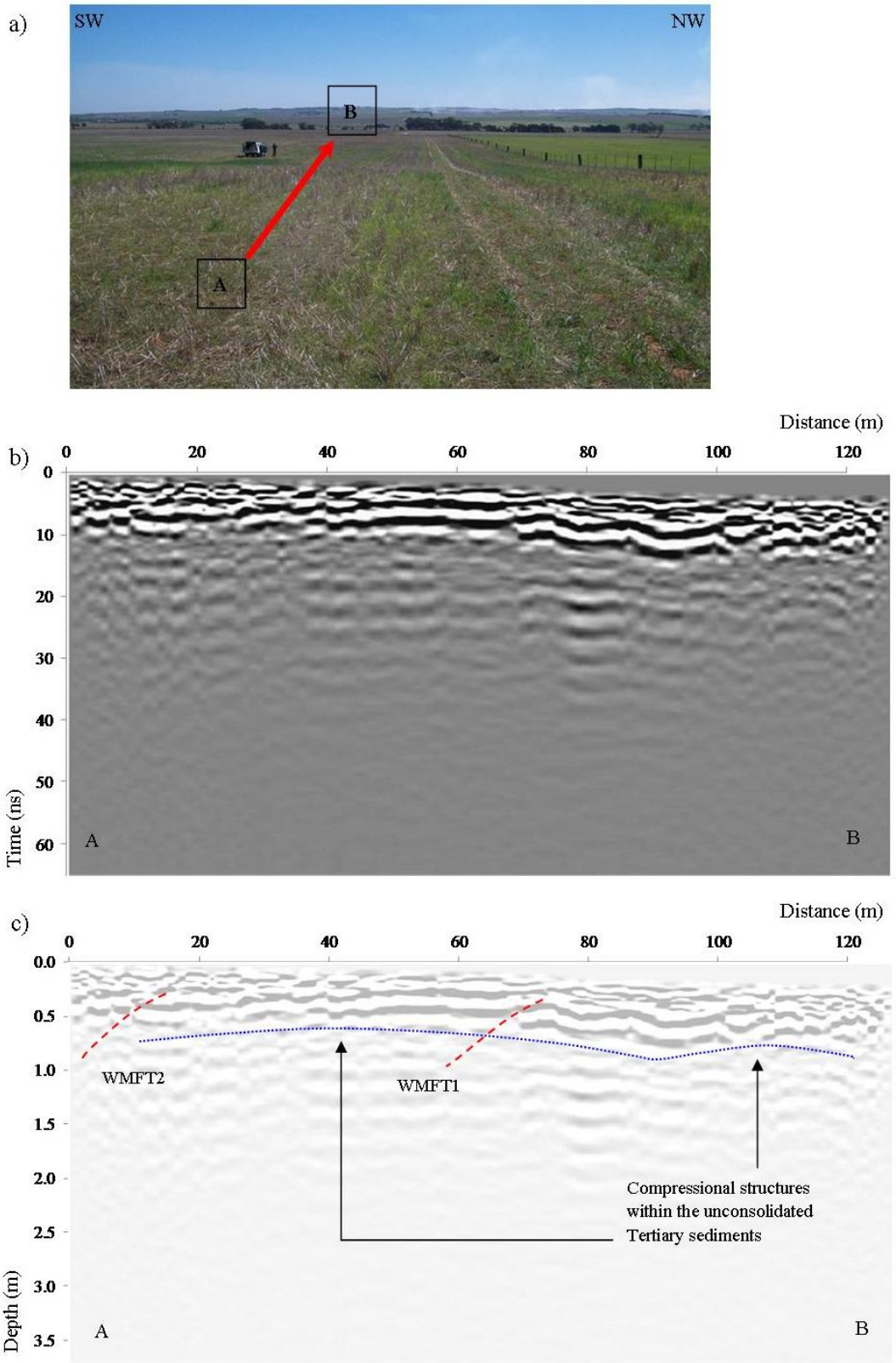

Figure 6.11 *GPR profiles with the 100 MHz antenna at Tarlee a) Field photograph, b) Processed radargram, c) Interpretation*

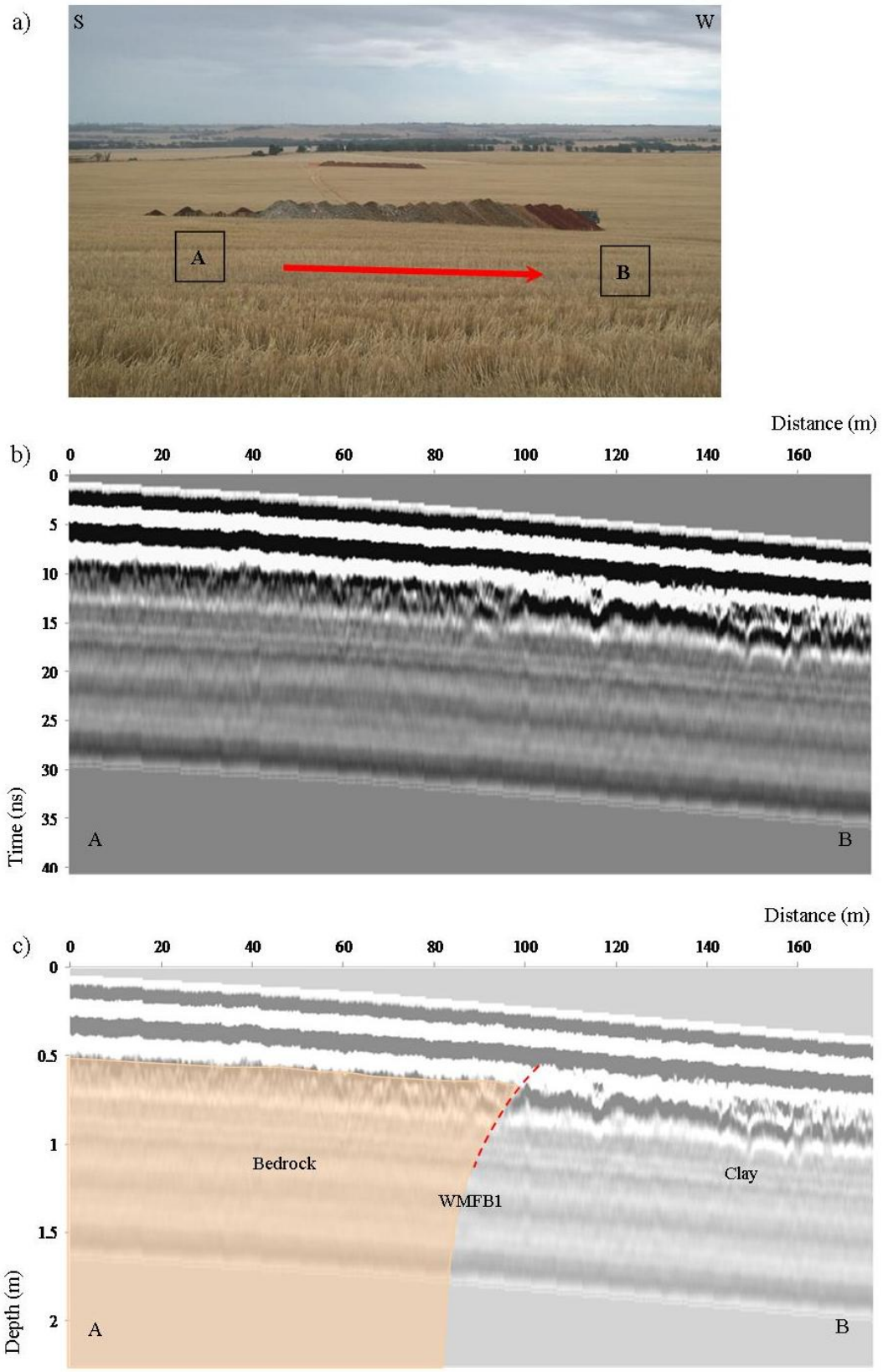

Figure 6.12 *GPR profiles with the 100 MHz antenna at Bethel a) Field photograph, b) Processed radargram, c) Interpretation*

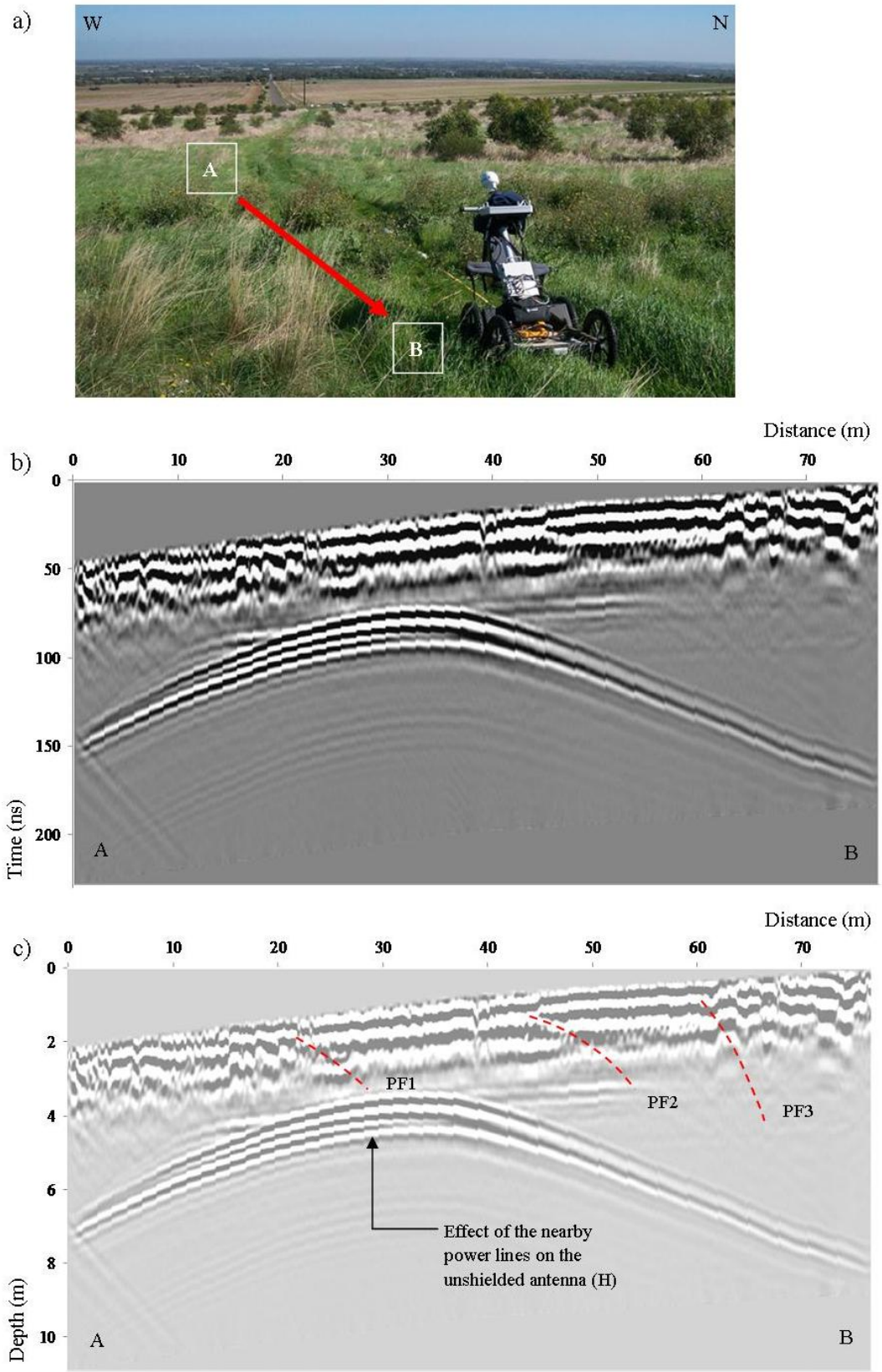

Figure 6.13 *GPR profiles with the 100 MHz antenna at Gawler a) Field photograph, b) Processed radargram, c) Interpretation*

Location & Fault name	**Length (m) & Line no**	**Antenna Frequency (MHz)**	**Traverse coordinates**				**Traverse Direction**	**Figure no**
			Start		*End*			
			N	E	N	E		
Sellicks - Willunga	325 (51)	100	6100454	251414	6100570	251251	Towards NW	(Figure 6.9)
Hoyelton - Alma	75 (108)	100	6234042	255778	6234042	255732	Towards W	(Figure 6.10)
Tarlee – W-Meadows	117 (61)	500	6215417	267333	6215425	267264	Towards W	(Figure 6.11)
Bethel – W-Meadows	165 (274)	500	6212707	267852	6212728	267949	Towards W	(Figure 6.12)
Gawler -Para	75 (114)	100	6190565	264318	6190564	264362	Towards E	(Figure 6.13)

Table 6.2 *Summary of the GPR profiles*

Selected profiles from Sellicks, Hoyelton, Tarlee and Bethel were chosen for detailed interpretations. Each radargram has been related to known subsurface information and faults. Information extracted through the interpretations can be summarised as follows.

1. Two of the high angle faults displayed on Sellicks profile relate to the thrust faults at Cactus Canyon and Waterfall Gully. The cross-section alignment of the identified faults resembles fault splays and positive flower structuring reflecting branching of the Willunga Fault at this locality.
2. The processed radargram from Hoyelton displays similar faulting characters to that of Sellicks. They are in agreement with the stratigraphic offsets revealed on the trench. In spite of the disturbances caused by the reflections from tree roots, the association of several low to high angle faults, related to the Alma Fault, is compelling.
3. Two possible thrust faults of the Williamstown-Meadows Fault and a compressional structure at a depth of ~0.5 m can be distinguished on the radargram from the Tarlee site. One of those faults was confirmed through trenching and the deformational characteristics within the unconsolidated sediments are in sympathy with the current stress regimes.
4. A high angle thrust fault of the Williamstown-Meadows Fault was recognised at Bethel. Reflection variations on the radargram clearly indicate the fault contact, which was covered by a thin layer of clay-rich topsoil stratum.
5. The radargram for Gawler indicate potential faults towards the middle and the eastern end of the traverse. Branching and the development of positive flower structures on the Para Fault at this locality may be responsible for the above observations. However, the strong hyperbolic reflectance from power-lines on the 100 MHz unshielded antenna distracts from the fault features of the radargram.

From the above results, it can be inferred that most of the neotectonic faults experience branching towards the surface, often obscured by thin layers of alluvium. Low to high-angle thrusts of these fault networks resemble positive flower structures possibly influenced by transpression similar to the situation at Sellicks. This characteristic nature of deformation in parts of the Mount Lofty Ranges reflects the

oblique movements on faults due to the present stress regimes. The GPR profiles clearly reveal evidence of transpressional faulting.

6.7 Limitations and factors influencing the GPR performance

The performance of a ground penetrating radar is site specific and mainly depends on the aspects of subsurface, the equipment, experience of the operator as well as the environment and weather conditions, before and during the survey (Benson 1995, Leucci 2008). Accurate data collection with appropriate surveying techniques and suitable parameters/unit configuration is essential to obtain useful subsurface information. In general, parameter selection results in a compromise between penetration depths and the degree of resolution (Rashed *et al.* 2003). Antenna type, frequency, parameter configuration, accuracy of spatial and elevation data are some of the equipment-related controlling factors of a survey, whereas subsurface mineralogy and moisture content (Rashed *et al.* 2003, Leucci 2008) are some of the environmental factors beyond the operator's control.

Generally, the antenna has to be in contact with the ground to achieve optimum results through a radargram. The resolution and depth penetration of a radar signal are governed by the antenna frequency and the conductive properties of the subsurface material. Antenna frequency is proportional to the profile resolution and inversely proportional to the signal penetration depth (Cooke & Gladwin 1999). Radar wave propagation is controlled by subsurface material properties such as dielectric permittivity, electrical conductivity, magnetic permeability, moisture content and density (Jol 2009). Moreover, high conductive environments may reduce the signal penetration depth due to wave attenuation (Leucci 2008). As such, GPR is effective in low-electrical-loss material (Jol 2009), and it is important to understand the subsurface properties of the area under investigation for effective surveying and interpretation.

Faulting signatures from clayey unconsolidated sediments are generally difficult to distinguish due to water content and higher signal attenuation rates (Bonilla & Lienkaemper 1990, Crone & Luza 1990). Unconsolidated clay-rich sedimentary

layers influenced signal scattering by masking, creating low-resolution profiles with the increase of depth. Absorptive losses are high on clayey soils and areas of high salinity, as well as in calcium carbonate rich environments, which reduce the wave penetration depth. Conduction based energy losses during radar wave propagation through unconsolidated soils are mainly due to the influence of ionic charge transport and electrochemical processes on clay minerals. The moisture content of the soil is a critical factor, as the conductivity is governed by hydrochemistry of the water, having an inverse linear relationship with the signal penetration depth (Smith & Jol 1995). Accordingly, a slight increase in moisture content could cause dramatic reductions in the radar range on typical soils based on clay, silt and sand (Cooke & Gladwin 1999). Hence, it is advisable to conduct a GPR survey during dry weather conditions. Dissolved and heavy minerals present and the pore spaces within the subsurface may also influence the above results (Benson 1995, Cooke & Gladwin 1999)

Determination of the ground velocity during slot F-K migration was treated as a common unique value for the entire volume regardless of the characteristics (dielectric properties) of the different stratigraphic sequences encountered. Searching for an alternative processing program (communication with Alpha-Geosciences, Australia) to compare the results was not possible due to time and financial restrictions. Distance measurements using the odometer connected to the cart or the hip chain required regular calibration. A measuring tape was used at the beginning of each traverse was to ensure and maintain the accuracy of distance measurements in surveying.

The readings from the attached GPS were directly recorded as a separate file within the GPR unit with the .cor extension. Hence, the RadExplorer program could not directly import the file to use with the topographic correction routine. The incompatibility issue with the column structure of the .cor file system and the program generated this issue during post-processing. Manual re-arrangement of the columns of .cor files by opening them in a notepad and saving as a text file eliminated this problem, which was a time consuming task. Furthermore, elevations were not recorded for each and every radar signal firing, and even the ones that have

been recorded were not consistently spaced. The spatial interpolation routine in post-processing did not accommodate for this problem and it was necessary to interpolate the elevations separately, in order to achieve a realistic topography.

Eliminating the interferences from outside sources such as vehicles and mobile transmitting devices can improve the radargram accuracy. The effects of vegetation, tree-roots and power-lines have to be considered, particularly when using the unshielded antennae. Some strong hyperbolic reflections were observed when passing trees and traversing under power lines (Figure 6.10 &Figure 6.13). The traverse should also be conducted away from gullies, steep cliffs or disturbed surfaces, at least a minimum distance of signal penetration depth for better results. The use of a high precision GPS device coupled with the GPR unit or conducting a surveying using a total station along the GPR traverse is essential for spatial interpolation and topographic correction at the post-processing stages.

6.8 Discussion

GPR wave form analysis (Villamor & Berryman 2006), has the potential to reveal the characteristics of subsurface fault zones, including their extents and stratigraphic offsets (Chow *et al.* 2001, Basson *et al.* 2003, Rossetti 2003). Despite the high costs and restricted applicabilities, trenching and drilling across fault contacts provide the most reliable and detailed information on palaeoseismic histories of fault zones. However, remote sensing with high resolution imaging such as LiDAR, coupled with a non-invasive geophysical technique such as GPR, may expedite locating appropriate sites for extensive field investigations.

The main objective of this study was to assess the feasibility of deploying GPR investigation techniques to image near-surface faults at selected locations intersecting active faults. The identification of fault splays with limited surface expression and covered by thin layers of unconsolidated alluvial sediments was significant, considering that this was the first-time use of the technique and equipment in this locality. Calculations of dip angles and the extent of vertical displacement on stratigraphic layers have not been addressed in this work, due to the

difficulties of maintaining traverses orthogonal to the strike of the faults. Varying dips and strikes of faults can mislead the orientation calculations on a subsurface GPR profile, particularly in regions where, the faults are subjected to complex branching.

The data from 100 MHz unshielded antenna provided reasonable information with greater detail in comparison to 250 MHz and 500 MHz shielded antennae. However, strong masking of the radar waves on all antennae was encountered in the shallow subsurface during the initial 30-40 ns. Multi-point source reflectors (Conyers & Cameron 1998) on the upper layers disturb most of the radargrams, which could possibly result from the influence of cultivation. Data from a total of 167 GPR profiles were collected and representative profiles were included within this chapter following a rigorous screening process. Some of the investigated profiles did not identify meaningful subsurface structures due to low-resolution of the radargrams and limited depths of penetration. Possible reasons for obtaining unsatisfactory results may include;

1. Unfavourable environmental and ground conditions:

   The survey was carried out in ideal, dry weather conditions and in areas where there were no high ground water conditions. Hence, the possible impacts of wet ground conditions hindering signal depths were avoided. Most of the locations subjected to GPR surveying had been used for cultivation and the top most soil layers could have been repeatedly disturbed. Furthermore, chemical alterations within the strata due to the use of fertiliser may have adversely affected the performance of the GPR. Hence, the observed multiple point reflectors on some profiles could be a result of such interferences. Some field locations displayed clay-dominant subsurface conditions, with reasonably thick gravelly layers. Layers of boulders within colluvial flows might have affected the GPR signals. Given the variety of study sites, a clay rich subsurface cannot be considered to be exclusively responsible for diminishing the radar signal. It is difficult to conclude that the environmental conditions were not suitable for a GPR study, except in the instances where unshielded antenna was used in the presence of high-tension power-lines at the Sellicks, Hoyelton and Gawler sites.

2. Complex deformational structures and inhomogeneous subsurface stratigraphy:
   GPR surveying on the trenched sites (Hoyelton, Tarlee and Bethel) was conducted parallel to the excavations with an offset of at least ~6-7 m, to avoid the influence of artefacts generated due to the excavation. Traverses were aligned in the best possible manner to intersect the inferred fault traces, based on the information of known faults contacts. Nonetheless, it does not assure a fault to be essentially displayed on the radargram, considering the amount of branching, step-overs and *en echelon* transpressional behaviours observed in active faults (Chapter 3 & 4). Presence of faults as complex subsurface structures, instead of as a discrete single structure, complicate the identification process, especially in unconsolidated soils. Hence, there can be instances where a fault behaves differently only a few metres away from a known exposure, in contrast to the trench observations and surface geomorphic expressions. As such, the GPR traverses may not record the same structural contacts on its radargram. This was evident at sites near Hoyelton and Bethel, where three separate trenches displayed different subsurface conditions within a space of a few tens of metres. Similarly, near Burra the trench only slightly intersected the fault, even within few metres of the naturally exposed fault contact. More evidence is available for the Willunga Fault at Sellicks, where two trenches failed to expose the fault contact only approximately 100 m from its natural exposure (Reid 2007).

   GPR surveying at Gawler across the inferred Para Fault was conducted prior to excavations of the trenches. The pre-trenching traverses at the two proposed trench locations indicated structural features similar to faulting within the unconsolidated sediments, complementing the geophysical exploration results of Finlayson (1978). However, subsequent excavations did not expose fault contacts within the trench depth of ~4 m. Nonetheless, a slight fault scarp-like feature is visible on aerial photos, and its presence is compatible with the geophysical surveying results presented in McPherson and Clark (2011). Given the known structural information related to the Para Fault, it should have a strike

that continues through this particular locality and there is no satisfactory explanation for these contradictory observations.

3. Use of inappropriate surveying parameters and lack of experience:

   Field parameters were mainly determined according to the user manual of the GPR unit and published data sources (Doolittle & Collins 1995, Cooke & Gladwin 1999, Jol 2009). Technical advice on the parameter settings was also obtained from the geophysicists of the unit distributor. However, the signal penetration depth (or the acquired reflected signal) was weak after the 30-40 ns time limit, mostly with the 500 MHz antenna. Irrespective of the parameter combinations, the radargram details fell short of expectations. The unit was calibrated each time before taking it into the field and signal search at the beginning of each profile helped to determine the *in-situ* effective depth of penetration. All the sites were surveyed using the three antennae available (100, 250 & 500 MHz) with varying configurations. Hence, if it were a frequency depth related issue generated from the parameter settings, it should have been eliminated, at least on some profiles.

   Discussions on the experienced signal dilution issue with the MALA representative (Toft 2011), similar MALA branded GPR academic users (Howman 2011, Dougherty 2012, Gontz 2012), commercial users (Shearsmith 2011, Suntharalingam 2011), was not of much assistance. Incorporating some of them in the field, and repeating the traverses with alternative parameters could not improve the survey results. Hence, the use of inappropriate parameters or lack of knowledge cannot be considered as a valid reason for some of the ambiguous observations on radar profiles.

4. Restrictions on post-processing:

   The purpose of post-processing is to enhance the appropriate features on a GPR profile, in order to facilitate interpretations. However, extensive post-processing can also destroy important field data. Despite the best attempts, poor quality raw data cannot be rescued with post-processing. Hence, it is advisable to begin with the simplest tools and extract features with a minimal amount of post-processing

(Cassidy 2009). In this study, only the recommended minimal post-processing steps were deployed on the profiles, eliminating adverse effects on genuine reflectors. However, signal masking was observed in most of the profiles and only a limited number could be enhanced, and useful features extracted. Consultations with the GPR unit distributor for technical assistance and advice related to post-processing did not achieve significant improvements.

5. A malfunctioning equipment:

   A brand new GPR unit should not be expected to malfunction. However, this cannot be ruled out as the control unit of the GPR behaved suspiciously when initialising communication with the antennae. The time delay of establishing communication was extended from a few minutes to several hours. Malfunctioning was also indicated by the signal masking observed on most of the profiles beyond the level of 30-40 ns, which an observation not limited to the potentially clay rich subsurface of southern South Australia. At perfect coastal settings (Riggs 2011, Dougherty 2012), in sandy environments (Kermode 2012) and even in the presence of MALA GPR technicians, the signal masking at ~ 30-40 ns, could not be eliminated.

   Ideally, the radargrams recorded with the 500 MHz antenna should record better resolution at shallow depths. However, in this particular instance the 100 MHz antenna gave better resolution (clarity) throughout the vertical profile, while achieving higher penetration depths. As the GPR unit was not following the norms, benchmarking the performance of the unit with another was the best option to try to resolve most of the ambiguities.

   As a test, the unit used for this study (MALA with 100 & 500 MHz antennae) was run in parallel with another GPR unit (GSSI with 250 & 400 MHz antennae). On an identical traverse, with similar parameters, the radargrams from the two units showed significant contrasts, in the field as well as when observed through the RadExplorer program. The comparison was not perfect due to frequency differences in antennae, but the MALA unit had the theoretical advantage of providing a better resolution in higher frequencies with greater

depth of penetration on lower frequencies. Comparison profiles for a few selected depths are given in Appendix III. The observations infer that the subsurface imaging strength and resolution capabilities of a GPR could vary, depending on the brand and the firmware on the control unit.

Eventually, courtesy of Gontz (2012), each of the components of the MALA GPR was tested using an identical MALA unit and the following list of malfunctioning items was identified.

i) The 500 MHz antenna produces poor signal strength when compared with an identical unit. Hence, the reduced depth of penetration and resolution has to be a result of the malfunctioning 500 MHz antenna.

ii) Intermittent problems with one of the antenna modules (slot-B) of the control unit introduce repetitions and noise to the radargram. Hence, frequent multiples and masking observed on most of the radargrams, was a technical issues related to the control unit.

iii) Malfunctioning of the fibre-optic contacts (springs) sporadically disconnected the signals while traversing. Hence, lack of continuity and clarity of some of the profiles may have largely due to the wobbly fiber-optic connectors.

The MALA GPR unit was working up to the expectations, when the faulty items were temporarily replaced with identical components. Successive investigations on improving the radargram on MALA GPR resulted in identifying the above technical defects, which were repaired. The effects caused by the malfunctioning were not significant for the purpose of this study as it did not require in-depth subsurface information on the fault zones with the advantage of using three different kinds of antenna. Nevertheless, the results would have been improved by acquiring more details, had the equipment not malfunctioned.

In conclusion, GPR is a rapid exploration tool, which is cost effective and easy to use, provided that an experienced surveyor operates the appropriate equipment. Being a non-invasive geophysical tool, it is useful and suitable even in environmentally sensitive areas. The accuracy of stratigraphic offsets obtained by the

GPR for subsurface fault identification, can be enhanced by data acquisition before trenching, identically along the trench locations, and after trenching at the base of the trench (Taylor 2010). Detection of progressive seismic events beyond the excavation depths of the trenches is a major advantage of GPR surveying.

Deploying a GPR for neotectonic structural investigations was a challenging endeavour considering the complex subsurface stratigraphy in southern South Australia. Trialling a few different brands and selecting the most appropriate GPR unit suitable for the purpose and site conditions, are important for a successful study. Despite the problems encountered, the results were sufficiently convincing to demonstrate the successful applicability of the GPR for subsurface imaging of faults in southern South Australia.

7 A REVISED TECTONIC MODEL FOR NEOTECTONIC DEFORMATIONS IN SOUTHERN SOUTH AUSTRALIA

7.1 Introduction

Orogenesis may span a few millions of years to 10's or 100's of million years, in spite of mountain erosion and planation (Dewey 1998, Vernant *et al.* 2013). Unroofing of orogens can be a rapid process (Schwartz & Askury 1989, Hill *et al.* 1992) as most orogens tend to be denuded and planated within 10's of millions of years (Ollier 2006). The Ural Mountains in Russia survived for some 250 Ma and still preserve a significant relief (Brown *et al.* 2008, Puchkov 2009b). Amongst the oldest extant mountains retaining unusually high elevations, they are similar to the Appalachian Mountains of eastern North America, (Webb 1969, Rankin 1975, Quinlan & Beaumont 1984). How long mountains persist after orogenesis, is an interesting topic relevant to long-term climate forcing and tectonic alterations (Raymo & Ruddiman 1992).

A significant topography around Adelaide at the time of the Permian glaciations is evident by the distribution and nature of the Permian glacial deposits (Crowell & Frakes 1971, Alley & Bourman 1995), and glaciated surfaces across Fleurieu Peninsula (Bourman & Lindsay 1989, Bourman *et al.* 1999, Bourman *et al.* 2010b). If the Mount Lofty and Flinders Ranges are the denuded core of the ~500 Ma Delamerian Orogen, they would represent an extant mountain range twice the age of the Urals or Appalachians. However, increasing recognition that most of the present day relief of the Mount Lofty and Flinders Ranges is a consequence of neotectonic processes (Sandiford 2003a, Quigley *et al.* 2010, Bourman *et al.* 2010a), exclude them from the list of long-lived mountains. As evident by faulted and disrupted Quaternary sediments along the flanks of the Mount Lofty and Flinders Ranges, neotectonic processes have been responsible for much of the present day relief, regardless of its long-term evolution. This localised, intraplate tectonism requires explanation in terms of the nature of deformation and recognition of a valid driving mechanism.

Attempts to explain the distribution and disruption of Cenozoic marine and terrestrial units in southern South Australia includes a number of hypotheses. Initially, Tertiary embayments represented by half-graben structures were postulated as the result of normal block faulting in an extensional setting (Sprigg 1945, 1946). The recognition of Delamerian basement rocks thrust over Quaternary sediments in places, such as Sellicks Beach, indicated the degree of compression involved with ongoing deformation. The realization that Cenozoic Embayments represent the footwall component of upthrown horsts thrusting over flanking Tertiary sediments, has led to the conclusion that the ranges were most likely created by compression (Bourman & Lindsay 1989, Sandiford 2003a). However, orientations of a few fault planes may not necessarily represent the present or past stress regimes as well as the extensional and/or compressional forces that it has experienced (Stiros 1988). Extensional and compressional stresses may enable discontinuities to demonstrate both normal and reverse movements at different stages of the deformation (Tokarev 2005). Consequently, perturbations in fault orientations may contain localised zones of compression and/or extension. Relative lateral movements may also facilitate simultaneous normal and reverse fault movements (Storti *et al.* 2003). Hence, it is important to identify contemporaneous reverse, normal and strike-slip faults and their unique orientations on a fault zone, to determine fault and fracture patterns, as well as overall stress regimes to account for regional deformation.

7.2 Seismic history

Seismicity indicates subsurface movements along lineaments or planes of weakness (Pavlides *et al.* 1999). Consistent, low-level, shallow-depth seismicity is a characteristic feature in the Mount Lofty and Flinders Ranges (Belperio 1995). Broadly spread, temporally isolated contemporary seismicity, occasionally display high magnitude events, including foreshocks and/or aftershocks (Belperio 1995), largely in regions where elevations exceed ~200 m (Wellman & Greenhalgh 1988). Deformations are not limited to the ranges, with the records of arbitrary seismicity from the surrounding on and offshore basins. Nevertheless, the distribution of seismic activity appears to be random, without recognizable rupture patterns, probably due to the complexity of the fault networks (Greenhalgh *et al.* 1986).

According to the palaeoseismic records, regular earthquakes are observed in intraplate strike-slip settings rather than in those experiencing dip-slip faulting (Sylvester 1988). Seismic evidence becomes more diffused in most strike-slip fault zones as seismicity is dispersed within heterogeneities of the upper continental crust, blanketing the expression of activity in deeper, confined structures (Sylvester 1988). Frequent, shallow-subsurface earthquakes in the Mount Lofty and Flinders Ranges (Figure 2.3), could also have a similar origin and merge into a deeper, low-angle dècollement similar to the San Andreas Fault, California and the Vienna Basin, in Austria-Czechoslovakia (Royden 1985).

Limited numbers of historic seismic records do not directly compliment the features observed on mapped fault zones. Computed epicentres from seismic events substantially deviate from known faults, with large error ellipses (Clark & Leonard 2003, Hillis *et al.* 2008). Corresponding shallow depth (<20 km) hypocentres also display vague relationships with the identified faults. Moreover, strike-slip focal plane solutions have been obtained for faults considered to demonstrate dip-slip movements (Greenhalgh *et al.* 1986). Inconsistent relationships between seismic sources and topographic features could be due to the presence of unidentified subsurface faults. Down-dip step-over branching or varying dip orientations could develop such faulting complexities. However, step-over geometries producing seismic heterogeneities along fault lines are commonly observed in strike-slip environments.

The diffuse relationship between earthquake epicentres and surface expressions of active, range-bounding faults could be a function of large epicentre error ellipses, or reflect a lack of understanding on the nature of faulting, including the possibility of the faults being low-angle and merging into a dècollement plane at depth. Nevertheless, the frequencies and magnitudes of seismic events recorded in the Mount Lofty and Flinders Ranges are relatively strong, given their intraplate setting remote from the plate boundaries. Uncertainties of the rupture lengths and patterns, slip variations along the strike, and possible branching of the faults have complicated estimations of the magnitudes, spatial extents and recurrence intervals of palaeo-earthquakes. Aseismic-slip within the upper most ~100 m of the crust is observed in

strike-slip fault zones, such as the San Andreas (Goulty & Gilman 1978, Schultz *et al.* 1982, Linde *et al.* 1996, Titus *et al.* 2005) and on the North Anatolian Fault (Ambraseys 1970, Barka 1996). Extensive dip-slip movements without a record of large earthquakes on most of the active faults within the Mount Lofty and Flinders Ranges may also be, a consequence of ongoing aseismic-slip (Crone *et al.* 2003).

Conversely, seismicity can be distributed over larger regions where major faults with networks of subsidiary fault splays occur. Faults in a network may be active, sequentially or concurrently accommodating stress at different levels and creating complex temporal rupture patterns (Jones & Wesnousky 1992, Wesnousky & Jones 1994) as well as relatively slow surface deformations (Braun *et al.* 2009). Shearing on steeply dipping faults encounters less friction during deformation and results in low levels of instantaneous seismic energy release. In particular, the mature stages of orogenic belts display low seismicity strike-slip tectonics, as some movements are accommodated by pre-existing structurally weak zones. Additionally, continuous micro-level brittle deformations may result in association with low seismic profiles with irregular larger events (Okal & Stewart 1982). Hence, most of the features observed in the Mount Lofty and Flinders Ranges has significant similarities with strike-slip zones.

7.3 Geomorphic expression

The Mount Lofty and Flinders Ranges have a characteristic sigmoidal shape (Figure 1.2), probably resulting from the interaction between the stable Gawler Craton, and the western boundary of the mountain range (Mancktelow 1981, Fraser *et al.* 2010). Laboratory scale strike-slip models (Dauteuil & Mart 1998, McClay & Bonora 2001, Schellart *et al.* 2007) display identical sigmoidal patterns, which can be correlated with the features of the Mount Lofty and Flinders Ranges. Furthermore, thrust faults on a terminal or step-over strike-slip zone can propagate with a curvature in their strike (Cunningham *et al.* 2003). Horsetail splay of thrust faults in the Northern Flinders Ranges and the southern Mount Lofty Ranges, and the composite sigmoidal shape could have also resulted from terminal or step-over strike-slip zone.

According to the lithological changes within the sedimentary successions of the ranges (Belperio 1995), and the Murray Basin (Brown & Stephenson 1991), the western side of the mountain range may have been uplifted earlier than the eastern. The timing differences between uplift on the western and eastern sides could have resulted from lateral movements against the stable Gawler Craton. Increasing elevations towards the NW and SE on southern and northern tips of the mountain range can be observed on topographic cross sections generated from elevation models (Figure 7.6). These can be considered as frontal thrust wedges developed in line with sinistral strike-slip movements (Christie-Blick & Biddle 1985).

Curvilinear faults in the Mount Lofty and Flinders Ranges display *en echelon* step-over patterns with variable dips resulting from episodic uplift and subsidence (Twidale & Campbell 1995, Buckman & Jayawardena 2009a). Block sliding in an extensional strain accommodation zone (Tokarev 2005) or regions under transpression may produce a non-linear strike of a fault (Harland 1971, Harding 1974, 1985). Curvilinear Willunga, Ochre-Cove, Eden-Burnside and Para fault scarps on the western flanks (Figure 2.8) of the southern Mount Lofty Ranges demonstrate horsetail splay structures (Figure 7.1), common to strike-slip fault systems. Prominent knick-point retreats in incision gullies near the Willunga, Wilkatana, Williamstown-Meadows and Milendella faults (Stubley 1990, Sandiford 2003a, Quigley *et al.* 2007b, Quigley *et al.* 2007c, Buckman *et al.* 2009b), and differentially elevated terraces (Quigley *et al.* 2007b, Bourman *et al.* 2010a), may reflect recurrent tectonic activity. A number of waterfalls and deeply incised valleys on the moderately steep western slope of the Mount Lofty Ranges may have been produced by ongoing block uplift (Tokarev 2005).

The height of a fault scarp generally indicates the minimum vertical displacement of the fault. The scarp heights vary along the strike of a fault, depending on the distribution of vertical slip components (Peltzer & Tapponnier 1988, Sylvester 1988). The Willunga and Burra faults, which are naturally exposed in erosion gullies, disappear within short distances of their exposures. Trench cross sections reveal that the Williamstown-Meadows and Alma faults exist in the shallow subsurface, without much surface expression. Indistinctive fault scarps at the Wilkatana Fault in the

Flinders Ranges have resulted from oblique movements (Quigley *et al.* 2006), and the same could be happening in other places as well. However, the lack of expression of fault scarps in a region dominated by thrust faulting is abnormal, unless rapid weathering or erosion has taken place.

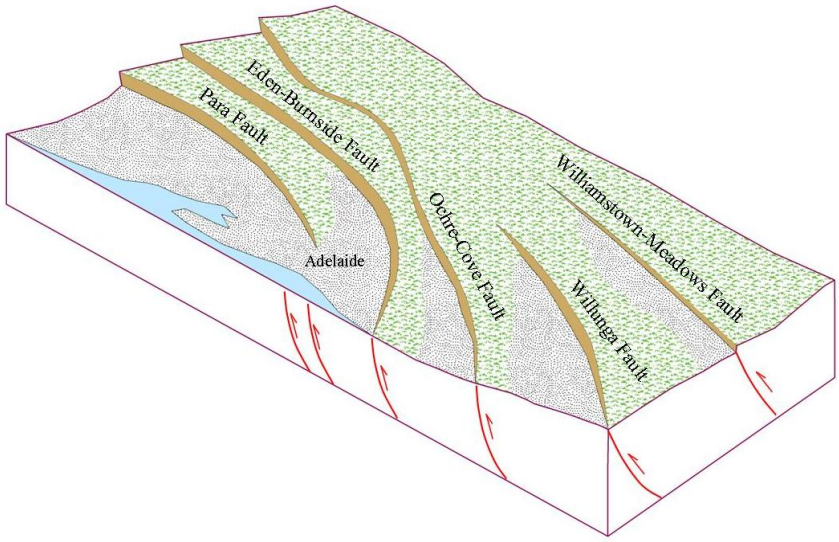

Figure 7.1 *A revised interpretation of the southern Mount Lofty Ranges (adapted from Talbot & Nesbitt (1968)*

The preservation of fault scarps may be hindered by the unconsolidated nature of sediments, local geological factors and high rates of degradation due to locally enhanced erosion (Sandiford 2003a, Quigley *et al.* 2007a). This is exacerbated if the nature of faulting is such that it does not generate sufficient vertical offsets to create long-lasting fault scarps and thick alluvial fans adjacent to the scarp (Sandiford 2003a, 2003b). Combined these factors, may have diluted the topographic evidence of faulting. Additionally, scarps generated by faults with slow slip-rates (Ihmle & Jordan 1994, Houston & Vidale 2007, Peng & Gomberg 2010), may be erased by active surface processes such as local erosion, sedimentation and colluvial flows (Sylvester 1988, Ihmle & Jordan 1994, Peng & Gomberg 2010, Vidale & Houston 2012). Most of the fault contacts of the Mount Lofty and Flinders Ranges are covered with veneers of unconsolidated sediments (Chapter 4). Studies on the Wilkatana (Quigley *et al.* 2007a), Willunga (Buckman *et al.* 2009b), Alma and Williamstown-Meadows faults, have revealed that, they are accompanied by several subsidiary fault networks. Hence, partitioning of slip on fault networks may collaboratively and concurrently release stresses, thereby experiencing deformation without significant scarp generation (Caskey & Wesnousky 1997).

The Mount Lofty and Flinders Ranges are surrounded by areas of subsidence such as Gulf St. Vincent, Spencer Gulf, Lake Gairdner, Lake Torrens, Lake Frome and the Murray Basin (Figure 1.2). Localised uplifts surrounded by subsidence may be best explained by strike-slip movements as they control shapes, sedimentation and deformation (Ballance & Reading 1980) by extensional and compressional lateral-slip. Evidence of extensional faulting on the basins may have been blanketed by active sedimentation. Nevertheless, occasional seismic events including large events NNW of the ranges confirm ongoing deformation, which would be difficult to explain using compressional forces.

7.4 Geometry of faults

The nature and the rate of fault movements change over geologic time. The geometry and style of faulting depends on spatial and temporal constraints such as the amount of strain accumulated, the vertical and horizontal slip components, pre-existing structures and the nature of the deformed material (Sylvester 1988). Current knowledge on the Mount Lofty and Flinders Ranges faults, infer dip-slip movements with dominant reverse faulting, largely due to E-W compression. Most of these classifications have not considered detailed local fault kinematics. They contradict the regional characteristics such as evidence of transpressional faulting (Clarke & Powell 1989) and dominantly strike-slip focal mechanism solutions for range interior faults (Clark & Leonard 2003).

Planation surfaces of various ages and stratigraphic offsets emphasise multiple episodes of landscape development (Bourman & Lindsay 1973, Bourman & Lindsay 1989) in response to changing stress regimes. Variably dislocated Cenozoic stratigraphy in the Mount Lofty and Flinders region indicates that the faults have produced large offsets, even though, many of these recognised faults have not been associated with large historical earthquakes. The Oligocene-Miocene Port Willunga Formation has been recorded ~200 m below present sea level near Adelaide, but close to sea level north of the Willunga Fault contact at Sellicks (Figure 3.4). Movements on the Ochre-Cove, Eden-Burnside and, most probably, the Para Fault, may have been collectively responsible for these dislocations. Conversely, there has

been more than ~240 m of vertical uplift of the Port Willunga Formation at Myponga (Figure 7.2), ~12 km south of Sellicks (May & Bourman 1984), revealing a total offset of the Port Willunga Formation of ~440 m in the past 20 Ma due to ongoing fault activity.

Faults on the western flanks of the Mount Lofty Ranges generally dip towards the SE, whereas, faults on the eastern flanks dip to the NW. The dip of the faults steepens towards the middle of the ranges, and the cross-sectional representation of the faults resembles positive flower structuring. Youthful faults are largely reported from the western Mount Lofty Ranges and the eastern Flinders Ranges (Belperio 1995), a pattern that cannot be solely explained in terms of simple E-W compression. Segmentation on the sections of the Wilkatana Fault in the central Flinders Ranges has been interpreted as merging with an unidentified major subsurface fault at depth (Quigley *et al.* 2007a). Topographic cross-sections perpendicular to the strike of the Willunga and Williamstown-Meadows faults also display, low to high angle thrusts branching towards the surface, and resembling positive flower structures. Accordingly, most of the range-bounding faults may be regarded as fault splays emanating from a major subsurface fault system.

Upward branching faults with recent reverse-oblique left-lateral movements have been recorded in the Wilkatana Fault Zone in the Flinders Ranges (Quigley *et al.* 2006, Quigley *et al.* 2007a). Varying dips along its strike, alternative dip directions and indistinctive fault scarps in the region reflect complexities in the faulting, the driving mechanisms of which are unclear. Dominant reverse-oblique slip on a series of *en echelon* vertical fault contacts of the Eden-Burnside Fault (Bourman *et al.* 2010a) exposed at the Anstey Hill Nature Reserve near Vista, provide further evidence that faulting is not limited to dip-slip movements. Based on the sub-horizontal slip lineations and extension-gash arrays, the behaviour of the fault at this locality has been interpreted to display sinistral movements resulting from transpression. The presence of sinistral oblique-slip *en echelon* fault segments along the strike of a fault as a result of transpression, contradicts the explanation of purely compressional reverse faulting generally attributed to this region.

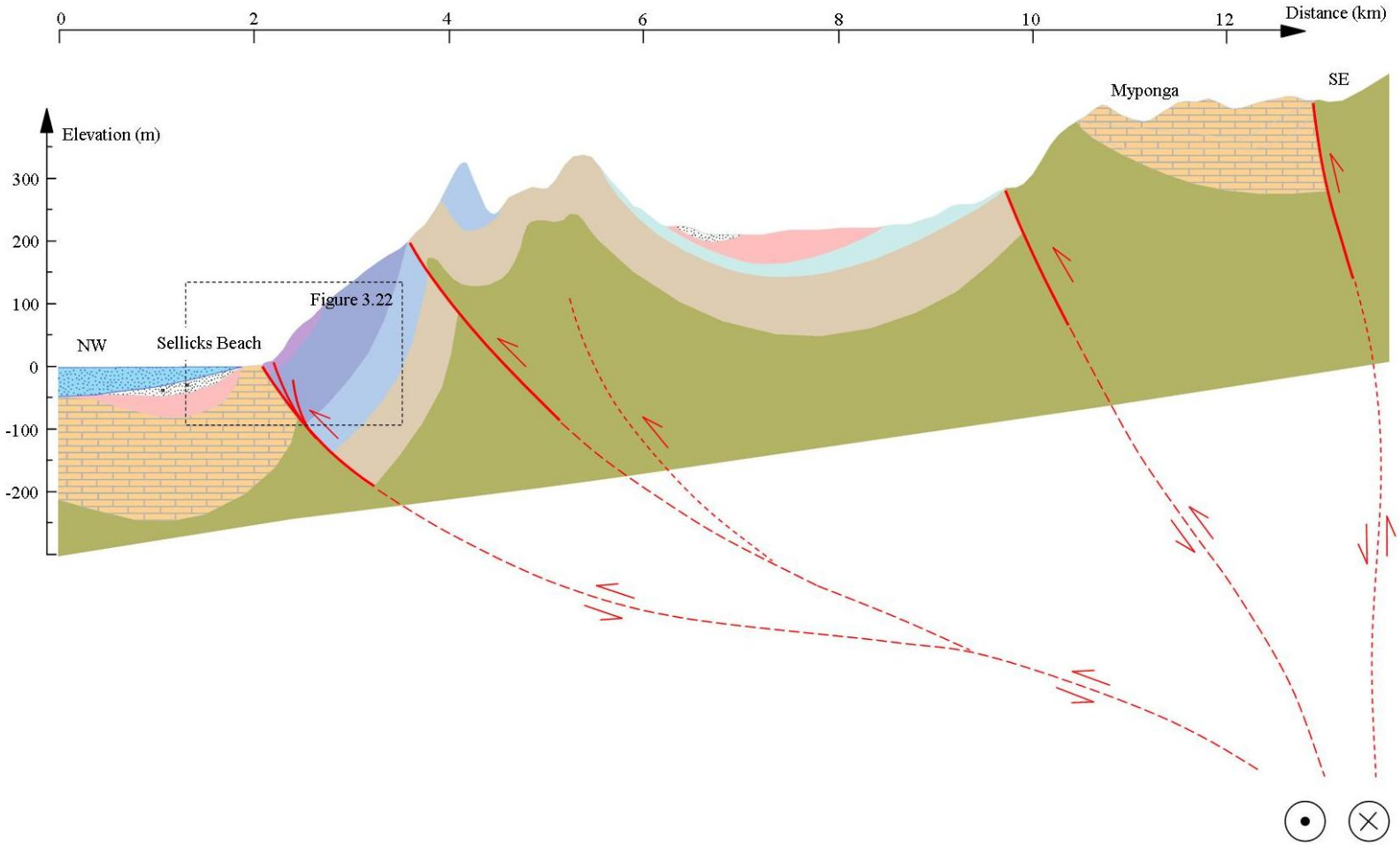

Figure 7.2 *Cross section from Sellicks to Myponga demonstrating regional scale deformation mechanism.*

Delamerian sinistral slip on the Paralana Fault (Paul *et al.* 1999) and dextral slip on the MacDonald's Fault zone in the Flinders Ranges, have also recorded significant oblique movements (Paul *et al.* 2000). Belperio (1995) documented post-Delamerian strike-slip movements on the Kingston Fault near the Burra Mine in the Mount Lofty Ranges, based on north plunging slickensides. There are also records of east trending strike-slip and oblique-slip faults in the southern Mount Lofty Ranges, but without proper spatial reference (Forbes & Pitt 1980, Clarke & Powell 1989). A series of parallel *en echelon* fault splays towards the southern end of the Para Fault, near Adelaide, has been identified by a gravity survey (Thomson 1969b, Finlayson 1978) as stated in McPherson & Clark (2011). On Kangaroo Island, south of the Mount Lofty Ranges there are reverse faults with east-west strike directions. These faults have been shown to display both sinistral and dextral movements in *en echelon* vein arrays, but the timing of their movements were not specified (Marshak & Flöttmann 1996).

Mineral lineations and slickensides trending east on thrust planes (Mancktelow 1981), do not sufficiently indicate the accurate orientations of recent faulting, for a region experienced multiple deformational episodes. According to Tokarev (2005), normal faulting from middle Eocene to middle Miocene times was associated with the breakup of Australia from Antarctica, and ongoing reverse faulting since the early-middle Pleistocene was considered to be responsible for the deformational features in this region. Middle Miocene to earliest Pleistocene was considered to be the period of transition, from extensional to compressional regimes. Prolonged activity on discontinuities and direction change in deformation, is a prominent feature of strike-slip zones (Mann 2007b), even though deformation within the Mount Lofty and Flinders Ranges have not been assessed from a strike-slip perspective. However, several studies have acknowledged oblique and lateral movements, during both neotectonic and Delamerian episodes.

High-angle subsidiary faults associated with the Willunga Fault in the Sellicks region (Howchin 1911), were examined in detail during the present study. Several branches emanating from the main Willunga Fault were observed on incised gullies, eroded sea-cliffs and road-cuttings, having varying dips and strikes. Some of the reverse and

normal faults display oblique movements based on sub-horizontal slickensides, and reflect recurrent fault activity. The orientation of reverse, normal and possible strike-slip faults have been interpreted to represent a zone of transpression with left-lateral movements (Chapter 3). High- to low-angle thrusts observed on the Paralana, Alma, Burra and Milendella faults reflect extensive branching to form a network of faults, even though it was sometimes difficult to extract fault kinematics on highly weathered fault contacts at these localities. Sub-vertical extensional fractures on most of the hanging-walls were considered to have resulted either from collapse after reverse faulting, or from continuous transpressional movements along the faults.

Trenches intersecting the Williamstown-Meadows Fault at two different locations (namely Tarlee and Bethel) also reveal branching (Figure 4.17) of recently active faults. Changes in sedimentation characteristics such as, from debris flows to conglomerate deposition and vice-versa, indicate source regions varying from unconsolidated soil strata to weathered bedrock. The stratigraphic offset of ~1.7 m along the dip of the Williamstown-Meadows Fault, with a subtle surface expression near Tarlee, is uncharacteristic for a region generally considered to be under compression with reverse movements. Similarly, almost ~17 m of vertical offset on the same fault with limited surface expression near Bethel, may be an indication of transpressional oblique-slip diverted from compressional dip-slip faulting. Apart from the sinistral transcurrent offsets reported on the subsurface Permian glacial troughs due to fault movements on the eastern side of the Mount Lofty Ranges (Stackler 1963), direct evidence for lateral component of the oblique-slip movements, is yet to be recorded from the southern South Australia. However, studies have shown that, large amounts of transpressional movements can be accommodated despite the absence of significant lateral movements (Wesnousky 1986).

7.5 Tectonic evolution

The Delamerides consist of metamorphosed, folded Neoproterozoic sedimentary rocks and granitic plutons emplaced during the ~500 Ma Delamerian Orogeny, culminating in the formation of a significantly high mountain range. The granite

plutons were exposed at the surface by the time of the Permian glaciation (~ 300 to 280 Ma) as evident by the widespread presence of granitic erratics in the Permian glacial deposits. This reveals a rate of landscape lowering of some 36 m/Ma, possibly accomplished during the Permian glaciation. A glaciated granite surface, the only one known from the area, glacigenic sediments and the profusion of granite erratics throughout Fleurieu Peninsula demonstrate that the granite was exposed during or just before the glaciations. A substantial relief would have been preserved, prior to the glaciation, which approached from the southeast and moved in a westerly direction across Fleurieu Peninsula. Occasional xenoliths, occurring as roof pendants, reveal that the roof of the pluton was close to the present land surface (Milnes & Bourman 1972). Following this, the landscape was subjected to ongoing weathering and erosion, and was bevelled to a surface of low relief, which was tectonically uplifted in the Neogene (Sandiford 2003a, 2003b, Celerier *et al.* 2005, Quigley *et al.* 2006, Müller *et al.* 2012) along range-bounding faults. Thus, most probably, the present Mount Lofty and Flinders Ranges bear limited resemblance to the folded Delamerides, but predominantly are a reflection of neotectonic faulting and uplift.

The field observations favour uplift of neotectonic structures, independent of Delamerian influences as the SE-NW tectonic movements of the Delamerian are oblique to the ongoing neotectonic block movements. Relatively steep, range bounding reverse faults also support this interpretation (Bourman & Lindsay 1989, Sandiford 2003a). Furthermore, the SE-NW ancient block movements along a major shear zone, accompanied by several low-angle dècollements (Preiss 1987, Jenkins 1990, Jenkins & Sandiford 1992, Flöttmann *et al.* 1994, Yassaghi *et al.* 2004), are unlikely to be functional during the Cenozoic. The tectonic settings of the Delamerian Orogeny were vastly different from the neotectonic faulting, with the first occurring within Gondwana and the other happening in a post-rifting environment. Hence, the behaviour of the steep neotectonic blocks can be regarded as being independent from the dynamics that operated during the Delamerian. However, pre-existing low angle basement thrusts and dècollements may be significantly involved, if the deformation complies with lateral-slip, as is evident by oblique movements on some of the faults.

Discrepancies between known faults and earthquake epicentres could possibly result from the reactivation of unidentified older tectonic structural networks under the present stress regimes (Belperio 1995). A correlation between regional seismicity and the elevations of the Mount Lofty and Flinders Ranges (Love *et al.* 1995), favours the compressional reactivation of E to NE trending Delamerian structures during the middle to late Eocene (Drexel & Preiss 1995, Benbow *et al.* 1995b, Müller *et al.* 2012). An east-dipping basement ductile shear zone, several hundred metres wide, associated with the Para Fault near Gawler, and recognized during a gravity survey by Thomson (1969a), overlaps with the NNW trending Palaeozoic sinistral shear zone (Figure 2.9) proposed by Coward (1976). Thus, Delamerian ductile shear structures could be influencing the present behaviour of the Para Fault. However, clear evidence of reactivation or independence from older structures could not be observed in the field. Trenches near Bethel and Hoyleton displayed obliqueness between the two regimes, with, most of the older structures dipping NNE, while the younger structures dipped towards the ESE.

Sedimentary basin inversion in an intraplate setting developed the topography during the Delamerian Orogeny (Sandiford *et al.* 1998b). The mountains were eroded and bevelled during the Palaeozoic and Mesozoic (Coats & Blissett 1971), setting the stage for a reformed phase of neotectonic deformations. Uplift of the Flinders Ranges could also have resulted from a renewed phase of basin inversion (Sandiford *et al.* 1998b) and elongated structures in the Mount Lofty region have a similar origin (Tokarev 2005). A spatially interconnected Tertiary extension distinguished by Pleistocene compression (Fenner 1930, Tokarev 2005) better accommodates uplift of the mountains and subsidence of the flanking basins. Accordingly to this hypothesis, movements during part of the Pleistocene and Holocene (~1 Ma) enforced compressional uplift on the reversely reactivated Tertiary normal faults, exclusive of the Delamerian structures. However, the general absence of older basement fabrics (Tokarev *et al.* 1999) makes it difficult to guarantee complete independence of the neotectonics: the notion that neotectonics are independent of Delamerian structures is only valid on the naturally exposed and shallow subsurface fault contacts, as the behaviours of the deeper subsurface structures are largely unknown.

7.6 Stress and modes of deformation

Considerable heterogeneity in the *in-situ* stress fields are displayed on the Australian stress map (Hillis *et al.* 1999). According to the stress models, the maximum horizontal stress distribution for most of South Australia has changed from ~ NNW-SSE to WNW-ESE, over the past ~50 Ma (Hillis & Reynolds 2003, Dyksterhuis & Muller 2004, Hillis *et al.* 2008). Bedding orientations of the Neogene Port Willunga Formation along the shoreline platform of Aldinga Bay, display evidence of NNW-SSE compression (Chapter 3). Gentle folding of the last interglacial Pleistocene Pooraka Formation emphasizes NW-SE compression on the western flanks of the ranges (Chapter 3). The approximate E-W compression on subsurface GPR profiles on unconsolidated sediments adjacent to the Williamstown-Meadows Fault near Tarlee (Figure 6.11) also reflects ongoing deformation. Variations in local stress orientations and consequent neotectonic structural responses are verified by these field observations.

Tectonically induced stresses are expressed by lineaments (Meinesz 1947, Boutaloff 1952), which can demonstrate both lateral and vertical differential movements (Twidale & Bourne 2004). These shear planes assist the development and propagation of conjugate fracture patterns, which display localized zones of tension and compression, in environments largely considered to be compressive (Weissenberg 1947). Approximately WNW-ESE oriented local maximum horizontal stress is determined in the context of southern South Australia, where the Mount Lofty and Flinders Ranges are bounded by active faults (Greenhalgh *et al.* 1986, Greenhalgh *et al.* 1994, Belperio 1995, Hillis & Reynolds 2000, 2003). The local stress vectors are mostly oblique to the strike of steeply dipping reverse faults (Greenhalgh *et al.* 1986, Greenhalgh *et al.* 1994, Belperio 1995), making the Cenozoic evolution of the region, far more complex than achieved by simple E-W compressional uplift. The oblique movements on normal and reverse faults in the Sellicks region align with the above interpretation of oblique-sinistral strike-slip movements (Section 3.5).

Sub-horizontal shearing on fault planes such as the, Wilkatana, Eden-Burnside and Willunga faults may have resulted from complex stress orientations that produce lateral movements. Potential strike-slip and thrust movements on the northern Flinders Ranges have been related to stress vectors varying between ~020°-120° (Hillis *et al.* 1999, Hillis & Reynolds 2000, Hillis & Muller 2003). However, paleostress reconstructions do not show direct relationships to most of the youthful deformational structures, because of the considerable heterogeneity in the post Miocene *in-situ* stress fields in the region (Dickinson *et al.* 2001, Dickinson *et al.* 2002, Sandiford 2003a). Nevertheless, palaeostress orientations derived from some of the Pliocene and Quaternary range-bounding reverse faults (Quigley *et al.* 2006) indicate the presence of a compressional tectonic regime, at least for the past 5 Ma (Sandiford 2003a, Quigley *et al.* 2006).

Deformation in parts of the Australian continent is considered to be similar to the folding and faulting observed in the Indian oceanic crust (Krishna *et al.* 2001), characterised by long wavelength (~200 km), low-amplitude (200-500 m) lithospheric folding (Sandiford & Quigley 2009a, Sandiford *et al.* 2009b) and widely distributed reverse faulting (Celerier *et al.* 2005). In general, this active deformation is described as approximately E-W, squeezing between the Indian-Himalayas and the New Zealand-Alps, with increasing resistance from the northern subduction boundaries. Ongoing Australian intraplate deformation is primarily triggered by plate boundary stress variations around 8-6 Ma (Hill 1995, Hillis & Reynolds 2000, Hillis *et al.* 2008), where increasing stress exceeding the threshold limits resulted in geological deformations (Paul 1998).

Considering the obvious variations in strike directions and the inhomogeneous continental landmass, it is unacceptable to agree that the neotectonic faults in the Mount Lofty and Flinders Ranges are simply a result of E-W compression. Composition and rheological discrepancies in the subsurface may also causing southern South Australia to undergo compression along axes of variable orientations (Greenhalgh & Singh 1988). Furthermore, structural geometries are inclined to develop along inherited discontinuities, as the stresses are likely to concentrate along pre-existing weak zones (Ruedemann 1922, Twidale & Bourne 2004). The strike-slip

focal plane solutions and inconsistency due to epicentres deviating from known dip-slip faults, are likely to be a result of neotectonic structural complexities. Hence, a seismicity-based approach to characterize the fault movements is of limited scope.

The basement of the Flinders Ranges and sections of the Mount Lofty Ranges overlap with an elevated heat anomaly resulted from mantle heat flow (Sandiford 1989) and high concentrations of heat producing elements (Sandiford *et al.* 1998b, Neumann *et al.* 2000, Celerier *et al.* 2005, Hillis *et al.* 2008). The localized distribution of strain may have influenced the dominant brittle deformation in the upper crust (Fleming & Offler 1968) due to the thermally weakened lithosphere in this region (Cull 1982, Sandiford *et al.* 1998b). The deformation of a region overlapping an elevated heat anomaly (Cull 1982, Paul 1998, McLaren *et al.* 2003), would be mutually facilitated by subsurface thermal and mechanical properties (Sandiford 1989, McLaren & Sandiford 2001, Holdsworth *et al.* 2001a, Holdsworth *et al.* 2001b), as well as structural discontinuities in order to replicate tectonic events (Roberts & Houseman 2001). However, considering the tectonic quiescence between the Delamerian and neotectonic events, given that the heat producing granite locations remain unchanged, the influence of heat on deformation becomes inconsistent and limited (Neumann *et al.* 2000, Celerier *et al.* 2005).

7.7 A strike-slip perspective of the Mount Lofty and Flinders Ranges

The faulting pattern in the Mount Lofty and Flinders Ranges is complex and obviously inconsistent with interpretations solely in terms of reverse faulting due to E-W compression. The existing hypotheses do not satisfactorily explain the faulting mechanisms that have contributed to the present topography and seismicity of the region. Evidence of normal and reverse faulting has been well established and indications of oblique-slip are emerging along the sections of the Willunga, Wilkatana, and Eden-Burnside faults. Hence, it is essential to evaluate the nature of faulting by evaluating the influence of lateral slip components in the region. The following sections assess the applicability of a strike-slip tectonic model in explanation of deformation in the Mount Lofty and Flinders Ranges.

7.7.1 Strike-slip characteristics

Strike-slip faults can be active throughout geologic time, extending deeply into the crust, at various scales (Kennedy 1946, Reading 1980, Sylvester 1988, Bluck 1995). Ductile shear zones represent strike-slip faults at depth (Burg 2011). Characteristic folding and faulting patterns are observed on strike-slip systems as the segments converge or diverge (Harland 1971) laterally along the strike, producing local zones of reverse or normal faulting (Reading 1980, Burg 2011). Converging and diverging zones are emphasised by curvature, braiding, side stepping and rotation of fault blocks (Christie-Blick & Biddle 1985, Buckman 2000). Hence, it is important to comprehensively understand the local scale fault movements, in order to determine the regional scale strike-slip deformation patterns.

Well known strike-slip systems such as the San Andreas (Crowell 1974, Blake *et al.* 1978, Sieh 1978a, Howell 1984), the Alpine Fault System (Lewis 1980), the Philippine Fault, the Anatolian Fault (Allen 1982, Honkura *et al.* 2000, Papazachos *et al.* 2002), the Mongolian Altai (Cunningham *et al.* 2003, Cunningham 2007), the Gobi-Altay (Vassallo *et al.* 2007), the Tien Shan Fault Zone (Buslov *et al.* 2003, Cunningham 2007), the Mid-Atlantic Ridge (Mohriak & Rosendahl 2003) and the Dead Sea Fault System (Manspeizer 1985), provide information towards understanding and identifying strike-slip systems and corresponding seismic risks. Of these, the Tien Shan provides the best example of rapid continental interior deformation, and the Mongolian Altai provides information on late Cenozoic intraplate strike-slip movements in response to the Indo-Eurasian plate collision.

Near surface, low angle oblique thrusts are common features along many converging strike-slip zones (Sylvester 1988). Lateral movements on converging systems or restraining bends due to transpression, fabricate local shortening and surface uplift. These convex shaped pop-up geometries (Figures 3.22, 4.18 and 4.25) (positive flower structures) largely contain networks of reverse faults on both sides, created by upward splaying subsidiary faults. These fault networks display gentle dips closer to the surface and merge into steep faults at depth (Wilcox *et al.* 1973, Harding 1974, 1985, Sylvester 1988). Conversely, areas of transtension create sedimentary basins,

due to subsidence along normal faults and resemble negative flower structures (Harding 1985, Harding *et al.* 1985).

The displacement may be distributed into several branches on a strike-slip fault network, when it terminates at a zone of brittle deformation (Wesnousky & Jones 1994). In contrast, a ductile zone produces *en-echelon* structures, made of subsidiary faults, which curve away from the main fault plane. Sometimes, they form an imbricate fan of faults (horsetail splay structures), due to compression on thrust faults and folds (Harland 1971, Harding 1985). Crustal shortening between parallel strike-slip segments or bends along the strike of a fault generate restraining-bends (Crowell 1974, Christie-Blick & Biddle 1985, Mann *et al.* 2007a). Restraining bends create complex structures with dominant oblique deformations and commonly expose basement rocks due to extensive thrusting followed by erosion (Cunningham 2007). In general, restraining-bends and step-overs are controlled by pre-existing structures (Storti *et al.* 2003).

Subsidiary fractures (riedel shears) in a strike-slip system propagate short distances from the main fault (Wilcox *et al.* 1973, Bartlett *et al.* 1981, Richard *et al.* 1995, Burg 2011), forming an *en echelon* or overstepping array of faults (step-overs) (Aydin & Nur 1985, Burg 2011). Step-overs commonly observed within the shallow depth sedimentary sequences, generate transpressional or transtensional deformation patterns (Woodcock & Fischer 1986, Sylvester 1988, Storti *et al.* 2003). A transfer fault, striking parallel to the regional trend of compression or extension (Nemser & Cowan 2009), may divert the displacement from one fault segment to another. These strike-slip duplexes are created by isolated regions bounded by parallel strike-slip fault segments, and show oblique faulting under compression or extension (Woodcock & Fischer 1986). Strike-slip duplexes may display both sinistral and dextral movements, depending on the stress variations.

Analogue experiments based on clay and sand models (Wilcox *et al.* 1973, Casas *et al.* 2001) reveal consistent patterns in strike-slip faulting and progressive development of offsets on distributed segments at different times. Hence, within a particular strike-slip network, certain sections of a fault could be active, while others

remain quiescent for extensive periods. The heterogeneous nature of rock properties and stress distributions mainly account for such behaviours leading to complex structural and seismic patterns along faults.

7.7.2 Accommodating stress and strain (The strain-ellipse model)

Strike-slip zones largely accommodate horizontal shearing within the crust. Their characteristic behaviour depends on their orientation, stress components, and the capacity of the subsurface to withstand seismic strain (Wallace 1970, Allen *et al.* 2005). The recognition of fault and fold axes orientations during instantaneous shearing is important for estimating the nature of deformation. The strain-ellipse model best explains the structural features of shear zones and their associated strike-slip fault systems (Wilcox *et al.* 1973, Christie-Blick & Biddle 1985, Harding 1985).

Structural patterns generated by a left-lateral strike-slip zone (Figure 7.3) can be presented as a sinistral shear-couple on a strain-ellipse (Reading 1980, Biddle & Christie-Blick 1985, Harding 1985). Conjugate sets of strike-slip faults occur oblique to the main fault as synthetic-antithetic shears. In reality, a progressive general shear is likely to result in the folding and rotation of faults soon after their initiation. The identification of the local compression axis (C), the Extension axis (E), Normal Faults (N), Thrust Faults (T), Strike-Slip Faults (S), and the Fold Axis is important in establishing the character of larger scale movements in a fault zone (Bartlett *et al.* 1981, Christie-Blick & Biddle 1985). Alternatively, analysing the orientations of structural features with respect to the strain ellipse model can determine potential tectonic movements for a region.

Establishment of structural discontinuities mainly depends on stress orientations, strain accommodation and the subsurface material as well as the intensity of convergence or divergence. Synchronous movements within subsidiary fractures accommodate stress/strain in a fault zone (Ghosh & Chattopadhyay 2008), although, in reality fault segments activate sequentially over a wide range of the geologic time (Sylvester 1988). Steeply dipping faults parallel or oblique to the primary direction of crustal extension/compression, act as stress/strain transfer zones (Gibbs 1990).

The structural design of crustal segmentation consists of stress/strain accommodation and stress/strain transfer zones (Faulds & Varga 1998), while the curvilinear shapes of the stress/strain accommodation zones is formed by block movements, which generally absorb the lateral movements along faults (Faulds & Varga 1998). Transfer zones are similar to oceanic transform faults, as they accommodate strike-slip motion without a physical separation (Wernicke 1992, Faulds & Varga 1998).

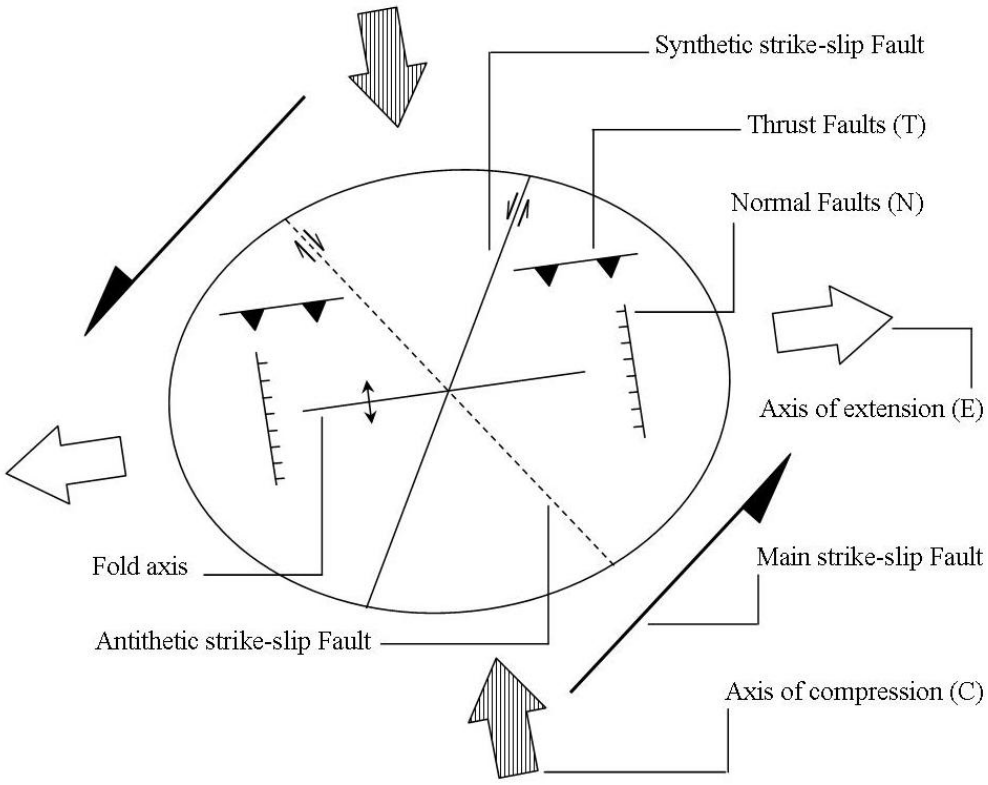

Figure 7.3 *Structural patterns of a sinistral strike-slip zone (Source: Harding 1974, Reading 1980, Biddle & Christie-Blick 1985)*

7.7.3 Lateral shearing in southern South Australia

There are proposals that emphasise shear movements in southern South Australia (Cleary & Simpson 1971, Stewart & Mount 1972, Crawford & Campbell 1973, Harrington *et al.* 1973, Coward 1976, Clarke & Powell 1989). Most of them relate to Palaeozoic times and are not comprehensively associated with supportive field evidence. Ambiguity on the specific timing of the movements and uncertainty of their present status does not provide sufficient information for their influence on

neotectonic movements. However, middle-Eocene to middle-Miocene (~43-14 Ma) activity on the ~NNW-SSE oriented strain transfer zone (Tertiary Transfer Zone – TTZ) proposed by Tokarev (2005), can be considered as the most reliable source of information at present. Accordingly, early-Tertiary crustal segmentation along the strain transfer zone (Figure 2.8) is responsible for the normal faulting and subsequent basin formation in southern South Australia.

Cenozoic dextral movements on the eastern Antarctic Plate (south of Tasmania) is a result of an active fracture zone in the Southern Ocean, transmitting lateral shear through the oceanic and continental crusts (Storti *et al.* 2003). An identical phenomenon could also operate possibly in the opposite direction, on the southern boundary of the Australian and Antarctic plates. There are records of sinistral strike-slip movements associated with the Tasman Fracture Zone, resulting from an irregular boundary between Australia and Antarctica (Moore *et al.* 2000). Oblique-slip movements between Tasmania and the Australian mainland have operated as left lateral movements (Moore *et al.* 2000, Norvick & Smith 2001, Miller *et al.* 2002). A possible relationship between the Tertiary Transfer Zone and the Tasmanian Fracture System (Tokarev 2005) suggests the occurrence of plate boundary influenced left-lateral intraplate neotectonic movements.

The strike of the Tertiary Transfer Zone overlaps with a Palaeozoic dextral shear zone (Stewart & Mount 1972), a sinistral mega-shear zone (Coward 1976) and Jurrassic-Cretaceous crustal extensions (Willcox & Stagg 1990). It is parallel to NW striking transform faults, which have undergone extensive intra-continental crustal extensions during the evolution of the southern Australian continental margin (Stagg *et al.* 1990, Willcox & Stagg 1990), and aligns obliquely to the present Mount Lofty Ranges. The Tertiary Transfer Zone also coincides with a hypothetical sub-plate boundary across South Australia (Cleary & Simpson 1971) and has been derived from limited records of seismic observations.

NW-SE directed block movements along shear zones with low angle dècollements were reported during the Delamerian structural evolution of southern South Australia (Preiss 1987, Jenkins & Sandiford 1992, Flöttmann *et al.* 1994, Yassaghi *et al.*

2004). The neotectonic structures are recognised as being different and independent from the low-angle thrusts and basement dècollements of Delamerian age, due to the diverse environments that they have created. However, the present local stress regimes of the Mount Lofty and Flinders Ranges are almost parallel to the ~NW oriented palaeo-shear zones; a potential reactivation along the pre-existing discontinuities may be inevitable, considering that the Pleistocene compressional reactivation of the middle-Eocene to middle-Miocene normal faults (Tokarev 2005) originated from a strain transfer zone background.

Transform faults are often associated with oceanic crusts, in addition to their existence as continental interior strain transfer zones (Wilson 1965). Strain transfer zones represent crustal weaknesses, which can be activated intermittently, in line with the stress variations. These steeply dipping transform faults may be inactive for prolonged periods of time, and may be triggered by tectonic plate velocity changes, propagating into new discontinuities (Furlong *et al.* 1989). Post-Delamerian to middle-Eocene tectonic serenity in the southern South Australia may be explained in a similar way, as the crustal segmentation associated with the Tertiary Transfer Zone was related to a major stress reorganization on the Indo-Australian tectonic plate.

In conclusion, primary lateral shearing in the southern South Australia may exist as a result of the obliqueness between the local maximum horizontal stress vectors and the strike of the faults (Section 7.4). Additionally, the lateral shearing may be enhanced by the possible reverse-reactivations along pre-existing structures such as strain transfer zones, which are also mostly oblique to the strike of the neotectonic faults. Sub-horizontal slickenside observations on some of the active fault contacts within the Mount Lofty and Flinders Ranges provide field evidence for the extent of lateral movements.

7.7.4 Plausible driving mechanisms for lateral movements

Plate boundary interactions are responsible for most global mountain building events. The relationships between plate tectonics and intraplate tectonics are complex (Molnar 1988, Dyksterhuis & Muller 2008) and the factors influencing intraplate deformations are not well understood (McLaren & Sandiford 2001). The seismicity

and geomorphic expression of the Mount Lofty and Flinders Ranges are significant given their intraplate setting well away from the plate boundaries. The driving mechanisms of the sigmoidal-shaped Mount Lofty and Flinders Ranges, located in the relatively stable Australian continent, remains enigmatic. A single tectonic process could not have created the current topographical curves of the Mount Lofty and Flinders Ranges (Marshak & Flöttmann 1996), and a simple and unique process could not have controlled the driving mechanisms of this intraplate mountain building.

Zones of strain transfer and lateral movements are generally inherited from oceanic transform faults generated by differential spreading rates at mid-oceanic ridges (Wilson 1965, Ranalli 1974, Horne 1975, Smith 1976). There are also strike-slip faults within continental interiors that do not directly relate to plate boundaries (Reading 1980). These include, the Great Glen Fault, the Highland Boundary Fault and the Southern Uplands Fault in Scotland, the North Pyrenean Fault Zone, the Insubric Line of the Alps and the Cabot Fault of Newfoundland (Hyde *et al.* 1988). Continental interior faults largely behave under the influence of current regional stress regimes and a particular fault may variably act normally, reversely or with strike-slip movements at different stages over geologic time.

A renewed phase of structural discontinuities in southern South Australia obviously originated during the Australian-Antarctic separation and continues to display episodic movements. The Tertiary Transfer Zone connects with an extensive Tasmanian Fracture System south of Australia, and is considered as a spatially and chronologically dependable link between intraplate neotectonics and the plate boundary interactions (Tokarev 2005). However, a ~NW trending hypothetical discontinuity better explains the structural differences in the region by dividing the continental margin into two segments (Tokarev 2005), similar to the sub-plate model of Cleary and Simpson (1971). Moreover, the South Australian Flinders Seismic Zone aligns directly north of a complex shaped southern boundary of the Indo-Australian Plate and a number of prominent fracture zones, possibly acting as transform faults, with differential spreading rates (Figure 7.4).

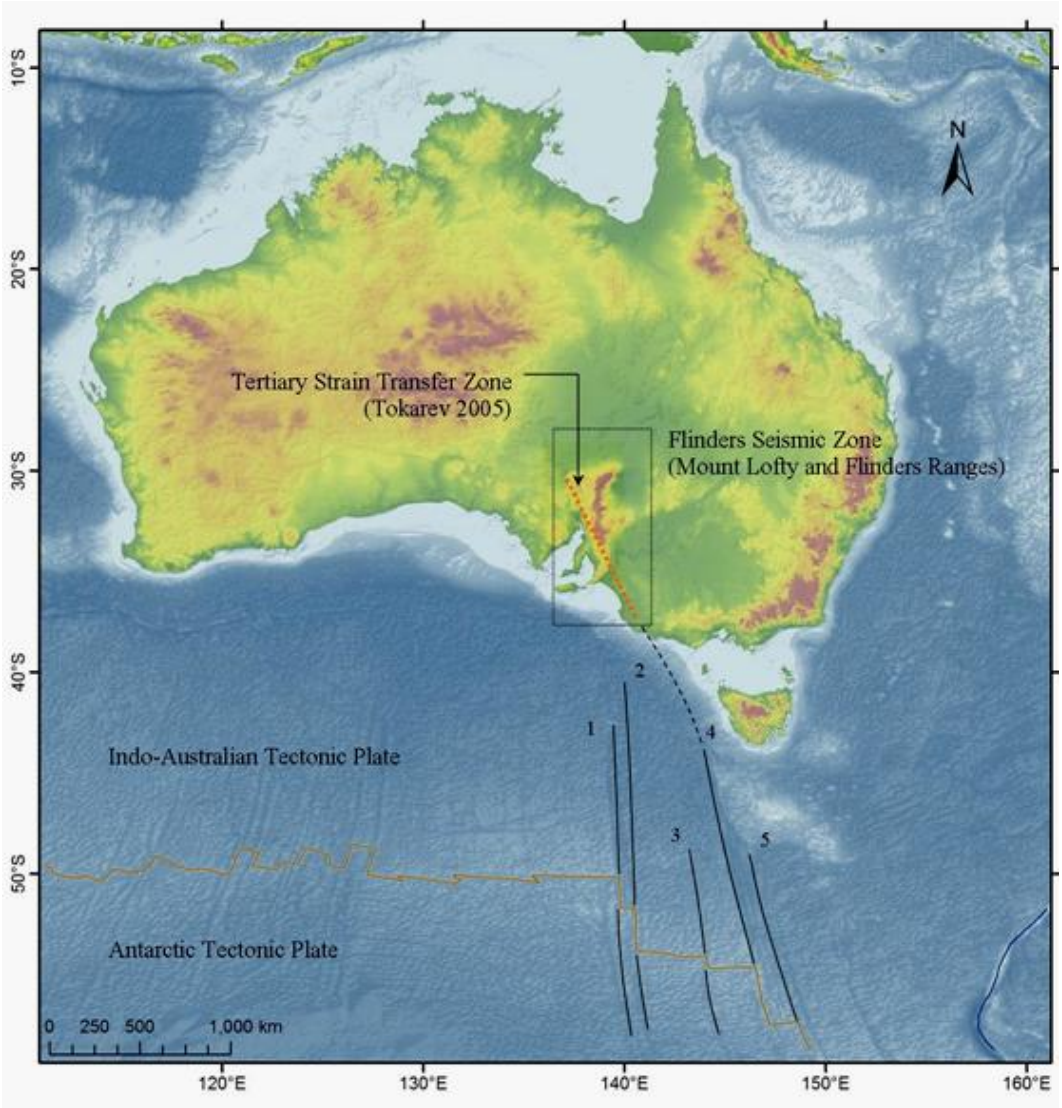

Figure 7.4 *Fracture zones at the Australian-Antarctic plate boundary (1-George V Fracture Zone, 2-Kangaroo Fracture Zone, 3-Carey Fracture Zone, 4-Tasman Fracture Zone (Muller et al. 2000), 5-Balleny Fracture Zone)*

Differential seafloor spreading in diverging plate boundaries creates transform faults (Smith 1976) that lead to rare intraplate strike-slip zones (Storti *et al.* 2003). These oceanic transform faults, showing considerable movements at the ridge segment (Ranalli 1974), become tectonically quiescent upon reaching the plate interior, and are known as oceanic fracture zones, (Storti *et al.* 2003). Aseismic movements along some of the oceanic transform faults are produced by extremely slow slip rates (Okal & Stewart 1982, Peng & Gomberg 2010). Stress induced movements along oceanic fractures could impinge onto comparatively weaker continental interiors, creating localised deformations (Braun & Shaw 2001). Thermally weakened southern South

Australian crust (McLaren *et al.* 2003) would have provided the ideal environment for such localized deformations.

Continental extension of the southern Australian margin largely took a N-S direction (Miller et al 2002) and the northward acceleration of the Australian plate and the rate of southern seafloor spreading, increased from 0.8 to 3.0 cm/yr (Cooper 1985, Royer & Rollet 1997) during ~43-25 Ma (Dalrymple & Clague 1976, Veevers 2000, Muller *et al.* 2000a). Of the total spreading between Australia and Antarctica, 88% occurred in the past 45 Ma compared with only 12% during the period 96-45 Ma (Veevers 2000). Amalgamation of the Australian-Indian plates (Aitchison *et al.* 2007), collision with the Eurasian plate (Liu *et al.* 1983, Veevers 2000) and initial subduction along the Papua-New Guinea margin (Pigram & Symonds 1991, Charlton 2000), could have also occurred concurrently during the middle-late Eocene times. Considerable stress reorganization and a new tectonic pulse on the Australian plate interior may be anticipated, as a result of intraplate stress field changes affected by plate boundary forces.

Plate motion since ~43 Ma is considered to be mid-oceanic ridge dominated (Le Pichon 1968), where the influence of slab-pull forces due to subduction is poorly expressed within the intraplate setting (Sandiford *et al.* 2005). Patterns and orientations of σH^{max} across the Australian continent reflect a balance in the plate driving forces, except for the resistance imposed by the Himalayan, Papua-New Guinea and New Zealand collision boundaries. (Coblentz *et al.* 1995, Coblentz *et al.* 1998, Reynolds 2001, Reynolds *et al.* 2003, Lithgow-Bertelloni & Guynn 2004, Sandiford *et al.* 2004). The consequent deformations were considered as extensional, with crustal segmentation along normal faults accommodating sediment deposition (Tokarev 2005), and overlapping with higher heat flows of southern South Australia (Dyksterhuis & Muller 2008). The sedimentation terminates ~14 Ma in the St.Vincent and Murray basins (Brown & Stephenson 1991), indicating possible changes in tectonic deformations.

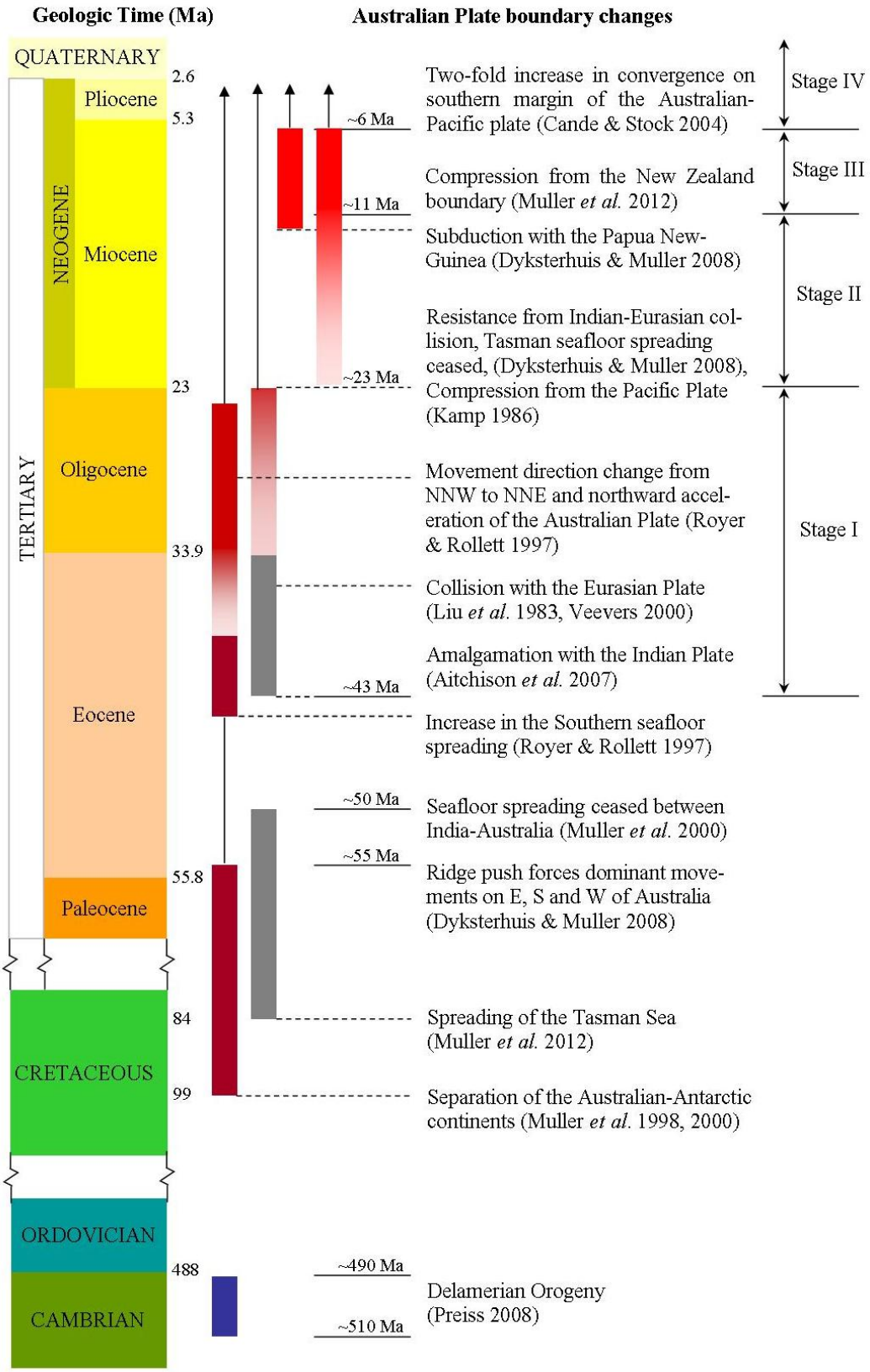

Figure 7.5 *A summary of the major changes in Australian Plate boundaries*

The Indo-Australian Plate began its collision from the east with the Pacific Plate ~23 Ma (Kemp 1986) ago, and from north with Papua New-Guinea at almost the same time (Hall 2001). Increased resistance on the Indo-Australian Plate from the Indian direction may have occurred between Oligocene-Miocene times due to interactions with the Eurasian Plate. Ridge-push forces from east of Australia ceased at ~23 Ma as a result of termination of Tasman Seafloor spreading. The above changes were associated with plate interior stress reorganization at this stage and the Flinders Ranges were aligned with NW-SE directed stress regimes for the period of ~25-11 Ma (Dyksterhuis & Muller 2008). An increase, a decrease, or reversing of the existing strike-slip movements are expected as intraplate transform faults are capable of changing direction with time, in sympathy with plate boundary interactions and the rates of movements. A summary of the major changes associated with the Australian Plate boundaries are given in Figure 7.5.

Absolute subduction along the Papua New Guinea margin occurred ~12 Ma (Hall 2001, Dyksterhuis & Muller 2008) and additional slab-pull forces from the Papua New Guinea region influenced Australian Plate movements that earlier were dominated by ridge-push forces. The coupling between the plates increased during ~10-5 Ma (Sandiford *et al.* 2004), ~11-6 Ma (Dyksterhuis & Muller 2008), establishing new stress regimes on the continental interior of Australia. Compressive forces from the E of the Australian Plate during ~13-7 Ma with the Pacific Plate interactions were also responsible for stress reorganizations (Dyksterhuis & Muller 2008). Rejuvenated ridge-push and slab-pull forces, in-conjunction with compression from E, would have caused a reverse reactivation on existing faults and a new phase of localized strike-slip deformations.

A two-fold increase in convergence along SE sections of the Australian-Pacific boundary during ~6 Ma (Cande & Stock 2004, Müller *et al.* 2012), established ~WNW-ESE oriented horizontal compressive stress regimes on the Australian continent, while lifting the Southern Alps in New Zealand (Dickinson *et al.* 2001, Dickinson *et al.* 2002, Sandiford 2003a, Sandiford *et al.* 2004). The imposed oblique component of stress during the terminal Miocene (~6 Ma) is considered to be active at present, generating complex maximum horizontal stress vectors on the Indo-

Australian plate. As a result, the plate movements previously dominated by ridge-push slab-pull forces and eastward compression, was subjected to an additional ~ESE compression with a change in relative plate velocities. Largely N-S oriented oceanic fracture zones and southern South Australian discontinuities may have accommodated the compressional reorganization of the cumulative oblique-stresses, possibly with a new episode of deformation. Increased movements along the southern fracture zones may have generated transpressional movements on existing faults, as evident by some of the sub-horizontal slickensides. In addition to the readjustments of existing faults, a new regime of oblique-faults would have developed, to accommodate most of the SE compressive forces imposed on the thermally weakened southern South Australian crust (Dyksterhuis & Muller 2008). Sinistral oblique-reverse movements displayed by some of the neotectonic faults in Mount Lofty and Flinders Ranges could be considered to be the combined effect of transpressional and compressional movements. Relatively rich record of neotectonic activity along the Paralana Fault (Sandiford & McLaren 2002) and oblique-sinistral slip on the Wilkatana, Eden-Burnside and Willunga faults confirm the above activity in this region.

7.8 A revised tectonic model

Most of the geomorphic features within the Mount Lofty and Flinders Ranges and their surrounding basins can best explained within the framework of transpression rather than compression. They resemble the characteristics of well documented strike-slip systems (Christie-Blick & Biddle 1985, Mann *et al.* 1985, Wesnousky & Jones 1994, Lopes Cardozo *et al.* 2002, Cunningham 2007, Cunningham & Mann 2007, Vassallo *et al.* 2007).

A strike-slip tectonic model is proposed (Figure 7.6), to better accommodate faulting characteristics reflected by the regional seismicity. The proposed tectonic model displays sinistral strike-slip movements for its ongoing transpressional deformation. It is identical to the local tectonic model proposed for ongoing deformation in the Sellicks region (Section3.5), and an expansion of the same is presented, within a broader view of the Mount Lofty and Flinders faults. The relationships between

topography, seismicity, local stress regimes and the active faults in the Mount Lofty and Flinders Ranges can be better explained through distributed sinistral strain ellipses.

The timing of major deformational episodes in southern South Australia is reviewed. Accordingly, the recent tectonic evolution of southern South Australia can be described as a four-stage development with respect to changes at the plate boundaries. An amendment is proposed for the South Australian Sprigg's Orogeny, incorporating the two-stage (Fenner 1930, Dyksterhuis & Muller 2008), three-stage (Sprigg 1946, Tokarev 2005) tectonic models and Australian Plate boundary interactions. The main stages of tectonic developments in southern South Australia are summarised in Table 7.1.

Stage	Timing (Ma)	Dominant mode of deformation	Description
I	~43-23	Extension	extensional strike-slip movements due to ridge-push forces
II	~23-11	Transition	Increase, decrease or reversing of strike-slip movements due to additional slab-pull forces
III	~11-6	Compression	Reverse reactivation of faults due to compression from E
IV	Since ~6	Transpression	Transpressional strike-slip movements due to the oblique compression from ESE

Table 7.1 *A Summary of the tectonic developments in southern South Australia since ~43 Ma with respect to the plate boundary interactions*

Based on the proposed tectonic model, two stages during the Sprigg's Orogeny can be identified. The Sprigg's Orogeny, which begins in middle Miocene times consists of a compressional stage (~11-6 Ma) and a transpressional stage (since ~6 Ma). Most of the uplift of the Mount Lofty and Flinders Ranges is considered to have been created by transpressional and compressional forces, with the present movements being dominated by oblique-slip fault movements. Conversely, the depressions are regarded as being created by extensional lateral slip during middle Eocene to late Oliocene times. Lake Eyre just beyond the northern tip of the Flinders Ranges could

have developed at the termination of a sinistral strike-slip zone. From a regional perspective, Kangaroo Island, Fleurieu Peninsula, Yorke Peninsula and possibly the south-eastern border of Eyre Peninsula may represent restraining bends and consequent uplift, possibly due to step-over faults of a major strike-slip fault zone.

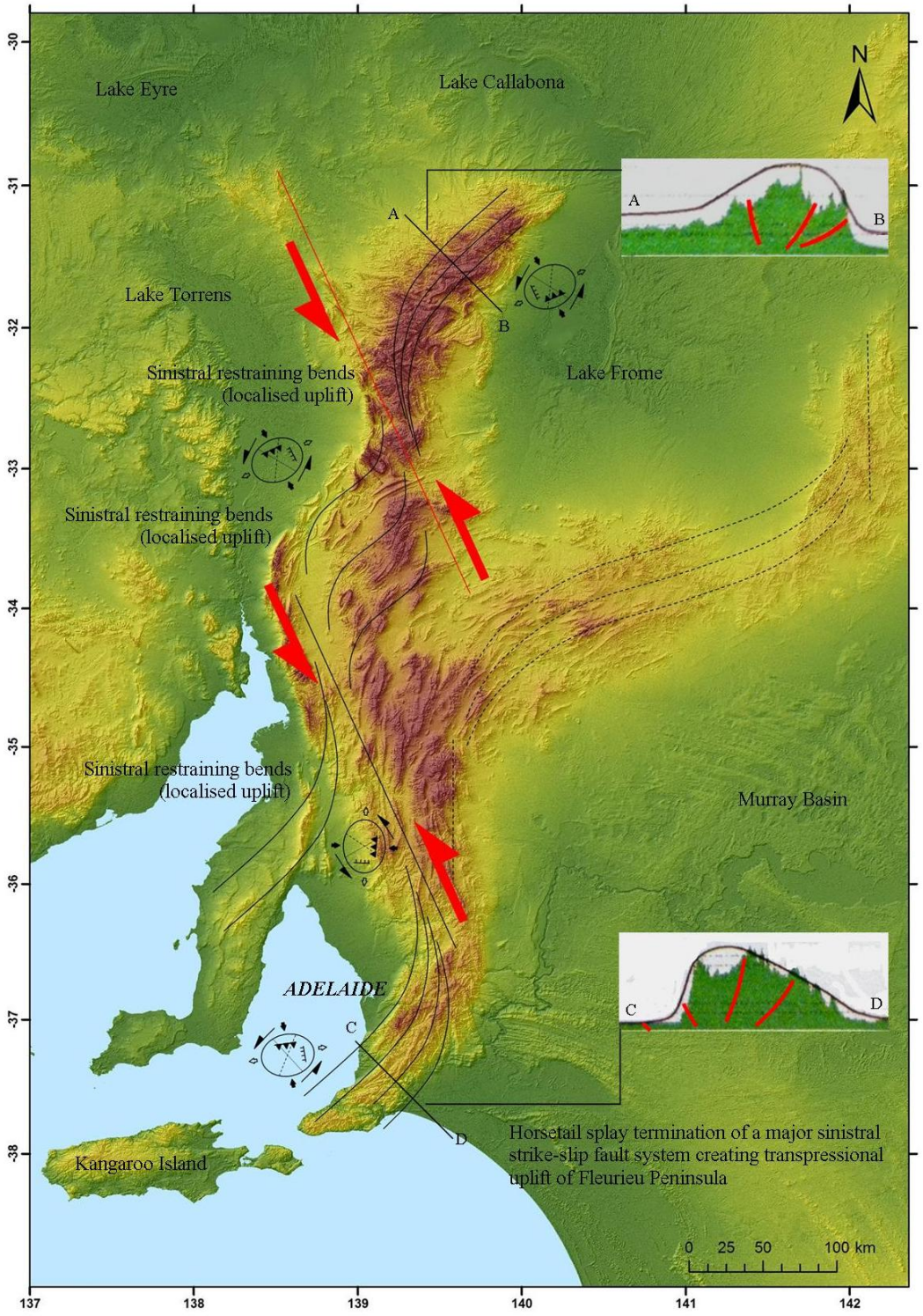

Figure 7.6 *A revised tectonic model for the deformations in the Mount Lofty and Flinders Ranges*

7.8.1 Earthquake potential

The faults have produced only a handful of large earthquakes in South Australia, for the period that seismic records are available. A map generated with magnitude 5 and above earthquakes of South Australia since 1887 (Figure 7.7) reveals a NNW-SSE trend for the events above magnitude 6 (Appendix IV). This parallels the Tertiary Transfer Zone and aligns with the southern oceanic Tasman Fracture System. However, the number and spatial distribution of the monitoring stations and the methods of earthquake magnitude calculations affect the reliability and accuracy of the magnitudes and locations of these events. Nonetheless, the absence of fault scarps associated with most of these events (except in Marryat Creek magnitude 6.0 and 5.6 events in 1986) suggests that the nature of faulting should not to be limited to dip-slip movements.

Estimates of potential earthquake magnitudes for the region range from 5.8 to 7.2, based on the rupture length, rupture depth and single-event displacements (Clark & McCue 2003, Quigley et al 2006). The calculated earthquake magnitudes can have a high degree of uncertainty and may not provide realistic estimates due to lack of understanding of the nature of faulting and associated driving mechanisms. Nevertheless, stratigraphic offsets and rugged topography with abundant scarps in the Mount Lofty and Flinders Ranges reflect the extent of fault activity that has obviously produced large earthquakes. As the deformation is ongoing, similar movements can be anticipated in the future.

This study presents a framework that better characterises the nature of faulting and deformational mechanisms currently in operation, in southern South Australia. The proposed sinistral strike-slip behaviour provides a seismic potential assessment that can be noted as follows.

1) The stresses are largely accommodated by *en echelon* faults and extensive fault branching, possibly scaling-down the earthquake magnitudes and fault rupture lengths
2) The region could be subjected to aseismic strike-slip movements, and subsequent oblique-slip movements to produce consistently lower magnitude earthquakes

3) Structurally weakened lithosphere due to pre-existing structures may be absorbing large amounts of stress and successive strike-slip movements, reducing the amount of higher magnitude earthquakes and fault ruptures
4) Strike-slip fault systems act as conduits for magma and hydrothermal fluid flows (Cox & Hart 1986, Storti *et al.* 2003). Hence, a thermally weakened crust could reduce the friction and dampen the seismicity of a region
5) Positive flower structuring reflects that the faults are merging into unidentified major subsurface strike-slip faults, in which case, a thermally weakened crust would promote elastic movements

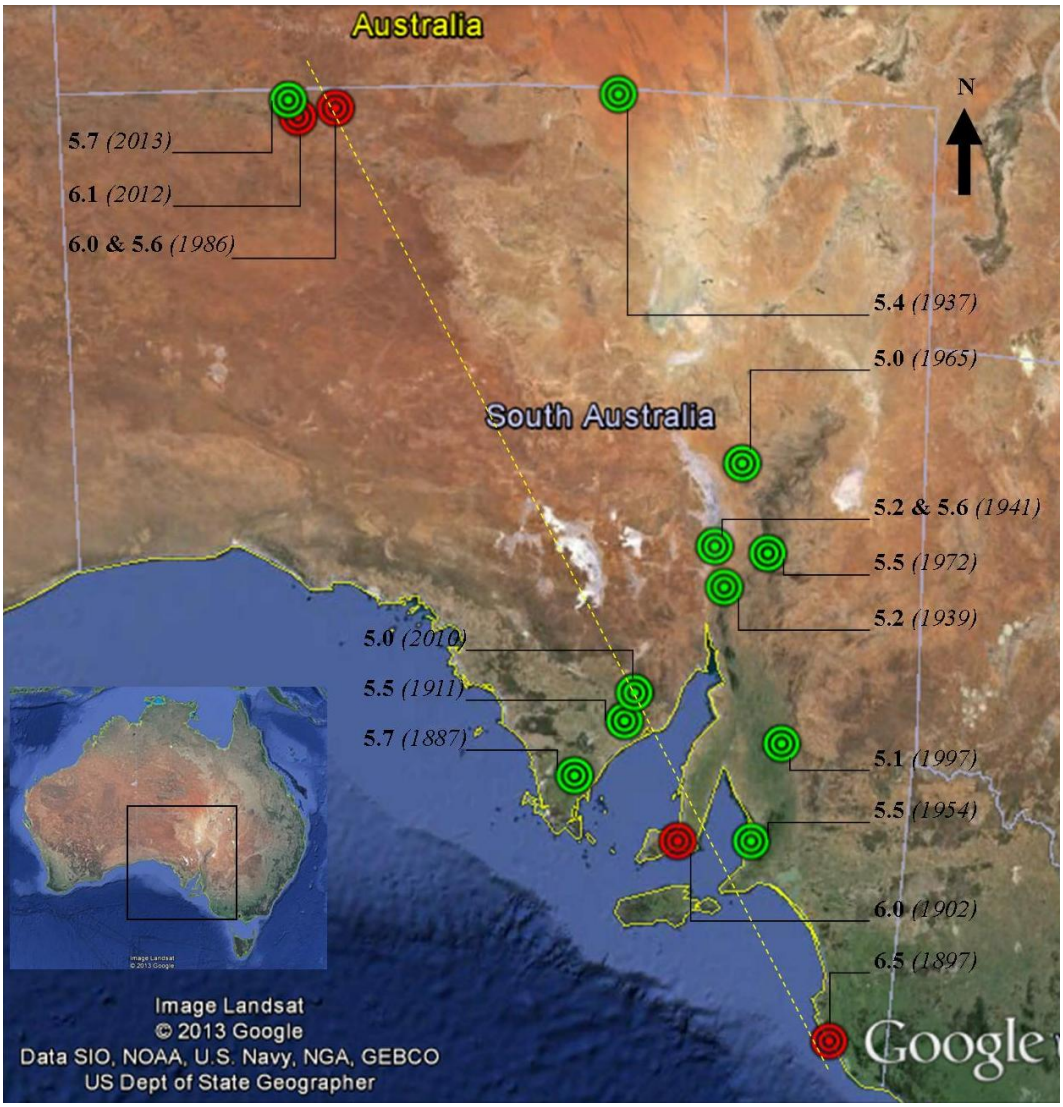

Figure 7.7 *South Australian earthquakes plotted on GoogleEarth (magnitude ≥ 5, from 1887 to 2013) displaying a NNW trend on magnitudes ≥ 6 events (data source: www.ga.gov.au/earthquakes, see also Appendix-IV)*

From a strike-slip perspective a high earthquake potential and low magnitude seismicity can be anticipated in southern South Australia. This is contradictory to the projections involving compressional reverse faulting, but is in sympathy with the present seismic records. However, subsurface inhomogeneities and complexities in the nature of faulting may intermittently produce anomalously higher magnitude events.

7.8.2 Recurrence intervals and slip ratios

Most of the active faults indicate multiple Quaternary movements, based on the evidence of stratigraphic offsets. Optically stimulated luminescence dating results from this study confirm the same, even though they did not establish a comprehensive framework of age estimates. There are no rupture patterns and established recurrence intervals for the faults in the Mount Lofty and Flinders region, and the exact timing of most of the seismic events are ambiguous (Crone *et al.* 1997, Crone *et al.* 2003). However, several estimates on localised fault movements are available (Crone *et al.* 1997, Crone *et al.* 2003, Quigley *et al.* 2006), the accuracy and validity of which are questionable. The mismatch of rupture patterns with respect to compressional reverse uplift may have caused many of the misleading estimates.

The proposed sinistral strike-slip deformation helps to assess the region from a transpressional perspective, and to recognise the deformational fronts as well as the potential rupture zones. Variable slip rates along the strikes and rupturing segments during a particular stress release event need to be investigated to identify localised rupture patterns. Approximate slip components for the Willunga Fault Zone, based on oblique-slip slickenside measurements, has resulted in a vertical to horizontal slip ratio of 5:7 in Sellicks region. Similar lateral movements may have occurred on the other active faults in the Mount Lofty and Flinders Ranges, in view of the similarities in their fault behaviours.

7.8.3 Limitations of neotectonic investigations

Identification of fault kinematics and their relationships to deformational episodes is a complicated process as the region has experienced multiple deformational events. However, the establishment of age constraints is rendered difficult because of the highly weathered, unconsolidated and reworked nature of the sediments. Hence, a degree of error could be present with the slip component and age calculations. The overlap of various deformational phases or remobilization of structures has to be carefully considered to minimize these errors.

The oblique-slip calculations on the Willunga Fault Zone were based on a limited number of slickenside observations. A larger data collection would have improved the accuracy of the calculations and provided more realistic values for regional scale horizontal offsets. Additionally, similar detailed structural data sets and age constraints from each of the active fault zones would have provided much more accurate slip estimates.

Limited seismic records and low levels of current seismic activity, mostly generating large error ellipses, assists minimally for focal plane solutions. Hence, determining rupture patterns, recurrence intervals and slip estimates has limited validity at a regional scale, unless verified for several locations. Identification of the extent of active faults may help to minimize the error associated with seismic and slip rate calculations.

There are elongated topographic features in the Mount Lofty and Flinders region, similar to fault scarps or escarpments on satellite imagery and elevation models. Only a few of those have been confirmed as faults, apart from the well established range-bounding thrust faults on both sides of the ranges. Therefore, little attention has been given to associated aspects of the rate of uplift, such as the magnitude of landscape lowering, isostatic adjustments and topographic variations due to mantle turbulence.

7.9 Discussion

Magnitudes of seismic events, their spatial distributions and topographic features in the Mount Lofty and Flinders Ranges cannot be satisfactorily explained with compressional reverse faulting. Limited knowledge on faulting characteristics complicates the process of determining plausible driving mechanisms for this localised intraplate deformation in southern South Australia. The available hypotheses explaining possible deformation criteria (Fenner 1930, Sprigg 1946, Cleary & Simpson 1971, Tokarev 2005, Dyksterhuis & Muller 2008, Sandiford & Quigley 2009a) do not sufficiently accommodate most of the local features, reflecting the inconsistency of present understanding. This study attempts to harmonize the field observations with hypothetical developments, in order to better explain the seismicity and mountain building in the Flinders Seismic Zone.

Tectonic plates travel great horizontal distances over geologic time (Sylvester 1988). Horizontal stresses that drive the plate movements are responsible for the elastic deformations mostly reflected through lithospheric buckling. Basin formation and mountain building events commonly reflect the topographic variations resulting from deformation episodes (Veevers 1980). Variations in plate velocity and stress may cause the episodic tectonic plate movements (Sylvester 1988). The complex distribution of local stresses interlinked with networks of shear zones and faults may result in distorted seismic patterns (Storti *et al.* 2003). Numerical modelling of stress and seismicity within the southern South Australia has revealed the influence of plate boundary forces (Cloetingh & Wortel 1985, Coblentz *et al.* 1995). Therefore, lithospheric buckling may also have contributed to the intraplate deformations in southern South Australia (Stephenson & Lambeck 1985, Sandiford & Quigley 2009a).

The behaviour of plate interiors may be largely influenced by crustal heterogeneities, intraplate stresses, local geology, tectonic history and plate velocity. The intraplate stress is mainly derived from plate boundary interactions (Hillis *et al.* 2008). Seismological and geodetic studies reveal that horizontal deformations in a plate interior is largely accommodated by strike-slip faulting (Molnar & Tapponnier 1975, Storti *et al.* 2003). Horizontal movements along faults occur over prolonged periods

(Sylvester 1988) causing long-term lithospheric inhomogeneities, that may reworked in several episodes over geologic time (Storti *et al.* 2003). Stress measurements indicate that Australia is dominated with regions of reverse and strike-slip faulting (Reynolds 2001). Similar observations are also reported from the focal plane solutions (Greenhalgh *et al.* 1986, Clark & Leonard 2003, Hillis *et al.* 2008).

The patterns of deformation associated with the Willunga Fault at Sellicks Beach reveal that local oblique sinistral fault movements can be better explained through transpression rather than compression. Subsequent orientations of normal, reverse and potential strike-slip faults coincide with the strain-ellipse model of (Harding 1985), which is generally used to describe strike-slip zones. Fault kinematics and topographic features displaying left-lateral movements at this locality define the region as a sinistral strike-slip zone. Assessing the features on the Eden-Burnside Fault near Vista, Bourman *et al.* (2010a) described deformation with sinistral oblique movements subjected to transpression. Similar investigations on the segments of Wilkatana Fault by Quigley *et al.* (2007a) also revealed oblique-slip movements, which have not yet been assessed from a strike-slip perspective. Sinistral oblique-slip indicators at three different locations on the western boundary of Mount Lofty and Flinders Ranges, shallow subsurface fault characteristics revealed by the trenches and ground penetrating radar studies, provide evidence for transpressional behaviour, in lieu of simple compressional uplift for the region. Hence, investigation of the features in the Flinders Seismic Zone from a sinistral strike-slip perspective could provide further insights into the southern South Australian intraplate deformation.

The major drawback of a strike-slip interpretation for the Mount Lofty and Flinders region is the absence of direct topographic evidence for lateral movements, except for the sinistral offsets reported on the Permian Valley deposits (Stackler 1963) of the south-eastern Mount Lofty Ranges. The northward migration of the Onkaparinga River mouth on the western side of the southern Mount Lofty Ranges (Benson 1911), may also have been influenced by the left-lateral movements. However, there are instances where, *en echelon* faults accommodate large amounts of localised crustal shear, without demonstrating horizontal movements (Wesnousky 1986, 1988). In addition to the series of *en echelon* faults, sometimes a substantial amount of crustal

rotation can also take place. Curvilinear range bounding faults displaying oblique-slip movements in the Mount Lofty and Flinders Ranges may be regions of transpression, whereas, subsequent *en echelon* fault splays may have resulted from lateral movements, even though they are not accompanied with clear surface evidence.

Identifying plausible driving mechanisms is a complicated endeavour, although, there is convincing topographic and structural evidence of possible strike-slip movements in the Mount Lofty and Flinders Ranges. However, the forces imposed on the Australian continent primarily includes, slab-pull along the northern subduction zone with Papua New-Guinea; ride-push from the southern mid-oceanic ridge along the Australian-Antarctic boundary; oblique compression from the colliding Australian-Pacific plates and resistance from the Indian-Eurasian plate interactions. Inhomogeneous subsurface material, buoyancy forces resulting from lithospheric density variations, the asymmetric distribution of gravitational potential and thermally weakened crust could also account for localized deformations. Additionally, southern South Australia has experienced multiple deformational episodes, which could have facilitated neotectonic mountain building since the mid to late Miocene.

The mineralogical alterations due to repeated deformations can produce structurally weak zones as well as much stronger bonds along the discontinuities (Passchier *et al.* 2005). Therefore, the effects of pre-existing structures, especially due to the Delamerian deformations are uncertain. Exhibited orientation disparities between neotectonic and Delamerian structures, as well as fault contacts not showing Delamerian characteristics, leave the issue unresolved. Nevertheless, structural independence or inheritance cannot be estimated from a limited number of shallow subsurface observations, without assessing the deep crustal interactions. Reactivations can take place along the E-W to NE-SW trending deep-seated Delamerian basement structures (Preiss 2008) due to the compressional forces generated from Australian-Pacific plate interactions (Benbow *et al.* 1995a). Provided that the ongoing deformations are influenced by reactivation of older structures, similar behavioural patterns may be expected from the neotectonic faults (Preiss

1993). There are reports of reverse reactivation on middle-Eocene extensional structures during the ongoing phase of deformation (Tokarev 2005).

Older faults and shear zones are vulnerable for reactivation as they accommodate local deformation creating inhomogeneous mechanical properties within the subsurface (Thatcher 1995, Holdsworth *et al.* 1997, Hand & Sandiford 1999, Holdsworth *et al.* 2001a, Storti *et al.* 2003). As the pre-existing structures influence the deformation (Holdsworth *et al.* 2001b), regions having multiple episodes of deformation may produce complex and overlapped structures (Storti *et al.* 2003). Episodic intraplate deformations cause upper mantle rocks to undergo several episodes of reworking (Holdsworth *et al.* 2001a, Storti *et al.* 2003) and repeated reactivation along existing structures, such as deep ductile shear zones and fault systems in the upper crust. The periodic behaviour of orogens is mostly connected with changes in the mode of deformation from compressional to extensional (Lister *et al.* 2001, Miller *et al.* 2002). There are studies on the reactivation of pre-existing strike-slip structures. They display a series of superimposed episodes, such as on the Carajas-Cinzento Fault in Brazil, where its Archaean dextral movement have been followed by subsequent sinistral shearing to form complex deformation patterns (Storti *et al.* 2003). Superimposed episodes of continental reactivation and reworking in the Australian context, were experienced during the Permian (Sandiford & Hand 1998) and Alice Springs (Shaw *et al.* 1992) orogenies in Central Australia (Holdsworth *et al.* 2001a).

Reverse reactivation of ancient structures in southern South Australia (Sprigg 1946) is acceptable from a strike-slip perspective. Identification of two major deformational episodes and plate boundary influenced deformational dynamics indicate prolonged tectonic instability rather than tectonic quiescence on this intraplate setting. The orientation and characteristic discrepancies between discontinuities of different deformational episodes may be due to the variably localised spatial, environmental and temporal stress conditions. The Delamerian structures beneath the neotectonic St. Vincent and western Murray Basins could be satisfactorily explained within an extensional strike-slip setting, but is difficult from a compressional perspective. On the other hand, the inappropriateness of simple compressional uplift for the Mount

Lofty and Flinders Ranges is reflected in the paucity of folding on soft sediments bordering the consolidated Proterozoic basement. However, there is some gentle folding within the unconsolidated sediments, at places such as Sellicks and Tarlee, possibly resulted from transpression.

Approximately NW-SE trending sinistral strike-slip movements inferred by the proposed revised tectonic model, complements the sub-plate model by Cleary & Simpson (1971), the mega-shear couple of Coward (1976) and the Tertiary strain transfer zone of Tokarev (2005). It is also in agreement with the primary orientation of lineaments in Australia (Twidale & Bourne 2004), which can be reactivated with differential movements demonstrating conjugate shear zones. The validity of the Cleary & Simpson (1971) sub-plate model derived from limited seismic evidence (1960-1973) was verified with a comparatively lager seismic data set from 1973 to 2012 for the Australian continent (Figure 2.13). The mega-shear couple and the Tertiary strain transfer zone display good agreement with the seismic records from 1840 to 2009 for the Mount Lofty and Flinders Ranges (Figure 2.3). Accordingly, the Mount Lofty and Flinders Ranges can be confirmed as a continental interior shear zone, which could also be influenced by a dècollement. The orientation of this intraplate shear and its sense of motion have been mostly discussed as NW to W orientations and dextral and sinistral movements (Cleary & Simpson 1971, Stewart 1972, Crawford & Campbell 1973, Harrington *et al.* 1973, Coward 1976, Clarke & Powell 1989).

The Tertiary Transfer Zone confirms the presence of NW-SE directed structural discontinuities, which would have largely deformed under the compressive stress regimes. They overlap with a series of NW-SE oriented sinistral strike-slip faults, which operated during the oblique extension of the southern Australian margin (Willcox & Stagg 1990). The Eden-Burnside, Para and Alma faults terminate at the Tertiary Transfer Zone (Tokarev 2005). Conversely, the faults may have developed from the Tertiary Transfer Zone, reflecting its influence on the structural evolution in the region. Strain transfer zones may contain regions of distributed shear (Axen 1998, Hudson *et al.* 1998), and there is a probability that they behave as strike-slip zones, in addition to transferring strain.

The lack of seismic records along the southern fracture zones is not helpful in establishing the driving mechanisms of the proposed tectonic model. However, aseismic slip largely accepted along several other oceanic fracture systems (Peng & Gomberg 2010), provides a reasonable correlation to this region. Elevated seismicity at the Australian-Antarctic spreading ridge provides additional evidence on inhomogeneous crustal production and associated lateral-slip, which can be transmitted to the continental interiors along fracture zones. The non-rigidity of tectonic plates (Gordon 1998) accommodates differences in spreading rates at mid-oceanic ridges. Horizontal stresses are transmitted over large distances through the mantle as well as lithosphere, and the concentration of stress or decreases in lithospheric strength could result in localised deformations (Braun & Shaw 2001). The Australian continent has a record of plate boundary forces being focused on areas of weak lithosphere, which had resulted from previous deformations (Braun & Shaw 2001). Having a relatively thin crust, the Flinders Ranges (Paul *et al.* 2000) could present as a zone of weak lithosphere due to previous deformations. Moreover, prominent lithospheric discontinuities (fracture zones) such as; the Spencer, King George V and Kangaroo Fracture Zone (Figure 7.4) reside directly south of the Mount Lofty and Flinders Ranges (Heezen & Tharp 1976). According to Storti *et al.* (2003) excessive shearing along the oceanic transform faults could terminate at plate interiors or continental passive margins, creating intraplate strike-slip zones

Geologic information from various parts of Australia indicates that the continent underwent a change in deformation patterns around ~8-6 Ma and has continued to deform consistently (Paul 1998). Sedimentary records from offshore basins transition from carbonate to siliclastic sedimentation (Dickinson *et al.* 2001) and a preserved offshore reverse fault record, parallel to onshore basin structures, implies that the modern NW-SE compressive stress regime in SE Australia has been active since 8-6 Ma (Sandiford 2003a, Sandiford *et al.* 2004). Regional Miocene-Pliocene unconformities, uplifted Miocene limestones and analysis on Pliocene-Quaternary faults (Sandiford 2003a, Quigley *et al.* 2006) provide further geological evidence of an active tectonic regime around 10-5 Ma. This deformational change coincides with the formation of the New Zealand Southern Alps 12-6 Ma (Sandiford *et al.* 2004),

compressional deformation and uplift along the Macquarie Ridge, transpressional deformation and uplift in Papua New Guinea, collision between the Java Plateau and the Solomon Arc, deformation in the central Indian Ocean (~8 Ma) and the transition of decelerating Indo-Australian-Somalia seafloor spreading, to the present phase of steady spreading (Paul 1998, Merkouriev & DeMets 2006). Late Miocene to early Pliocene coarser alluvial sediments in the Flinders Ranges (Callen & Tedford 1976, May 1992) and a two-fold increase in convergence on the southern margin of the Australian-Antarctic plates since ~6 Ma (Cande & Stock 2004) supports the notion of the proposed fourth stage of deformation being a transpressional tectonic regime.

Middle to late Miocene (~11-6 Ma) subduction along the Papua New-Guinea margin (Dyksterhuis & Muller 2008), compression from the New Zealand boundary (Müller *et al.* 2012) and continental tilting due to slab-pull forces while travelling though a geoid high (Sandiford & Quigley 2009a, Sandiford *et al.* 2009b) may be considered as the evolution of a compressive stress regime. E-W dominant compressional forces have reactivated the faults with reverse movements (Dyksterhuis & Muller 2008), which is proposed as the evolution stage III for southern South Australia. Tasman seafloor spreading ceased and resistant forces from the Indian-Eurasian collision initiated ~23 Ma (Dyksterhuis & Muller 2008). The beginning of the compressive forces from the Australian-Pacific collision also happens to fall ~23 Ma (Kemp 1986). Therefore, plate boundary force changes during ~23 Ma can be interpreted as a considerable reorganization of the plate interior stresses without significant deformation. The period ~23 to 11 Ma has experienced limited strike-slip movements controlled by the ridge-push forces (Dyksterhuis & Muller 2008) possibly leading to widespread tectonic quiescence.

The proposed four-stage deformation in southern South Australia provides a better description of interactions between the plate boundary forces and intraplate tectonics. The gradual evolution of neotectonics in the southern South Australian context may have begun during early Miocene times. However, much of the uplift of the Mount Lofty and Flinders Ranges may have taken place since the mid Miocene, which is considered to be Sprigg's Orogeny by Sandiford (2003a). An expansion of the Sprigg's Orogeny towards the middle Eocene can be made by the inclusion of

tectonic transition stages (~23-11 Ma) and extensional stages (~43-23 Ma). On the other hand, continuous evolution of the Australian plate boundary dynamics (Figure 7.5) can be traced beyond early-late Cretaceous times, reflecting obvious continuity of the intraplate deformations even though it is commonly considered as intermittent.

8 CONCLUDING REMARKS AND FUTURE DIRECTIONS

Tectonically active landscapes in plate interiors are sources of seismic hazard. Therefore, identification of faulting characteristics and driving mechanisms for intraplate deformation is essential, even though it is complicated. The processes leading to the present topography and seismicity of the Mount Lofty and Flinders Ranges are enigmatic, as southern South Australia has experienced multiple orogenic episodes. Regional stress fields in South Australia fail to explain the localized deformation, probably due to the stress models not accommodating the spatially varying inhomogeneous nature of the earth's subsurface. Complexities of linking the field observations and plate boundary conditions inhibit the derivation of credible driving mechanisms accountable for intraplate deformations.

An attempt to understand the behavioural characteristics of the neotectonic faults in the Mount Lofty and Flinders Ranges has revealed that the ongoing deformation is a result of sinistral strike-slip movements. Accordingly, the range bounding faults are largely derived from localized transpressional movements, instead of regional compression. In-depth field observations identifying sub-horizontal slickensides complement the evidence of oblique fault movements. A link between the localized deformations and the plate boundary force changes has been established primarily based on the differential movements along the Southern Oceanic Fracture Systems.

According to the established link with the plate boundary force reorganizations, the South Australian Sprigg's Orogeny mainly consists of two episodes of mountain building events dominated by compression (~11-6 Ma) and transpression (since ~ 6 Ma). The beginning of the Sprigg's Orogeny may even reach as old as middle Eocene times, making it much older than the east Australian Kosciusko Orogeny. The latest and ongoing deformations are likely to have been in operation, since late-Miocene to early-Pliocene times, due to the oblique forces enforced from increased collision between the SE Australian and Pacific plates.

8.1 Methodological potentials

The present study provides an example of a composite methodological framework for the rapid assessment of neotectonic movements in southern South Australia. The utilization of LiDAR images and the ground penetrating radar (GPR) technique to extract subtle topographic and subsurface features related to faulting can be enhanced with trenching. In addition to the fault kinematics and stratigraphic offsets, topographic features such as, erosion gullies and knickpoints on incised stream channels facilitate as sources of information to establish fault movements. Recurrent fault movements were primarily observed from subsurface stratigraphy, with dating techniques providing age estimates for recurrence intervals or the latest fault movements.

The lateral movements largely demonstrated by sub-horizontal slickensides and oblique-slip faulting due to transpression provide a new perspective for neotectonic studies in this region. Assessment of the fault components based on the slickensides offer a new set of data for horizontal displacement estimates, exposing an avenue for further investigation of potential lateral movements. These movements may be validated through topographic features such as, stream channel migrations, valley-in-valley structures (Zhang *et al.* 2004) and long-term ground positioning system (GPS) based studies. Importantly, stream offsets must be used with caution to determine the lateral direction of movement (Higgins 1961, Allen 1962, Sylvester 1988).

By obtaining estimates for localized horizontal and vertical displacements, an average value can be computed for the rate of regional scale deformation. Identification of substantial strike-slip characteristics in the Mount Lofty and Flinders Ranges helps to expedite investigations of its neotectonic intraplate deformation.

8.1.1 Impact on local tectonics

Adelaide has the highest seismic risk among the Australian state capitals, being adjacent to a seismically active mountain belt. Three major earthquakes (1897, 1902 and 1954) have been recorded since 1837, causing minor damages to the city of Adelaide. A magnitude 3.8 earthquake, the strongest within the last two decades, was recorded on 17th April 2010. The epicentre of the event was located southeast of Adelaide, near Mount Barker, and the hypocentre was calculated at ~20 km depth, with no association to the known fault lines. The proposed sinistral strike-slip model provides a new dimension for neotectonic investigations in this region. Accordingly, the identification of fault networks, their inter-relationships and rupture patterns will improve the accuracy of calculations on the amount of slip, rate of movements, recurrence intervals and rupture patterns. Therefore, social impacts from the earthquakes may be reduced, by providing essential information for seismic hazard assessments and regional planning.

Additionally, a better explanation can be provided for the seismic observations in the Flinders Seismic Zone. An overestimation of earthquake magnitudes and seismic hazards may be eliminated, as the stress is most likely being partitioned along the networks of oblique-slip faults, continuous slow-slip and pre-existing structures, instead of localised reverse fault movements.

8.1.2 Impact on regional and global tectonics

The sinistral strike-slip tectonic model proposed in the present study complements the regional scale seismic observations and some of the previous hypotheses concerning deformation in the Mount Lofty and Flinders Ranges. Long-term strike-slip movements in southern South Australia probably behave according to the sub-plate model proposed by Cleary & Simpson (1971). Dextral strike-slip neotectonics recorded from the north-south trending Mt Narryer Fault Zone on Western Australia (Whitney & Hengesh 2011), also favours a sub-plate hypothesis for the Australian continent.

Plate boundary forces and tectonic plate movements evolve continuously, making it difficult to extract specific timing of the changes that take place. Consequently, the intraplate deformations compensate for much of the boundary force changes, the intensities of which are unclear. A link established between microtectonic features and plate boundary interactions, may mutually facilitate understanding of the nature of intraplate deformations and corresponding tectonic plate interactions.

REFERENCES

Aidamiec, G. and Aitken, M. J. (1998). "Dose-rate conversion factors: Update." *Ancient TL* 16: 37-50.

Aitchison, J. C., Ali, J. R. and Davis, A. M. (2007). "When and where did India and Asia collide?" *Journal of Geophysical Research* 112(B5): B05423.

Aitken, A. R. A. (2010). "Moho geometry gravity inversion experiment (MoGGIE): A refined model of the Australian Moho, and its tectonic and isostatic implications." *Earth and Planetary Science Letters* 297(1–2): 71-83.

Aitken, M. J. (1985). Thermoluminescence dating. London, Academic press.

Aitken, M. J. (1994). "Optical dating, a non-specialist review." *Quaternary Science Reviews* 13: 503-508.

Aitken, M. J. (1998). An introduction to Optical Dating: the dating of Quaternary sediments by the use of photon-stimulated luminescence. New York, Oxford University Press.

Aitken, M. J. and Xie, J. (1990). "Moisture correction for annual gamma dose." *Ancient TL* 8: 6-9.

Allen, C. R. (1962). "Circum-Pacific faulting in the Philippines-Taiwan region." *Journal of Geophysical Research* 67: 4795-4812.

Allen, C. R. (1982). "Comparisions between the North Anatolian Fault of Turkey and the San Andreas Fault, California."

Allen, T. I., Gibson, G. and Cull, J. P. (2005). "Stress-field constraints from recent intraplate seismicity in southeastern Australia." *Australian Journal of Earth Sciences* 52(2): 217-230.

Alley, N. F. (1973). "Landsurface development in the mid north of South Australia." *Transactions of the Royal Society of South Australia* 97: 1-17.

Alley, N. F. and Bourman, R. P. (1984). "Sedimentology and origin of late Palaeozoic glacigene deposits at Cape Jervis, South Australia." *Transactions of the Royal Society of South Australia* 108: 63-75.

Alley, N. F. and Bourman, R. P. (1995). Troubridge Basin. *The geology of South Australia*. (Drexel, J. F. and Preiss, W. V., Ed.), South Australia Geological Survey. 2**:** 65-70.

Ambraseys, N. N. (1970). "Some characteristic features of the Anatolian Fault Zone." *Tectonophysics* 9(143-165).

Amold, L. J., Bailey, R. M. and Tucker, G. E. (2007). "Statistical treatment of fluvial dose distributions from southern Colorado arroyo deposits." *Quaternary Geochronology* 2: 162-167.

Anderson, K. B., Spotila, J. A. and Hole, J. A. (2003). "Application of geomorphic analysis and ground-penetrating radar to characterization of paleoseismic sites in dynamic alluvial environments: an example from southern California." *Tectonophysics* 368(1-4): 25-32.

Andrews, E. C. (1933). "The origin of modern mountain ranges. with special reference to the eastern Australian highlands." *Journal and Proceedings of the Royal Society of New South Wales* 67(part 2): 251-350.

Annan, A. P. (2009). Electromagnetic principles of ground penetrating radar. *Ground penetrating radar: Theory and applications*. (Jol, H. M., Ed.). Amsterdam, Elsevier**:** 3-40.

Aranha, P. R. A., Augustin, C. H. R. R. and Sobreira, F. G. (2002). "The use of GPR for characterizing underground weathered profiles in the sub-humid tropics." *Journal of Applied Geophysics* 49(4): 195-210.

Atkinson, G. M. (2007). "Challenges in seismic hazard analysis for continental interiors." *Geological Society of America Special Papers* 425: 329-344.

Audemard, F., Pantosti, D., Machette, M., Costa, C., Okumura, K., Cowan, H., Diederix, H. and Ferrer, C. (1999). "Trench investigation along the Mérida section of the Boconó fault (central Venezuelan Andes), Venezuela." *Tectonophysics* 308(1–2): 1-21.

Axen, G. J. (1998). The Caliente-Enterprice Zone, southeastern Nevada and southwestern

Utah. *Accommodation zones and transfer zones: The regional segmentation of the Basin and Range Province*. (Faulds, J. E. and Stewart, J. H., Ed.), Geological Society of America. 323**:** 181-194.

Aydin, A. and Nur, A. (1985). "The types and role of stepovers in strike slip tectonics." *The Society of Economic Paleontologists and Mineralogists*: 35-44.

Azzaro, R., Bella, D., Ferreli, L., Maria Michetti, A., Santagati, F., Serva, L. and Vittori, E. (2000). "First study of fault trench stratigraphy at Mt. Etna volcano, Southern Italy: understanding Holocene surface faulting along the Moscarello fault." *Journal of Geodynamics* 29(3–5): 187-210.

Ballance, P. F. and Reading, H. G. (1980). Sedimentation in oblique-slip mobile zones: an introduction. *International Association of Sedimentologists Special Publication*. (Ballance, P. F. and Reading, H. G., Ed.). London, Blackwell Scientific Publications. 4**:** 1-5.

Banerjee, D., Hildebrand, A. N., Murray-Wallace, C. V., Bourman, R. P., Brooke, B. P. and Blair, M. (2003). "New quartz SAR-OSL ages from the stranded beach dune sequences in southeast South Australia." *Quaternary Science Reviews* 22: 1019-1025.

Barka, A. (1996). "Slip distribution along the North Anatolian Fault associated with the large earthquakes of the period 1939 to 1967." *Bulletin of the Seismological Society of America* 86: 1238-1254.

Bartlett, W. L., Friedman, M. and Logan, J. M. (1981). "Experimental folding and faulting of rocks under confining pressure - wrench faults in limestone layers." *Tectonophysics* 79: 255-277.

Basson, U., Gev, I. and Ben-Avrahsm, Z. (2003). "Ground penetrating radar as a tool for mapping of moisture content and stratigraphy of sand dunes." *International Water Technology Journal* 19: 11-13.

Bell, W. T. and Zimmerman, D. W. (1978). "The effect of HF etching on the morphology of quartz inclusions for thermoluminescence dating." *Archaeometry* 20: 63-65.

Belperio, A. P. (1988). Fowlers Bay rotary drilling report and revision of the Quaternary geology around Fowlers Bay, South Australia, Department of Mines and Energy**:** 93.

Belperio, A. P. (1995). Quaternary. *The Geology of South Australia*Ed.). 2**:** 219-280.

Belperio, A. P. and Bateman, J. (1986). Cainozoic stratigraphy and structure of the Gawler and Vincent 1:50000 map sheet. 86/49.

Benbow, M. C., Alley, N. F., Callen, R. A. and Greenwood, D. R. (1995). Geological history of paleoclimate. *The geology of South Australia*. (Drexel, J. F. and Preiss, W. V., Ed.), South Australia, Geological Survey, Bulletin. 2**:** 208-217.

Benbow, M. C., Alley, N. F., Callen, R. A. and Greenwood, D. R. (1995a). Geological history and palaeoclimate. *The geology of South Australia.Vol. 2, The Phanerozoic*. (Drexel, J. F. and Preiss, W. V., Ed.), South Australia, Geological Survey, Bulletin. 2**:** 208-217.

Benbow, M. C., Callen, R. A., Bourman, R. P. and Alley, N. F. (1995b). Deep weathering, ferricrete and silcrete. *Bulletin 54 The geology of South Australia: The Phanerozoic*. (Drexel, J. F. and Preiss, W. V., Ed.), Geological Survey, South Australia.

Benson, A. K. (1995). "Applications of ground penetrating radar in assessing some geological hazards: examples of groundwater contamination, faults, cavities." *Journal of Applied Geophysics* 33(1-3): 177-193.

Benson, W. N. (1911). "Note descriptive of a stereogram of the Mt.Lofty Ranges, South Australia." *Transactions of the Royal Society of South Australia* 35: 108-111.

Berger, G. W. (1998). "Dating Quaternary events by luminescence." *Geological society of America Special Paper* 227: 13-50.

Bergman, E. A. (1986). "Intraplate earthquakes and the state of stress in oceanic lithosphere." *Tectonophysics* 132(1–3): 1-35.

Biddle, K. T. and Christie-Blick, N. (1985). Glossary - Strike-slip deformation, basin formation, and sedimentation. *Strike-slip deformation, basin formation, and sedimentation*. (Biddle, K. T. and Christie-Blick, N., Ed.), Society of Economic

Paleantologists and Mineralogists. Special publication no.37**:** 375-386.

Bierman, P. R. and Nichols, K. K. (2004). "Rock to sediment - slope to sea with 10Be - Rates of landscape change." *Annu. Rev. Earth Planet. Sci.* 32: 215-255.

Blake, M. C., Campbell, R. H., Dibblee, T. W., Howell, D. G., Nilsen, T. H., Normark, W. R., Vedder, J. C. and Silver, E. A. (1978). "Neogene basin formation in relation to plate-tectonic evolution of San Andreas Fault System, California." *Bulletin of the American Association of Petroleum Geologists* 62: 344-372.

Bluck, B. J. (1995). "W. Q. Kennedy, the Great Glen Fault and strike-slip motion." *Geological Society, London, Memoirs* 16(1): 57-65.

Bommer, J., Douglas, J. and Strasser, F. (2003). "Style-of-Faulting in Ground-Motion Prediction Equations." *Bulletin of Earthquake Engineering* 1(2): 171-203.

Bonilla, M. J. and Lienkaemper, J. J. (1990). "Visibility of fault strands in exploratory trenches and timing of rupture events." *Geology* 18: 153-156.

Bøtter-Jensen, L. and Mejdahl, V. (1988). "Assessment of beta dose rate using a GM multicounter system." *Muclear tracks and radiation measurements* 14: 187-191.

Bourman, R. P. (2006). "River terraces of the Fleurieu Peninsula, South Australia." *South African Geographical Journal* 105: 1-24.

Bourman, R. P., Belperio, A. P., Murray-Wallace, C. V. and Cann, J. H. (1999). "A Last Interglacial Embayment Fill at Normanville, South Australia, and its Neotectonic Implications." *Transactions of the Royal Society of South Australia* 123 (1): 1-15.

Bourman, R. P., Buckman, S., Pillans, B., Williams, M. A. J. and Williams, F. (2009). "The Age and Origin of the Gun Emplacement, A Ferricreted Terrace, Adelaide, South Australia : Evidence of Neotectonic Dislocation and Surface Rupture on the Eden-Burnside Fault."

Bourman, R. P., Buckman, S., Pillans, B., Williams, M. A. J. and Williams, F. (2010a). "Traces from the past: the Cenozoic regolith and intraplate neotectonic history of the Gun Emplacement, a ferricreted bench on the western margin of the Mt. Lofty Ranges, South Australia." *Australian Journal of Earth Sciences* 57(5): 577-595.

Bourman, R. P. and Lindsay, J. M. (1973). "Implications of Fossiliferous Eocene Marine Sediments Underlying Part of the Waitpinga Drainage Basin, Fleurieu Peninsula, South Australia." *Search* 4(3): 77.

Bourman, R. P. and Lindsay, J. M. (1989). "Timing, Extent and Character of Late, Cainozoic Faulting on the Eastern Margin of the Mt.Lofty Ranges, South Australia." *Transactions of the Royal Society of South Australia* 113 part I & 2: 63-67.

Bourman, R. P., Martinaitis, P., Prescott, J. R. and Belperio, A. P. (1997). "The Age of the Pooraka Formation and its Implications, with some Preliminary Results from Luminescence Dating." *Transactions of the Royal Society of South Australia* 121 (3): 83-94.

Bourman, R. P. and May, R. I. (1984). "Coastal Rotational Landslump." *Australian Geographer* 16: 144-146.

Bourman, R. P. and Murray-Wallace, C. V. (2002). "Amino Acid Racemisation Dating of a Raised Gravel Beach Deposit, Sellicks beach, South Australia." *Transactions of the Royal Society of South Australia* 126 (1): 21-28.

Bourman, R. P., Murray-Wallace, C. V., Belperio, A. P. and Harvery, N. (2000). "Rapid coastal geomorphic change in the River Murray Estuary of Australia." *Marine Geology* 170: 141-168.

Bourman, R. P. and Pillans, B. (1997). "The Use of the Geomagnetic Polarity Time Scale in Elucidating Pleistocene Landscape Evolution: An Example from South Australia." *South African Geographical Journal* 79 (Special Edition): 75-82.

Bourman, R. P., Prescott, J. R., Banerjee, D., Alley, N. F. and Buckman, S. (2010b). "Age and origin of alluvial sediments within and flanking the Mt Lofty Ranges, southern South Australia: a Late Quaternary archive of climate and environmental change." *Australian Journal of Earth Sciences: An International Geoscience Journal of the*

Geological Society of Australia 57(2): 175-192.

Boutaloff, N. (1952). "The great circle stress pattern of the earth." *Australian Journal of Science* 14: 198-111.

Bowler, J. M., Johnston, H., Olley, J. M., Prescott, J. R., Roberts, R. G., Shawcross, W. and Spooner, N. A. (2003). "New ages for human occupation and climatic change at Lake Mungo, Australia." *Nature* 421(6925): 837-840.

Braun, J., Burbidge, D. R., Gesto, F. N., Sandiford, M., Gleadow, A. J. W., Kohn, B. P. and Cummins, P. R. (2009). "Constraints on the current rate of deformation and surface uplift of the Australian continent from a new seismic database and low-T thermochronological data." *Australian Journal of Earth Sciences* 2009(56): 99-110.

Braun, J. and Shaw, R. (2001). "A thin-plate model of Palaeozoic deformation of the Australian lithosphere: implications for understanding the dynamics of intracratonic deformation." *Geological society, London, special publications* 184(1): 165-193.

Brown, C. M. and Stephenson, A. E. (1991). "Geology of the Murray Basin, Southeastern Australia." *Bureau of Mineral Resources Bulletin*(235): 430.

Brown, D., Juhlin, C., Ayala, C., Tryggvason, A., Bea, F., Alvarez-Marron, J., Carbonell, R., Seward, D., Glasmacher, U., Puchkov, V. and Perez-Estaun, A. (2008). "Mountain building processes during continent–continent collision in the Uralides." *Earth-Science Reviews* 89(3–4): 177-195.

Brugger, J., Long, N., McPhail, D. C. and Plimer, I. (2005). "An active amagmatic hydrothermal system: The Paralana hot springs, Northern Flinders Ranges, South Australia." *Chemical Geology* 222(1–2): 35-64.

Buckman, S. (2000). Tectonics and mineralization of West Junggar, NW China. Ph.D., University of Hong Kong.

Buckman, S. and Jayawardena, C. L. (2009a). Adelaide seismicity and neotectonics. Geodynamics of the Australian Plate - research meeting, Monash University.

Buckman, S., Jayawardena, C. L. and Bourman, R. P. (2010). What is driving intraplate deformation in South Australia? Australian earth sciences convention, Canberra.

Buckman, S., Jayawardena, C. L., Bourman, R. P. and Murray-Wallace, C. V. (2009b). What's up with the Willunga fault? Structural and topographic characteristics of restraining bends in the Southern Mt.Lofty Ranges using SRTM and LIDAR DEM's. Geomorphology 2009, Melbourne.

Bull, W. B. (2007). Tectonic geomorphology of mountains - A new approach to paleoseismology, Blackwell publishing.

Burg, J.-P. (2011) "Strike-slip and oblique-slip tectonics." Tectonics - strike slip faults, 145-164.

Buslov, M. M., Klerkx, J., Abdrakhmatov, K., Delvaux, D., Batalev, V. Y., Kuchai, O. A., Dehandschutter, B. and Muraliev, A. (2003). "Recent strike-slip deformation of the northern Tien Shan." *Geological society, London, special publications* 210(1): 53-64.

Cagnoli, B. and Russell, J. K. (2000). "Imaging the subsurface stratigraphy in the Ubehebe hydrovolcanic field (Death Valley, California) using ground penetrating radar." *Journal of Volcanology and Geothermal Research* 96(1-2): 45-56.

Callen, R. A. (1983). "Late Tertiary 'grey billy' and the age and origin of surficial silicifications (silcrete) in South Australia." *Journal of the Geological Society of Australia* 30: 393-410.

Callen, R. A. and Tedford, R. H. (1976). "New late Cainozoic rock units and depositional environments, Lake Frome area, South Australia." *Transactions of the Royal Society of South Australia* 100: 125-167.

Campana and Wilson (1953). The geology of the Gawler Military Sheet. Geological survey of South Australia. 4**:** 24.

Campana, B. (1954). "The structure of the Eastern South Australian Ranges: The Mt.Lofty - Olary arc." *Geological Society of Australia* 2: 47-61.

Campbell, J. B. (1996). Introduction to Remote Sensing. New York, The Guilford Press.

Cande, S. C. and Stock, J. M. (2004). "Pacific—Antarctic—Australia motion and the formation of the Macquarie Plate." *Geophysical Journal International* 157(1): 399-414.

Casas, A. M., Gapais, D., Nalpas, T., Besnard, K. and Roman-Berdiel, T. (2001). "Analogue models of transpressive systems." *Journal of Structural Geology* 23: 733-743.

Caskey, S. J. and Wesnousky, S. G. (1997). "Static stress changes and earthquake triggering during the 1954 Fairview Peak and Dixie Valley earthquakes, Central Nevada." *Bulletin of the Seismological Society of America* 87: 521-527.

Cassidy, N. J. (2009). Ground penetrating radar data processing, modelling and analysis. *Ground penetrating radar: Theory and application*. (Jol, H. M., Ed.). Amsterdam, Elsevier**:** 141-176.

Catchpole, H. (2009). Australians unaware of earthquake risk. General Interest Periodicals--Australia. Sydney, ABC Premium News.

Celerier, J., Sandiford, M., Hansen, D. L. and Quigley, M. C. (2005). "Modes of active intraplate deformation, Flinders Ranges, Australia." *Tectonics* 24: 1-17.

Charlton, T. R. (2000). "Tertiary evolution of the Eastern Indonesia Collision Complex." *Journal of Asian Earth Sciences* 18(5): 603-631.

Chow, J., Angelier, J., Hua, J. J., Lee, J. C. and Sun, R. (2001). "Paleoseismic event and active faulting: from ground penetrating radar and high-resolution seismic reflection profiles across the Chihshang Fault, eastern Taiwan." *Tectonophysics* 333(1-2): 241-259.

Christie-Blick, N. and Biddle, K. T. (1985). "Deformation and basin formation along strike-slip faults." *The Society of Economic Paleontologists and Mineralogists*: 1-34.

Clark, D. (2006). A seismic source model based on neotectonics data. Australian Earthquake Engineering Society.

Clark, D. (2010). What is an "active" fault in the Australian intraplate context? A discussion with examples from eastern Australia. Australia, G. Canberra, Geoscience Australia.

Clark, D. and Leonard, M. (2003). "Principal stress orientations from multiple focal-plane solutions: new insight into the Australian intraplate stress field." *Geological Society of Australia Special Publication* 22: 91-105.

Clark, D. and McCue, K. (2003). "Australian paleoseismology: towards a better basis for seismic hazard estimation." *Annals of Geophysics* 46(N5): 1087-1105.

Clark, D. and McPherson, A. (2011). Large earthquake recurrence in the Adelaide region: a palaeoseismological perspective. Australian Earthquake Engineering Society. Barossa Valley, South Australia.

Clark, D. and McPherson, P. (2010, 2011). Trenching program - Geoscience Australia. Jayawardena, C. L. and Buckman, S. Adelaide.

Clark, D., Van Dissen, R., Cupper, M., Collins, C. and Prendergast, A. (2008). Temporal clustering of surface ruptures on stable continental region faults: A case study from the Cadell Fault Scarp, southeastern Australia Geoscience Australia**:** 5.

Clarke, G. L. and Powell, R. (1989). "Basement-cover interaction in the Adelaide Foldbelt, South Australia: the development of an arcuate foldbelt." *Tectonophysics* 158(1–4): 209-226.

Cleary, J. R. and Simpson, D. W. (1971). "Seismotectonics of the Australian continent." *Nature* 230(Mar-Apr): 239-241.

Cleary, J. R., Simpson, D. W. and Muirhead, K. J. (1972). "Variations in Australian upper mantle structure, from observations of the Cannikin explosion." *Nature* 236(Mar-Apr): 111-112.

Cloetingh, S. and Wortel, R. (1985). "Regional stress field of the Indian Plate." *Geophys. Res. Lett* 12: 77-80.

Cloetingh, S. and Wortel, R. (1986). "Stress in the Indo-Australian plate." *Tectonophysics* 132(1–3): 49-67.

Coats, R. P. (1973). Copley map sheet, South Australia. Geological Series Explanatory Notes, Geological Survey of South Australia.

Coats, R. P. and Blissett, A. H. (1971). "Regional and economic geology of the Mount Painter Province." *Geological Survey of South Australia Bullatin* 43.

Coblentz, D. D., Sandiford, M., Richardson, R. M., Zhou, S. and Hillis, R. (1995). "The origins of the intraplate stress field in continental Australia." *Earth and Planetary Science Letters* 133: 299-309.

Coblentz, D. D., Zhou, S., Hillis, R. R., Richardson, R. M. and Sandiford, M. (1998). "Topography, boundary forces, and the Indo-Australian intraplate stress field." *Journal of Geophysical Research* 103(B1): 919-931.

Cohen, T. J., Nanson, G. C., Jansen, J. D., Jones, B. G., Jacobs, Z., Treble, P., Price, D. M., May, J., Smith, A. M., Ayliffe, L. K. and Hellstrom, J. C. (2011). "Continental aridification and the vanishing of Australia's megalakes." *Geology* 39(2): 167-170.

Conyers, L. B. and Cameron, C. M. (1998). "Finding buried archaeological features in the American Southwest: a new ground-penetrating radar techniques and three-dimensional mapping." *Journal of Field Archaeology* 25: 417-430.

Cooke, J. A. and Gladwin, M. T. (1999). Ground penetrating radar performance in typical Australian Soils. *CSIRO Exploration and Mining Reserach Review*Ed.)**:** 159-163.

Cooper, B. J. (1979). Eocene to Miocene stratigraphy of the Willunga Embayment, Department of Mines and Energy, Geological Survey of South Australia. 50**:** 101.

Cooper, B. J. (1985). "The Cainozoic St Vincent Basin - tectonics, structure, stratigraphy." *South Australian Department of Mines and Energy, special publication* 5: 35-49.

Costa, C. H., Cesco, J. C. and Morán, R. J. (1997). "A simple graphical method for estimating the components of the fault-slip vector." *Journal of Structural Geology* 19(9): 1245-1247.

Coward, M. P. (1976). "Large scale Palaeozoic shear zone in Australia and present extension to the Antarctic ridge." *Nature* 259(February): 648-649.

Cox, A. and Hart, R. B. (1986). Plate Tectonics, How it works. Melbourne, Blackwell Scientific Publications.

Crawford, A. R. and Campbell, K. S. W. (1973). "Large-scale horizontal displacement within Australo-Antarctica in the Ordovician." *Nature Physical Science* 241(January): 11-14.

Crone, A. J., DeMartini, P. M., Machette, M. N., Okumura, K. and Prescott, J. R. (2003). "Paleoseismicity of aseismic Quaternary faults in Australia: Implications for fault behaviour in stable continental regions." *Bulletin of the Seismological Society of America* 93: 1913-1934.

Crone, A. J. and Luza, K. V. (1990). "Style and timing of Holocene surface faulting on the Meers Fault, southwestern Oklahoma." *Geological Society of America Bulletin* 102: 1-17.

Crone, A. J., Machette, M. N. and Bowman, J. R. (1997). "Episodic nature of earthquake activity in stable continental regions revealed by palaeoseismicity studies of Australian and North American Quaternary faults." *Australian Journal of Earth Sciences* 44: 203-214.

Crowell, J. C. (1974). "Sedimentation along the San Andreas Fault, California." *Modern and Ancient Geosynclinal Sedimentation* 19: 292-303.

Crowell, J. C. and Frakes, L. A. (1971). "Late Paleozoic Glaciation: Part IV, Australia." *Geological Society of America Bulletin* 82(9): 2515-2540.

Cull, J. (1982). "An appraisal of Australian heat-flow data." *Bureau of Mineral Resources Journal of Australian Geology and Geophysics* 7: 11-21.

Cunningham, D., Dijkstra, A., Howard, J., Quarles, A. and Badarch, G. (2003). "Active intraplate strike-slip faulting and transpressional uplift in the Mongolian Altai." *Geological society, London, special publications* 210(1): 65-87.

Cunningham, W. D. (2007). "Structural and topographic characteristics of restraining bend mountain ranges of the Altai, Gobi Altai and

easternmost Tien Shan." *Geological society, London, special publications* 290: 219-237.

Cunningham, W. D. and Mann, P. (2007). "Tectonics of strike-slip restraining and releasing bends." *Geological society, London, special publications* 290: 1-12.

Dagallier, G., Laitinen, A. I., Malartre, F., Van Campenhout, I. P. A. M. and Veeken, P. C. H. (2000). "Ground penetrating radar application in a shallow marine Oxfordian limestone sequence located on the eastern flank of the Paris Basin, NE France." *Sedimentary Geology* 130(3-4): 149-165.

Daily, B., Firman, J. B., Forbes, B. G. and Lindsay, J. M. (1976). Geology.

Daily, B., Jago, J. B. and Milnes, A. R. (1973a). "Large-scale horizontal displacement within Australo-Antarctica in the Ordovician." *Nature Physical Science* 244(July): 61-64.

Dalgarno, C. R., Johnson, J. E., Forbes, B. G. and Thomson, B. P. (1968). Port Augusta map sheet, South Australia, Sheet SI53-4. Geological Atlas of South Australia, 1:250 000 series, Geological Survey of South Australia, Adelaide.

Dalrymple, G. B. and Clague, D. A. (1976). "Age of the Hawaiian - Emperor bend." *Earth and Planetary Science Letters* 31: 313-329.

Daniels, F., Boyd, C. A. and Saunders, D. F. (1953). "Thermoluminescence as a research tool." *Science* 117: 343-349.

Dauteuil, O. and Mart, Y. (1998). "Analogue modeling of faulting pattern, ductile deformation, and vertical motion in strike slip fault zones." *Tectonics* 17(2): 303-310.

Davey, J. E. (2009). Tectonostratigraphic evolution of an intracontinental terrain: The geological evolution of the Frome Embayment, Eromanga Basin, Australia. School of Earth and Environmental Sciences, Geology and Geophysics and Australian School of Petroleum.

Davis, J. L. and Annan, A. P. (1989). "Ground penetrating radar for high resolution mapping of soil and rock stratigraphy." *Geophysical Prospecting* 37: 531-551.

DeLong, S. B. and Arnold, L. J. (2007). "Dating alluvial deposits with optically stimulated luminescence, AMS 14C and cosmogenic techniques, western Transverse Ranges, California, USA." *Quaternary Geochronology* 2(1–4): 129-136.

DeMets, C. and Dixon, T. H. (1999). "New kinematic models for Pacific-North America motion from 3 Ma to present: Evidence for steady motion and biases in the NUVEL-1A model." *Geophys. Res. Lett* 26: 1921-1924.

Denham, D., Alexander, I. G. and Worontinicki, G. (1979). "Stresses in the Australian crust: evidence from earthquake and in situ stress measurements." *Bureau of Mineral Resources journal of Australian geology and geophysics* 4: 289-295.

Denis, A., Huneau, F., Hoerlé, S. and Salomon, A. (2009). "GPR data processing for fractures and flakes detection in sandstone." *Journal of Applied Geophysics* 68(2): 282-288.

Dewey, J. F. (1998). "Extensional collapse of orogens." *Tectonics* 7: 1123-1139.

Dickinson, J. A., Wallace, M. W., Holdgate, G. R., Daniels, J., Gallagher, S. J. and Thomas, L. (2001). "Neogene tectonics in SE Australia; Implications for petroleum systems." *Australian petroleum production and exploration association journal* 41: 37-52.

Dickinson, J. A., Wallace, M. W., Holdgate, G. R., Gallagher, S. J. and Thomas, L. (2002). "Origin and Timing of the Miocene-Pliocene Unconformity in Southeast Australia." *Journal of sedimentary research* 72: 288-303.

Doolittle, J. A. and Collins, M. E. (1995). "Use of soil information to determine application of ground penetrating radar : J. A. Doolittle & M. E. Collins, Journal of Applied Geophysics, 33(1-3), 1995, pp 101-108." *International Journal of Rock Mechanics and Mining Science & Geomechanics Abstracts* 32(8): A383-A383.

Dougherty, A. J. (2009). Evolution of prograded coastal barriers in Northern New Zealand. PhD, University of Auckland.

Dougherty, A. J. (2012). Field surveying in coastal regions with a GPR. Jayawardena, C. L. Wollongong.

Doyle, H. A., Everingham, I. B. and Sutton, D. J. (1968). "Seismicity of the Australian

continent." *Geological Society of Australia Journal* 15: 295-312.

Drexel, J. F. and Preiss, W. V. (1995). The geology of South Australia, South Australia, Geological Survey, Bulletin.

Duller, G. A. T. (2003). "Distinguishing quartz and feldspar in single grain luminescence measurements." *Radiation measurements* 37: 161-165.

Dumont, J. F., Santana, E., Vilema, W., Pedoja, K., Ordóñez, M., Cruz, M., Jiménez, N. and Zambrano, I. (2005). "Morphological and microtectonic analysis of Quaternary deformation from Puná and Santa Clara Islands, Gulf of Guayaquil, Ecuador (South America)." *Tectonophysics* 399(1-4): 331-350.

Dury, G. H. (1964). "Australian geochronology: checklist 1." *Australian Journal of Sciences* 278: 103-109.

Dyksterhuis, S. and Muller, R. D. (2004). "Modelling the contemporary and palaeo stress field of Australia using finite-element modelling with automatic optimisation." *Exploration geophysics* 35: 236-241.

Dyksterhuis, S. and Muller, R. D. (2008). "Cause and evolution of intraplate orogeny in Australia." *Geology* 36(6): 495-498.

Dyster, T. (1995). Strong shock of earthquake: The story of the four greatest earthquakes in the history of South Australia, PIRSA. 3**:** 86.

Fairburn, B. (1998). "The Willunga Embayment - A stratigraphic revision." *MESA Journal* 11(October 1998): 35-41.

Faulds, J. E. and Varga, R. J. (1998). The role of accommodation zones and transfer zones in the regional segmentation of extended terranes. *The Regional Segmentation of the Basin and Range province*. (Faulds, J. E. and Stewart, J., Ed.), Geological Society of America, Special Paper. 323**:** 1-45.

Feathers, J. K. (2003). "Single-grain OSL dating of sediments from the Southern High Plains, USA." *Quaternary Science Reviews* 22(10-13): 1035-1042.

Fenner, C. (1930). "The major structural and physiographic features of South Australia." *Transactions of the Royal Society of South Australia* 54: 1-36.

Findlay, R. H. (2003). "Collision tectonics of northern Papua New Guinea: key field relationships demand a new model." *Geological Society of America Special Papers* 372: 291-307.

Finlayson, B. (1978). Para Fault gravity survey - West Adelaide. Department of mines & energy report book. Adelaide, Department of mines & energy, South Australia.

Firman, J. B. (1967). "Stratigraphy of late Cainozoic deposits in South Australia." *Transactions of the Royal Society of South Australia* 91: 165-180.

Firman, J. B. (1976). "Limestone at the base of the Pleistocene sequence in South Australia." *Geological survey of South Australia quarterly geological notes* 58: 2-5.

Fisher, S. C., Stewart, R. R. and Harry, M. J. (1992). Processing ground penetrating radar (GPR) data. report, C. r. 4.

Fisher, S. C., Stewart, R. R. and Jol, H. M. (1996). "Ground penetrating radar (GPR) data enhancement using seismic techniques." *J. Environ. Eng. Geophys.* 1: 89-96.

Fitzgerald, P. (1978). "Excursion to the Eden Fault." *Bulletin of the Field Geology Club of South Australia* 7(10): 5-8.

Fleming, P. D. and Offler, R. (1968). "Pre-tectonic metamorphic crystallization in the Mt. Lofty Ranges, South Australia." *Geological Magazine* 105(4): 356-359.

Flottmann, T., Gibson, G. and Kleinschmidt, G. (1993). "Structural continuity of the Ross and Delamerian orogens of Antarctica and Australia along the margin of the paleo-Pacific." *Geology* 21: 319-322.

Flottmann, T. and James, P. (1997). "Influence of basin architecture on the style of inversion and fold-thrust belt tectonics--the southern Adelaide Fold-Thrust Belt, South Australia." *Journal of Structural Geology* 19(8): 1093-1110.

Flöttmann, T., James, P., Rogers, J. and Johnson, T. (1994). "Early Palaeozoic foreland thrusting and basin reactivation at the Palaeo-Pacific margin of the southeastern Australian Precambrian Craton: a reappraisal of the structural evolution of the Southern

Adelaide Fold-Thrust Belt." *Tectonophysics* 234(1–2): 95-116.

Forbes, B. G. and Pitt, G. M. (1980). Geology of the Olary region, South Australia. Department of Mines and Energy, Report, Department of Mines and Energy.

Fraser, G., McAvaney, S., Neumann, N., Szpunar, M. and Reid, A. (2010). "Discovery of early Mesoarchean crust in the eastern Gawler Craton, South Australia." *Precambrian Research* 179(1–4): 1-21.

Furlong, K. P., Hugo, W. D. and Zandt, G. (1989). "Geometry and evolution of the San Andreas Fault." *Journal of Geophysical Research* 94: 3100-3110.

Galbraith, R. F. (1988). "Graphical Display of Estimates Having Differing Standard Errors." *Technometrics* 30(3): 271-281.

Galbraith, R. F. (1990). "The radial plot: Graphical assessment of spread in ages." *International Journal of Radiation Applications and Instrumentation. Part D. Nuclear Tracks and Radiation Measurements* 17(3): 207-214.

Galbraith, R. F. and Roberts, R. G. (2012). "Statistical aspects of equivalent dose and error calculation and display in OSL dating: An overview and some recommendations." *Quaternary Geochronology* 11(0): 1-27.

Galbraith, R. F., Roberts, R. G., Laslett, G. M., Yoshida, H. and Olley, J. M. (1999). "Optical dating of single and multiple grains of quartz from Jinmium Rock Shelter, Northern Australia: Part I, Experimental design and statistical models." *Archaeometry* 41(2): 339-364.

Garmin (2002). GPS 72 Personal Navigator, Garmin Limited.

Ghosh, N. and Chattopadhyay, A. (2008). "The initiation and linkage of surface fractures above a buried strike-slip fault: An experimental approach." *Journal of earth system science* 117: 23-32.

Gibbs, A. D. (1990). "Linked fault families in basin formation." *Journal of Structural Geology* 5(5/6): 795-803.

Glaessner, M. F. (1953). "Some problems of Tertiary geology in southern Australia." *Journal and Proceedings of the Royal Society of New South Wales* 87: 31-45.

Glaessner, M. F. and Wade, M. (1958). "New Fossils from the base of the Cambrian in South Australia." *Transactions of the Royal Society of South Australia* 81: 185-188.

Glanville, D. H. (2010). Australian seismological report 2010, Geoscience Australia. record 2011/16**:** 77.

Gontz, A. (2012). Fault finding in a MALA GPR unit. Jayawardena, C. L. Bundanoon.

Goodman, D. and Piro, S. (2013). Basic GPR Signal Processing. *GPR Remote Sensing in Archaeology*Ed.), Springer Berlin Heidelberg. 9**:** 11-36.

Gordon, R. G. (1998). "The plate tectonic approximation: Plate nonrigidity, diffuse plate boundaries, and global plate reconstructions." *Annual Review of Earth and Planetary Sciences* 26(1): 615-642.

Goulty, N. R. and Gilman, R. (1978). "Repeated creep events on the San Andreas fault near Parkfield, California, recorded by a strainmeter array." *Journal of Geophysical Research* 83: 5415-5419.

Graham, D. and Midgley, N. (2000). "Tri-plot: Ternary diagram plotting software." 2009, from http://www.lboro.ac.uk/research/phys-geog/tri-plot/index.html.

Greenhalgh, S. A., Love, D., Malpas, K. and McDougall, R. (1994). "South Australian earthquakes, 1980-92." *Australian Journal of Earth Sciences* 41: 483-495.

Greenhalgh, S. A. and Singh, R. (1988). "The seismicity of the Adelaide Geosyncline, South Australia." *Bulletin of the Seismological Society of America* 78: 243-263.

Greenhalgh, S. A., Singh, R. and Parham, R. T. (1986). "Earthquakes in South Australia." *Transactions of the Royal Society of South Australia* 110(4): 145-154.

Hall, R. (2001). Cenozoic reconstructions of SE Asia and the SW Pacific: Chainging patterns of land and sea. *Faunal and floral migrations and evolution in SE Asia - Australasia*. (al, M. e., Ed.). Lisse, Netherlands, Balkema**:** 35-56.

Hancock, P. L. (1988). "Neotectonics." *Geology Today* 4(2): 57-61.

Hand, M. and Sandiford, M. (1999). "Intraplate deformation in central Australia, the link between subsidence and fault reactivation." *Tectonophysics* 305(1–3): 121-140.

Harding, T. P. (1974). "Petroleum traps associated with wrench faults." *The American Association of Petroleum Geologists Bulletin* 58(7): 1290-1304.

Harding, T. P. (1985). "Seismic characteristics and identification of Negative flower structures, positive flower structures, and positive structural inversion." *The American Association of Petroleum Geologists Bulletin* 69(4): 582-600.

Harding, T. P., Vierbuchen, R. C. and Christie-Blick, N. (1985). "Structural styles, plate-tectonic settings and hydrocarbon traps of divergent (transtensional) wrench faults." *The Society of Economic Paleontologists and Mineralogists*: 51-77.

Harland, W. B. (1971). "Tectonic transpression in Caledonian Spitzbergen." *Geological Magazine* 108: 27-42.

Harrington, H. J., Burns, K. L. and Thompson, B. R. (1973). "Gambier - Beaconsfield and Gambier - Sorell fracture zones and the movement of plates in the Australia - Antarctica - New Zealand region." *Nature Physical Science* 245: 109-112.

Heezen, B. C. and Tharp, M. (1976). The floor of the oceans, United States Navy, Office of Naval Research.

Heidbach, O., Tingay, M., Barth, A., Reinecker, J., Kurfeß, D. and Müller, B. (2010). "Global crustal stress pattern based on the World Stress Map database release 2008." *Tectonophysics* 482(1–4): 3-15.

Heirtzler, J. R., Dickson, G. O., Herron, E. M., Pitman, W. C. and Le Pichon, X. (1968). "Marine magnetic anomalies, geomagnetic field reversals, and motion of the ocean and continents." *Journal of Geophysical Research* 73(6): 2119-2136.

Higgins, C. G. (1961). "San Andreas Fault north of San Francisco, California." *Geological Society of America Bulletin* 72: 51-68.

Hill, A. J. (1995). Source rock distribution and maturity modelling. *The petroleum geology of South Australia*. (Morton, J. G. G. and Drexel, J. F., Ed.). Volume 1: Otway Basin**:** 103-125.

Hill, E. J., Baldwin, S. L. and Lister, G. S. (1992). "Unroofing of active metamorphic core complexes in the D'Entrecasteaux Islands, Papua New Guinea." *Geology* 20(10): 907-910.

Hillis, R. R., Enever, J. R. and Reynolds, S. D. (1999). "In-situ Stress Field of Eastern Australia." *Australian Journal of Earth Sciences* 46: 813-825.

Hillis, R. R., Monte, S. A., Tan, C. P. and Willoughby, D. R. (1995). "The contemporary stress field of the Otway Basin, South Australia: Implications for hydrocarbon exploration and production." *Australian petroleum production and exploration association journal* 23: 494-506.

Hillis, R. R. and Muller, R. D. (2003). Evolution and Dynamics of the Australian Plate. Sydney, Geological Society of Australia Special Publication 22

Geological Society of America Special Paper 372.

Hillis, R. R. and Reynolds, S. D. (2000). "The Australian Stress Map." *Journal of the Geological Society, London* 157: 915-921.

Hillis, R. R. and Reynolds, S. D. (2003). "In situ stress field of Australia." *Geological Society of Australia Special Publication* 22: 49-58.

Hillis, R. R., Sandiford, M., Reynolds, S. D. and Quigley, M. C. (2008). "Present-day stresses, seismicity and Neogene-to-Recent tectonics of Australia's 'Passive' margins: intraplate deformation controlled by plate boundary forces." *Geological society, London, special publications* 306: 71-89.

Holcombe, R. (2009). "Structural Geology - Mapping/GIS Software." 2009, from http://www.holcombe.net.au/software/rodh_software.htm.

Holdsworth, R. E., Butler, C. A. and Roberts, A. M. (1997). "The recognition of reactivation

during continental deformation." *Journal of Geological Society, London* 154: 73-78.

Holdsworth, R. E., Handa, M., Miller, J. A. and Buick, I. S. (2001a). "Continental reactivation and reworking: an introduction." *Geological society, London, special publications* 184(1): 1-12.

Holdsworth, R. E., Stewart, M., Imber, J. and Strachan, R. A. (2001b). "The structure and rheological evolution of reactivated continental fault zones: a review and case study." *Geological society, London, special publications* 184(1): 115-137.

Honkura, Y., Isikara, A. M., Oshiman, N., Ito, A., Ucer, B., Baris, S., Tuncer, M. K., Matsushima, M., Pektas, M. and Celik, C. (2000). "Preliminary results of multidisciplinary observations before, during and after the Kocaeli (Izmit) earthquake in the western part of the North Anatolian Fault Zone." *Earth and Planetary Science Letters* 52(4): 293-298.

Horne, R. R. (1975). "Transverse fault systems in fold belts and oceanic fracture zones." *Nature* 255(5510): 620-621.

Houseman, G. and Molnar, P. (2001). "Mechanisms of lithospheric rejuvenation associated with continental orogeny." *Geological society, London, special publications* 184(1): 13-38.

Houston, H. and Vidale, J. E. (2007). "Earthquakes: Relationships in a slow slip." *Nature* 447(7140): 49-50.

Howchin, W. (1911). "Description of a disturbed area of Cainozoic rocks in South Australia, with remarks on its geological significance." *Transactions of the Royal Society of South Australia* 35: 47-59.

Howchin, W. (1926). "The geology of the Victor Harbour, Inman Valley, and Yankalilla Districts, with special reference to the great Inman Valley glacier of Permo-Carboniferous age." *Transactions of the Royal Society of South Australia* 50: 89-119.

Howell, B. F. (1984). "On the variation of seismic hazard along the San Andreas fault." *Bulletin of the Seismological Society of America* 74(2): 709-723.

Howman, D. (2011). Use of MALA GPR equipment for effective gorund surveying and best practises of post-processing. Jayawardena, C. L. Perth.

Hudson, M. R., Rosenbaum, J. G., Gromme, C. S., Scott, R. B. and Rowley, P. D. (1998). Paleomagnetic evidence for counter-clockwise rotation in a broad sinistral shear zone, Basin and Range province, southeastern Nevada and southwestern Utah. *Accommodation zones and transfer zones: The regional segmentation of the Basin and Range Province*. (Faulds, J. E. and Stewart, J. H., Ed.), Geological Society of America, Special Paper. 323**:** 149-180.

Huntley, D. J., Godfrey-Smith, D. I. and Thewalt, M. L. W. (1985). "Optical dating of sediments." *Nature* 313: 105-107.

Huntley, D. J., Hutton, J. T. and Prescott, J. R. (1993). "The stranded beach-dune sequence of south-east South Australia: A test of thermoluminescence dating, 0-800 Ka." *Quaternary Science Reviews* 12: 1-20.

Huntley, D. J., Hutton, J. T. and Prescott, J. R. (1994). "Further thermoluminescence dates from the dune sequence in south-east of South Australia." *Quaternary Science Reviews* 13: 201-207.

Hutton, J. T., Prescott, J. R., Bowman, J. R., Dunham, M. N. E., Crone, A. J., Machette, M. N. and Twidale, C. R. (1994). "Thermoluminescence dating of Australian palaeo-earthquakes." *Quaternary Science Reviews* 13(2): 143-147.

Hyde, R. S., Miller, H. G., Hiscott, R. N. and Wright, J. A. (1988). "Basin architecture and thermal maturation in the strike-slip Deer Lake Basin, Carboniferous of Newfoundland." *Basin Research* 1: 85-105.

Ihmle, P. F. and Jordan, T. H. (1994). "Teleseismic search for slow precursors to large earthquakes." *Science* 266: 1547-1551.

Jacobs, Z., Duller, G. A. T. and Wintle, A. G. (2003). "Optical dating of dune sand from Blombos Cave, South Africa: ii - single grain data." *Journal of Human Evolution* 44: 613-625.

Jacobs, Z., Duller, G. A. T. and Wintle, A. G. (2003b). "Optical dating of dune sand from Blombos Cave, South Africa: II—single grain

data." *Journal of Human Evolution* 44(5): 613-625.

Jacobs, Z., Duller, G. A. T. and Wintle, A. G. (2006). "Interpretations of single grain De distributions and calculation of De." *Radiation Measurements* 41: 264-277.

Jacobs, Z. and Roberts, R. G. (2007). "Advances in optically stimulated luminescence dating of individual grains of quartz from archeological deposits." *Evolutionary Anthropology: Issues, News, and Reviews* 16(6): 210-223.

Jacobs, Z., Wintle, A. G. and Duller, G. A. T. (2003a). "Optical dating of dune sand from Blombos Cave, South Africa: I—multiple grain data." *Journal of Human Evolution* 44(5): 599-612.

Jenkins, R. J. F. (1990). "The Adelaide Fold Belt: tectonic reappraisal." *Geological Society of Australia Special Publication* 16: 395-420.

Jenkins, R. J. F. and Sandiford, M. (1992). "Observations on the tectonic evolution of the southern Adelaide Fold Belt." *Tectonophysics* 214(1–4): 27-36.

Jol, H. M. (2009). Ground Penetrating Radar theory and applications. Amsterdam, Elsevier.

Jol, H. M., Lawton, D. C. and Smith, D. G. (2003). "Ground penetrating radar: 2-D and 3-D subsurface imaging of a coastal barrier spit, Long Beach, WA, USA." *Geomorphology* 53(1-2): 165-181.

Jones, C. H. and Wesnousky, S. G. (1992). "Variations in Strength and Slip Rate Along the San Andreas Fault System." *Science* 256(5053): 83.

Jonston, S. Y., Potter, C. J. and Armentrout, J. M. (1994). "Origin and evolution of the Seattle Fault and Seattle Basin, Washington." *Geology* 22: 71-74.

Kelly, P. G., Peacock, D. C. P., Sanderson, D. J. and McGurk, A. C. (1999). "Selective reverse-reactivation of normal faults, and deformation around reverse-reactivated faults in the Mesozoic of the Somerset coast." *Journal of Structural Geology* 21(5): 493-509.

Kemp, P. J. J. (1986). "The mid Cenozoic Challenger Rift System of western New Zealand and its implications for the age of Alpine Fault inception." *geological Society of America Bulletin* 97: 255-281.

Kennedy, W. Q. (1946). "The Great Glen Fault." *Quarterly Journal of the Geological Society of London* 102: 41-76.

Kermode, S. J. (2012). GPR surveying in the Shoalhaven River flood plains, Nowra, NSW-Australia. Jayawardena, C. L.

Kimber, R. W. L. and Milnes, A. R. (1984). "The extent of racemisation of amino acids in Holocene and Pleistocene marine molluscs in southern South Australia: Priliminary data on a time-frame-work for calcrete formation." *Australian Journal of Earth Sciences* 31: 279-286.

Klose, C. D. (2007). "Geomechanical modeling of the nucleation process of Australia's 1989 M5.6 Newcastle earthquake." *Earth and Planetary Science Letters* 256(3–4): 547-553.

Krishna, K. S., Bull, J. M. and Scrutton, R. A. (2001). "Evidence for multiphase folding of the central Indian Ocean lithosphere." *Geology* 29: 715-718.

Lanbo, L. and Yong, L. (2001). "Identification of liquefaction and deformation features using ground penetrating radar in the New Madrid seismic zone, USA." *Journal of Applied Geophysics* 47(3-4): 199-215.

Le Pichon, X. (1968). "Sea-floor spreading and continental drift." *Journal of Geophysical Research* 73(12): 3661-3697.

Lemon, N. M. and McGowran, B. (1989). Structural Development of the Willunga Embayment, St.Vincent Basin, South Australia. Field Excursion**:** 15.

Leonard, M. (2006). "One hundred years of earthquake recording in Australia." *Bulletin of the Seismological Society of America* 97.

Leucci, G. (2008). "Ground penetrating radar: The electromagnetic signal attenuation and maximum penetration depth." *Scholarly Research Exchange* 2008.

Lewis, K. B. (1980). "Quaternary sedimentaion on the Hikurangi oblique subduction and transform margin, New Zealand." *International association of*

sedimentologists special publication 4: 171-189.

Li, Z. X. and Powell, C. M. C. A. (1993). Late Proterozoic to Early Palaeozoic palaeomagnetism and the formation of Gondwanaland. *Gondwana*Ed.). Rotterdam, Balkema.

Lian, O. B. and Roberts, R. G. (2006). "Dating the Quaternary: progress in luminescence dating of sediments." *Quaternary Science Reviews* 25(19-20): 2449-2468.

Lian, O. B. and Scott, A. E. (2007a). Luminescence Dating | Thermoluminescence. *Encyclopedia of Quaternary Science*Ed.). Oxford, Elsevier**:** 1480-1491.

Lian, O. B. and Scott, A. E. (2007b). Luminescence Dating | Optically-Stimulated Luminescence. *Encyclopedia of Quaternary Science*Ed.). Oxford, Elsevier**:** 1491-1505.

Linde, A. T., Gladwin, M. T., S.;, J. M. J., Gwyther, R. L. and Bilham, R. B. (1996). "A slow earthquake sequence on the San Andreas Fault." *Nature* 383(6565): 65-68.

Lindsay, J. M. (1981). Tertiary stratigraphy and foraminifera of the Adelaide city area, St. Vincent Basin, South Australia. M.Sc., University of Adelaide.

Lindsay, J. M. (1986). New record and tectonic implication of a high level Lepidocyclina-bearing limestone, Bremer Vally, Eastern Mount Lofty Ranges, Department of Mines and Energy, Geological Survey.

Lindsay, J. M. and Alley, N. F. (1995). Tertiary. *Geology of South Australia*. (Drexel, J. F. and Preiss, W. V., Ed.), Geological survey - South Australia. 2**:** 163-172.

Lister, G. S., Forster, M. A. and Rawling, T. J. (2001). "Episodicity during orogenesis." *Geological society, London, special publications* 184(1): 89-113.

Lithgow-Bertelloni, C. and Guynn, J. H. (2004). "Origin of the lithospheric stress field." *Journal of Geophysical Research B: Solid Earth* 109(1): 1-32.

Liu, C. S., Curray, J. R. and McDonald, J. M. (1983). "New constraints on the tectonic evolution of the eastern Indian Ocean." *Earth and Planetary Science Letters* 65: 331-342.

Lopes Cardozo, G., Bada, G., Lankreijer, A. and Nieuwaland, D. (2002). "Analogue modelling of a prograding strike-slip fault: Case study of the Balatonfo Fault, western Hungary." *EGU Stephan Mueller Special Publication Series* 3: 217-226.

Love, D. N., Preiss, W. V. and Belperio, A. P. (1995). Seismicity, neotectonics and earthquake risk. *The geology of South Australia*. (Drexel, J. F. and Preiss, W. V., Ed.). 2**:** 268-270.

Ludbrook, N. H. (1961). "Stratigraphy of the Murray Basin in South Australia." *Geological Survey of South Australia Bullatin* 36.

Ludbrook, N. H. (1983). "Molluscan faunas of the early Pleistocene Point Ellen formation and Burnham Limestone, South Australia." *Transactions of the Royal Society of South Australia* 107: 37-49.

Ma, S. and Beroza, G. C. (2008). "Rupture Dynamics on a Bimaterial Interface for Dipping Faults." *Bulletin of the Seismological Society of America* 98(4): 1642-1658.

MALA-Geosciences (2009). MALA XV monitor for ProEX and X3M-Ethernet operating manual v.1.3. Geosciences, M. Skolgatan, MALA Geosciences.

Mancktelow, N. S. (1981). "Variation in fold axis geometry and slaty cleavage microfabric associated with a major fold arc, Fleurieu Peninsula, South Australia." *Journal of the Geological Society of Australia* 28(1-2): 1-12.

Mancktelow, N. S. (1990). "The structure of the southern Adelaide fold belt, South Australia." *Special Publications of Geological Society of Australia* 16: 369-395.

Mann, P. (2007b). "Global catalogue, classification and tectonic origins of restraining- and releasing bends on active and ancient strike-slip fault systems." *Geological society, London, special publications* 290(1): 13-142.

Mann, P., Demets, C. and Wiggins-Grandison (2007a). "Toward a better understanding of the late Neogene strike-slip restraining bend in Jamaica: geodetic, geological and seismic

constraints." *The Geological Society of London, special publication* 290: 239-253.

Mann, P., Draper, G. and Burke, K. (1985). "Neotectonics of a strike-slip restraining bend system, Jamaica." *The Society of Economic Paleontologists and Mineralogists*.

Manspeizer, W. (1985). "The Dead Sea Rift: Impact on climate and tectonism in Pleistocene and Holocene sedimentation." *Society of Economic Paleontology and Mineralogy special publication* 37: 143-158.

Marrett, R. and Allmendinger, R. W. (1990). "Kinematic analysis of fault-slip data." *Journal of Structural Geology* 12(8): 973-986.

Marshak, S. and Flöttmann, T. (1996). "Structure and origin of the Fleurieu and Nackara Arcs in the Adelaide fold-thrust belt, South Australia: Salient and recess development in the Delamerian Orogen." *Journal of Structural Geology* 18(7): 891-908.

May, R. I. (1992). Origin, mineralogy and diagenesis of Quaternary sediments from the Noarlunga and Willunga Embayments, South Australia. PhD, University of Adelaide.

May, R. I. and Bourman, R. P. (1984). "Coastal landslumping in the Pleistocene sediments at Sellicks beach, South Australia." *Transactions of the Royal Society of South Australia* 108: 85-94.

McCalpin, J. P. and Carver, G. (2009). Palaeoseismology - International Geophysics. (McCalpin, J. P., Ed.). Burlington, Academic Press**:** 315-419.

McClay, K. and Bonora, M. (2001). "Analog models of restraining stepovers in strike slip fault systems." *American Association of Petroleum Geologists Bulletin* 85(2): 233-260.

McCue, K. (1990). "Australia's large earthquakes and recent fault scarps." *journal of Structural Geology* 12: 761-766.

McCue, K., Gregson, P., Sinadinovski, C. and Hodgson, L. (1997). Earthquakes - Australian Seismological Report 1997, Geoscience Australia. 18.

McGarr, A. (1984). "Scalling of ground motion parameters, state of stress, and focal depth." *Journal of Geophysical Research* 89: 6969-6979.

McGowran, B. (1978a). "Early Tertiary foraminiferal biostratigraphy in southern Australia: A progressive report." *Bureau of Mineral Resources Journal of Australian Geology and Geophysics* 192: 83-95.

McGowran, B. (1978b). "Stratigraphic record of early Tertiary oceanic and continental events in the Indian Ocean region." *Marine Geology* 26: 1-39.

McKenzie, D. (1978). "Active tectonics of the Alpine—Himalayan belt: the Aegean Sea and surrounding regions." *Geophysical Journal of the Royal Astronomical Society* 55(1): 217-254.

McLaren, S. and Sandiford, M. (2001). "Long-term thermal consequences of tectonic activity at Mount Isa, Australia: Implications for polyphase tectonism in the Proterozoic." *Geological society, London, special publications* 184(1): 219-236.

McLaren, S., Sandiford, M., Hand, M., Neumann, N., Wyborn, L. and Bastrakova, I. (2003). The hot southern continent: heat flow and heat production in Australian Proterozoic terranes. *Evolution and dynamics of the Australian plate*. (Hillis, R. and Muller, R. D., Ed.), Geological Society of Australia Incorporated**:** 157-167.

McLennan, S. M. and Taylor, S. R. (1996). "Heat Flow and the Chemical Composition of Continental Crust." *The Journal of Geology* 104(4): 369-377.

McPherson, P. and Clark, D. (2011). Preliminary results of palaeoseismological investigations on the Para Fault**:** 8.

Meinesz, F. A. V. (1947). "Shear patterns in the earth's crust." *Transactions of the American Geophysical Union* 28: 1-61.

Mejdahl, V. (1979). "Thermoluminescence dating: beta-dose attenuation in quartz grains." *Archaeometry* 21: 61-72.

Merkouriev, S. and DeMets, C. (2006). "Constraints on Indian plate motion since 20 Ma from dense Russian magnetic data: Implications for Indian plate dynamics." *Geochemistry, Geophysics, Geosystems* 7(2): Q02002.

Miles, K. R. (1952). "Geology and underground water resources of the Adelaide

Plains area." *Geological Survey of South Australia Bullatin* 27.

Miller, J. M., Norvick, M. S. and Wilson, C. J. L. (2002). "Basement controls on rifting and the associated formation of ocean transform faults—Cretaceous continental extension of the southern margin of Australia." *Tectonophysics* 359(1–2): 131-155.

Miller, J. M., Norvick, M. S. and Wilson, C. J. L. (2002). "Basement controls on rifting and the associated formation of ocean transform faults - Cretaceous continental extension of the southern margin of Australia." *Tectonophysics* 359: 131-155.

Mills, K. J. (1965). The structural petrology of the Milendella area of South Australia. Ph.D., University of Adelaide.

Milnes, A. R. and Bourman, R. P. (1972). "A late Palaeozoic glaciated granite surface at Port Elliot, South Australia." *Transactions of the Royal Society of South Australia* 96: 151-155.

Mohriak, W. U. and Rosendahl, B. R. (2003). "Transform zones in the South Atlantic rifted continental margins." *Geological society, London, special publications* 210(1): 211-228.

Molnar, P. (1988). "Continental tectonics in the aftermath of plate tectonics." *Nature* 335: 131-137.

Molnar, P. and Tapponnier, P. (1975). "Cenozoic tectonics of Asis: Efects of a continental collision." *Science* 189: 419-426.

Moore, A. M. G., Stagg, H. M. J. and Norvick, M. S. (2000). "Deep-water Otway Basin: a new assessment of the tectonics and hydrocarbon prospectivity." *Australian petroleum production and exploration association journal* 40: 66-85.

Mote, T. I., Rothwell, M. and Bowden, A. (2011). Identification of neotectonic features in the Gladstone region, Central Queensland. Australian Earthquake Engineering Society. Barossa Valley, South Australia.

Müller, R. D., Dyksterhuis, S. and Rey, P. (2012). "Australian paleo-stress fields and tectonic reactivation over the past 100 Ma." *Australian Journal of Earth Sciences* 59(1): 13-28.

Muller, R. D., Gaina, C., Tikku, A., Mihut, D., Cande, S. C. and Stock, J. M. (2000a). Mesozoic/Cenozoic tectonic events around Australia. *The History and Dynamics of Global Plate Motions*Ed.). Washington, DC, AGU. 121**:** 161-188.

Muller, R. D., Roest, W. R. and Royer, J. (1998). "Asymmetric sea-floor spreading caused by ridge-plume interactions." *Nature* 396(December): 455-459.

Murray-Wallace, C. V. (2002). "Pleistocene coastal stratigraphy, Sea-level highstands and Neotectonism of the Southern Australian passive continental margin - A Review." *Journal of Quaternary Sciences* 17: 469-489.

Murray-Wallace, C. V. and Belperio, A. P. (1991). "The Last interglacial shoreline in Australia - A review." *Quaternary Science Reviews* 10: 441-461.

Murray-Wallace, C. V. and Bourman, R. P. (2002). "Amino acid racemisation dating of a raised gravel beach deposit, Sellicks beach, South Australia." *Transactions of the Royal Society of South Australia* 126(1): 21-28.

Murray, A. S. and Roberts, R. G. (1998). "Measurement of the equivalent dose in quartz using a regenerative-dose single-aliquot protocol." *Radiation measurements* 29: 503-515.

Murray, A. S. and Wintle, A. G. (2000). "Luminescence dating of quartz using improved single-aliquot regenerative-dose protocol." *Radiation measurements* 32(57-73).

Nanson, G. C., Callen, R. A. and Price, D. M. (1998). "Hydroclimatic interpretation of Quaternary shorelines on South Australian playas." *Palaeogeography, Palaeoclimatology, Palaeoecology* 144(3–4): 281-305.

Neal, A. (2004). "Ground-penetrating radar and its use in sedimentology: principles, problems and progress." *Earth-Science Reviews* 66(3–4): 261-330.

Nemser, E. S. and Cowan, D. S. (2009). "Downdip segmentation of strike-slip fault zones in the brittle crust." *Geology* 37(5): 419-422.

Neumann, N., Sandiford, M. and Foden, J. (2000). "Regional geochemistry and

continental heat flow: implecations for the origin of the South Australian heat flow anomaly." *Earth and Planetary Science Letters* 183: 107-120.

Neumann, N., Sandiford, M. and Foden, J. (2000). "Regional geochemistry and continental heat flow: implications for the origin of the South Australian heat flow anomaly." *Earth and Planetary Science Letters* 183(1–2): 107-120.

Norvick, M. S. and Smith, A. M. (2001). "Mapping the plate tectonic re-construction of southern and southeastern Australia and implications for petroleum systems." *Australian petroleum production and exploration association journal* 41: 15-35.

Offler, R. and Fleming, P. D. (1968). "A synthesis of folding and metamorphism in the Mt Lofty Ranges, South Australia." *Geological Society of Australia Journal* 15: 245-266.

Offler, R., Och, D. J., Phelan, D. and Zwingmann, H. (2009). "Mineralogy of gouge in north-northeast striking faults, Sydney region, New South Wales." *Australian Journal of Earth Sciences* 56: 889-905.

Okal, E. A. and Stewart, L. M. (1982). "Slow earthquakes along oceanic fracture zones: evidence for asthenospheric flow away from hotspots?" *Earth and Planetary Science Letters* 57(1): 75-87.

Olley, J. M., Caircheon, G. G. and Roberts, R. G. (1999). "The origin of dose distribution in fluvial sediments and the prospect of dating single grains from fluvial deposits using optically stimulated luminescence." *Radiation measurements* 30: 207-217.

Olley, J. M., Pietsch, T. and Roberts, R. G. (2004). "Optical dating of Holocene sediments from a variety of geomorphic settings using single grains of quartz." *Geomorphology* 60: 337-358.

Ollier, C. D. (2006). "Mountain uplift and the neotectonic period." *Annals of Geophysics* 49(N 1): 14.

Papazachos, B. C., Savvaidis, A. S., Karakaisis, G. F. and Papazachos, C. B. (2002). "Precursory accelerating seismic crustal deformation in the Northwestern Anatolia Fault Zone." *Tectonophysics* 347: 217-230.

Passchier, C. W., Zhang, J. S. and Konopasek, J. (2005). "Geometric aspects of synkinematic granite intrusion into a ductile shear zone - an example from Yunmengshan core complex, northern China." *Geological society, London, special publications* 245: 65-80.

Paul, E. G. (1998). The geometry and controls on basement-involved deformation in the Adelaide Fold Belt, South Australia. PhD, University of Adelaide.

Paul, E. G., Flo¨ttmann, T. and Sandiford, M. (1999). "Structural geometry and controls on basement-involved deformation in the northern Flinders Ranges, Adelaide Fold Belt, South Australia." *Australian Journal of Earth Sciences* 46: 343-354.

Paul, E. G., Sandiford, M. and Flo¨ttmann, T. (2000). "Structural geometry of a thick-skinned fold-thrust belt termination: the Olary Block in the Adelaide Fold Belt, South Australia." *Australian Journal of Earth Sciences* 47: 281-289.

Pavlides, S. B., Zhang, P. and Pantosti, D. (1999). "Earthquake, active faulting, and paleoseismological studies for the reconstruction of the seismic history of faults." *Tectonophysics* 308(1-2): vii-x.

Peltzer, G. and Tapponnier, P. (1988). "Formation and evolution of strike-slip faults, rifts, and basins during India-asia collision: an experimental approach." *Journal of Geophysical Research* 93: 15085-15172.

Peng, Z. and Gomberg, J. (2010). "An integrated perspective of the continuum between earthquakes and slow-slip phenomena." *Nature Geoscience* 3(Sep 2010): 599-607.

Phillips, S. E. and Milnes, A. R. (1988). "The Pleistocene terrestrial carbonate mantle on the southeastern margin of the St Vincent Basin, South Australia." *Australian Journal of Earth Sciences: An International Geoscience Journal of the Geological Society of Australia* 35(4): 463-481.

Pigram, C. J. and Symonds, P. A. (1991). "A review of the timing of the major tectonic events in the New Guinea Orogen." *Journal of*

Southeast Asian Earth Sciences 6(3–4): 307-318.

Pillans, B. and Bourman, R. P. (1996). "The Brunhes/Matuyama polarity transition (0.78 Ma) as a chronostratigraphic marker in Australian regolith studies." *AGSO Journal of Australian Geology & Geophysics* 16(3): 289-294.

Pillans, B. and Bourman, R. P. (2001). "Mid Pleistocene Arid Shift in South Australia, Dated by Magnetostratigraphy." *Australian Journal of Soil Research* 39(2001): 89-98.

Pizzi, A. and Scisciani, V. (2000). "Methods for determining the Pleistocene–Holocene component of displacement on active faults reactivating pre-Quaternary structures: examples from the Central Apennines (Italy)." *Journal of Geodynamics* 29(3–5): 445-457.

Pledge, N. S., Prescott, J. R. and Hutton, J. T. (2002). "A late Pleistocene occurrence of Diprotodon at Hallett Cove, South Australia." *Transactions of the Royal Society of South Australia* 126: 39-44.

Preiss, W. V. (1986). Adelaide Geosyncline and Steward shelf:Precambrian and Palaeozoic Geology (with special reference to the Adelaidean)). 1:600 000 scale, Department of Mines and Energy, Adelaide.

Preiss, W. V. (1987). "The Adelaide Geosyncline - late Proterozoic stratigraphy, sedimentation, palaeontology and tectonics." *Geological Survey of South Australia Bullatin* 53.

Preiss, W. V. (1993). Geology of South Australia, Mines and Energy, South Australia.

Preiss, W. V. (1995). "RbSr dating of differentiated cleavage from the upper Adelaidean metasediments at Hallett Cove, southern Adelaide fold belt: Discussion." *Journal of Structural Geology* 17(12): 1797-1800.

Preiss, W. V. (1999). Parachilna, South Australia. 1:250000 Geological Series - Explanatory Notes, Primary Industries and Resources SA, Adelaide.

Preiss, W. V. (2008). New oppertunities in the Delamerian Orogen of South Australia. South Australian Resources and Energy Investment Conference. Adelaide.

Prescott, J. R. and Hutton, J. T. (1994). "Cosmic ray contributions to dose rates for luminescence and ESR dating: large depths and long-term time variations." *Radiation measurements* 23: 497-500.

Preusser, F., Chithambo, M. L., Gotte, T., Martini, M., Ramseyer, K., Sendezera, E. J., Susino, G. J. and Wintle, A. G. (2009). "Quartz as a natural luminescence dosimeter." *Earth Science Reviews* 97: 184-214.

Puchkov, V. N. (2009b). "The controversy over plumes: Who is actually right?" *Geotectonics* 43(1): 1-17.

Quigley, M. C. (2006). Continental tectonics and landscape evolution in south-central Australia and southern Tibet. Ph. D., University of Melbourne.

Quigley, M. C., Clark, D. and Sandiford, M. (2010). "Tectonic geomorphology of Australia." *Geological Society London Special Publication* 346: 243-265.

Quigley, M. C., Cupper, M. L. and Sandiford, M. (2006). "Quaternary faults of South-Central Australia: palaeoseismicity, slip rates and origin." *Australian Journal of Earth Sciences* 53: 285-310.

Quigley, M. C., Sandiford, M. and Cupper, M. L. (2007c). "Distinguishing tectonic from climatic controls on range-front sedimentation." *Basin Research*.

Quigley, M. C., Sandiford, M., Fifield, L. K. and Alimanovic, A. (2007a). "Landscape responses to intraplate tectonism: Quantitative constraints from Be nuclide abundances." *Earth and Planetary Science Letters* 261: 120-133.

Quigley, M. C., Sandiford, M., Fifield, L. K. and Alimanovic, A. (2007b). "Bedrock erosion and relief production in the northern Flinders Ranges, Australia." *Earth Surface Processes and Landforms* 32: 929-944.

Quinlan, G. M. and Beaumont, C. (1984). "Appalachian thrusting, lithospheric flexure, and the Paleozoic stratigraphy of the Eastern Interior of North America." *Canadian Journal of Earth Sciences* 21(9): 973-996.

Ranalli, G. (1974). "Tectonic role of oceanic fracture zones." *Marine Geology* 17(1): M27-M34.

Rankin, D. W. (1975). "The continental margin of eastern north America in the Southern Appalachians: The opening and closing of the proto-Atlantic Ocean." *American Journal of Science* 275(A): 298-336.

Rashed, M., Kawamura, D., Nemoto, H., Miyata, T. and Nakagawa, K. (2003). "Ground penetrating radar investigations across the Uemachi fault, Osaka, Japan." *Journal of Applied Geophysics* 53(2-3): 63-75.

Raymo, M. E. and Ruddiman, W. F. (1992). "Tectonic forcing of late Cenozoic climate." *Nature* 359: 117-122.

Reading, H. G. (1980). Characteristics and Recognition of Strike-Slip Fault Syatems. *Sedimentation in Oblique-Slip Mobile Zones*. (Ballance, P. F. and Reading, H. G., Ed.). Melbourne, Blackwell Scientific Publications. 4**:** 7-26.

Reid, B. (2007). A neotectonic study of the Willunga and Milendella faults, South Australia. B.Sc. (Hons), University of Melbourne.

Reynolds, M. A. (1953). "The Cainozoicsuccession of Maslin and Aldinga bays, South Australia." *Transactions of the Royal Society of South Australia* 76: 114-140.

Reynolds, S. D. (2001). Characterization and modelling of the regional insitu stress field of continental Australia. PhD, Adelaide University.

Reynolds, S. D., Coblentz, D. D. and Hillis, R. R. (2003). "Influences of plate-boundary forces on the regional intraplate stress field of continental Australia." *Geological Society of Australia Special Publication* 22: 59-70.

Richard, P. D., Naylor, M. A. and Koopman, A. (1995). "Experimental models of strike-slip tectonics." *Petroleum Geoscience* 1(1): 71-80.

Richardson, R. M. (1992). "Ridge forces, absolute plate motions, and the intraplate stress field." *Journal of Geophysical Research* 97(11739-11748).

Riggs, N. (2011). GPR surveying of the southern coastal New South Whales and selected regions of Tasmania, Australia. Jayawardena, C. L.

Riordan, S. J. (2009). Characterization of Adelaidean rocks as potential geothermal reservoirs. PIRSA project TIG, University of Adelaide. 4.3**:** 37.

Roberts, E. A. and Houseman, G. A. (2001). "Geodynamics of central Australia during the intraplate Alice Springs Orogeny: thin viscous sheet models." *Geological society, London, special publications* 184(1): 139-164.

Roberts, R. G. (1997). "Luminescence dating in archaeology: from origins to optical." *Radiation measurements* 27: 819-892.

Roberts, R. G., Galbraith, R. F., Yoshida, H., Laslett, G. M. and Olley, J. M. (2000). "Distinguishing dose populations in sediment mixtures: a test of single-grain optical dating procedures using mixtures of laboratory-dosed quartz." *Radiation Measurements* 32(5–6): 459-465.

Roberts, R. G., Yoshida, H., Galbraith, R., Laslett, G., Jones, R. and Smith, M. (1998). "Single-aliquot and single-grain optical dating confirm thermoluminescence age estimates at Malakunanja II rock shelter in northern Australia." *Ancient TL* 16: 19-24.

Rossetti, D. F. (2003). "Delineating shallow Neogene deformation structures in northeastern Pará State using Ground Penetrating Radar." *Anais da Academia Brasileira de Ciências* 75: 235-248.

Rowett, A. I. (1997). Preliminary report of palaeodrainage in the St Vincent Basin and Mt Lofty Ranges, South Australia. Department of Mines and Energy, Report Book. 25.

Royden, L. H. (1985). The Vienna Basin: a thin-skinned pull-apartbasin. *Strike-slip deformation, sedimentation, basin formation*. (Biddle, K. T. and Christie-Blick, N., Ed.)**:** 319-338.

Royer, J. Y. and Rollet, N. (1997). "Plate-tectonic setting of the Tasmanian region." *Australian Journal of Earth Sciences* 44: 543-560.

Ruedemann, R. (1922). The Existence and Configuration of Precambrian Continents, University of the State of New York.

Sandiford, M. (1989). "Horizontal structures in granulite terrains: A record of mountain

building of mountain collapse?" *Geology* 17: 449-452.

Sandiford, M. (2003a). "Neotectonics of southeastern Australia: Linking the Quaternary faulting record with seismicity and In-situ stress." *Geological Society of Australia* Special Publication(22): 101-113.

Sandiford, M. (2003a). "Neotectonics of southeastern Australia: linking the Quaternary faulting record with seismicity and in situ stress." *Geological Society of America Special Papers* 372: 107-119.

Sandiford, M. (2003b). "Geomorphic Constraints on the Late Neogene Tectonics of the Otway Range, Victoria." *Australian Journal of Earth Sciences* 50: 69-80.

Sandiford, M. (2010a). "Geodynamics: Complex subduction." *Nature Geoscience* 3(8): 518-520.

Sandiford, M., Coblentz, D. D. and Richardson, R. M. (1995). "Focusing ridge-torque during continental collision in the Indo-Australian plate." *Geology* 23: 653-656.

Sandiford, M., Coblentz, D. D. and Schellart, W. P. (2005). "Evaluating slab-plate coupling in the Indo-Australian Plate." *Geology* 33: 113-116.

Sandiford, M., Foden, J., Zhou, S. and Turner, S. P. (1992). "Granite genesis and the mechanics on convergent orogenic belts with application to the southern Adelaide Fold Belt." *Geological Society of America, Special Paper* 273: 83-93.

Sandiford, M. and Hand, M. (1998). "Controls on the locus of Phanerozoic intraplate deformation in central Australia." *Earth and Planetary Science Letters* 162: 97-110.

Sandiford, M. and McLaren, S. (2002). "Tectonic feedback and the ordering of heat producing elements within the continental lithosphere." *Earth and Planetary Science Letters* 204: 133-150.

Sandiford, M., Paul, E. and Flo¨ttmann, T. (1998b). "Sedimentary thickness variations and deformation intensity during basin inversion in the Flinders Ranges, South Australia." *Journal of Structural Geology* 20(12): 1721-1731.

Sandiford, M. and Quigley, M. C. (2009a). "TOPO-OZ: Insights into the various modes of intraplate deformation in the Australian continent." *Tectonophysics* 474(1–2): 405-416.

Sandiford, M. and Quigley, M. C. (2009a). "TOPO-OZ: Insights into the various modes of intraplate deformation in the Australian continent." *Tectonophysics* Article in press.

Sandiford, M., Quigley, M. C., De Broekert, P. and Jakica, S. (2009b). "Tectonic framework for the Cenozoic cratonic basins of Australia." *Australian Journal of Earth Sciences* 56: S5-S18.

Sandiford, M., Wallace, M. and Coblentz, D. D. (2004). "Origin of the in situ stress field in South-Eastern Australia." *Basin Research* 16: 325-338.

Schellart, W. P., Freeman, J., Stegman, D. R., Moresi, L. and May, D. (2007). "Evolution and diversity of subduction zones controlled by slab width." *Nature* 446(March): 308-311.

Schmidt, S., Tsukamoto, S., Salomon, E., Frechen, M. and Hetzel, R. (2012). "Optical dating of alluvial deposits at the orogenic front of the andean precordillera (Mendoza, Argentina)." *Geochronometria* 39(1): 62-75.

Schultz, S. S., Mavko, G. M., Burford, R. O. and Stuart, W. D. (1982). "Long-term fault creep observations in central California." *Journal of Geophysical Research* 87: 6977-6982.

Schwartz, M. O. and Askury, A. K. (1989). "Geologic, geochemical, and fluid inclusion studies of the tin granites from the Bujang Melaka Pluton, Kinta Valley, Malaysia." *Economic Geology* 84(4): 751-779.

Selby, J. and Lindsay, J. M. (1982). "Engineering geology of the Adelaide city area." *Geological Survey of South Australia Bullatin* 51: 121.

Shackleford, P. R. J. and Sutton, D. J. (1981). "A first interpretation of crustal structure in the Adelaide Geosyncline in South Australia using quarry blasts." *Journal of the Geological Society of Australia* 28: 491-500.

Shaw, R. D., Zeitler, P. K., McDougall, I. and Tingate, P. R. (1992). "The Paleozoic history of an unsual intracratonic thrust belt in central

Australia based on 40Ar-39Ar, K-Ar and fission track dating." *Journal of Geological Society, London* 149: 937-954.

Sheard, M. J. (2009). Explanatory notes for Callabonna 1:250000 geological map, sheet SH 54-6, South Australia, Department of Primary Industries and Resources. Report Book 2009/01.

Sheard, M. J. and Bowman, G. M. (1987). "Definition of the Keswick Clay, Adelaide/Golden Grove Embayment, Para and Eden blocks, South Australia." *Geological survey of South Australia quaterly geological notes* 103: 4-9.

Sheard, M. J. and Bowman, G. M. (1996). Soils, stratigraphy and engineering geology of the near surface materials of the Adelaide Plains.

Shearsmith (2011). Industrial applications of MALA GPR unit and field observations. Jayawardena, C. L. Perth.

Shelkoplyas, V. N. and Morozov, G. V. (1965). Some results of an investigation of Quaternary deposits by the thermoluminescence method. 7th International Quaternary Association Congress, Keiv.

Sieh, K. E. (1978a). Geological studies of the Holocene behaviour of the San Andreas Fault, California. California, California institute of technology, Pasadena.

Sinadinovski, C., Greenhalgh, S. A. and Love, D. (2006). Historical earthquakes: A case study for the Adelaide 1954 earthquake. Australian Earthquake Engineering Society. Conference (2006 : Canberra, A.C.T.). Canberra, Australian Earthquake Engineering Society**:** 151-158.

Singhvi, A. K., Banerjee, D., Pande, K., Gogte, V. and Valdiya, K. S. (1994). "Luminescence studies on neotectonic events in south-central Kumaun Himalaya -- a feasibility study." *Quaternary Science Reviews* 13(5-7): 595-600.

Smith, D. G. and Jol, H. M. (1995). "Ground penetrating radar: antenna frequencies and maximum probable depths of penetration in Quaternary sediments." *Journal of Applied Geophysics* 33(1-3): 93-100.

Smith, P. J. (1976). "Transform faults to spreading offsets." *Nature* 260(March): 13-14.

Spitzak, S. and DeMets, C. (1996). "Constraints on present-day plate motions south of 30°S from satellite altimetry." *Tectonophysics* 253: 167-208.

Sprigg, R. C. (1942). "The geology of the Eden-Moana fault block." *Transactions of the Royal Society of South Australia* 66(2): 185-215.

Sprigg, R. C. (1945). "Some aspects of the geomorphology of a portion of the Mount Lofty Ranges." *Transactions of the Royal Society of South Australia* 69: 227-304.

Sprigg, R. C. (1946). "Reconnaissance geological survey of portion of the Western escarpment of the Mount Lofty Ranges." *Transactions of the Royal Society of South Australia* 70(2): 313-346.

Stackler, W. F. (1963). Milang gravity survey, South Australia (Transcurrent offset of Permian Valley), Geosurveys of Australia Limited**:** 10.

Stagg, H. M. J., Cockshell, C. D., Willcox, J. B., Hill, A. J., Needham, D. J. L., Thomas, B., O'brien, G. W. and Hough, L. P. (1990). Basins of the Great Australian Bight Region: Geology and Petroleum Potential. Continental margins Program. 5.

Stephenson, R. and Lambeck, K. (1985). "Isostatic response of the lithosphere with in-plane stress: Application of Central Australia." *Journal of Geophysical Research* 90: 77-85.

Stevens, B. P. J. and Corbett, G. J. (1993). "The Redan geophysical zone; part of the Willyama Supergroup? Broken Hill, Australia." *Australian Journal of Earth Sciences* 40: 319-338.

Stevens, C. W., Moorman, B. J., Solomon, S. M. and Hugenholtz, C. H. (2009). "Mapping subsurface conditions within the near-shore zone of an Arctic delta using ground penetrating radar." *Cold Regions Science and Technology* 56(1): 30-38.

Stewart, I. C. F. (1972). "Seismic interpretation of crustal structure in the Flinders - Mt Lofty ranges and Gulf regions, South Australia." *Journal of the Geological Society of Australia* 19(3): 351-362.

Stewart, I. C. F. (1976). "Fractures and movement in the Adelaide rift zone." *Nature* 264: 198-199.

Stewart, I. C. F. and Mount, T. J. (1972). "Earthquake mechanisms in South Australia in relation to plate tectonics." *Journal of the Geological Society of Australia* 19(1): 41-52.

Stewart, I. C. F. and Sutton, D. J. (1971). "The South Australian earthquake of January 7, 1971 and aftershocks." *Journal of the Geological Society of Australia* 18(3): 201-205.

Stiros, S. C. (1988). "Model for the northern Peloponnesian (central Greece) uplift." *Journal of Geodynamics* 9: 199-214.

Stokes, S., Ingram, S., Aitken, M. J., Sirocko, F., Anderson, R. S. and Leuschner, D. (2003). "Alternative chronologies for late Quaternary (Last Interglacial-Holocene) deep sea sediments via optical dating of silt-sized quartz." *Quaternary Science Reviews* 22: 925-941.

Storti, F., Holdsworth, R. E. and Salvini, F. (2003). "Intraplate strike-slip deformation belts." *Geological society, London, special publications* 210(1): 1-14.

Stubley, M. P. (1990). "The geometry and kinematics of a suite of conjugate kink bands, southeastern Australia." *Journal of Structural Geology* 2(8): 1019-1031.

Suntharalingam (2011). How to improve the results with post-processing of a GPR profile obtained from a MALA branded GPR. Jayawardena, C. L. Perth.

Sutton, D. J. (1976). "Deformation within continental plates." *Nature* 260(March): 15-16.

Sutton, D. J. and White, R. E. (1968). "The seismicity of South Australia." *Journal of the Geological Society of Australia* 15: 25-32.

Switzer, A. D., Bristow, C. S. and Jones, B. G. (2006). "Investigation of large-scale washover of a small barrier system on the southeast Australian coast using ground penetrating radar." *Sedimentary Geology* 183(1-2): 145-156.

Sykes, L. R. and Sbar, M. L. (1973). "Intraplate earthquakes, lithospheric stresses and the driving mechanism of plate tectonics." *Nature* 245: 298-302.

Sylvester, A. G. (1988). "Strike-slip faults." *Geological Society of America Bulletin* 100(11): 1666-1703.

Talbot, J. L. and Nesbitt, R. W. (1968). Geological excursions in the Mount Lofty Ranges and the Fleurieu Peninsula, Angus and Robertson.

Taylor, H. (2010). Recognising active faults in regions of rapid resurfacing - A Ground Penetrating Radar (GPR) approach. M.Sc., University of Auckland.

Taylor, H. (2010). Recognising active faults in regions of rapid resurfacing - A ground penetrating radar approach. M. Sc., Univeristy of Auckland.

Thatcher, W. (1995). "Microplate versus continuum descriptions of active tectonic deformation." *Journal of Geophysical Research* 100: 3885-3894.

The Sydney Morning Herald. (2007). "Quake fears for new Adelaide hospital." Retrieved 03-10-2012, from http://www.smh.com.au/news/National/Quake-fears-for-new-Adelaide-hospital/2007/08/13/1186857416300.html.

Thomas, M., Jonathan, D. A. C., Gostin, V. A. and Williams, G. E. (2012). The Flinders Ranges and sorrounds, South Australia: a window on astrobiology and planetary geology.

Thomson, B. P. (1969a). Adelaide 1:25000 geological series map sheet, Department of Mineral Resources, South Australia.

Thomson, B. P. (1969b). Precambrian basement cover - the Adelaide system. *Handbook of South Australian Geology*. (Parkin, L. W., Ed.), Geological Survey of South Australia. 1**:** 49-83.

Titus, S. J., Dem, C. and Tikoff, B. (2005). "New slip rate estimates for the creeping segment of the San Andreas Fault, California." *Geology* 33(3): 205-208.

Toft, M. (2011). Lack of penetration of GPR signal and possible equipment errors. Jayawardena, C. L. Wollongong, Adelaide.

Tokarev, V. (2005). Neotectonics of the Mount Lofty Ranges (South Australia). PhD thesis, University of Adelaide.

Tokarev, V., Sandiford, M. and Gostin, V. (1999). "Landscape evolution in the Mount Lofty Ranges: implications for regolith development.": 131-139.

Toshioka, T., Tsuchida, T. and Sasahara, K. (1995). "Application of GPR to detecting and mapping cracks in rock slopes." *Journal of Applied Geophysics* 33(1-3): 119-124.

Twidale, C. R. and Bourne, J. A. (1975). "Geomorphological evolution of part of the eastern Mount Lofty Ranges, South Australia." *Transactions of the Royal Society of South Australia* 99(4): 197-209.

Twidale, C. R. and Bourne, J. A. (2004). "Neotectonism in Australia: its expressions and implications / Néotectonique en Australie : ses manifestations et ses implications." *Géomorphologie : relief, processus, environnement*: 179-193.

Twidale, C. R. and Campbell, E. M. (1995). "Pre-Quaternary landforms in the low latitude context: the example of Australia." *Geomorphology* 12: 17-35.

Valenzuela, R. W. and Wysession, M. E. (1993). "Intraplate earthquakes in the southwest Pacific ocean basin and the seismotectonics of the southern Tasman Sea." *Geophys. Res. Lett* 20: 2467-2470.

van der Pluijm, B. A., Hall, C. M., Vrolijk, P. J., Pevear, D. R. and Covey, M. C. (2001). "The dating of shallow faults in the Earth's crust." *Nature* 412(6843): 172-175.

Vassallo, R., Ritz, J. F., Braucher, R., Jolivet, M., Carretier, S., Larroque, C., Chauvet, A., Sue, C., Todbileg, M., Bourles, D., Arzhannikova, A. and Arzhannikov, S. (2007). "Transpressional Tectonics and Stream Terrace of the Gobi-Altay, Mongolia." *Tectonics* 26.

Veevers, J. J. (1980). Basins of the Australian craton and margin - Dynamics of plate interiors. Washington D.C.

Veevers, J. J. (2000). Billion-year earth history of Australia and neighbours in Gondwanaland. North Ryde, N.S.W., Gemoc Press.

Vernant, P., Hivert, F., Chéry, J., Steer, P., Cattin, R. and Rigo, A. (2013). "Erosion-induced isostatic rebound triggers extension in low convergent mountain ranges." *Geology* 41(4): 467-470.

Vidale, J. E. and Houston, H. (2012). "Slow slip: A new kind of earthquake." *Physics Today* 65(1): 38-43.

Villamor, P. and Berryman, K. R. (2006). "Late Quaternary geometry and kinematics of faults at the southern termination of the Taupo Volcanic Zone." *New Zealand journal of geology and geophysics* 49(1): 1-21.

von der Borch, C. C. (1980). "Evolution of late Proterozoic to early Paleozoic Adelaide fold belt, Australia: Comparisons with post-Permian rifts and passive margins." *Tectonophysics* 70: 115-134.

Walker, M. (2005). Quaternary dating methods. West Sussex, John Wiley & Sons.

Wallace, R. E. (1970). "Earthquake Recurrence Intervals on the San Andreas Fault." *Geological Society of America Bulletin* 81(10): 2875-2890.

Wallinga, J. (2002). "Optically stimulated luminescence dating of fluvial deposits: a review." *Boreas* 31(4): 303-322.

Ward, W. T. (1965). "Eustatic and climatic history of the Adelaide area, South Australia." *Journal of Geology* 73: 592-602.

Ward, W. T. (1966). Geology, geomorphology and soils of the south-western part of county Adelaide, South Australia. CSIRO Soil Publication. Melbourne. 23**:** 115.

Watchman, A. L. and Twidale, C. R. (2002). "Relative and 'absolute' dating of land surfaces." *Earth Science Reviews* 58: 1-49.

Webb, B. P. (1957). "Summary of the tectonics and sedimentation." *Journal of the Geological Society of Australia* 5: 136-148.

Webb, G. W. (1969). Paleozoic wrench faults in the Canadian Appalachians. *North Atlantic Geology and Continental Drift*. (Kay, M., Ed.). 40**:** 457-476.

Weissenberg, K. (1947). "Continuum theory of rheological phenomena." *Nature* 159: 310-311.

Wellman, P. and Greenhalgh, S. A. (1988). "Flinders/Mount Lofty Ranges, South Australia. Their uplift, erosion and relationship to crustal structure." *Transactions of the Royal Society of South Australia* 112(1): 11-19.

Wernicke, B. (1992). Cenozoic extensional tectonics of the U.S. Cordillera. *The Cordilleran Orogen: Conterminous U.S., The Geology of North America*. (Burchfiel, B. C., Lipman, P. W. and Zoback, M. L., Ed.). Boulder, Colorado, Geological Society of America**:** 553-582.

Wesnousky, S. G. (1986). "Earthquakes, quaternary faults, and seismic hazard in California." *Journal of Geophysical Research: Solid Earth* 91(B12): 12587-12631.

Wesnousky, S. G. (1988). "Seismological and Structural evolution of strike-slip faults." *Nature* 335(22): 340-343.

Wesnousky, S. G. and Jones, C. H. (1994). "Oblique slip, slip partitioning, spatial and temporal changes in the regional stress field, and the relative strength of active faults in the Basin and Range, Western United States." *Geology* 22(November): 1031-1034.

Whitney, B. and Hengesh, J. (2011). Neotectonic deformation in the Stable Continental Region of Western Australia: Paleoseismology of the Mt. Narryer fault zone. Australian New Zealand Geomorphology Group Conference, Oamaru, New Zealand.

Whittaker, A. C. and Boulton, S. J. (2012). "Tectonic and climatic controls on knickpoint retreat rates and landscape response times." *Journal of Geophysical Research: Earth Surface* 117(F2): F02024.

Wilcox, R. E., Harding, T. P. and Seely, D. R. (1973). "Basic wrench tectonics." *Association of petroleum geologists bulletin* 57(1): 74-96.

Willcox, J. B. and Stagg, H. M. J. (1990). "Australia's southern margin: a product of oblique extension." *Tectonophysics* 173(1–4): 269-281.

Williams, B. B. (2007). Tectonic geomorphology of mountains: A new approach to paleoseismology. Malden, Blackwell.

Williams, G. E. (1973). "Late Quaternary piedmont sedimentation, soil formation and palaeoclimates in arid South Australia." *Zeit Geomorphologie* 17(1): 102-125.

Williams, G. E. and Goode, A. D. T. (1978). "Possible western outlet for an ancient Murray River in South Australia." *Search* 9.

Wilson, J. T. (1965). "A new class of faults and their bearing on continental drift." *Nature* 207(July): 343-347.

Wintle, A. G. (2008). "Luminescence dating: where it has been and where it is going." *Boreas* 37: 471-482.

Wintle, A. G. and Murray, A. S. (2006). "A review of quartz optically stimulated luminescence characteristics and their relevance in single aliquot regeneration dating." *Radiation measurements* 41: 369-391.

Wolin, E., Stein, S., Pazzaglia, F., Meltzer, A., Kafka, A. and Berti, C. (2012). "Mineral, Virginia, earthquake illustrates seismicity of a passive-aggressive margin." *Geophysical Research Letters* 39: 1-7.

Woodcock, N. H. and Fischer, M. (1986). "Strike-slip duplexes." *Journal of Structural Geology* 8(7): 725-735.

Yassaghi, A., James, P. R., Flöttmann, T. and Winsor, C. N. (2004). "P–T conditions and kinematics of shear zones from the southern Adelaide Fold-Thrust Belt, South Australia: Insights into the dynamics of a deeply eroded orogenic wedge." *Australian Journal of Earth Sciences* 51(2): 301-317.

Zhang, K., Liu, K. and Yang, J. (2004). "Asymmetrical valleys created by the geomorphic response of rivers to strike-slip fault." *Quaternary Research* 62(3): 310-315.

Zoback, M. L., Zoback, M. D., Adams, J., Assumpcao, M., Bell, S., Bergman, E. A., Blumling, P., Bereton, N. R., Denham, D., Ding, J., Fuchs, K., Gay, N., Gregersen, S., Gupta, H. K., Gvishiani, A., Jacob, K., Klein, R., Knoll, P., Magee, M., Mercier, J. L., Muller, B. C., Paquin, C., Rajendran, K., Stephansson, O., Suarez, G., Suter, M., Udias, A., Xu, Z. H. and Zhizhin, M. (1989). "Global patterns of tectonic stress." *Nature* 341: 291-298.

APPENDIX I - CHAPTER 3

Reverse faults

Easting	Northing	Dip Dir^{n}	Dip
268220	6085606	132	74
267507	6085036	172	58
267517	6085000	177	22
267527	6084965	167	65
267538	6084934	167	68
267538	6084934	180	52
268220	6085606	137	73
268220	6085606	150	71
266149	6084406	178	88
268117	6085632	127	71
267182	6084766	320	62
267474	6085019	320	75
267370	6084949	215	42
267519	6084989	300	35
267519	6084989	144	65
267519	6084989	305	35
267938	6086777	150	14
267509	6085029	342	64
267508	6085021	181	46
267441	6085020	168	70
267389	6084967	302	44
267374	6084953	194	59
267365	6084946	163	54
267341	6084907	244	27
267314	6084906	310	20
267314	6084906	304	38
267248	6084856	205	54
267248	6084856	200	23
267237	6084854	167	50
267204	6084834	331	80
266287	6084454	306	40
267030	6084818	168	72
266902	6084789	340	63
267512	6084980	302	36
267512	6084980	153	70

Easting	Northing	Dip Dir^{n}	Dip
267512	6084980	173	44
267509	6084997	152	65
267720	6084907	151	37
267603	6084752	165	56
267534	6084784	160	43
267640	6084772	350	68
267726	6084882	352	68
267726	6084883	164	73
267716	6084902	342	66
267315	6084916	035	63
267315	6084916	026	73
266701	6084763	356	58
266229	6084435	014	70
266169	6084394	006	86
266467	6084408	175	89
266149	6084406	178	88
267229	6084842	311	78
267314	6084897	320	82
267509	6085029	010	80
267347	6084929	358	84
266220	6084446	014	74
266146	6084414	190	87
266639	6084712	000	54
266588	6084664	028	67
266411	6084509	015	52
266340	6084486	004	62
266340	6084486	005	61
266288	6084450	008	73
267229	6084853	306	74
267510	6085023	188	73
267720	6084907	195	70
267706	6084911	022	56
266135	6084418	016	89
266538	6084639	005	36

Normal faults

Easting	Northing	Dip Dir^{n}	Dip
267431	6085000	251	46
267431	6085052	255	79
267341	6084917	280	24
267005	6084812	258	72
267441	6085020	072	60
267426	6085000	226	51
267365	6084946	094	47
267326	6084905	100	75
267674	6085094	250	78
266220	6084446	266	84
266756	6084768	304	70
266680	6084735	010	23
266340	6084486	292	84
266288	6084450	334	26
266229	6084435	275	81
266131	6084415	332	20
266169	6084394	075	73
267332	6084917	278	22
267332	6084917	264	20
267308	6084901	256	68
267293	6084898	095	60
267260	6084477	208	69
267229	6084853	225	78
267229	6084853	232	70
267229	6084853	238	84
267229	6084853	250	76
267229	6084853	079	82
267512	6084980	126	68
267764	6084853	263	38
267767	6084850	278	42
267784	6084802	267	73
267726	6084882	252	68
267726	6084883	234	73
267716	6084902	242	66
267360	6084510	232	30
267397	6084972	267	74

Easting	Northing	Dip Dir^{n}	Dip
267327	6084916	268	51
267248	6084856	205	54
267248	6084856	200	23
267640	6084772	250	68
267426	6085000	082	44
266646	6084709	074	56
267393	6084997	271	30
267423	6084999	281	48
267376	6084981	274	25

Strike-slip faults

Easting	Northing	Dip Dir^{n}	Dip
267160	6084791	311	84
267160	6084791	330	80
267595	6084856	317	73
266467	6084408	166	76
266149	6084406	163	81
267335	6084521	332	78
267786	6084731	347	69
267768	6084854	162	64
267397	6084972	160	25
266131	6084415	350	85
267736	6084866	150	74
267742	6084868	138	69
267791	6084794	340	71
267791	6084794	338	77
267360	6084510	162	30
267397	6084972	167	74
267327	6084916	168	51
267397	6084972	337	74

Bedding on Port Willunga Formation

Easting	Northing	Dip Dir^{n}	Dip
267930	6086727	317	6
267930	6086727	339	11
267906	6086379	127	15
267217	6084850	320	35
267001	6084823	328	45
266915	6084809	335	65
266782	6084813	350	65
266350	6084542	340	60
266277	6084497	355	65
266142	6084467	335	70
266142	6084466	300	70
266697	6084635	320	20
266642	6084687	310	26
266915	6084812	332	78
266915	6084812	334	57
266915	6084812	330	77
266915	6084812	328	64
266915	6084812	334	74
266902	6084789	290	24
266902	6084789	321	26
266845	6084792	347	62
266788	6084780	346	78
266756	6084768	355	54
266701	6084763	342	65
266701	6084763	344	48
266639	6084712	298	28
266494	6084711	334	56
266494	6084711	334	52
266541	6084711	335	89
266529	6084647	328	43
266548	6084651	298	46
266558	6084649	316	24
267930	6086727	317	6
267930	6086727	339	11
267906	6086379	127	15
267561	6085886	250	9
267557	6085909	253	9
267652	6086082	079	13
267729	6086227	183	12
267707	6086269	221	11
267757	6086409	136	9
267752	6086424	115	2

Easting	Northing	Dip Dir^{n}	Dip
267046	6084851	304	43
267037	6084829	323	45
267033	6084832	126	30
267034	6084831	336	59
267021	6084838	322	52
267006	6084822	335	45
266998	6084814	334	45
266967	6084812	327	49
266967	6084812	329	49
266954	6084821	340	70
266942	6084826	348	62
266936	6084830	334	60
266887	6084816	349	71
266888	6084820	342	80
266865	6084830	342	71
266823	6084824	345	75
266815	6084825	343	64
266770	6084766	352	74
266775	6084759	348	60
266722	6084803	337	60
266722	6084803	343	52
266724	6084808	339	48
266672	6084791	352	52
266634	6084769	341	58
266633	6084714	346	56
266641	6084709	336	47
266644	6084716	346	47
266578	6084712	349	38
266552	6084649	323	27
266482	6084640	328	65
266485	6084652	336	43
266449	6084649	321	59
266404	6084604	312	40
266346	6084563	319	59
266280	6084536	314	57
266290	6084567	348	35
266211	6084513	325	48
266274	6084715	357	38
266161	6084480	360	56
266163	6084485	327	62
266886	6084833	154	78

Bedding on bedrock

Easting	Northing	Dip Dir^{n}	Dip
267431	6085015	160	80
267414	6084999	260	33
267416	6084997	160	64
267371	6084953	320	45
267366	6084945	280	32
267250	6084865	220	18
267315	6084898	255	20
267315	6084898	260	22
267267	6084906	320	60
267283	6084894	000	52
267283	6084894	332	35
267249	6084876	310	38
267234	6084866	305	59
267229	6084865	168	45
267245	6084846	150	80
267246	6084850	155	75
267245	6084849	140	80
267220	6084848	325	55
267220	6084848	215	33
267217	6084848	150	72
266149	6084451	010	64
267703	6084918	285	24
267703	6084918	150	49
267706	6084916	142	60
267706	6084916	158	55
267706	6084910	267	25
267710	6084903	278	24
267714	6084896	140	58
267729	6084880	306	57
267745	6084865	127	65
267729	6084873	325	70
267597	6084748	295	76
267600	6084749	325	34
267366	6084490	167	44
267368	6084492	342	48
267317	6084531	160	42
267509	6085029	166	50
267509	6085000	335	36
267500	6084995	325	48
267502	6084981	325	55
267526	6084990	320	55
267528	6084985	260	14
266247	6084444	010	60
266247	6084444	170	52

Easting	Northing	Dip Dir^{n}	Dip
266247	6084444	297	71
266220	6084446	285	77
266107	6084385	180	66
266107	6084385	306	47
266031	6084349	358	81
266031	6084349	286	65
266340	6084486	004	62
266340	6084486	292	84
266340	6084486	005	61
266229	6084435	358	30
266161	6084436	316	29
266161	6084436	000	82
267319	6084911	260	32
267308	6084901	246	16
267293	6084898	355	70
267293	6084898	302	75
267245	6084859	210	18
267245	6084859	147	80
267245	6084859	305	51
267229	6084853	250	24
267229	6084853	158	54
267229	6084853	312	80
267229	6084853	338	71
267158	6084838	325	54
267158	6084838	162	45
267158	6084838	326	65
267228	6084894	337	44
267228	6084894	354	36
267228	6084894	308	68
267221	6084849	330	72
267225	6084889	157	77
267272	6084888	322	54
267317	6084938	320	53
267380	6084988	284	28
267380	6084988	308	31
267281	6084910	322	63
267249	6084867	325	53
267203	6084854	309	44
267185	6084844	322	56
266133	6084413	175	73
266213	6084440	007	78
266232	6084449	012	57
266327	6084473	003	77

Foliation on bedrock

Easting	Northing	Dip Dir^{n}	Dip
267433	6085017	240	60
267433	6085017	050	85
267431	6085015	140	50
267430	6085014	190	40
267414	6084999	250	40
267416	6084997	080	80
267366	6084944	200	78
267298	6084900	335	80
267296	6084899	050	46
267296	6084898	020	75
267251	6084866	035	70
267421	6085001	240	45
267421	6085001	246	50
267420	6085000	205	47
267420	6085000	200	55
267251	6084893	075	65
267251	6084892	210	24
267252	6084893	330	72
267283	6084894	228	35
267248	6084875	050	57
267250	6084875	190	32
267245	6084847	180	33
267245	6084847	055	89
267246	6084850	145	26
267245	6084849	030	52
267245	6084849	195	22
267217	6084848	174	28
267230	6084836	325	70
267218	6084836	164	20
267218	6084836	338	71
267216	6084836	263	82
266151	6084451	120	20
266129	6084439	025	55
266129	6084439	115	28
266126	6084439	110	30
267704	6084918	235	88
267706	6084911	040	56
267708	6084908	320	78
267729	6084880	244	81
267729	6084880	070	75
267727	6084876	085	65
267308	6084544	330	75
267302	6084548	326	65
267502	6084997	320	72
267502	6084997	210	35

Easting	Northing	Dip Dir^{n}	Dip
267500	6084995	100	60
267500	6084979	220	38
267500	6084983	076	45
267525	6084992	200	42
269742	6097040	264	64
269779	6100568	310	24
267798	6100591	290	18
267780	6100560	305	20
269524	6099740	120	40
268220	6085606	202	36
268220	6085606	244	37
268220	6085606	211	30
268220	6085606	320	84
268220	6085606	076	76
268220	6085606	354	38
267431	6085000	132	45
267517	6085000	252	89
267517	6085000	338	79
266220	6084446	020	51
266220	6084446	162	25
266031	6084349	124	49
266161	6084436	074	68
267332	6084917	262	53
267332	6084917	074	52
267332	6084917	050	72
267332	6084917	062	54
267319	6084911	085	70
267293	6084898	238	35
267293	6084898	072	56
267293	6084898	028	50
267272	6084885	226	31
267272	6084885	020	54
267272	6084885	226	30
267260	6084477	068	40
267260	6084477	258	82
267260	6084477	042	44
267229	6084853	272	77
267229	6084853	129	30
267171	6084838	330	77
267175	6084852	064	70
267175	6084852	212	26
267192	6084845	330	80
267192	6084845	030	73
267213	6084857	038	46
267213	6084857	333	71

Foliation on bedrock (continued)

Easting	Northing	Dip Dir^{n}	Dip
267213	6084857	200	41
267213	6084857	080	68
267213	6084857	025	67
267237	6084885	326	79
267237	6084885	020	56
267237	6084885	050	59
267256	6084894	325	74
267256	6084894	115	47
267259	6084899	332	66
267259	6084899	123	57
267259	6084899	065	81
267259	6084899	075	63
267302	6084901	265	77
267302	6084901	336	68
267322	6084924	042	79
267322	6084924	260	47
267322	6084924	069	72
266153	6084442	133	30
266133	6084459	116	36
266229	6084437	161	38
266273	6084449	149	34
266281	6084465	201	30
267301	6084939	194	32
267266	6084924	166	32
267159	6084867	176	46

Meta data of the LiDAR images

Column	Description	Units
1	Longitude	Degrees
2	Latitude	Degrees
3	Elevation	Meters
4	Signal Amplitude	Receiver units
5	Echo half peak width	1/10 ns
6	Class ID (unidentified=0)	0
7	Total no of echo’s received	NA
8	Index of the current echo	NA

Slickenside recordings and fault components

Easting	Northing	Dip Dir^{n}	Dip (β)	Slicks (δ)	L	T	V	Type
268220	6085606	132	74	-85	0.087	0.275	0.958	R
268220	6085606	137	73	-36	0.809	0.172	0.562	R
268220	6085606	150	71	-65	0.423	0.295	0.857	R
267360	6084510	162	30	60	0.5	0.75	0.433	SS?
267335	6084521	332	78	55	0.574	0.17	0.801	SS?
267431	6085000	251	46	90	0	0.695	0.719	N
267431	6085052	255	79	55	0.191	0.563	0.804	N
266149	6084406	178	88	22	0.927	0.013	0.374	R
267397	6084972	167	74	0	1	0	0	SS
267674	6085094	250	78	52	0.616	0.164	0.771	N
267327	6084916	168	51	15	0.966	0.163	0.201	SS
267315	6084916	035	63	18	0.951	0.14	0.275	R
267315	6084916	022	56	48	0.669	0.416	0.616	N
267315	6084916	026	73	12	0.978	0.061	0.199	R
267248	6084856	205	54	34	0.829	0.329	0.452	N
267248	6084856	200	23	65	0.423	0.834	0.354	N
267237	6084854	167	50	-31	0.857	0.331	0.395	R?
267204	6084834	331	80	-27	0.891	0.079	0.447	R?
266287	6084454	306	40	-42	0.743	0.513	0.43	R?
266220	6084446	014	74	73	0.292	0.264	0.919	R
266220	6084446	266	84	36	0.809	0.061	0.585	N
266146	6084414	190	87	90	0	0.052	0.999	R
266701	6084763	356	58	5	0.996	0.046	0.074	R
266131	6084415	350	85	0	1	0	0	SS
266169	6084394	006	86	3	0.999	0.004	0.052	SS?
266169	6084394	075	73	24	0.914	0.119	0.389	N
267512	6084980	302	36	-68	0.375	0.75	0.545	R
267519	6084989	305	35	-32	0.848	0.434	0.304	R
267726	6084882	352	68	-30	0.866	0.187	0.464	R
267726	6084883	164	73	-28	0.883	0.137	0.449	R
267716	6084902	342	66	-67	0.391	0.374	0.841	R
267720	6084907	151	37	-44	0.719	0.555	0.418	R
267603	6084752	165	56	-36	0.809	0.329	0.487	R
267534	6084784	160	43	-52	0.616	0.576	0.537	R
267720	6084907	195	70	52	0.616	0.27	0.74	R
267764	6084853	263	38	45	0.707	0.557	0.435	N
267767	6084850	278	42	40	0.766	0.478	0.43	N
267784	6084802	267	33	57	0.545	0.703	0.457	N
267640	6084772	250	68	49	0.656	0.283	0.7	N
267786	6084731	347	69	42	0.743	0.24	0.625	SS
267768	6084854	162	64	18	0.951	0.135	0.278	SS
267397	6084972	337	74	0	1	0	0	SS
267736	6084866	150	74	20	0.94	0.094	0.329	SS
267742	6084868	138	69	23	0.921	0.14	0.365	SS
267791	6084794	340	71	28	0.883	0.153	0.444	SS
267791	6084794	338	77	39	0.777	0.142	0.613	SS

This map is to be printed in landscape A3 paper

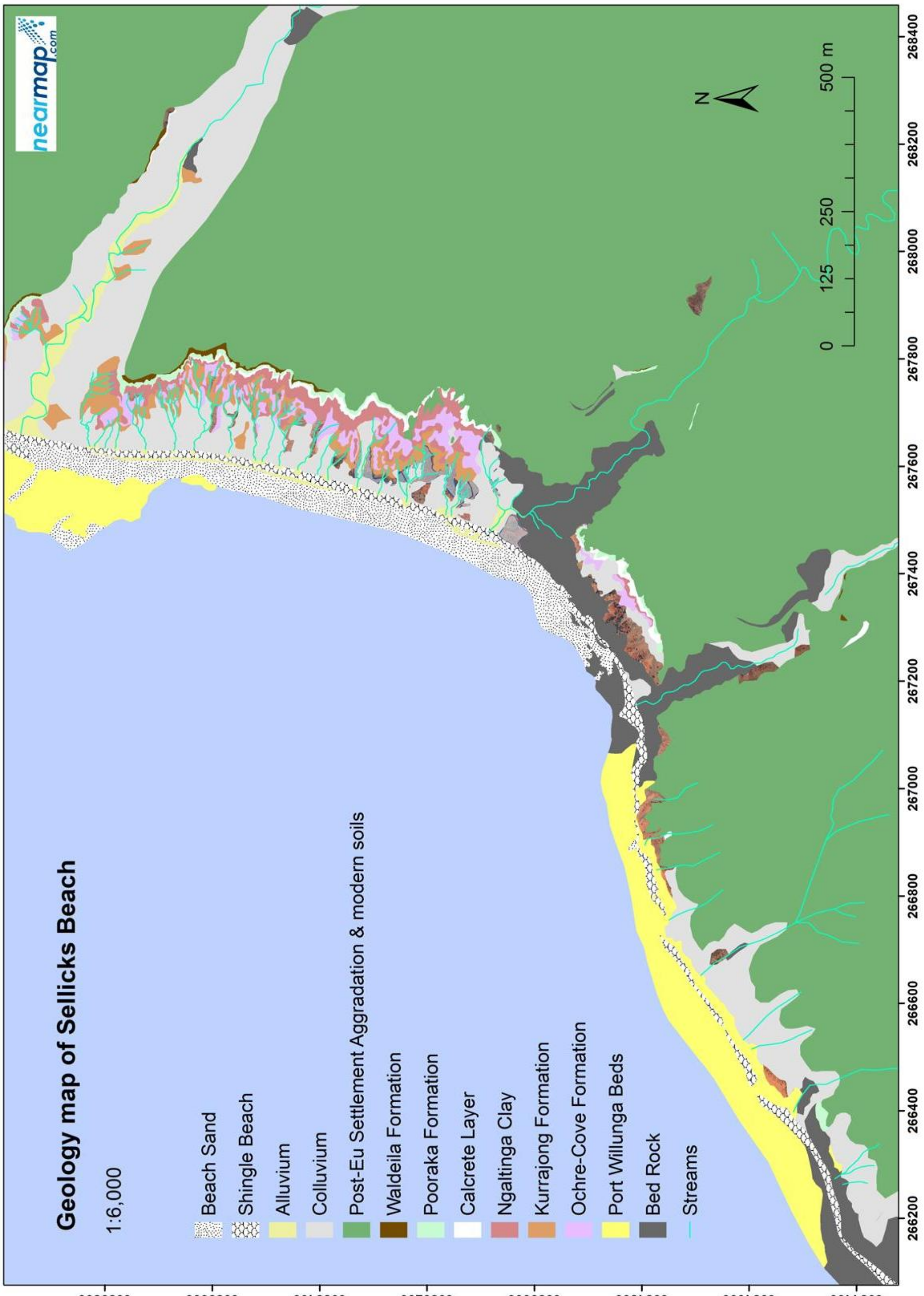

This map also to be printed in landscape A3 paper

APPENDIX II - CHAPTER 5

Overview of total dose rates for the samples from Moolawatana as estimated from airborne and laboratory measurements

Name	**Lab code**	**Stratigraphy**	**Lat**	**Lon**	**Depth** (m)	**Total Airborne D** (nGy hr^{-1})	**K** (%)	**err** ±	**Th** (ppm)	**err** ±	**U** (ppm)	**err** ±	**W field** (%)	**W** (%)	**Cosmic D** (Gy ka^{-1})	**Total D** (Gy ka^{-1})	**err** ±
MW 100	UOW 405	Holocene	-29.9268	139.7416	0.30	229.9	2.02	0.24	41.12	1.69	14.74	0.49	1.1	2 ± 1	0.202	8.59	0.34
MW 105	UOW 407	Holocene	-29.9274	139.7383	0.55	204.8	2.17	0.20	32.45	1.50	9.86	0.43	1.5	3 ± 2	0.201	6.85	0.32
MW 109	UOW 406	Pooraka	-29.9271	139.7376	0.55	204.8	2.46	0.21	36.67	1.71	7.67	0.50	2.9	3 ± 2	0.196	6.88	0.33
MW 104	UOW 408	Pooraka	-29.9271	139.7297	0.50	292.7	3.16	0.25	38.40	1.15	12.80	0.33	1.3	2 ± 1	0.197	8.91	0.38

Report on the OSL dating results
Samples A1, B1, T1 and T2

Version 02

27th May, 2013

M. Meyer

University Innsbruck

OSL equipment and dating procedures

OSL dating provides an estimate of the time since sediment grains were last exposed to sunlight. The burial age of the sediment is calculated using equation (1) by dividing the equivalent dose (D_e), the radiation energy absorbed by the natural sediment, by the environmental dose rate (D_r), the rate of exposure of the sediment to naturally-occurring ionising radiation.

$$\text{Burial age (ka)} = \frac{\text{Equivalent dose } (D_e)\ [\text{Gy}]}{\text{Dose rate } (D_r)\ [\text{Gy/ka}]}$$

Chemical preparation to obtain quartz grains from the bulk sediment samples followed standard procedures (Wintle, 1997). Carbonates were dissolved in 10% hydrochloric (HCl) acid and organic matter was oxidised in 30% hydrogen peroxide (H_2O_2) solution. The 180-212 μm grain size fraction was obtained by dry sieving, and quartz was isolated from feldspar and heavy mineral grains by density separation, using sodium polytungstate solutions with a specific gravity of 2.62 and 2.7, respectively. The remaining quartz grains were then etched in 48% HF for 40 minutes to destroy any remaining feldspar grains and to remove the alpha-irradiated outer rinds (~9 μm) of each quartz grain. The HF etched sample was then re-sieved and only those grains retained in the 180 μm diameter sieve were used for optical dating.

The OSL signal of the purified quartz grains was measured using an automated Risø TL/OSL –DA20 reader equipped with blue light emitting diodes (LEDs) for stimulation of multi-grain aliquots, each consisting of ~ 50-100grains (used for initial tests of quartz OSL behaviour), and a focussed green laser for measurement of individual sand-sized grains of quartz (Bøtter-Jensen et al., 2000). The light emitted from both, single aliquots and single grains was detected with an EMI 9235 photomultiplier tube after passing through 6 mm of Hoya U-340 filter to isolate the ultraviolet wavelength.

The measurement procedures employed in this study followed the single aliquot regenerative dose (SAR) procedure introduced for multi-grain aliquots by Murray and Wintle, 2000 and first applied to single-grains of quartz by Jacobs et al., 2006. Routine checks of OSL protocol performance were made for thermal transfer, test dose sensitivity correction and dose response behaviour using a number of different tests (Murray and Wintle, 2000; Duller 2003; Jacobs et al., 2006). Aliquots or grains were rejected from further analyses if : (1) the OSL signal was weak (T_N< 3 times the background signal), (2) the sensitivity-corrected zero dose value was > 5% of the sensitivity-corrected natural value, (3) the repeat dose points at the end of the measurement procedure were not consistent with the initial value for the same dose (> 2σ different from unity), (4) the sensitivity- corrected natural OSL signal did not intercept the dose-response curve, and (5) the OSL-IR depletion ratio was more than 2σ below unity, suggesting the presence of feldspar grains or inclusions.

To determine the most appropriate experimental and measurement conditions for the samples, and the usefulness of the analytical procedures, a series of dose recovery tests (Murray &Wintle, 2003) were performed on single aliquots of quartz from sample T1. It involved zeroing the natural OSL signal at room temperature by exposing a sub-sample of grains to natural sunlight for at least 3 days. A known laboratory dose was then administered, and the SAR procedure used to evaluate whether the known dose value can be recovered accurately while the preheat temperatures administered prior to measurement of the regenerative and test dose OSL signals, were varied systematically.

Further measurement details of single-grains of quartz were as follows: OSL measurements were made with 2 seconds of laser stimulation. SAR dose response curves were constructed by administering five regenerative doses that ranged from 21 to up to a maximum value of 500 Gy (sample dependent). A test dose of either 30 Gy or 5 Gy (sample dependent) was used to correct for sensitivity changes that might occur during the SAR measurement sequence. Furthermore, two recycling points were integrated into the SAR protocol, one at 100 Gy and a second at 400 Gy (and both were used as rejection cirtierias – see above). The dose response curves were fitted with a single exponential function or – if more appropriate – a single exponential plus linear function and fitting errors were determined via 500 Monte Carlo iterations.

Results

Dose recovery experiments

On the multi-grain level (single aliquots with ~50 grains each) the most accurate and precise results were obtained when a preheat of 160ºC for 10 s (PH1) was applied prior to measurement of the natural (L_N) and each regenerative dose (L_x), and a preheat of 160 ºC for 5 s (PH2) prior to measurement of the test dose (T_N and T_x) OSL signals. Under this preheat regime the measured/given dose ratio was found to be consistent with unity, i.e. 0.98 ± 0.05 (average of four aliquots; weighted average: 0.98 ± 0.01; Fig. 1). The recycling ratio for this preheat combination is 0.97 ± 0.03 (average of four aliquots; weighted average of the recycling ratio: 0.98 ± 0.01) and the averaged recuperation is negligible (i.e. 0.25 ± 0.05 %; Fig. 1).

Using the same measurement conditions (i.e. PH 1 at 160°C for 10 s; PH 2 at 160°C for 5 s) and rejection criteria, a dose recovery test was also performed on single grains from sample T1, resulting in a measured/given dose ratio of 1.06 ± 0.03 (n=89) and an overdispersion value of 7.3 ± 3% (Fig. 2A). In this experiment the recovered dose is slightly overestimating the given dose (i.e. by 5.5 ± 3%), but on the 2 sigma level this ratio is still consistent with unity. An additional single-grain dose recovery experiment with a higher preheat combination (i.e. PH 1 at 260°C for 10 s; PH 2 at 220°C for 5 s; Fig. 2B) underestimated the given doseby 23% (measured/given dose ratio of 0.77 ± 0.01 (n=69); overdispersion value of 8.4 ± 2%; recycling ratio of 0.97 ± 0.01). Hence, all further OSL measurements were made with a PH1 of 160 ºC for 10 s and a PH2 of 160 ºC for 5 s.

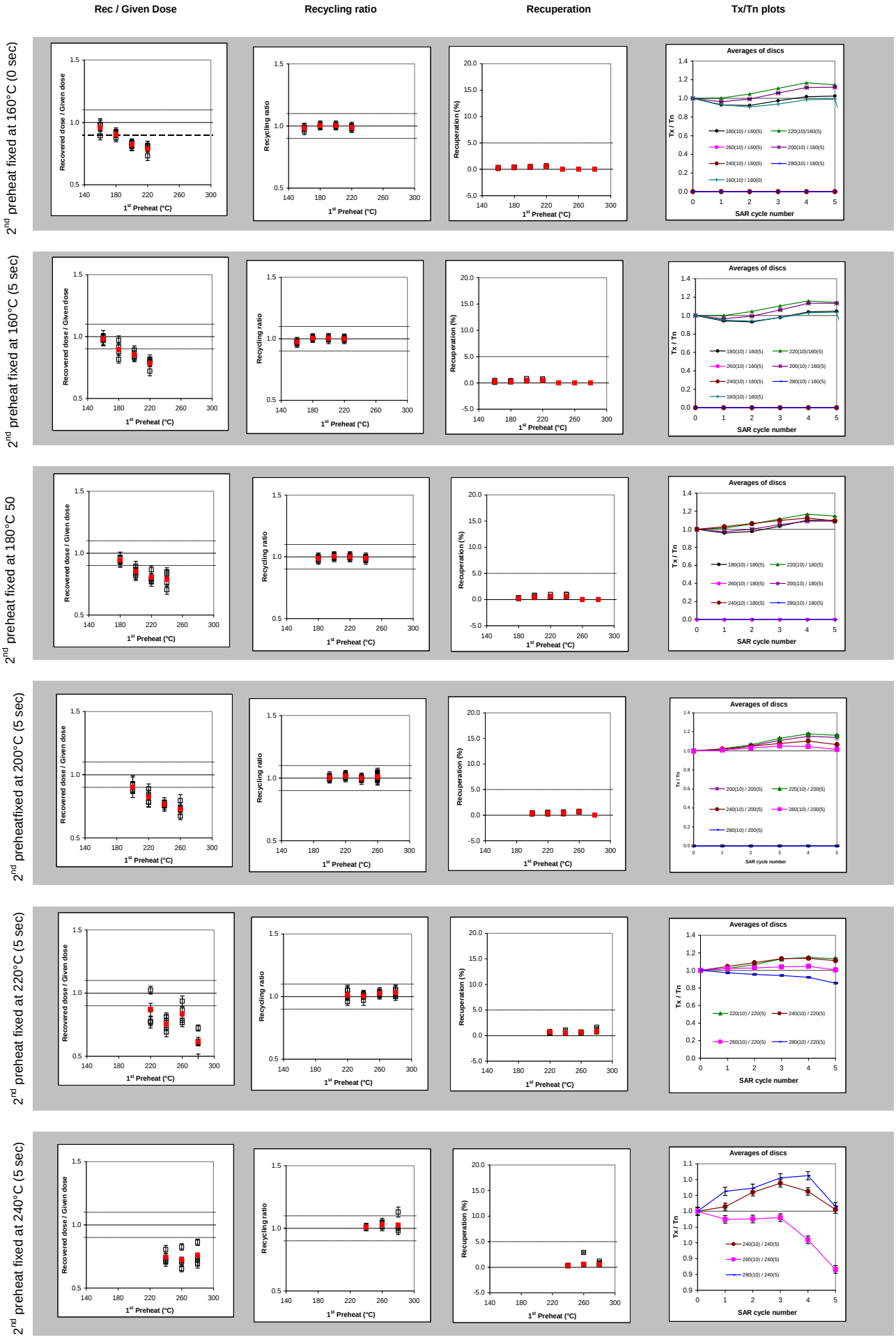

Figure 1: Results of dose recovery experiments for sample T1 conducted on multi grain

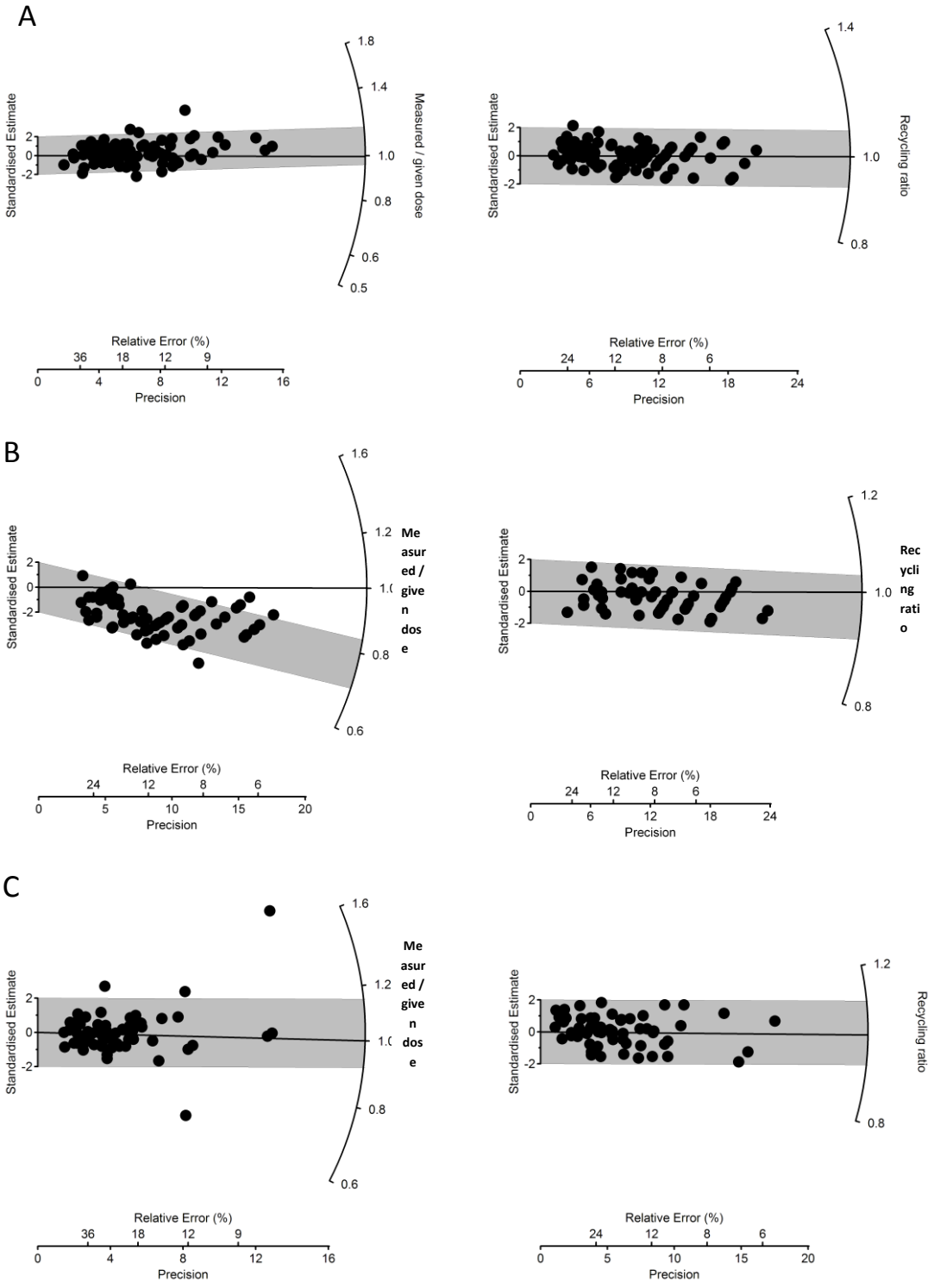

Figure 2: Results of the single-grain dose recovery experiments for sample T1. A:Ratio of the measured to given dose (left) and the recycling ratio (right) using a preheat combination of 160°C for 10 seconds for preheat 1 (PH 1) and 160°C for 5 seconds for preheat 2 (PH 2). B: Ratio of the measured to given dose (left) and the recycling ratio (right) using a preheat combination of 260°C for 10 seconds for PH 1 and 220°C for 5 seconds for PH 2. C: Same data as in A (i.e. measured to recovered dose ratio obtained with a PH 1 of 160°C for 10 s and a PH 2 at 160°C for 5 s (left) and recycling ration (right)), but analysed using the early background subtraction method.

OSL signal characteristics and early background subtraction

All samples investigated in this study generally reveal bright to very bright luminescence signals (i.e. 10^3 – 10^5 counts in the initial signal channels; Fig. 3). However, background build-up was observed for several of the quartz grains that otherwise passed all the rejection criteria (Fig. 3). Background build-up might result from (i) thermally unstable medium and / or slow OSL components that are sensitizing throughout the SAR measurement sequence or (ii) because the OSL signal cannot be completely stimulated to the background level. Appearance of the medium or slow components in the initial part of OSL signals (where they might interfere with the fast component) potentially complicates De determination (see Wintle and Murray, 2006 or Bailey, 2010 for discussion) and typically results in De underestimation (e.g. Choi et al., 2003; Li and Li, 2006; Steffen et al., 2009). Several methods have been proposed to isolate the fast OSL component or maximise the contribution of the fast OSL component to the net OSL signals (see Wintle and Murray, 2006; Bailey, 2010, Cunningham and Wallinga, 2010 for discussion). We opted for the early background (EBG) subtraction method, i.e. an approach first suggested by Ballarini et al. 2007 for single-grains of quartz and since then successfully applied in many different OSL studies dealing with samples from diverse sedimentary environments of various depositional ages. This approach (i) integrates the initial interval of the OSL decay curve to derive the OSL signals for the natural, regenerated and test-dose OSL responses and (ii) estimates the background signal from the curve interval that immediately follows the signal interval. The net OSL signal is then derived by subtracting this early background interval from the signal interval (as opposed to the commonly applied late background subtraction, where the background is derived from the last few channels of an OSL decay curve). OSL net signals derived via the EBG subtraction method have been shown to contain almost no slow components and have only minor contributions (if any) from the medium component (Ballarini et al. 2007; Cunningham and Wallinga, 2010). The advantage of the EBG subtraction method thus lies in its simplicity and efficiency in obtaining a predominantly fast–component derived signal.

The single-grain dose recovery data that were obtained via the low preheat combination (i.e. PH 1 at 160°C for 10 s; PH 2 at 160°C for 5 s; Fig. 2A) were re-analysed using the early background subtraction method of Ballarini et al., (2007). As signal interval for the natural OSL signal as well as for the regenerated OSL signal and test-dose responses the initial 0.02 s of the decay curve were used, while the background was estimated from the subsequent 0.02 s (Fig. 3B and 3F). This resulted in an improvement of the measured/given dose ratio that is now consistent with unity (i.e. 1.03 ± 0.04; recycling ratio: 1.01 ± 0.02; n=61) while the overdispersion value increased to 16.7 ± 4% (Fig. 2C). Hence, all further OSL measurements were made with a PH1 of 160 ºC for 10 s and a PH2 of 160 ºC for 5 s and the single-grain OSL data were analysed using the above mentioned rejection criteria as well as the EBG subtraction method (signal and background integration intervals as specified above).

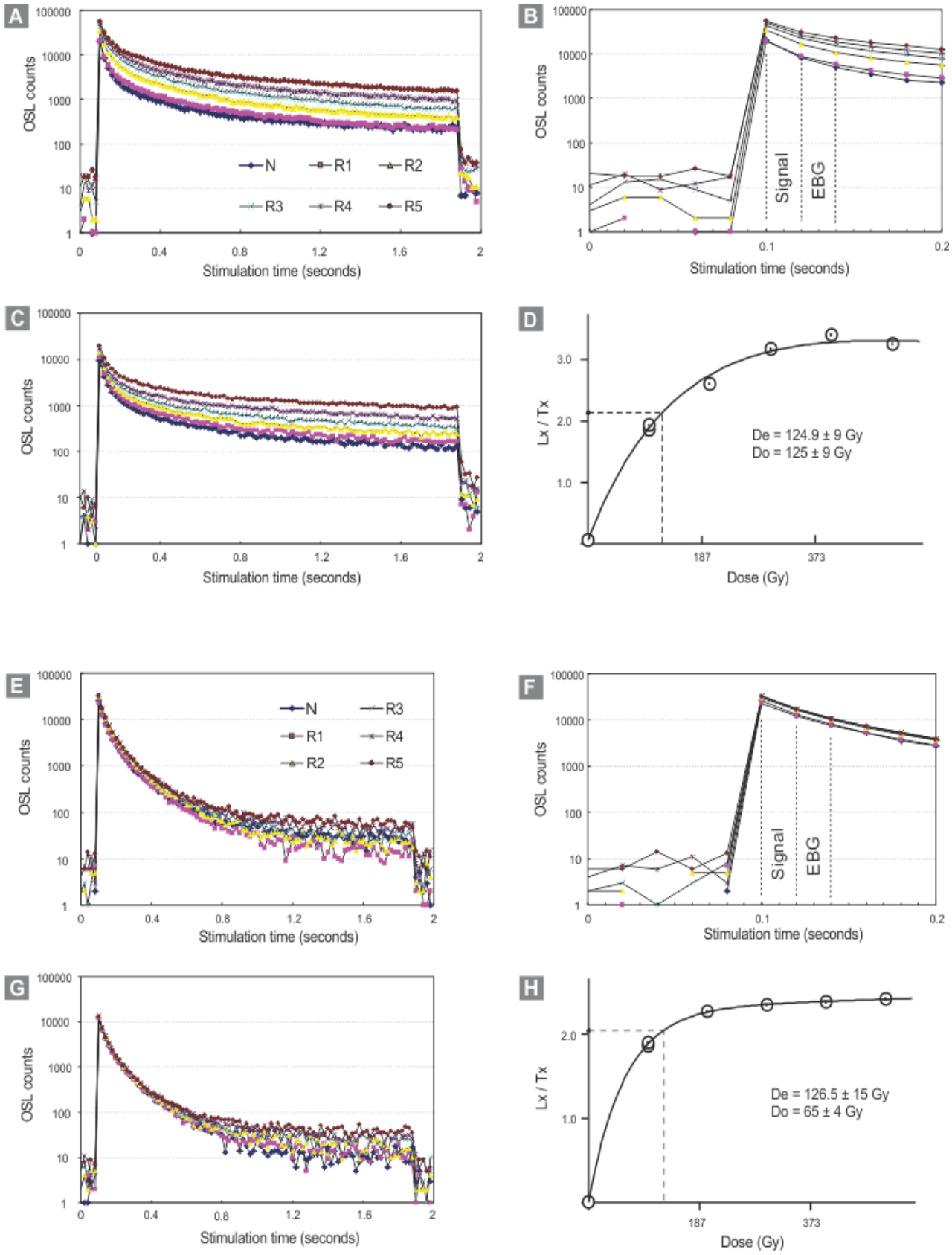

Figure 3: Examples of OSL decay curves and sensitivity corrected dose-response curves for two characteristics grains of quartz from sample A1. Note the logarithmic scale on the y-axis in A, B, C as well as E, F and G. A-D: Grain Uibk104_11_44 revealing strong background build-up; A: Natural and regenerated OSL decay curves;

B: Same data as in A but only the initial 0.2 seconds of stimulation time are plotted with the signal and background integration intervals indicated; C: OSL responses to the administered test dose (30 Gy). D: Dose response curve (De and Do values indicated). E-F: grain Uibk 104_15_93 with no significant background build-up. E: Natural and regenerated OSL decay curves; F: Same data as in E but only the initial 0.2 seconds of stimulation time are plotted with the signal and background integration intervals indicated; G: OSL responses to the administered test dose (30 Gy). H: Dose response curve (De and Do values indicated). Both grains passed the SAR rejection criteria and were accepted for De estimation.

Dosimetry

A1	B1	T1	T2	
1.70	7.10	9.70	1.40	U (ppm)
11.60	14.10	1.30	13.40	Th (ppm)
3.44	1.99	1.39	1.95	K (%)

Table 1: U, Th and ^{40}K concentrations determined via ICP-MS measurements.

De distribution analysis

Figure 4A-D: Single-grain De distributions for the samples A1 (A), B1 (B), T1 (C) and T2 (D). For each sample two radial plots are presented: the one on the left side shows the entire single-grain De data set, i.e. accepted grains (black dots) are plotted together with those grains for which a De could only be obtained via linear extrapolation of the dose response curve beyond the highest regenerated dose point (so called “extrapolated grains”, displayed as triangles). On the right side the De distributions and age modelling results for each sample are presented; i.e. for sample A1 (right plot in A): finite mixture model – 3 component fit; for sample B1 (right plot in B): central age model; for sample T2 (right plot in C): finite mixture model – 3 component fit; for sample T1 (right plot in D) – 3 component minimum age model (for optical ages see Table 2 and 3). All radial plots are centred on the central De value as calculated via the central age model for the accepted grains. The 2 sigma uncertainty ranges for these central De estimates are indicated as a grey bars in each radial plot on the left hand side (for central De values and the associated overdispersion see Table 2).

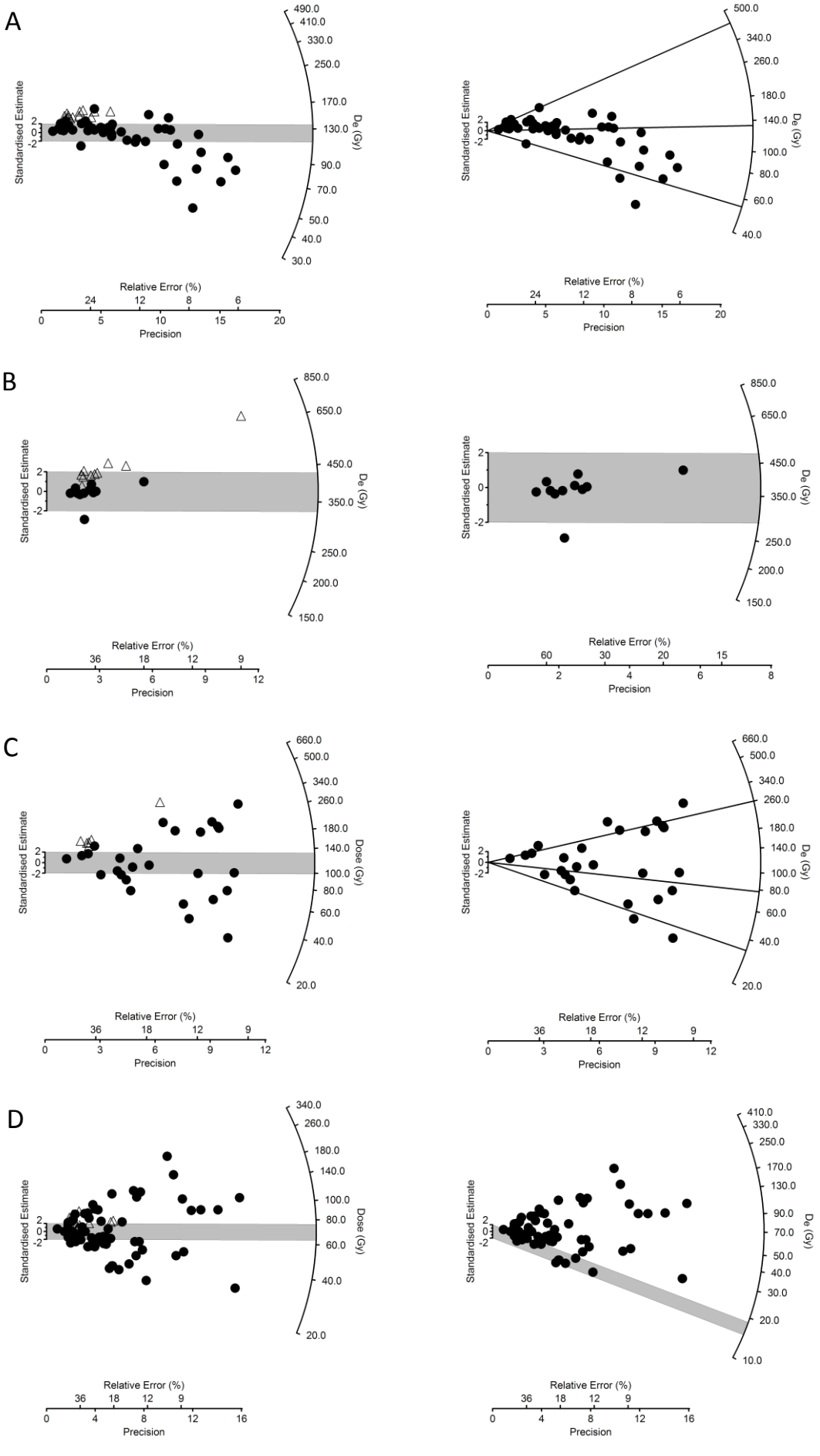
A
Standardised Estimate
De (Gy)
Relative Error (%)
Precision
B
Standardised Estimate
De (Gy)
Relative Error (%)
Precision
C
Standardised Estimate
Dose (Gy)
Relative Error (%)
Precision
D
Standardised Estimate
Dose (Gy)
De (Gy)
Relative Error (%)
Precision

Foot notes for Table 2:

[a] Given is the present field water content for each sample that was also applied for age calculation.

[b + c] The U, Th and K concentrations was determined on sub-samples of dried, homogenised and powdered samples by IC-PMS measurements by the Activation Laboratories Ltd, Ancaster, Canada. Elemental concentrations were converted to dry dose rates using the conversion factors of Stokes et al., 2003 and adjusted for the water content (expressed as % of dry mass of sample using the dose correction factors of Adamiec and Aitken, 1998).

[d] Cosmic dose rates have been calculated using the equations provided by Prescott and Hutton (1994) taking into account the latitude, longitude and altitude of the sites. The dose rates calculated were also adjusted for the water content and a relative uncertainty of 10% has been assigned to each cosmic dose rate estimate.

[e] Mean ± total uncertainty (68% confidence interval), calculated as the quadratic sum of the random and systematic uncertainties.

[f] Includes an assumed internal alpha dose rate of 0.03±0.01 Gy/ka.

[g] The total uncertainty includes a systematic component of ±2% associated with laboratory beta-source calibration.

[h] The central age model (CAM) and finite mixture model (FMM) were applied as discussed in the text.

Samples	grain size used for dating (µm)	Moisture content (weight %)[a]	Dose rates (Gy / ka)								De[a] (Gy) via CAM	sd	Number of grains		Over-dispersion (σ_b in %)	sd	Age Model[h]	Optical Age (ka)	sd (ka)
			Beta[b]	sd	Gamma[c]	sd	Cosmic[d]	sd	Total[e, f]	sd			Measured	Accepted					
A1	180 - 212	10.1	2.64	0.11	1.42	0.09	0.19	0.02	4.28	0.21	125.2	9.4	1000	48	47	6	FMM	see Table 3	
B1	181 - 212	12.2	2.29	0.09	1.72	0.10	0.18	0.02	4.22	0.20	376.3	42.5	1000	11	0	0	CAM	89.1	11.1
T1	182 - 212	14	1.92	0.08	1.29	0.10	0.18	0.02	3.42	0.19	114.6	18.3	1000	27	80	12	FMM	see Table 3	
T2	183 - 212	21	1.49	0.07	1.02	0.07	0.17	0.02	2.72	0.14	70.4	8.6	1000	96	96	9	MAM	6.2	1.0

Table 2: Dose rate data, water content, equivalent doses and optical ages for the samples A1, B1, T1 and T2.

sample	over-dispersion (δd in %)	k (number of components)	llik (max log likelihood)	BIC (bayesian info criterion)	Component	Proportion (%)	se (%)	De (Gy)	se (Gy)	Age (ka)	se (ka)
A1	20	3	-70.3	161.5	1	11.2	4.4	55.5	6.0	13.0	1.6
					2	57.4	7.1	133.3	7.1	31.2	2.3
					3	31.4	6.6	423.9	44.2	99.1	11.6
T1	20	3	-26.6	69.6	1	17.6	9.3	34.3	5.6	10.0	1.7
					2	37.4	11.2	77.8	8.6	22.7	2.8
					3	44.9	10.1	262.1	21.4	76.7	7.7

Table 3: Results of the finite mixture model for the samples A1 and T1.

References

Adamiec, G. and Aitken, M. (1998): Dose-rate conversion factors: update. Ancient TL 16, 37-50.

Bailey, R.M. (2010): Direct measurement of the fast component of quartz optically stimulated luminescence and implications for the accuracy of optical dating. Quaternary Geochronology 5, 559-568.

Choi, J.H.; Murray, A.S.; Cheong, C.S.; Hong, D.G., Chang, H.W. (2003): The resolution of stratigraphic inconsistency in the luminescence ages of marine terrace sediments from Korea. Quaternary Science Reviews22, 1201-1206.

Cunningham, A.C. and Wallinga, J. (2010): Selection of integration time intervals for quartz OSL decay curves. Quaternary Geochronology 5, 657-666.

Duller, G.A.T. (2003): Distinguishing quartz and feldspar in single grain luminescence measurements. Radiation Measurements.37, 161-165.

Jacobs, Z., Duller, G.A.T. Wintle, A.G. (2006): Interpretation of single grain De distributions and calculation of De. Radiation Measurements 41,264-277.

Murray, A.S. and Wintle, A.G. (2000): Luminescence dating of quartz using an improved single-aliquot regenerative-dose protocol. Radiation Measurements 32,57-73.

Li, B. and Li, S.H. (2006): Comparison of De estimates using the fast component and the medium component of quartz OSL. Radiation Measurements41, 125-136.

Steffen, D., Preusser, F., Schlunegger, F. (2009): OSL quartz age underestimation due to unstable signal components: Dating the Recent Past. Quaternary Geochronology 4, 353-362.

Stokes, S.; Aitken, M.J., Sirocko, F., Anderson, R., Leuschner, D. (2003): Alternative chronologies for Late Quaternary (Last Interglacial-Holocene) deep sea sediments via optical dating of silt-sized quartz. Quaternary Science Reviews 22, 925-941.

Wintle, A.G. and Murray, A. S. (2006): A review of quartz optically stimulated luminescence characteristics and their relevance in single-aliquot regeneration protocols. Radiation Measurements 41, 369-391.

Amendment: FMM for T2

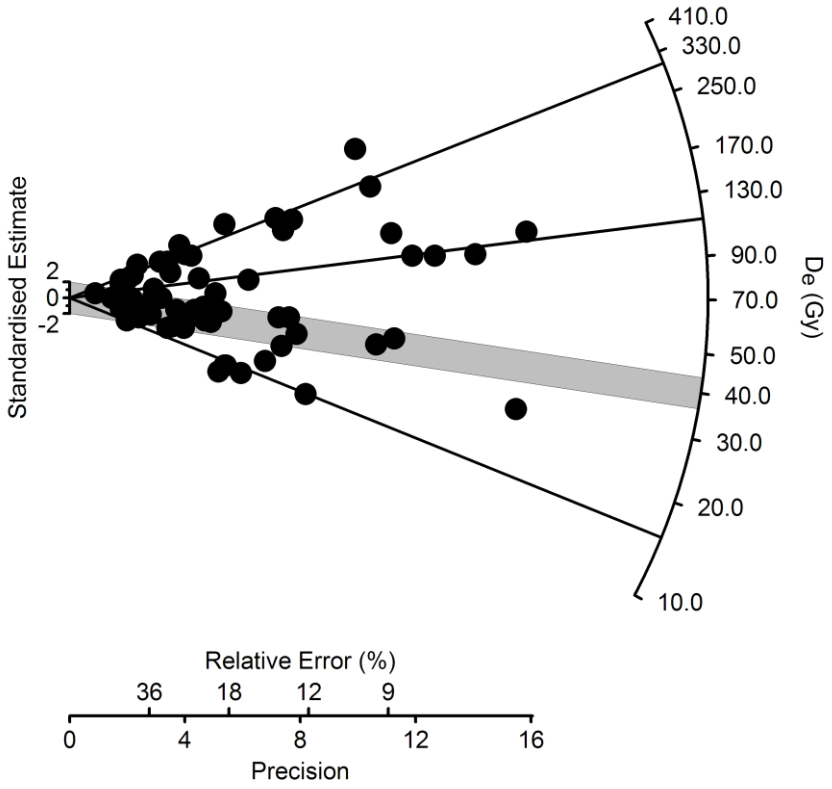

δ_d (overdisp %)	k (number of components)	llik (max log likelihood)	BIC (bayes info criterion)	Component	Proportion (%)	se (%)	De (Gy)	se (Gy)	optical age (ka)	se
20	4	**-84.6**	**198.7**	1	11.6	4.7	15.7	2.0	5.8	0.8
				2	46.2	7.2	40.4	2.7	14.8	1.3
				3	19.0	5.9	111.3	10.0	40.9	4.3
				4	23.3	5.5	302.1	24.2	110.9	10.9

APPENDIX III - CHAPTER 6

Material	Dielectric constant	Conductivity (mS/m)	Velocity (m/ns)	Attenuation (dB/m)
Air	1	0	0.3	0
Fresh water	80	0.5	0.033	0.1
Sea water	80	30000	0.01	1000
Dry sand	3 - 5	0.01	0.15	0.01
Saturated sand	20 - 30	0.1 - 1.0	0.06	0.03 - 0.3
Limestone	4 - 8	0.5 - 2	0.12	0.4 - 1
Shale	5 - 15	1 - 100	0.09	1 - 100
Silt	5 - 30	1 - 100	0.07	1 - 100
Clay	4 - 40	2 - 1000	0.06	1 - 300
Granite	4 - 6	0.01 - 1	0.13	0.01 - 1
Salt (dry)	5 - 6	0.01 - 1	0.13	0.01 - 1
Ice	3 - 4	0.01	0.16	0.01

Electrical Properties of Geological Media (Source: Davis & Annan 1989)

File extension	**Description of information content**
.add	Records the additional parameters for grid projects
.cor	Consists of coordinates for each measured trace (from the GPS)
.ele	Elevation data
.em	Electromagnetic data from high frequency antennae
.mrk	Surface markers
.rad	Contains the field measurement parameters
.rd3	Standard 2D radargram data files

File extensions associated with MALA radargrams

File No	Antenna Frequency	Signal Velocity	Sampling Frequency	Time Window	Point Interval	Signal Depth	No of Samples	Stacks	Location	Direction	Comments
51	100	129	1014.28	475.2	0.1	6.04	176	Auto	Sellicks	towards NW	Cactus Canyon - before the Pooraka formation
52	500	129	5000	104	0.1	4.77	544	Auto	Sellicks	towards NW	Cactus Canyon
53	250	129	4792	195	0.1	4.77	544	Auto	Sellicks	towards NW	Cactus Canyon
54	100	129	4792	475.2	0.1	14.99	344	Auto	Sellicks	towards NNW	Monastery - SM1 at electricity lines
55	500	129	5000	104	0.1	4.77	544	Auto	Tarlee	South to North	Trial runs across the trench
56	500	140	5000	104	0.1	4.77	544	Auto	Tarlee	N to S	Trial runs across the trench
57	500	75	5000	104	0.1	4.77	544	Auto	Tarlee	S to N	Trial runs across the trench
58	500	75	5000	104	0.1	4.77	544	Auto	Tarlee	N to S	Trial runs across the trench
59	500	75	5000	104	0.1	4.77	544	Auto	Tarlee	East to West	Trench - Forward, SM1 at A and SM2 at B
60	500	75	5000	104	0.1	4.77	544	Auto	Tarlee	Backward	Trench
61	500	90	5000	104	0.1	4.77	544	Auto	Tarlee	E to W	Trench
62	500	90	5000	104	0.1	4.77	544	Auto	Tarlee	Backward	Trench
63	500	129	5000	104	0.1	4.77	544	Auto	Tarlee	E to W	Trench
64	500	129	5000	104	0.1	4.77	544	Auto	Tarlee	Backward	Trench
65	500	140	5000	104	0.1	4.77	544	Auto	Tarlee	E to W	Trench
66	500	140	5000	104	0.1	4.77	544	Auto	Tarlee	Backward	Trench
67	500	55	1014.28	104	0.1	4.77	544	Auto	Tarlee	E to W	Trench
68	500	55	1014.28	104	0.1	4.77	544	Auto	Tarlee	Backward	Trench
69	100	55	1014.28	475.2	0.1	6.04	176	Auto	Tarlee	E to W	Trench
70	100	55	1014.28	475.2	0.1	6.04	176	Auto	Tarlee	Backward	Trench
71	100	75	1014.28	475.2	0.1	6.04	176	Auto	Tarlee	E to W	Trench
72	100	75	1014.28	475.2	0.1	6.04	176	Auto	Tarlee	Backward	Trench
73	100	90	1014.28	475.2	0.1	6.04	176	Auto	Tarlee	E to W	Trench
74	100	90	1014.28	475.2	0.1	6.04	176	Auto	Tarlee	Backward	Trench
75	100	129	1014.28	475.2	0.1	12.32	264	Auto	Tarlee	E to W	Trench

76	100	129	1014.28	475.2	0.1	12.32	264	Auto	Tarlee	Backward	Trench
77	100	140	1014.28	475.2	0.1	12.32	264	Auto	Tarlee	E to W	Trench
78	100	140	1014.28	475.2	0.1	12.32	264	Auto	Tarlee	Backward	Trench
79	250	129	2472.3	195	0.1	6.09	336	Auto	Tarlee	E to W	Trench
80	250	129	2472.3	195	0.1	6.09	336	Auto	Tarlee	Backward	Trench
81	250	140	2472.3	195	0.1	6.09	336	Auto	Tarlee	E to W	Trench
82	250	140	2472.3	195	0.1	6.09	336	Auto	Tarlee	Backward	Trench
83	250	90	2472.3	195	0.1	6.09	336	Auto	Tarlee	E to W	Trench
84	250	90	2472.3	195	0.1	6.09	336	Auto	Tarlee	Backward	Trench
85	250	75	2472.3	195	0.1	6.09	336	Auto	Tarlee	E to W	Trench
86	250	75	2472.3	195	0.1	6.09	336	Auto	Tarlee	Backward	Trench
87	250	55	2472.3	195	0.1	6.09	336	Auto	Tarlee	E to W	Trench
88	250	55	2472.3	195	0.1	6.09	336	Auto	Tarlee	Backward	Trench
89	250	129	2472.3	195	0.1	6.09	336	Auto	Tarlee	S to N	Across the trench to see fill recorded
90	100	90	1014.28	475.2	0.1	31.73	512	Auto	Tarlee	W to E	Paddick - Trial Driving speed 6km/h with hip chain
91	100	90	1014.28	475.2	0.01	31.73	512	Auto	Tarlee	W to E	Paddick - Trial Driving speed 6km/h with hip chain
92	100	90	1014.28	475.2	0.5	31.73	512	Auto	Tarlee	E to W	Paddick - Trial Driving speed 6km/h with hip chain
93	100	90	1014.28	774.9	0.1	35.96	816	Auto	Tarlee	In CAR	Paddick - Trial Driving speed 6km/h with hip chain
94	100	90	1014.28	534.4	0.1	25	552	Auto	Tarlee	E to W	Paddick - Trial Driving speed 6km/h with hip chain
95	100	90	1014.28	313.5	0.01	15.17	328	Auto	Tarlee	Forward	Trench - Perpendicular
96	100	90	1014.28	140	0.1	7.32	152	Auto	Tarlee	Backward	Trench - Perpendicular
97	100	90	1014.28	250	0.05	12.32	264	Auto	Tarlee	Forward	Trench - Perpendicular
98	100	129	1014.28	250	0.05	12.32	264	Auto	Tarlee	Backward	Trench - Perpendicular
99	100	90	1014.28	132	0.05	6.96	144	Auto	Tarlee	Forward	Trench - Perpendicular
100	100	90	1014.28	258.3	0.05	12.68	272	Auto	Tarlee	Backward	Trench - W to E parallel to the trench
101	250	90	1014.28	131.9	0.05	6.09	336	Auto	Tarlee	Forward	Trench
102	250	90	1014.28	131.9	0.05	8.66	336	Auto	Tarlee	Backward	Trench
103	250	100	1014.28	148	0.05	7.56	336	Auto	Tarlee	Forward	Trench
104	250	100	1014.28	148	0.1	7.56	376	Auto	Tarlee	Backward	Trench
105	100	100	1014.28	148	0.1	10	179	Auto	Tarlee	Forward	Trench
106	100	90	1014.28	179.4	0.1	9.11	192	Auto	Tarlee	E to W	Paddick

107	100	90	1014.28	179.4	0.1	9.11	192	Auto	Tarlee	E to W	Paddick
108	100	90	1014.28	179.4	0.1	9.11	192	1	Hoyleton	Forward	Trench 1
109	100	90	1014.28	179.4	0.1	9.11	192	1	Hoyleton	Backward	Trench 1
110	100	90	1014.28	189.3	0.1	9.11	192	1	Hoyleton	Forward	Error
111	100	90	1014.28	179.4	0.1	9.11	192	1	Hoyleton	Forward	Paddick - towards W, parallel to the second trench
112	100	90	1014.28	313.5	0.1	15.17	328	Auto	Gawler	to SE	Paddick - From entrance along the GA traverse
113	100	90	1014.28	313.5	0.1	15.17	328	Auto	Gawler	Backward	Paddick - reverse, SM1-powerline, others pegs
114	100	90	1014.28	199.2	0.1	10	232	Auto	Gawler	Forward	Paddick - starting from entrance
115	100	90	1014.28	427.9	0.1	20.33	464	Auto	Gawler	Backward	Paddick - reverse on 114, SM1 power line
116	100	90	1014.28	199.2	0.1	10	232	Auto	Gawler	Forward	Paddick - parallel to the previous, from entrance
117	100	90	1014.28	427.9	0.1	20.33	464	Auto	Gawler	Backward	Paddick - reverse on 116, SM1&2-start & middle
118	100	90	1014.28	309.6	0.1	15	344	1	Vista	W to E	Hill - from Gun Emplaycement to the hill, hip chain
119	100	90	1014.28	309.6	0.1	15	344	1	Vista	E to W	Across the benches down-wards
120	100	90	1014.28	309.6	0.1	15	344	1	Vista	W to E	from the terraces upwards
121	100	90	1014.28	309.6	0.1	15	344	1	Vista	towards NE	Across the recent fault scarp
122	250	90	1014.28	140	0.1	6.45	376	Auto	Sellicks	towards NW	Cactus Canyon - Top to bottom at the paddick
123	250	100	1014.28	140	0.1	6.45	376	Auto	Sellicks	Backward	Cactus Canyon - Reverse on 122
124	500	90	1014.28	104	0.1	4.77	544	Auto	Sellicks	Forward	Cactus Canyon - Top to bottom at the paddick
125	500	140	1014.28	104	0.1	7.37	544	Auto	Sellicks	Backward	Cactus Canyon - Reverse on 124
126	100	90	1014.28	309.6	0.1	14.99	344	Auto	Sellicks	Forward	Cactus Canyon
127	100	140	1014.28	309.6	0.1	22.74	344	Auto	Sellicks	Backward	Cactus Canyon
128	500	90	1014.28	104	0.1	4.77	544	Auto	Sellicks	towards SE	Pipe - Towards the main road
129	500	140	1014.28	104	0.1	4.77	544	Auto	Sellicks	Backward	Pipe
130	100	90	1014.28	309.6	0.1	22.74	544	Auto	Sellicks	Forward	Pipe - Towards the main road, SM for the pipe
131	100	129	1014.28	309.6	0.1	21.04	344	Auto	Sellicks	Backward	Pipe
132	250	90	4944.6	104	0.1	4.77	544	Auto	Sellicks	Forward	Pipe - Towards the main road
133	250	129	4944.6	104	0.1	4.77	544	Auto	Sellicks	Backward	Pipe - higher sampling Fz for 132 & 133
134	250	129	4944.6	104	0.1	4.77	544	Auto	Sellicks	Forward	Error
135	250	90	4944.6	140	0.1	6.45	544	Auto	Sellicks	towards SE	Compression - Towards the road
136	250	129	4944.6	140	0.1	6.45	544	Auto	Sellicks	Backward	Compression - SM for the pipe
137	500	90	4944.6	104	0.1	4.77	544	Auto	Sellicks	Forward	Compression

138	500	129	4944.6	104	0.1	4.77	544	Auto	Sellicks	Backward	Compression
139	100	90	4944.6	309.6	0.1	14.99	344	Auto	Sellicks	Forward	Compression
140	100	129	4944.6	309.6	0.1	21.04	344	Auto	Sellicks	Backward	Compression
141	500	90	4944.6	104	0.1	4.77	544	Auto	Sellicks	N - NW	Monastery - Top to bottom on line 54
142	500	129	4944.6	104	0.1	4.77	544	Auto	Sellicks	Backward	Monastery - Reverse on 141
143	250	129	4944.6	104	0.1	6.45	376	Auto	Sellicks	Forward	Top to bottom line 54 SM1-power line, SM2-fault
144	250	90	2472.3	140	0.1	6.45	376	Auto	Sellicks	SE	Monastery - bottom to top of the monastery road
145	500	90	4944.6	104	0.1	4.77	544	Auto	Sellicks	NW	Monastery
146	100	90	1014.28	309.6	0.1	14.99	344	Auto	Monastery	SE	Monastery - bottom to top on road SM-power lines
230	100	100	1014.28	96.6	0.1	5.83	128	Auto	Bethel	towards W	T3 - Test SM for trenches
231	100	100	1014.28	96.6	0.1	5.83	128	Auto	Bethel	towards W	T3 -Test
232	100	100	1014.28	175.5	0.1	9.81	208	Auto	Bethel	Backward	T3
233	100	100	1014.28	161	0.1	9	160	16	Bethel	towards N	In-between the trenches T 2 & T3
234	100	100	1014.28	161	0.1	9	160	16	Bethel	Towards W	north of the trench - parallel to T2
235	100	80	1014.28	175.2	0.1	8.04	208	2	Bethel	Backward	T2 - towards up hill
236	100	80	1014.28	175.2	0.1	8.04	208	2	Bethel	towards S	perpendicularly in-between the trenches T2 & T3
237	100	100	1014.28	104.5	0.1	6.23	136	16	Bethel	towards W	on the grid - near T3
238	100	100	1014.28	104.5	0.1	6.23	136	16	Bethel	towards E	T3
239	100	70	1014.28	143.9	0.1	6.04	176	8	Bethel	towards W	T3 - Test
240	100	120	1014.28	88.7	0.1	6.33	120	8	Bethel	towards E	T3 - Test
241	100	100	1014.28	104.5	0.1	6.23	136	8	Bethel	towards W	T2 and T3 - on the grid
242	100	100	1014.28	104.5	0.1	6.23	136	8	Bethel	towards E	T2 and T3 - on the grid
243	100	100	1014.28	104.5	0.1	6.23	136	8	Bethel	towards W	T2 and T3 - on the grid
244	100	100	1014.28	104.5	0.1	6.23	136	8	Bethel	towards E	T2 and T3 - on the grid
245	100	100	1014.28	104.5	0.1	6.23	136	8	Bethel	towards W	T2 and T3 - on the grid
246	100	100	1014.28	104.5	0.1	6.23	136	8	Bethel	towards E	T2 and T3 - on the grid
247	100	100	1014.28	104.5	0.1	6.23	136	8	Bethel	towards W	T2 and T3 - on the grid
248	100	100	1014.28	104.5	0.1	6.23	136	8	Bethel	towards E	T2 and T3 - on the grid
249	100	100	1014.28	104.5	0.1	6.23	136	8	Bethel	towards W	T2 and T3 - on the grid
250	100	100	1014.28	104.5	0.1	6.23	136	8	Bethel	towards E	T2 and T3 - on the grid
251	100	100	1014.28	104.5	0.1	6.23	136	8	Bethel	towards W	T2 and T3 - on the grid

252	100	100	1014.28	104.5	0.1	6.23	136	8	Bethel	towards E	on the grid - north of T2
253	500	100	1014.28	104.5	0.1	3.48	136	8	Bethel	towards W	test
254	500	100	1014.28	104.5	0.1	3.48	136	8	Bethel	towards E	test
255	100	100	1014.28	96.6	0.1	4.92	128	8	Bethel	towards W	T3
256	100	100	1014.28	96.6	0.1	4.92	128	8	Bethel	towards E	Error
257	100	100	1014.28	80.8	0.1	5.02	112	8	Bethel	E to W	near T2 - 450m
258	100	100	1014.28	80.8	0.1	5.02	112	8	Bethel	towards E	T1 - from trees to up hill
259	100	100	1014.28	80.8	0.1	5.02	112	8	Bethel	S to N	T2 - along the road
260	100	100	807.28	71.8	0.1	4.56	88	8	Bethel	towards SW	T2 - from hill - down slope
261	100	100	1014.28	73	0.1	4.62	104	8	Bethel	Backward	T2 - towards the hill - NE
262	100	100	608.57	82.2	0.1	5.09	80	8	Bethel	towards SW	T2
263	100	100	1014.28	159.7	0.1	9.02	192	8	Bethel	Backward	T2
264	100	100	1014.28	80.8	0.1	5.02	112	16	Bethel	towards SW	T2 - down hill
265	100	100	1014.28	112.4	0.1	6.63	144	16	Bethel	Backward	T2 - up hill
266	100	100	1014.28	65.1	0.1	4.21	96	Auto	Bethel	towards SW	T2 - down hill
267	100	100	1014.28	65.1	0.1	4.21	96	8	Bethel	Backward	T2
268	500	100	500.72	67.9	0.1	3.48	64	8	Bethel	to SW	Test
269	500	100	500.72	67.9	0.1	3.48	64	8	Bethel	to SW	T2 - 100m length
270	500	100	4944.6	53.8	0.1	2.78	296	8	Bethel	to SW	T2
271	500	100	4944.6	48.9	0.1	2.54	272	8	Bethel	to SW	towards T1 - from T2
272	500	100	4944.6	32.8	0.1	1.73	192	16	Bethel	W to E	north to T1
273	500	100	4944.6	29.5	0.1	1.56	176	8	Bethel	to NE	between T2 & T3 - towards T2
274	500	100	4944.6	29.5	0.1	1.56	176	8	Bethel	towards W	T2 - north to T1, down hill SM for trench and fault
275	500	100	4944.6	23.1	0.1	1.56	176	8	Bethel	backwards	T2 - up hill - SM for the fault
276	500	100	4944.6	23.1	0.1	1.24	144	8	Bethel	to SW	T2 - down hill aligned T1
277	500	100	4944.6	18.2	0.1	1	120	8	Bethel	to NE	T2 - up hill
278	500	100	4944.6	13.3	0.1	0.75	96	16	Bethel	to SW	T2 - down hill aligned T1
279	500	100	3042.83	19.1	0.1	1.04	88	16	Bethel	to NE	T2 - up hill
280	500	100	3042.83	13.8	0.1	0.77	72	8	Bethel	to SW	T2 - down hill
281	500	100	3042.83	11.2	0.1	0.64	64	8	Bethel	to NE	T2 - up hill
282	100	100	1014.28	57.2	0.1	3.8	88	8	Bethel	to SW	T2 - down hill aligned T1

283	100	100	599.35	70.1	0.1	4.47	72	8	Bethel	to NE	T2 - up hill
284	100	100	1014.28	65.1	0.1	4.21	96	8	Bethel	to W	north of T2
285	100	100	1014.28	65.1	0.25	4.21	96	8	Bethel	to E	north of T2
286	100	100	1014.28	80.8	0.1	5.02	112	8	Bethel	to S	East of the T2 and T3 - SM for the T3
287	100	100	1014.28	80.8	0.1	5.02	112	8	Bethel	to W	south of T3 towards T1
288	100	100	1014.28	80.8	0.1	5.02	112	8	Bethel	to E	south of T1 - SM at the end of T1
289	100	100	1014.28	80.8	0.1	5.02	112	8	Bethel	to W	south of T1
290	100	100	1014.28	80.8	0.1	5.02	112	8	Bethel	to E	south of T1 towards T3
291	100	100	1014.28	80.8	0.1	5.02	112	8	Bethel	to W	Error
292	100	100	1014.28	80.8	0.1	5.02	112	8	Bethel	to E	Error
293	100	100	1014.28	73	0.1	4.62	104	8	Bethel	to W	to the bottom of T2
294	100	100	1014.28	88.7	0.1	4.52	120	8	Bethel	to S	towards T2 to T3
295	100	100	1014.28	88.7	0.1	4.52	120	8	Bethel	to E	south of T3
296	100	100	1014.28	88.7	0.1	4.52	120	8	Bethel	to W	south of T3
297	100	100	1014.28	88.7	0.1	4.52	120	8	Bethel	to E	south of T3
298	100	100	1014.28	65.1	0.1	4.21	96	8	Bethel	to W	bottom of T3
299	100	100	1014.28	65.1	0.1	4.21	96	8	Bethel	to W	T3 towards T1
300	100	100	1014.28	65.1	0.1	4.21	96	8	Bethel	to E	bottom of T1
301	100	100	1014.28	80.8	0.1	5.02	112	8	Tarlee	towards W	Trench - 75m
302	100	100	1014.28	120.3	0.1	7.03	152	8	Tarlee	towards E	Trench - up scarp
303	100	100	1014.28	104.5	0.1	6.23	136	8	Tarlee	towards N	across the trench - towards the fence
304	500	100	4944.6	48.9	0.1	2.54	272	8	Tarlee	towards S	Test - starting from fence across the trench
305	500	100	4944.6	48.9	0.1	1.3	104	8	Tarlee	backwards	Trench - 40m
306	500	100	3042.83	24.3	0.1	1.3	104	8	Tarlee	towards S	Trench
307	500	100	4944.6	18.2	0.1	1	120	8	Tarlee	to W	Trench - 85m
308	500	100	4944.6	24.26	0.1	0.91	112	8	Tarlee	towards N	across the trench - towards the fence
309	500	100	4944.6	24.26	0.1	0.91	112	8	Tarlee	to S	Error

Details of the GPR surveying

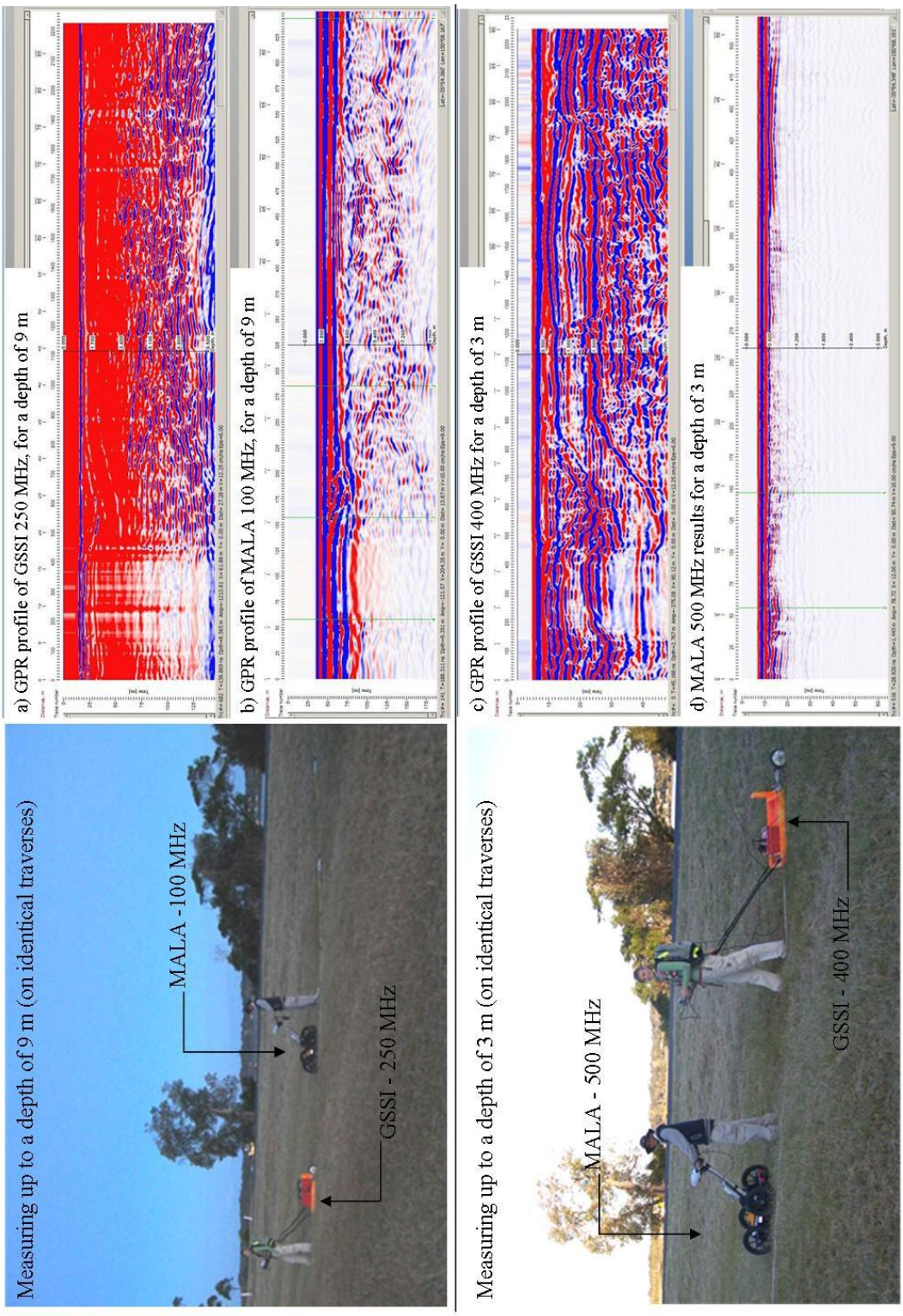

Comparision of the penetration depth and resulting radargram using MALA and GSSI GPR units

APPENDIX IV - CHAPTER 7

Richter magnitude	Depth (km)	Approximate location	Date
5.7	-	Eyre Peninsula	1887
6.5	-	Beachport	1897
6.0	14	Warooka	1902-09-19
5.5	-	Cleve	1911
5.4	0	Simpson Desert	1937-10-28
5.2	0	Motpena	1939-03-26
5.2	33	Simpson Desert	1941-05-05
5.6	33	Simpson Desert	1941-05-05
5.4	4	Adelaide	1954-03-01
5.0	10	Flinders Rangers	1965-03-03
5.5	12	Wilpena	1972-04-19
6.0	5	Marryat Creek	1986-03-30
5.6	5	Marryat Creek	1986-07-11
5.1	-	South of Burra	1997
5.0	-	Cleve	2010
6.1	-	Pukatja-Ernabella	2012-03-23
5.7	-	Near Ernabella	2013-06-09

Summary of the magnitude ≥ 5 earthquakes in South Australia from 1887 to 2013 (date source: www.ga.gov.au/earthquakes)